

**Development of biosensors using novel bioreceptors;
Investigation and optimisation of fundamental
parameters at the nanoscale**

By

Jack Antony Goode

Submitted in accordance with the requirements for the
degree of Doctor of Philosophy

The University of Leeds

School of Biomedical Sciences

Faculty of Biological Sciences

August 2015

Declaration

The candidate confirms that the work submitted is his own, except where work which has formed part of jointly authored publications has been included. The contribution of the candidate and the other authors to this work has been explicitly indicated below. The candidate confirms appropriate credit has been given within this these where reference has been made to the work of others. Copies of publications (or sections contributed by the candidate) are included with this thesis.

Jointly Authored publications:

- 1- Parts of chapter one have appeared in the following publication:

Biosensor Regeneration: A Review of Common Techniques and Outcomes.

2014, **Goode J A**, Rushworth J V, Millner P A.

Langmuir, 2015, 31 (23), pp 6267–6276

Jack Goode wrote the article with editorial and critical assistance from Jo Rushworth.

Copyright © 2014, American Chemical Society.

- 2- Some parts of chapter one have been adapted from a monograph :

Impedimetric biosensors for medical applications: current progress & challenges

2013, Rushworth JV, Hirst N A, Goode J A, Pike D J, Ahmed A, Millner P A.

Jack Goode contributed equally with other authors in this publication. copyright © 2013 ASME

Publications with work not in this thesis:

- 1- Comparative electrochemical analysis of two flow cell systems

Goode J A, Ahmed A, Millner P A, Kapur N, Stewart D,

Journal of the Electrochemical Society 161: B143-146

This work was done in collaboration with Prof. Nik Kapur, Faculty of Engineering, University of Leeds. Jack Goode & Asif Ahmed contributed equally in lab work and wiring the manuscript. Other authors assisted in flow cell design and critical discussions, Copyright © 2014, Journal of the Electrochemical Society.

This copy has been supplied on the understanding that it is copyright material and that no quotation from the thesis may be published without proper acknowledgment

© The University of Leeds and Jack A. Goode

“It is through science that we prove,

But through intuition that we discover.”

- **Henri Poincaré**

Acknowledgments

I would like to thank firstly my sponsors who have made this work possible; BBSRC for financial support as well as external training and providing the opportunity to do a policy internship with the Welsh Assembly Research Service. I would also like to thank AbCam for their continuous support and feedback throughout my project as well as access to interesting and novel technologies. Particular thanks go to Matt, Gary, the whole R&D team as well as other members of the office who helped me during my internship down in Cambridge.

I would like to express my thanks to Paul for his friendly manner and for giving me the freedom to steer this project in new directions, allowing me to follow my intuition and independently grow. Within the lab I wish to thank members both past and present for helpful discussion, coffee breaks and the motivation I have needed to come in and continue. Particular thanks go to Carolyn for her kind editorial assistance and advice along the way. Thanks go to the ECBU group (Gareth, Gina and Izma) as well as Andrew for providing distraction and brightening up long experiment days.

I would like to thank my family for getting me this far, and helping me to achieve everything I have to date, obviously the champagne & self-belief paid off. Finally thanks for those closest to me for keeping me sane over the last few years, without the support various friends I wouldn't have got through this. The friends I have made over the course of my PhD have consistently been at hand for drinks, lunches, brunches and parties to help me unwind and have given me many cherished memories.

Shout outs for my non-science friends both near and far that have ensured I've had the respite necessary along the way in the forms of holidays, hijinks and hurrahs all of which I have needed from time-to-time. My everlasting thanks go to David who has kept me (vaguely) sane, helped me edit and practically held me together throughout the process, I cannot articulate how much it has meant.

I dedicate this work to all of you guys and can't wait to start the next adventure.

Abstract

Point of care diagnostics is hailed as a potential revolution which could lower the significant cost of diagnosis, lead to earlier interventions and lower the mortality and morbidity of a variety of diseases. In spite of the early promises made and notable breakthroughs such as the glucose biosensor, the field of biosensors has yet to achieve the commercial and societal gains it promises. One of the primary reasons for this is the cost of testing a remaining obstacle in biosensor development. The work in this thesis aims to address different approaches to address this which may help accelerate the development of impedimetric immunosensors and enhance their adoption in diagnostic and field applications.

Initial work in this thesis has focussed on the development of a biosensor which could be regenerated, permitting repeated use. This work was done using a previously demonstrated biosensor where the signal behaviour was known and the process of regeneration could be studied in isolation. This proof-of-concept work it was discovered that regeneration and therefore re-use of impedimetric immunosensors was possible

The biosensors throughout this thesis were constructed using electropolymer to which proteins were attached before interrogating the sensor using electrochemical impedance spectroscopy (EIS). The fully constructed sensors were then incubated with analyte of increasing concentrations before repeating interrogations. EIS was used to monitor receptor - analyte binding and provide a method of sensor calibration.

Later work in this thesis explored the role of the bioreceptor in signal generation in EIS. The recent move towards the use of antibody mimetic receptors may have profound implications for biosensor development. There is however, limited demonstration of their use in biosensors and even less so in EIS based sensors. In this thesis nanobodies have been used to fabricate biosensors. They have also been re-engineered to include oriented peptide spacer arms with terminal cysteines to allow both oriented conjugation onto the transducer surface and precise positioning above it. This work has highlighted the importance of spacing and physical constraints at the nanoscale which may be important for determining signal generation in reagentless impedimetric immunosensors.

Abbreviations

2-ABA	2-aminobenzylamine
2-MEA	2-mercaptoethylamine (a.k.a β - mercaptoethylamine)
4-AAP	4- Amino antipyrine
aa	Amino acid
AC	Alternating current
AFM	Atomic force microscopy
AuNP	Gold Nanoparticles
BCA	Bicinchoninic acid
Biotin-Caproyl-DPPE	1,2 Dipalmitoyl- <i>sn</i> -glycero-3-phosphoethylamine-N-caproyl biotin
Biotin-NHS	Biotin –tagged N-Hydroxysuccinimide
BOI	Band of interest
BSA	Bovine serum albumin
CHAPS	[(3-Cholamidopropyl)dimethylammonio]-1-propanesulfonate
CCD	Charge coupled Device
C _{DL}	Double layer Capacitance
CDR	Complementarity Determining Region
C _{PE}	Constant Phase Element
CV	Cyclic voltammetry
DAPI	4',6-Diamino-2-phenylindole
DC	Direct current
DPPE	1,2 Dipalmitoyl- <i>sn</i> -glycero-3-phosphoethylamine-N-
DLL1	Delta like-1 protein
DMSO	Dimethyl sulphoxide
DMF	Dimethyl formidamide
DS	Dropsens®
DTT	Dithiothreitol
FRA	Frequency Response Analyser
<i>E.Coli</i>	<i>Escherichia Coli</i>
ECL	Enhanced Chemiluminescence
EDC	1-Ethyl-3-(3-dimethylaminopropyl)carbodiimide
EDTA	Ethylenediaminetetracetic acid
ELISA	Enzyme Linked Immunosorbent Assay

EIS	Electrochemical impedance spectroscopy
EtOH	Ethanol
FFA	Fixed frequency analysis
GOx	Glucose Oxidase
GPES	General purpose electrochemistry software
HRP	Horseradish peroxidase
IF	Immuno-fluorescence
IgG	Immunoglobulin type G
IPTG	Isopropyl β -D-1-thiogalactopyranoside
IHC	Immuno-histochemistry
IHP	Inner Helmholtz plane
ITO	Indium tin oxide
K_a	Association constant
K_b	Dissociation constant
K_d	Binding constant
KLH	Keyhole limpet haemocyanin
LB	Luria-Bertani
Mb	Myoglobin
MCH	Mercaptohexanol
MEA	Mercaptoethylamine
MES	2-Morpholino-ethanesulphonic acid
MHDA	Mercaptohexadecanoic acid
MOPS	2-Morpholino-propanesulphonic acid
mSAM	Molecular self-assembled monolayer
NABP	Non Antibody Binding Protein
NHS	N-Hydroxysuccinimide ester
NSB	Non-specific binding
OHP	Outer Helmholtz plane
o-PD	Ortho-phenylene diamine
PANI	Polyaniline
PBS	Phosphate buffered saline
PDADM	Polydiallyldimethyl ammonium chloride
PDDM	polydiphenyldiazomethane
PDPH	;3-(2-Pyrdyldithiolpropionyl Hydrazide 3-

PEG	Polyethylene glycol
PEI	Polyethylenimine
ppm	Parts per million
PSS	polystyrene sulphonate
PTyr	Polytyramine
QCM	Quartz crystal microbalance
R_{CT}	Charge transfer resistance
R_s	Solution resistance
SAM	Self-assembled monolayer
SAW	Surface acoustic wave
ScFv	Single chain variable Fragment
SELEX	Systematic evolution of ligands by exponential enrichment
SEM	Scanning electron microscopy
SDS	Sodium Dodecyl Sulphate
SDS-PAGE	Sodium Dodecyl Sulphate- Poly Acrylamide Gel Electrophoresis
SEM	Scanning electron microscopy
SPR	Surface plasmon resonance
Sulfo-SMCC	Sulphosuccinimidyl-4-(N-maleimidomethyl)cyclohexane-1-carboxylate
TA	Tris acetate
TB	Terrific Broth
TBST	Tris buffered saline, with 0.05% Tween-20
TCEP	Tris (2-carboxyethyl) phosphine
TMB	Tetra methyl benzidine
Z_w	Warburg Impedance
Z'	Real impedance
$-Z''$	Imaginary impedance

Table of Contents

Declaration.....	2
Acknowledgments.....	4
Abstract.....	5
List of Tables	17
List of Equations.....	18
1 Chapter One: Introduction.....	20
1.1 Overview	21
1.2 Biosensors	22
1.2.1 Optical biosensors.....	24
1.2.2 Mass based biosensors	27
1.2.3 Electrochemical biosensors	28
1.3 Construction of the biosensor	31
1.3.1 Transducer surface.....	31
1.3.2 Tethering layer	34
1.4 Bioreceptor conjugation	39
1.5 Bioreceptors.....	48
1.5.1 Oligonucleotides	48
1.5.2 Proteins	49
1.5.3 Validating receptors for use in biosensors.....	57
1.6 Biosensor regeneration.....	60
1.6.1 Enthalpic interactions	60
1.6.2 Entropic Interactions.....	62
1.6.3 Role of pH and electronic environment.....	63
1.6.4 Electrochemical regeneration.....	65
1.7 Electrochemistry	66
1.7.1 The three-electrode system.....	66
1.7.1 Double layer theory	67
1.7.2 Amperometry.....	69
1.7.3 Potentiometry.....	70
1.7.4 Voltammetry	71
1.7.5 Impedance	75
1.8 Project aims	84
2 Chapter Two: Materials & Methods	85

2.1	Materials	86
2.1.1	Inorganic materials	86
2.1.2	Organic materials	86
2.1.3	Antibodies	86
2.1.4	Plasmids for nanobodies.....	86
2.1.5	Agarose gels	86
2.1.6	Bacterial strains.....	87
2.1.7	Growth media for bacteria	87
2.1.8	Buffers and solutions	87
2.1.9	Consumables.....	87
2.2	Methods.....	89
2.2.1	Synthesis of nanobodies	89
2.2.2	SDS- PAGE and western blots	90
2.2.3	Immunoprecipitation experiments.....	91
2.2.4	Biotinylation of antibodies.....	92
2.2.5	Reduction of nanobody dimers.....	92
2.2.6	Electrode preparation	92
2.2.1	Electrochemical instrumentation.....	94
2.2.2	Interrogation of sensors.....	95
2.2.3	Regeneration of electrodes	96
2.2.4	Octet studies	96
3	Chapter Three: Fabrication and Regeneration of Immunosensors	98
3.1	Introduction	99
3.1.1	Chemical regeneration.....	100
3.1.2	Electro-reduction of nitrate	100
3.2	Results.....	102
3.2.1	Fabrication of myoglobin sensors.....	102
3.2.2	Interrogation of myoglobin sensors.....	104
3.2.3	Chemical Regeneration of myoglobin sensors.....	106
3.2.4	Return to chemical approach using a complex regeneration buffer.....	122
3.2.5	Verification of incubation times, using fluidics.....	123
3.3	Discussion.....	126
4	Chapter Four: Results: Nanobody production, optimisation and characterisation.	128
4.1	Antibodies	129

4.2	Nanobodies.....	130
4.2.1	Vector selection and recombinant molecular biology.....	130
4.2.2	Sequencing data.....	132
4.2.3	Expression of nanobody peptide.....	133
4.2.4	Disulphide cleavage using TCEP beads.....	134
4.2.5	Disulphide cleavage using β -MEA.....	135
4.2.6	Immunoprecipitation of rabbit IgG from serum.....	137
4.3	Analysis of binding parameters using BLI.....	142
4.4	Bioreceptor parameters.....	146
4.5	Discussion.....	151
5	Chapter Five: Results: Using nanobodies in electrochemical biosensors.....	153
5.1	Introduction.....	154
5.2	Antibody based sensors.....	155
5.2.1	Control data.....	156
5.3	Nanobody based biosensor.....	158
5.3.1	Optimisation.....	159
5.3.2	Controls.....	161
5.4	Oriented nanobody biosensors.....	164
5.4.1	P8D8-S5 Based biosensor interrogation.....	164
5.4.2	P8D8-S10 Based biosensor interrogation.....	165
5.4.3	P8D8-S15 Based biosensor interrogation.....	166
5.5	Comparison of bioreceptor systems.....	168
5.6	Testing of optimised nanobody biosensor.....	169
5.7	Discussion.....	171
6	Chapter Six: Discussion.....	174
6.1	General Discussion.....	175
6.2	Binding biophysics and regeneration.....	176
6.3	Nanobodies in reagentless immunosensors.....	178
6.4	Discovered opportunities.....	180
6.5	Requirements for sensor commercialisation.....	181
6.6	Future Work.....	183
6.6.1	Limitations within the field.....	184
7	References.....	186
8	Appendices.....	203

8.1	Variety of electrodes used	204
8.2	Buffers Used.....	205
8.3	Sequencing data for P8D8 nanobody	206
8.4	Poster presented at BBI 2013	207
8.5	Poster Presented at MMT 2015.....	208

List of Figures

Figure 1-1: Schematic of a biosensor	21
Figure 1-2: The number of publications including “biosensor” in the title	22
Figure 1-3: Typical SPR Instrumentation.....	24
Figure 1-4: Principles of Bio-Layer interferometry	25
Figure 1-5: The enzymatic oxidation of glucose	28
Figure 1-6: 22 years of glucose biosensor evolution (1983-2005).....	29
Figure 1-7: Comparing different electrode production techniques	31
Figure 1-8: Deposition of nanotubes on a gold transducer surface	32
Figure 1-9: Comparison of typical alkane-thiol SAM's	33
Figure 1-10: Disruption of mSAM by binding of a large analyte.....	34
Figure 1-11: Electrostatic entrapment of bioreceptor.....	37
Figure 1-12: Conjugation of carboxyl group to amine group using EDC.....	39
Figure 1-13: Conjugation of Thiol group to Amine group using SMCC.....	41
Figure 1-14: The conjugation of a carboxyl moiety to a thiol group using PDPH.....	43
Figure 1-15: The structure of avidin homo tetramer.....	44
Figure 1-16: Modification of IgG for biosensor applications	50
Figure 1-17: A comparison of IgG antibodies and camelid antibodies	53
Figure 1-18: An illustration of different bioreceptors used.....	55
Figure 1-19: Binding data in a typical interferometry experiment.....	56
Figure 1-20: A schematic of biosensor regeneration.....	58
Figure 1-21: Forces governing analyte: receptor binding and regeneration.....	61
Figure 1-22: A schematic of Guoy-Chapman theory.....	66
Figure 1-23: CV obtained in the ferri- ferrocyanide system.	70
Figure 1-24: Phase shift in complex impedance.	73
Figure 1-25: The Nyquist plot schematic.	77

Figure 1-26: The Randles' equivalent cell	78
Figure 1-27: A sample Bode plot.....	79
Figure 3-1: Electroreduction of nitrate ions	97
Figure 3-2: Electropolymerisation of PANI 2-ABA copolymer onto a gold electrode.....	99
Figure 3-3: Impedance scans of consecutive construction steps	100
Figure 3-4: Nyquist Plots of a PANI-2-ABA myoglobin sensor	101
Figure 3-5: Charge transfer resistance of a myoglobin biosensor on PANI-2ABA	102
Figure 3-6: pH study of myoglobin biosensor regeneration.....	103
Figure 3-7: Time study of myoglobin biosensor regeneration	104
Figure 3-8: The Dropsens microfluidics rig	105
Figure 3-9: Monitoring myoglobin biosensor regeneration across frequencies	106
Figure 3-10: Different electronic configurations of PANI: 2ABA copolymer	108
Figure 3-11: The stability of PANI:2-ABA	108
Figure 3-12: Analysed R_{CT} on stability of PANI:2-ABA.....	109
Figure 3-13: Electropolymerisation of polytyramine film.....	110
Figure 3-14: The stability of PTyr	111
Figure 3-15:Analysed R_{CT} on the stability of PTyr.	112
Figure 3-16: Stability of PTyr after 10s periods of electroreduction of nitrate	113
Figure 3-17: Analysed R_{CT} of PTyr film after electroreduction of nitrate.....	114
Figure 3-18: Monitoring the electroreduction of nitrate.....	115
Figure 3-19: Electro-reduction of nitrate at -2.0 V.	116
Figure 3-20: Nyquist plots of PTyr based sensor construction	117
Figure 3-21: Calibration of a PTyr based immunosensor for myoglobin	118
Figure 3-22: Regeneration of a myoglobin sensor using complex regeneration buffer.....	119
Figure 3-23: Nyquist plots of the successful regeneration of a myoglobin sensor.....	120
Figure 3-24: Successful regeneration of a myoglobin biosensor	121
Figure 4-1: Schematic of different bioreceptor constructs used.....	125

Figure 4-2: Map of <i>pHEN6</i> vector used for expression of nanobodies in <i>E.Coli</i>	127
Figure 4-3: E-gel image of vectors after digestion.....	128
Figure 4-4: SDS-PAGE of nanobodies.....	129
Figure 4-5: SDS-PAGE of nanobodies subjected to TCEP reduction	130
Figure 4-6: SDS-PAGE of nanobodies subjected to 2-MEA reduction.....	131
Figure 4-7: Size exclusion chromatography of reduced nanobody dimers	133
Figure 4-8: Schematic for immunoprecipitation experiments.....	134
Figure 4-9: Blotting experiments from immunoprecipitation fractions	136
Figure 4-10: Real time binding data for an antibody based rabbit IgG sensor.....	138
Figure 4-11: Calibration using R_{max} data from the Octet	139
Figure 4-12: Real time binding data from a full titration of nanobody based sensor	140
Figure 4-13: A comparison of R_{max} for the detection of IgG using various receptors.....	141
Figure 4-14: Comparison of one-site and two stage binding model to fit data.....	143
Figure 4-15: Comparison of binding constants of different bioreceptor systems.....	146
Figure 5-1: Sample Nyquist Plot.....	150
Figure 5-2: Nyquist plot of antibody based sensor for rabbit IgG	151
Figure 5-3: The calibration of a rabbit IgG sensor using IgG receptor.....	152
Figure 5-4: Calibration of a rabbit IgG biosensor constructed using IgG receptor	153
Figure 5-5: Initial calibration of a nanobody based sensor for rabbit IgG	154
Figure 5-6: Optimising nanobody concentration.....	156
Figure 5-7: Nyquist plots of a nanobody based sensor with increasing analyte	157
Figure 5-8: Calibration of a rabbit IgG biosensor using biotinylated P8D8 nanobodies.....	158
Figure 5-9: Comparison of specific and nonspecific signal for a GFP biosensor.....	159
Figure 5-10: Calibration of a sensor using P8D8-S5 nanobody.....	161
Figure 5-11: Calibration of a sensor using P8D8-S10 nanobody.....	162
Figure 5-12: Calibration of a sensor using P8D8-S15 a nanobody.....	163
Figure 5-13: Comparison of the specific signal generated different receptors.....	164

Figure 5-14: Testing of the P8D8-S5 biosensor in serum..... 165

Figure 5-15: Guoy-Chapman theory in nanobody based sensors..... 169

List of Tables

Table 1-1: Polymers used as biosensor tethering layers	38
Table 1-2: Antibody mimetic systems.....	54
Table 2-1 : Sources for antibodies and sera for purification studies	86
Table 4-1: Densitometry data from 2-MEA reduction of nanobody dimers.....	136
Table 4-2: Data from one site binding model	149
Table 4-3: Data from two site binding model.	149

List of Equations

Equation 1-1: The Sauerbrey equation	27
Equation 1-2: Calculating On rate from one site saturation curve	59
Equation 1-3: Calculating Off rate from one site binding	59
Equation 1-4: Calculation of affinity from rate constants	59
Equation 1-5: Calculation of system Enthalpy	61
Equation 1-6: Calculation of Gibb's free energy	62
Equation 1-7: The Debye layer equation	69
Equation 1-8: Faraday's Law	70
Equation 1-9: The Nernst equation.....	71
Equation 1-10: The Randle's- Sevçik equation.....	74
Equation 1-11: Simplified Randle's-Sevçik equation.....	74
Equation 1-12: Calculating area from Randle's Sevçik equation	74
Equation 1-13: Ohm's Law	76
Equation 1-14: Calculating voltage in an AC circuit	76
Equation 1-15: Calculating current from phase shift.....	77
Equation 1-16: Total impedance from potential and current	77
Equation 1-17: Ohms Law in a resistor subject to oscillating potential	78
Equation 1-18: Calculating charge from capacitance and potential.....	78
Equation 1-19: Integrating charge with respect to time	78
Equation 1-20: Emergence of capacitance in observed current.....	78
Equation 1-21: Euler's identity	79
Equation 1-22: Calculation of phase angle	79
Equation 1-23: Calculation of total impedance	79
Equation 2-1: One site saturation signal.....	97
Equation 2-2: One Site desaturation signal	97
Equation 2-3: Binding affinity	97

Equation 2-4: Two site saturation signal.....	97
Equation 2-5: Two site desaturation signal	97

1 | Chapter One: Introduction

1.1 Overview

Despite the increasing volume of research into biosensors, there have been disappointingly few sensors which have achieved commercial success (Luong et al., 2008). Though the glucose biosensor accounts for ~80% of the market (Newman & Turner, 2005) it does not satisfy the wider needs of the research, diagnostic and sensing fields.

Immunosensors, a much more widely applicable type of biosensor, have enabled the discovery of a large array of relevant biomarkers (Luppa et al., 2001). Within the literature, a commonly identified method for improving the quality of a sensor is to modify the receptor, found at the biosensor interface either by altering it chemically or replacing it with another category of receptor for the same analyte. This crucial component dictates the sensors specificity and sensitivity and has been widely proven to have a large impact in sensor performance (Zourob, 2009).

One trend within the field of biosensors and more widely in biochemical research is the adoption of antibody mimetics. Whilst this is hailed as a revolution in terms of both fundamental research and in applied fields such as diagnostics and therapeutics there is still fairly limited published output on the application of such binding proteins (Gilbreth & Koide, 2012; Skottrup, 2010).

Much attention has been devoted to the development of antibody mimetics with the aim of reducing the use of animals. The work in this thesis focusses on the application of such binding proteins, in particular on their use in biosensors. Nanobodies, essentially re-engineered camelid antibodies have been used in impedimetric immunosensors; this is a promising technique but has yet to prove its commercial viability. Work in this thesis has additionally re-engineered the nanobodies to optimise them for biosensor applications.

Work has also been carried out to investigate the possibility of biosensor regeneration, another approach which may help to reduce the cost per test. Whilst this has been previously demonstrated for a number of biosensor systems, it has only achieved limited success in reagentless impedimetric immunosensors.

1.2 Biosensors

A biosensor is a three component system comprising a biological recognition element; a transducer and a signal processing unit (Figure 1-1). Typically the analyte which interacts with a receptor is part of a complex mixture such as in blood or other biological fluids.

The biosensor must therefore generate signal specific only to the analyte given the large number of non analyte proteins which may be present in a given sample. The biosensor should also be sensitive in detecting the analyte at an appropriate level, e.g. to determine between physiological and pathological levels for a disease biomarker. These ranges are from pico-molar up through to nanomolar concentrations. Though this range will change for different diseases this is a technically achievable range and one which is often relevant to distinguish a biomarker and help determine where it is within the physiological (normal) or pathological (disease) range for a given illness or disorder.

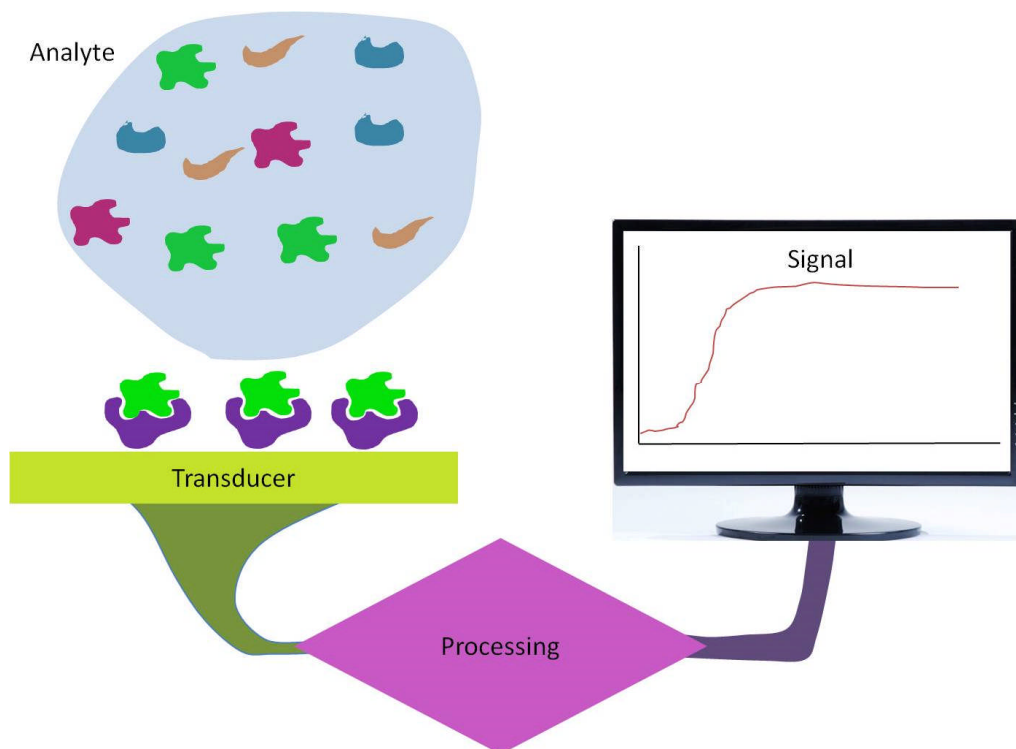


Figure 1-1: Schematic of a biosensor

Whilst *in-vitro* tests have been around for many decades now, the idea of developing biosensors is fairly recent and a brief search of the literature shows just how much growth in the field has accelerated in the last thirty years (Figure 1-2). It is important to note that whilst the landmark paper was published in 1962(Clark & Lyons, 1962), the term biosensor was coined at a later date and has since grown into its own field.

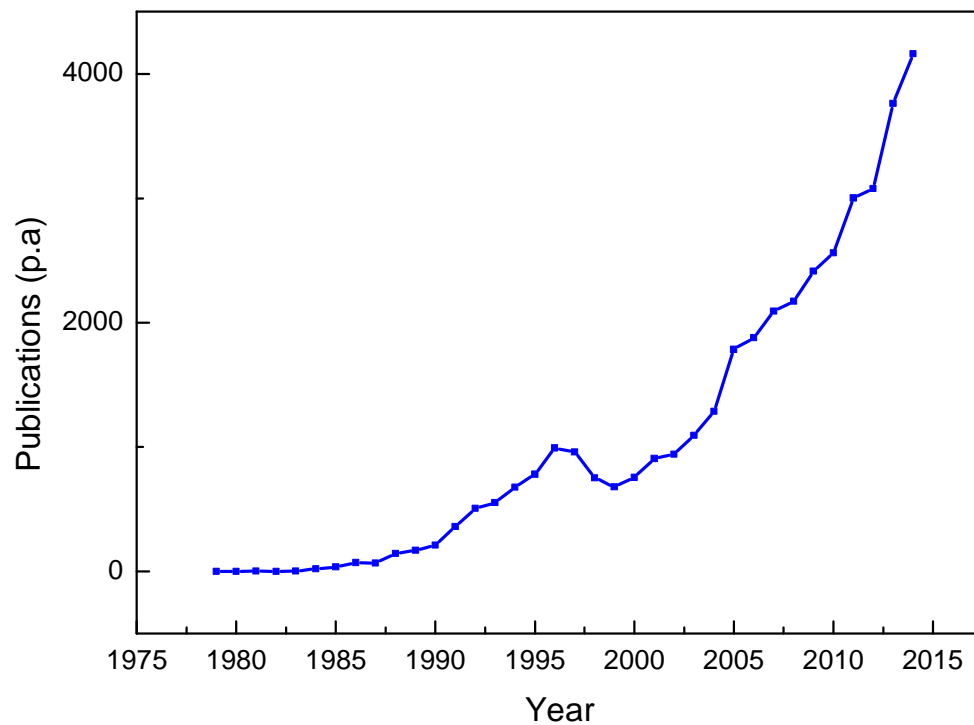


Figure 1-2: The number of publications including “biosensor” in the title. Data obtained by using Science Direct

The field of biosensors and In-vitro diagnostics has become increasingly diverse, in an aim to meet the expanding needs of researchers, within industry and by medical professionals. This has been additionally driven by discoveries in molecular medicine which have identified previously unknown biomarkers for a wide host of diseases and disorders. These potentially enable more stringent diagnostic tools to be developed, reducing mortality and morbidity by hastening positive intervention.

1.2.1 Optical biosensors

One of the most widely demonstrated biosensor categories are optical biosensors. They include methods such as surface plasmon resonance, interferometry and ellipsometry. Optical biosensors have enjoyed particular success due to the fact that binding can be monitored in real time, generating data which does not suffer from electrical interference (Albert et al., 2002). Optical sensing can be broadly grouped into methods which require the use of chromophores or fluorophores and label-less sensing. Label free detection is often considered the preferred option as it does not require the time and labour intensive steps associated with the use of tagging protocols. These steps may also adversely affect molecular interactions between receptor and analyte (Giepmans et al., 2006). In addition to operational difficulties, optical biosensor systems are often instrumentally complex and expensive to establish.

SPR based sensors operate using the principle that light travelling through biological materials will travel at a different speed than when travelling through a buffer or air. This causes a change in the refractive index which is used to assess binding of the analyte at the surface (Homola et al., 1999). The SPR chip is covered in a thin metal film coupled to a glass prism. When light is beamed at the prism total internal reflection occurs. As the light is diffused through the prism, a spectrum of wavelength is reflected across a range of angles. At a given angle, the energy of the incident photons interacts with the energy levels of evanescent waves at the prism -metal interface resulting in the propagation of plasmons. This process means that energy from the incident light is absorbed and that the intensity in reflected light is reduced, a diagram of a typical SPR setup is shown in Figure 1-3.

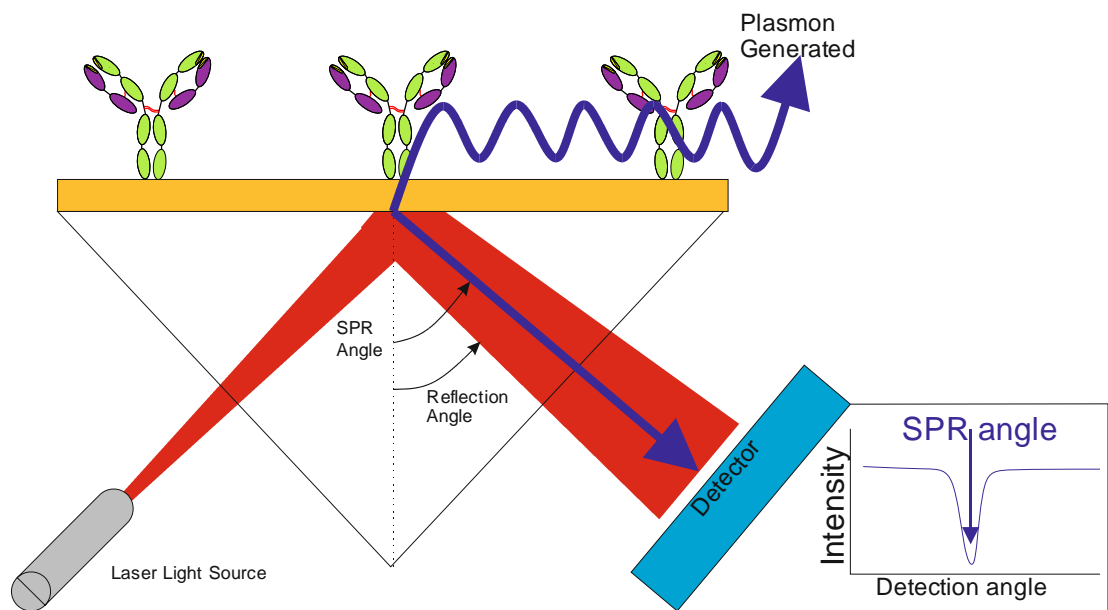


Figure 1-3: Typical SPR Instrumentation. As more biomaterial is attached at the surface, the plasmon generated absorbs light at a different angle causing the point of minimum intensity at the detector to shift; this change in shift is used to monitor binding in real time.

As the angle of reflected angle corresponds to the wavelength, the changing energy of the evanescent wave can be detected by a change in the SPR Angle. This is controlled by a number of parameters, the critical one being the refractive index at the film. Therefore, any change in refractive index at will result in a changing SPR. The change in this angle ($\delta\theta$) is used to generate SPR binding data in real time angle (Barnes et al., 2003; Suzuki et al., 2008).

Though SPR is a well-established method with successful commercialisation by Biacore and the Texas Instruments 'Spreeta' system (Karlsson, 2004), SPR equipment remains expensive and applications are primarily towards the investigation of binding phenomena rather than the development of clinical diagnostic tools.

Interferometry, another widely-used method of optical detection of biomolecules, is often achieved using fibre optic probes. By conjugating the receptor at the end of an optic probe, a biosensor surface is created which is perpendicular to the incident light. As the change in refractive index between the fibre and the buffer are so large, a proportion of the light is reflected back down the fibre as in Figure 1-4 .

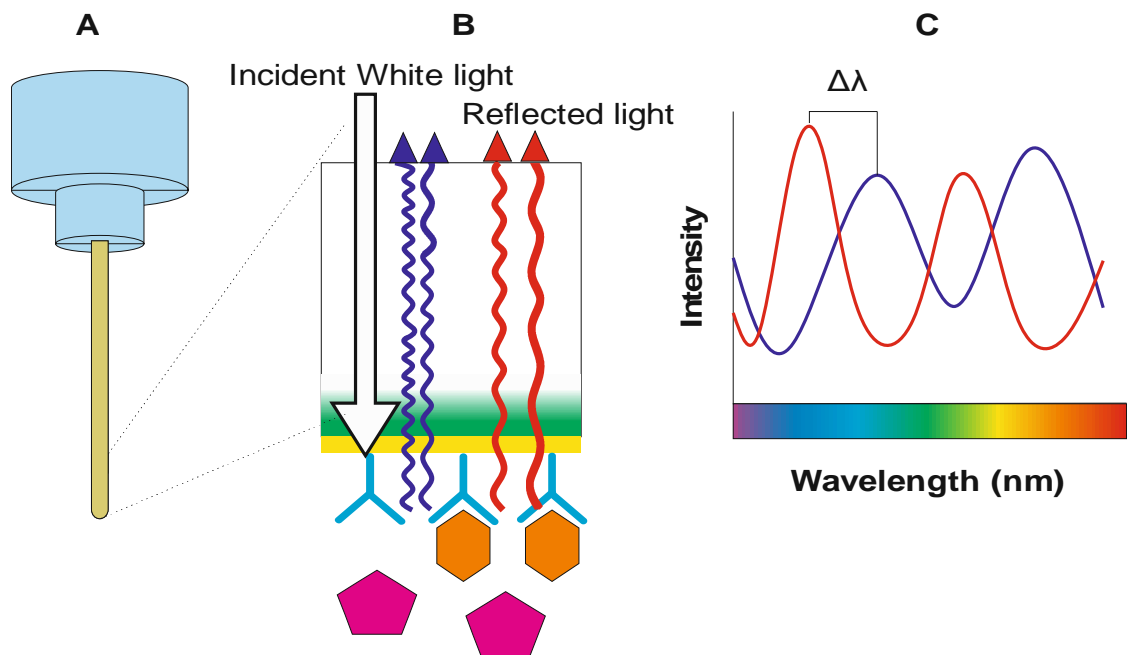


Figure 1-4: Principles of Bio-Layer interferometry. Incident white light is shone down a fibre optic probe(A) to which bioreceptors are covalently attached(B), the change in intensity across the various wavelength (C) can then be used to calculate an effective thickness as more matter binds at the sensor surface this thickness increases(B).

When white light is shone down the fibre optic probe a different pattern of wavelengths and intensities may be reflected back to a photodiode. Using a similar principle as in SPR the more matter that is bound at a surface, the thicker the reflecting surface will become. This leads to changes the constructive and destructive interference of both incident and reflected beams of light through the probe which can be measured. This is used to calculate an effective change in thickness at the biosensor interface, which can be measured in real-time. As with SPR, successful commercialisation of this has been achieved with the Fortebio Blitz and Octet systems. Again, many applications are research lead and the main use of these systems is to investigate binding parameters rather than for diagnostic sensors.

Another category of optical biosensor uses ellipsometry, a technique which can investigate the dielectric properties of surfaces and thin films. This technique exploits the fact that a given dielectric surface, with a refractive index much greater than the medium (either air or water), will reflect a proportion of light at a given angle (Bally et al., 2006). At a particular angle, known as the Brewster's angle, polarised light will be perfectly transmitted through the dielectric and there will be no light reflected. By shining a beam of

polarized light at the surface at an angle similar to the Brewster's angle, any changes in the surface will alter the amount of light reflected. This reflected light can be then detected using a photodiode. As the data is generated by the interaction of light over a surface, the surface must be very regular to generate high quality data. This method therefore requires highly ordered flat surfaces to operate and commonly uses ordered tethering layers such as self-assembled monolayers (Demirel et al., 2008).

As data obtained using this method provides information on the refractive index and thickness of any optical layer at the interface, any binding data must be calculated indirectly. This often requires lengthy calculations in order to achieve good simulation of binding processes at the sensor interface. In a variety of studies such simulation has resulted in successful calibration for biosensors for a variety of analytes including DNA (Demirel et al., 2008), toxins (Nabok et al., 2011) and bacteria (Gonzalez-Martinez et al., 2007) as well as proteins (Bombarová et al., 2015) and peptides such as amyloid peptide (Mustafa et al., 2010).

1.2.2 Mass based biosensors

Mass sensing biosensors, include piezoelectric methods such as the quartz crystal microbalance (QCM) and micro-cantilever based sensors. These sensors operate by exploiting the piezoelectric nature of the transducer. In QCM, a harmonic oscillating frequency is established in the material which is maintained. The QCM chip has the transducer layer of the biosensor attached covalently and so as there is any change on the transducer surface, this affects the oscillating wave through the piezoelectric substrate. As the mass at the surface increases, the input frequency is slowed to maintain the harmonic frequency through the substrate. The change in frequency can be converted using the Sauerbrey relation into mass on the binding surface (Kankare, 2002). As analysis can be done in real time, QCM is an effective way for studying binding events.

$$\Delta f = - \frac{2 f_0^2}{A \sqrt{\rho_q \mu_q}} \Delta m$$

Equation 1-1: The Sauerbrey equation

Where:

Δf = change in frequency (Hz)

f_0 = Resonant frequency (Hz)

A = Piezoelectrically active crystal area (cm²)

ρ_q = Density of quartz (2.648 g.cm⁻³)

μ_q = Shear modulus of Quartz (2.947x10¹¹ g.cm⁻¹.s⁻²)

Δm = Change in mass (g)

Whilst QCM is a useful and relatively low cost method, as signal is based on mass detection, it is particularly difficult to detect small molecules using QCM. Because the data collected is affected by the dissipation of the harmonic oscillating wave, a modified method known as dissipation monitoring QCM, or QCM-D, was established in which the mechanical properties of the interface can also be ascertained. This is achieved by monitoring the dissipation of the harmonic wave when the applied frequency is withdrawn as the time taken for the material to no longer oscillate is dependent on its viscoelastic properties.

The other principal mass based method is force spectroscopy. This is commonly achieved using piezoelectric cantilevers such as those used in atomic force microscopy (AFM). Though this sensing method is instrumentally more complex, it may allow the observation of individual binding events and direct data can be obtained on the strength of interactions between receptor and analyte proteins (Neuman & Nagy, 2008). Though piezoelectric systems have been widely demonstrated, their practical deployment in diagnostics are limited to applications such as HIV testing (Haleyur Giri Setty & Hewlett, 2014). The most successful biosensors have been demonstrated where analyte recognition results in a large change in mass at the biosensor interface (O'Sullivan & Guilbault, 1999).

1.2.3 Electrochemical biosensors

Electrochemical biosensors have been established as market leaders and account for a large proportion of the market share (~85%) (Grieshaber et al., 2008; Joseph, 2006; Laschi & Mascini, 2006; Lazcka et al., 2007; Pohanka, 2008). They are preferred to other methods due to their practical simplicity, speed and low capital costs (Caygill et al., 2010). It is for these reasons that electrochemical sensors are the focus of this thesis.

The field of electrochemical biosensors has been steadily developing since the creation of the first biosensor by Clark and Lyons (Clark & Lyons, 1962). This early sensor was for glucose and operated by confining glucose oxidase in a membrane bound dialysis chamber and monitoring the consumption of oxygen in the system, the reaction is outlined in Figure 1-5.

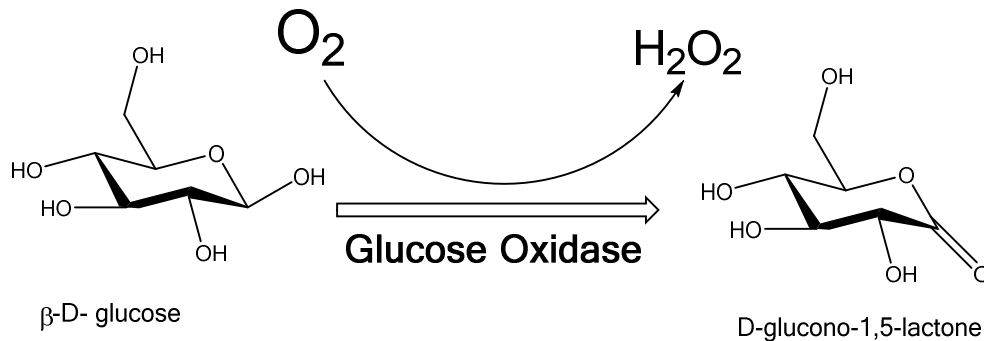


Figure 1-5: The enzymatic oxidation of glucose

These first generation sensors were unreliable as varying oxygen concentrations in the local environment commonly caused errors and a high potential (voltage) was needed to detect the oxygen generated in the sample (Habermüller et al., 2000).

In the 1980's, second generation sensors were developed which operated at much lower potentials, allowing greater specificity. This was enabled by the use of electron mediators (Cass et al., 1984; Kulys et al., 1980) in these sensors, the liberated electron from the glucose could be directly transferred to the transducer (Cass et al., 1985). This prevented non-specific redox of other species at the electrode surfaces. These electron mediators were either mixed into the sampling solution, or directly tethered to the transducer surface. These sensors were then superseded in the 90's by third generation biosensors where the enzymes used could directly transfer electrons to the surface of the electrode allowing direct specific signal. This was often achieved using materials such as conducting polymers. Whilst mediating electron transfer through the polymer matrix, the polymer could also itself be used to immobilise the enzyme. This is the form in which most amperometric sensors are found today (Gerard et al., 2002; Reiter et al., 2001; Schuhmann et al., 2000). The development of the glucose sensor over a period of 22 years, since the release of the first commercial sensor is shown in

Figure 1-6.

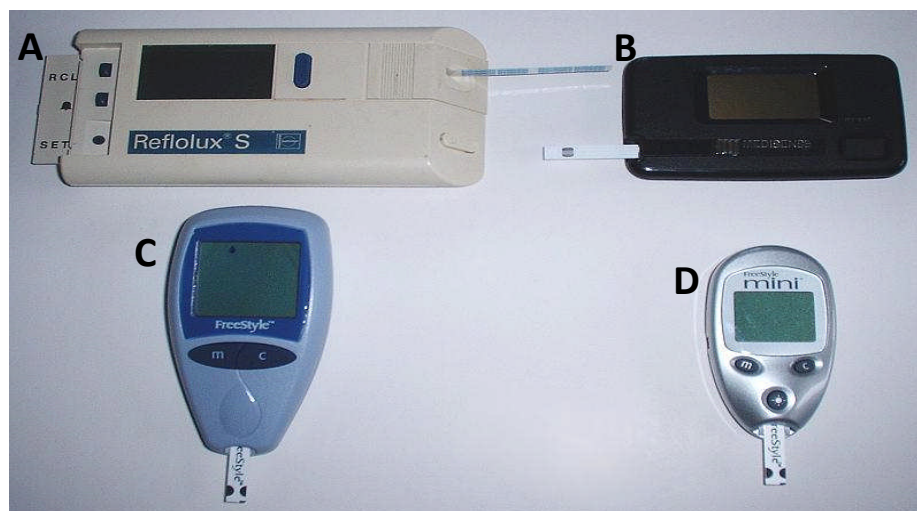


Figure 1-6: 22 years of glucose biosensor evolution (1983-2005). (Commons, 2014). A Reflolux S, by Boehringer Mannheim, introduced 1991. This device offered a 2 minute read time, based on reflectance. B: ExacTech Card, by MediSense introduced 1987 was capable of a 30 second read time using an electrochemical test strip which used much less blood as it operated using a capillary. C: FreeStyle, by TheraSense, Introduced 2003. A drop of blood could be assayed in 15 seconds electrochemically. D: Freestyle Mini, by Abbott. Introduced 2004, this is a smaller version of the FreeStyle and the interrogation time was reduced to 7 seconds.

The early types of metabolic biosensors were often enzyme based. This proved a powerful approach for analytes which had appropriate oxido-reductase enzymes available. However, as the needs for developing sensors have become more diverse, sensors are required for analytes which do not have a relevant enzyme specific to the analyte.

This has led to the expansion of the field of affinity based sensors. Whilst technologically less developed, lateral flow devices have been a large sector of the market in binding based assays to date (Luppa et al., 2001). A well-known example is the pregnancy test which is a biosensor for chorionic gonadotropin, a hormone which is immediately and greatly elevated in pregnancy (Cole, 2015). Whilst lateral flow devices are good for some analytes, they have intrinsic limitations in that they give a qualitative measure of an analyte and use a large amount of both receptor and sample (del Campo, 2014). This makes them unsuitable for a large range of analytes. In particular, their qualitative nature limits their application in medical diagnostics where the differences between physiological and pathological ranges of a biomarker cannot be distinguished using a lateral flow device (Singh et al., 2014).

1.3 Construction of the biosensor

When constructing a biosensor there are many aspects which must all be considered as the large number of variables and lack of established standards in the field mean that each biosensor system may give different data. Thus the fabrication process must be considered when analysing data.

1.3.1 Transducer surface

The electrode surface is a primary consideration when fabricating a biosensor. A number of factors must be considered including: stability, both mechanical and chemical, surface texture, surface chemistry and the ability to undergo conjugation reactions, cost, conductivity, quality and reproducibility of signal, and ease of use.

The transducer architecture (both size and shape) as well as relative position of other necessary electrodes in the electrochemical cell are also key parameters. Some electrodes are built into a system with external counter and reference electrodes which must be manually assembled upon use. This may not be ideal as it can introduce a level of variability into the system before experimentation even begins. Therefore, the aim is to develop an integrated transducer including the relevant electrodes which could result in more reproducible properties at the biosensing interface.

Over the years, many different electrodes have been proposed. In established biosensor fields such as the GOx sensor, a clear leader exists, in this case the carbon ink screen printed electrode (Niu et al., 2012). In developing areas such as in the field of reagentless impedimetric sensors, there are yet to emerge any optimum solutions. Indeed only a limited sample of the wide range of transducers has been successfully demonstrated for use in impedimetric sensors. Within the scope of this thesis, many electrodes have been trialled and a comprehensive list is given in Appendix 1. Though the majority of work has been done on Dropsens electrodes, it must be highlighted that this was also a compromise as the screen printing of the gold electrodes introduced a larger than optimum surface roughness and variability within the electrodes.

1.3.1.1 Sputter coated silicon wafer

A particularly good sensor substrate is a sputter coated silicon wafer. Silicon wafers are routinely produced for use in the semiconductor industry and have virtually atomically flat surfaces (typically $\text{RMS} \leq 1 \text{ nm}$) making them very useful as substrates for electrode construction. To achieve this, the wafer is placed in a vacuum chamber attached to which

is an ion accelerator. This ionises gas atoms such as argon or nitrogen which are then released into the main chamber where they are drawn towards a metal target. When they hit the target, it results in the displacement of gold particles which travel through the vacuum and collide with the substrate to condense and form a gold film. The design of the electrode can be controlled by doing this through a template, known as a mask shown in Figure 1-7 (A). Though this provides an excellent surface it often requires bespoke templates to be made and requires skilled technicians and expensive clean room instrumentation. This often results in prohibitively expensive electrodes, typically \geq £5 per chip for even a basic design (Millner et al., 2009).

1.3.1.2 Screen printed surfaces

One way of producing cheaper electrodes is to use screen printed electrodes (SPEs). These are produced by printing a suspension of carbon, metal or polymer particles. A suspension is held in a reservoir which runs over the flexible template and the ink or suspension is then squeezed through the template Figure 1-7 (B). As this relies on the use of a particulate suspension which is later heated in order to remove any organic components and sinter together particles, it often produces electrodes with a very rough surface which has more of an agglomeration of smaller particles than one continuous smooth surface (Alonso-Lomillo et al., 2010; Li et al., 2012; Niu et al., 2012). Carbon SPEs are often used for the creation of amperometric sensors as they allow direct coupling of an electroactive enzyme and the nano-topology does not prevent the small metabolite analyte molecules from reaching the receptor sites.

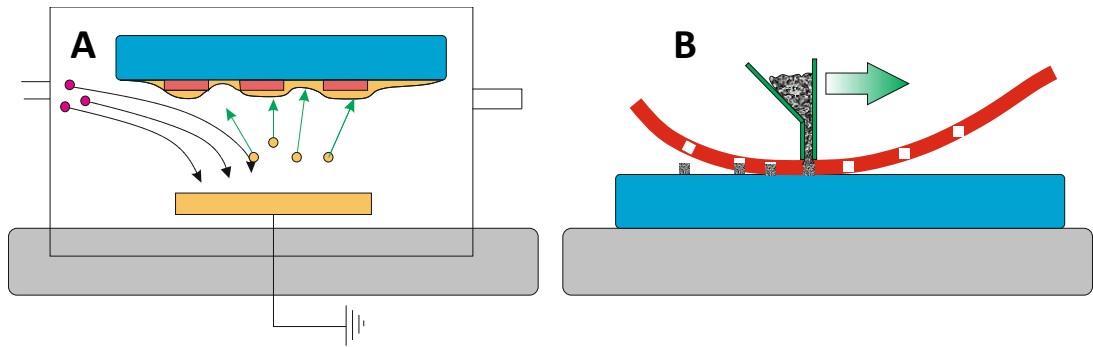


Figure 1-7: Comparing different electrode production techniques. Sputter coating of a resist for electrode manufacture (A) in which charged gas atoms (magenta) accelerate towards the metal target (yellow) this causes a displacement of metal particles which travel through the vacuum chamber (green arrows) and pass through a mask (red) where they condense upon the substrate (blue). In Screen-Printing (B) of electrodes, a slurry or liquid conducting ink is held in a reservoir (green) which is passed over a flexible mask (red) the ink is then deposited on the substrate (blue) either approach can be achieved for the patterning of a printed electrode material on an inert substrate.

Screen printing of electrodes often uses carbon inks as carbon is a good semiconductor which is cheap and can readily be made in a suspension form to enable screen printing. Though basic graphite slurry can be made which is then cured, most screen printed sensors use polymer binding agents or particles. These can have preferential conduction mechanisms such as with conducting polymer particles like polyaniline (Caygill et al., 2012). Gold particles may also be held in a suspension and printed in a similar way before heating to remove organic solvents (van Noort & Mandenius, 2000). This results in electrodes with superior conduction and the gold surface may be used for conjugation pathways (e.g. the Gold thiol interaction) which may be an advantage when fabricating biosensors.

One approach which has been tried to rectify the issue of surface irregularity when using screen printed electrodes is to fill in the surface with a conducting polymer, for example by electropolymerisation (Caygill et al., 2010; Gerard et al., 2002; Vakurov et al., 2009). This is advantageous as it can not only fill in voids, helping to make a more regular surface, but also it can incorporate tethering moieties to permit conjugation of the bioreceptor

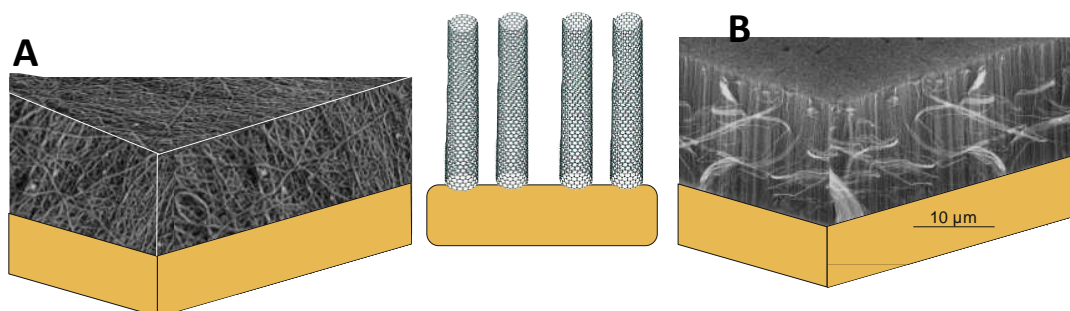


Figure 1-8: Deposition of nanotubes on a gold transducer surface. Though Ideally CNTs grow axially from the surface (centre) a forest formation as in (B), they often form a random tangle on the surface(A), Images adapted from (Delong America, n.d.; Ewels, n.d.; Williamson, n.d.).

Other improvements have been achieved by coating the surface of the electrode in nanotubes (Barsan et al., 2015; Boujtita, 2014; Yang et al., 2015). Applying nanotubes to a biosensor surface may aid in obtaining very high analyte specific responses as their highly conducting nature means that any signal generated can be easily relayed. However, creating an oriented array of nanotubes as in Figure 1-8 (B) may still be expensive and technically difficult (Zhu et al., 2013). Work involving an uncharacterised “tangle” of carbon nanotubes, as in Figure 1-8 (A), has still proven to be beneficial in a wide number of applications. In particular amperometric and enzyme based assays have benefitted from this approach (Boero et al., 2011; Manso et al., 2008; Wan et al., 2011).

1.3.2 Tethering layer

The bioreceptor component is commonly tethered to the transducer surface using an intermediary layer. This is done to prevent direct contact between the bioreceptor and the electrode surface. Early sensors worked on the primitive method of direct protein adsorption, in which the metal surface would bind the protein in a thermodynamic process driven by the interaction of the high surface energies with charge groups on the receptor. Often this would lead to the unfolding of the receptor protein and a consequent inhibition of its catalytic activity or binding capacity (Rushworth, Goode, et al., 2014; Millner et al., 2009).

It is for this reason that the use of a tethering layer has been widely adopted in biosensor construction and is a common theme across the field. This can be achieved in a number of ways (Abbas et al., 2011; Göpel & Heiduschka, 1995; Millner et al., 2009).

1.3.2.1 SAM based biosensors

Self-assembled monolayers (SAMs) are well-defined “liquid-crystal” films which allow immobilisation of biomolecules (Bain et al., 1989). These structurally defined layers form spontaneously when given time to assemble to provide well-ordered arrays of molecules as illustrated in Figure 1-9. There are many strategies that can be exploited to form SAMs for the fabrication of successful biosensors such as the interaction of silanes with hydroxyl groups (Bhatia et al., 1989; Song et al., 2007) or thiol–gold interaction (Ghindilis et al., 2009; Losic et al., 2001; Schuhmann et al., 2000).

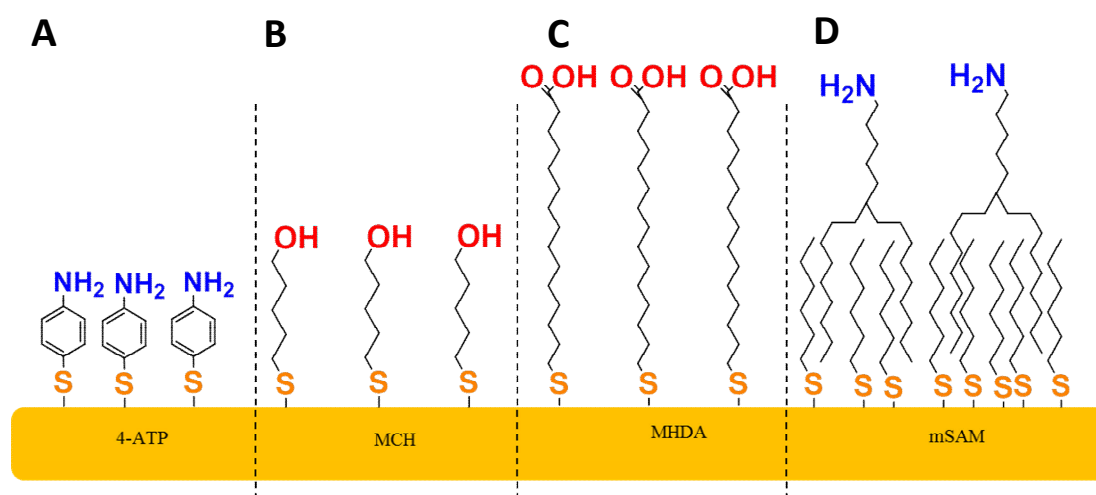


Figure 1-9: Comparison of typical alkane-thiol SAM's. From left to right monolayers of; (A) 4-aminothiophenol, (B) mercaptohexanol, (C) mercaptohexadecanoic acid and (D) a mixed SAM layer of mercaptohexane with a branched amino alkane. SAMs provide accessible functional groups for conjugation chemistry on the biosensor interface.

Typically, SAM formation has two kinetic steps. The first is binding of the SAM-forming agent to the surface e.g. alkane thiol to gold electrode. This stage typically occurs within minutes. It is followed by a slower phase (typically hours) in which the SAM reagents order themselves into a well-defined molecular array. This leads to maximising the Van der Waals interactions between adjacent alkyl chains which completes the SAM and makes it a much more stable tethering layer which may also be highly insulating.

Biosensors have also been constructed using mixed-SAMs (mSAMs) based on this thiol-gold interaction (Billah et al., 2010; Davis & Higson, 2005; Hays et al., 2006; Rodgers et al., 2010). One crucial aspect of the electrode which must be considered when constructing the mSAM is the surface. Continuous SAMs are only usually successful on a surface which is planar within the nanometre domain. Any roughness will interrupt the SAM, rendering the biosensor useless (Gerard et al., 2002).

SAMs are a dynamic system which behaves as a mobile film. This has consequences for analyte recognition as the relative sizes of the SAM and the analyte must be considered. The tethering forces of the sensor must also be considered as, when analysing small molecules, the force required to tether to the surface is relatively small compared to the forces holding the mSAM together. However, as the size of analyte increases, not only does the mass of the analyte but also the possibility that the analyte may have multiple binding sites. If this happens on a mobile SAM surface, binding may cause strain in the SAM and potentially in the development of nano- fissures which interrupt the mSAM and destroy the tethering layer as shown in Figure 1-10. (Arya et al., 2009; Billah et al., 2010; Caygill et al., 2012).

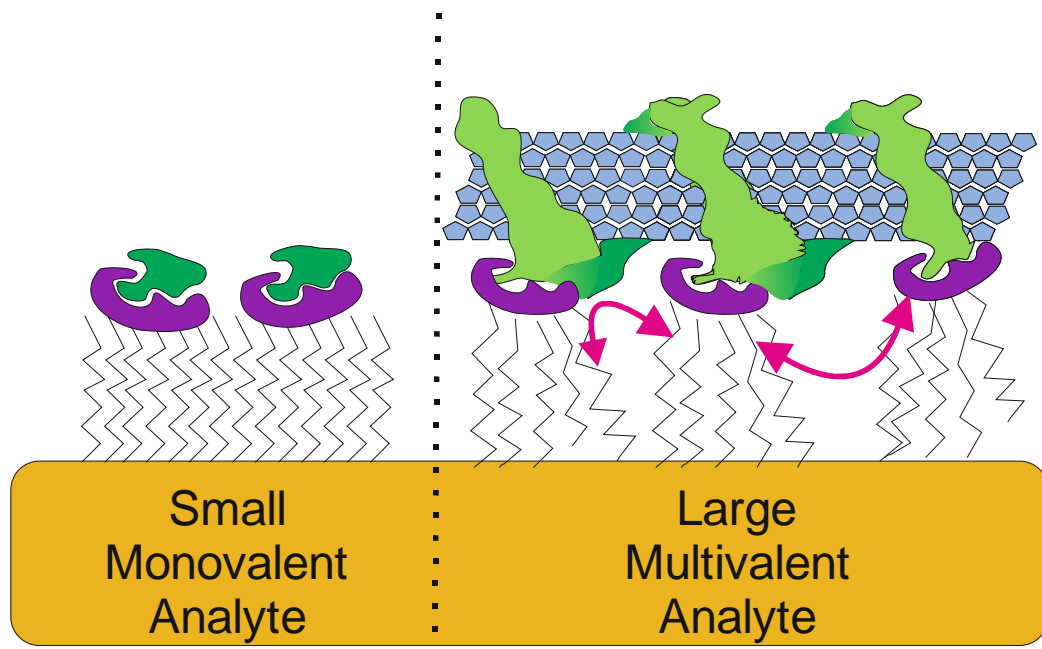


Figure 1-10: Disruption of mSAM by binding of a large analyte. For example a bacteria or virus where the paratope motif may be repeated many times or may attach something of a significantly larger size than the receptor. This can cause strain in the Tethering layer (magenta) and potentially a disruption in the SAM tethering layer.

1.3.2.2 Thiol - Gold Interaction

Although gold is often considered to be unreactive it can conveniently undergo a specific reaction, the oxidation of sulphur groups. If a thiol group is present, it will be oxidised to form a gold-sulphur bond which is dative, a form of covalent bond so is therefore particularly strong. This bond has an associated energy of $\sim 425 \text{ kJ} \cdot \text{Mol}^{-1}$ Making it very stable and useful for the construction of biosensors (Evans & Ulman, 1990). Whilst this reaction is not exclusive to gold (other transition metals may undergo the same reaction)

gold is particularly useful owing to its low reactivity with other chemicals and high electrical conductivity.

1.3.2.3 Polymer based biosensors

To overcome the problems of dealing with larger analytes, an alternative is to construct biosensors based on a conducting polymer matrix base layer (Ates, 2013; Barlett & Cooper, 1993; Gerard et al., 2002). This can be achieved by selectively electro-polymerising monomers onto the working electrode, typically using cyclic voltammetry (Hwang et al., 2001). When choosing the polymer, its electrical properties must be considered as well as its chemical features. A particularly good conducting polymer which is well characterised is polyaniline (Hwang et al., 2001; Lacroix et al., 2000). Many of its derivatives have also been polymerised (Kennedy et al., 2007). The analogue 2-aminobenzylamine (2-ABA) has been found to be particularly useful for the construction of biosensors when co-polymerised with aniline (Raffa et al., 2006) as it provides pendant amine groups to enable tethering of the bioreceptor. In using a polymer it is also possible to coat fairly rough surfaces evenly, reducing surface roughness as well as providing a solid structure. A wide variety of polymers have been used in the development of biosensors as shown in Table 1-1.

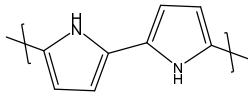
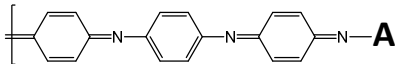
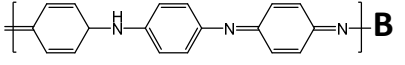
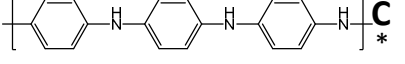
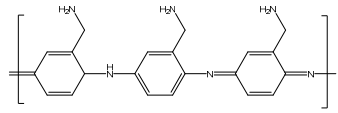
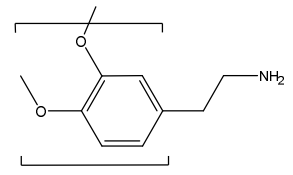
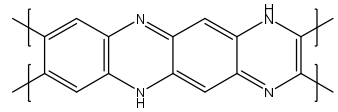
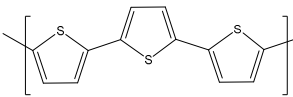
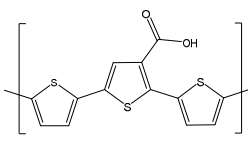
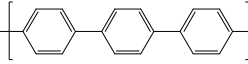
Polymer Used	Structure	Sensor type(s)	References
Polypyrrole		Amperometric Potentiometric Capacitive	(Lawal & Adeloju, 2013; Ramanavicius et al., 1999; Reiter et al., 2001; Schuhmann et al., 2000; Warriner et al., 1997)
Polyaniline	  	Amperometric Potentiometric	(Chawla et al., 2011; Jin et al., 2001; Sergeyeva et al., 1996; Trojanowicz & Krawczyński vel Krawczyk, 1995)
Poly-2-aminobenzylamine		Impedimetric	(Caygill et al., 2012)
Polytyramine		Impedimetric Capacitive Amperometric	(Labib et al., 2010; Pournaras et al., 2008; Tsuji et al., 1990)
Polyphenylenediamine		Potentiometric Amperometric	(Chirizzi & Malitesta, 2011; Windmiller et al., 2011; Zain et al., 2010)
Polythiophene		Piezoelectric Amperometric	(Giannetto et al., 2006; Nien et al., 2009)
Poly tert-thiophene-3'-carboxylic acid		Amperometric	(Darain et al., 2003)
Polyphenylene		Amperometric	(Gerard et al., 2002)

Table 1-1: Polymers used as biosensor tethering layers. * Polyaniline is shown as three structures as it has a different electronic configurations, the fully reduced form pernigraniline (A), the half oxidised, half reduced form emeraldine(B) and the fully oxidised form leucoemeraldine (C)

1.4 Bioreceptor conjugation

Once the transducer has been chosen and an appropriate tethering layer has been deposited the bioreceptor may then be attached to the surface. The tethering of the receptor is a crucial step as the bond must be robust, long lasting and resistant to the interrogation method as well as any further processing steps in the manufacture of the biosensor. There are a number of strategies which have been employed to ensure that the bioreceptor is fully integrated with the biosensor assembly.

1.4.1.1 Matrix entrapment

To provide both a spatial and energetic barrier between the electrode surface and the receptor, some early work focused on matrix entrapment. In this method a large polymeric matrix was deposited in conjunction with the bioreceptor to enable attachment. One particular example was the use of separate matrices of opposing charge which led to the electrostatic entrapment of the biorecognition component (Cosnier, 2005) as outlined in Figure 1-11.



Figure 1-11: Electrostatic entrapment of bioreceptor. Either using a bilayer (A) or multi-layer approach (B) the receptor can be held between polymer layers of opposing charge in both approaches polymers of opposing charge, commonly a positive polymer (blue) such as polydiallyldimethyl ammonium chloride (PDADM) is used which attaches to the negative electrode, an opposing negatively charged polymer (red) such as polystyrene sulphonate (PSS) can then be used to entrap the bioreceptor between layers. This can be repeated to gradually fabricate a multi-layer tethering component.

Multipoint electrostatic entrapment is a similar approach whereby polymeric layers of opposing charge can be bonded to multipoint charges within the bioreceptor itself. This is a particularly effective way of localising the receptor at the interface very gently. Bonding is achieved by soaking the electrode in a polycationic polymer such as polyethylenimine (PEI), polydiphenyldiazomethane (PDDM) or polydiallyldimethyl ammonium chloride (PDADM) along with the bioreceptor (Millner et al., 2009; Vakurov et al., 2009). The polymer forms many salt bridges with the receptor and attaches it to the electrode surface. By then soaking in a polyanionic polymer such as polystyrene sulphonate (PSS) the surface can be epitaxially grown and a stable sensor surface can be fabricated complete with embedded bioreceptors.

1.4.1.2 Carboxyl to amine coupling

Some of the most commonly used chemical moieties for conjugation employ the COOH and NH₂ groups. These are either at unmodified N and C termini or, more commonly, as external residue side chains (Asp, Glu providing COOH, and Lys providing NH₂ moieties). Therefore, they are a readily available route for the conjugation of receptor to the transducer surface.

The carboxyl group is often functionalised using 1-ethyl-3-(3-dimethyl aminopropyl) carbodiimide (EDC) as shown in Figure 1-12. This compound readily activates any COOH groups, making them more reactive and thus encouraging conjugation of the NHS Ester. This creates an acyl-isourea intermediate which is then susceptible to nucleophilic attachment from the lone pair of electrons located on the amine functional group. This causes the formation of an amide bond and an iso-urea by-product which is a chemically stable good leaving group (Hermanson, 2008).

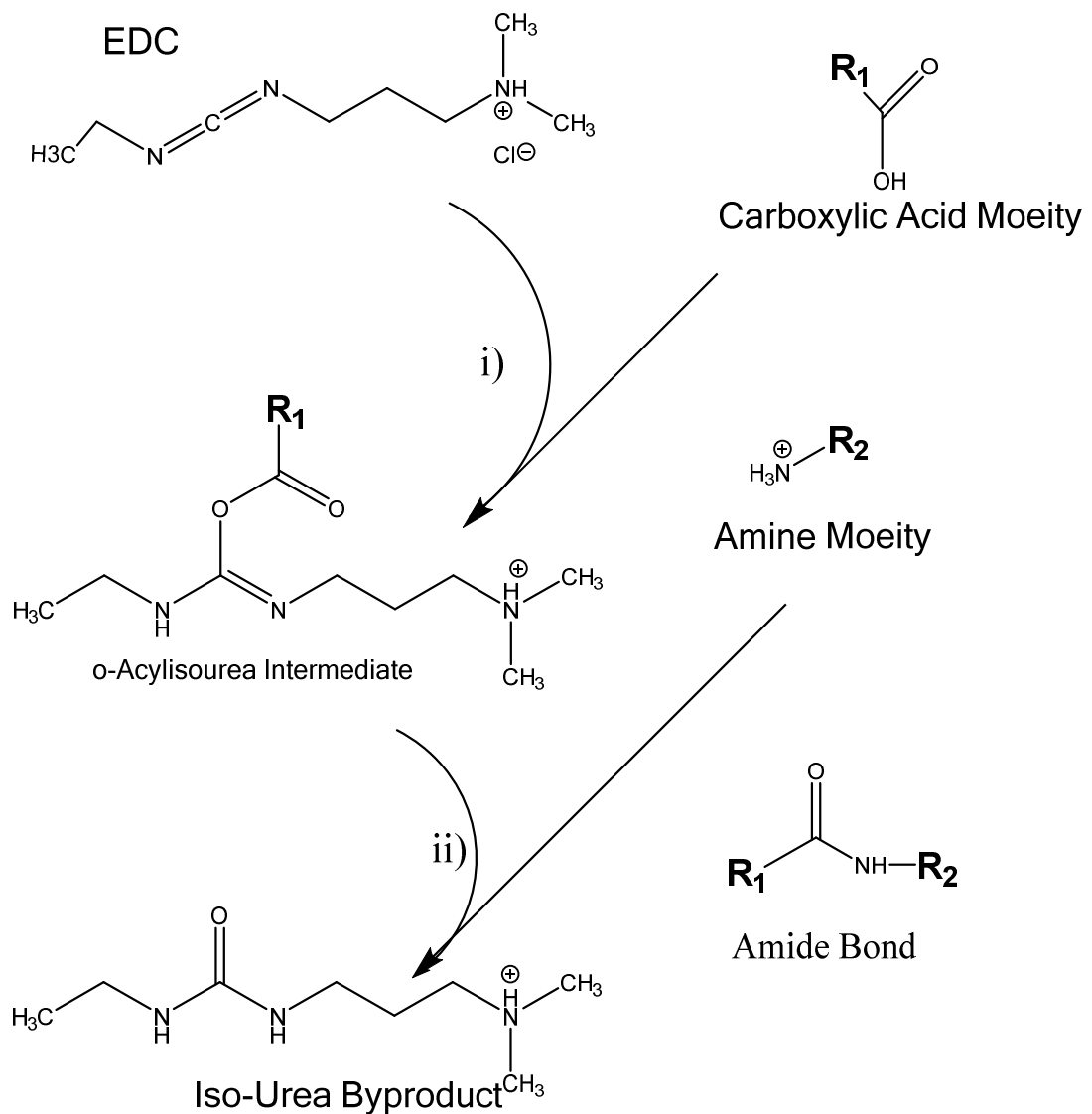


Figure 1-12: Conjugation of carboxyl group to amine group using EDC. The activation of the COOH moiety by EDC (i) is followed by the nucleophilic attack from the amine functional group (ii) resulting in a stable amide bond and the iso-urea leaving group. Scheme adapted from (Hermanson, 2008)

This provides an easy method for the conjugation of a carboxyl to an amine group, forming an amide bond which is chemically very stable. Though this method is commonly used it does have limitations including the fact that the optimum pH for the reaction is ~pH 4.5 which is potentially damaging the receptor protein. If the protein of interest includes many amine groups, which due to their hydrophilicity are often located on the protein surface, conjugation can occur at any of these sites. This makes it difficult to control orientation using this conjugation pathway.

1.4.1.3 Thiol coupling chemistry and heterobifunctional linking agents

Another functional group which is commonly exploited in conjugation chemistry is the thiol group. This group is particularly useful as it allows cysteine residues in a protein structure to be targeted. As cysteine residues tend to be relatively rare, even in native proteins the number of sites available to undergo this conjugation pathway is restricted and this may help to limit the orientation possibilities of a conjugated protein on the biosensor surface.

One way of further enhancing the receptor orientation is to engineer the protein and introduce a cysteine residue at a defined position, such as at the end of a peptide spacer. This enables the spatially controlled conjugation of the bioreceptor and ensures that all receptors are attached in a coherent manner. The orthogonal chemistry involved in amine to thiol chemistry is often mediated using heterobifunctional cross-linkers which allow specific oriented tethering.

One of the most widely used linkers, is sulfo-SMCC (Figure 1-13) which is an amine to thiol linker and is usually used in a two stage coupling process. First, the cross linker is incubated with the amine containing partner (in the case of this thesis, the polymer surface). This results in nucleophilic attack which causes the N-Hydroxysuccinimide group to leave and covalent linking between the amine containing surface and the crosslinker which is left with a labile –SH reactive maleimide group. When the bioreceptor thiol group is later introduced, the maleimide undergoes nucleophilic addition and a covalent carbon – sulphur bond is formed.

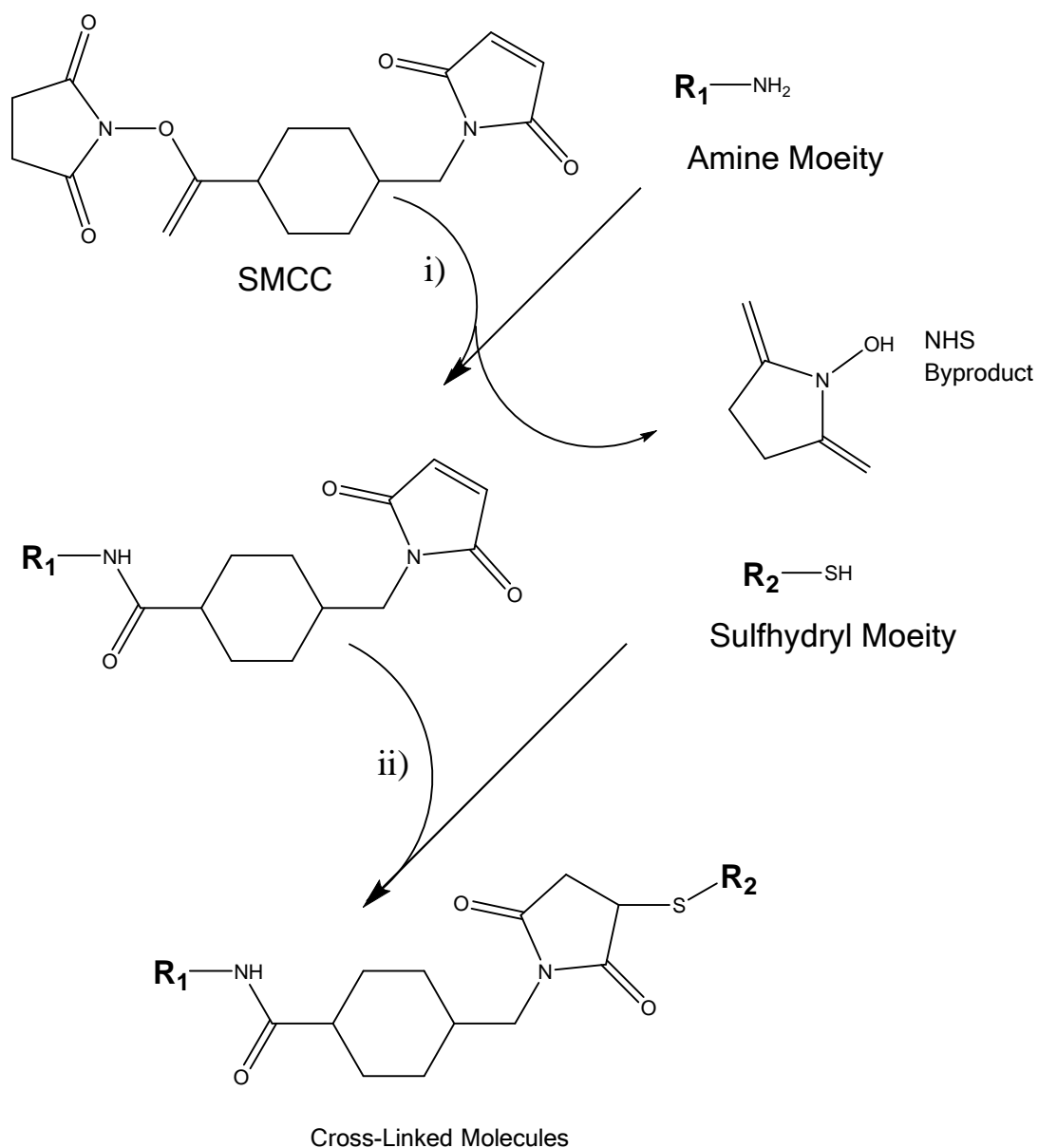


Figure 1-13: Conjugation of Thiol group to Amine group using SMCC. The primary amine is attached to the SMCC via nucleophilic attack resulting in the loss of an NHS leaving group (i). The amine is then covalently attached to a maleimide moiety which is susceptible to nucleophilic addition by a thiol functional group (ii). This results in thio-ether linking of the amine and thiol groups with a spacer arm length ~ 8.3 Å. Scheme adapted from (Hermanson, 2008).

Amine to thiol coupling is particularly effective since it is easy to ensure amine groups are incorporated into the transducer surface and also because exposed surface thiol groups are fairly rare in a protein's structure. Cysteines are commonly located deep within a protein structure and play a critical role in the structure or function of the protein. Though the amine coupling step of this occurs most rapidly at a similar pH as in EDC: NHS coupling (pH 4.5) coupling of the maleimide to a thiol group is optimal at pH ≥ 7 which is beneficial

in minimising damage to the receptor protein. This is useful as the amine crosslinking reaction is commonly used to attach SMCC to the tethering layer so; the receptor is not exposed to the high pH buffer at all. The use of Sulfo-SMCC allows the specific and oriented tethering of receptors to the biosensor interface. Using this principle many sensors have been constructed (Billah et al., 2010; Caygill et al., 2012; Makaraviciute & Ramanaviciene, 2013; Spitznagel & Clark, 1993; Tajima et al., 2011).

Sometimes it may be preferable to couple the thiol group to a carboxylated surface, for example when amine surfaces are unavailable or when the use of an intermediary such as di-glycine would add undesired steps to a conjugation reaction. One easy way of doing this is to use the crosslinker 3-(2-pyridyldithio) propionyl hydrazide (PDPH).

PDPH has a primary amine group which can be coupled to the carboxylated surface using EDC-NHS coupling as in Figure 1-12. As the PDPH is then covalently bound via an amide bond to the surface, it can undergo further reactions. The pyridyl disulphide group may then react with a thiol containing group in a step which may require cleavage with DTT. This is a nucleophilic substitution which results in a pyridyl-2-thione leaving group and the formation of a disulphide bond between the crosslinker and the target molecule.

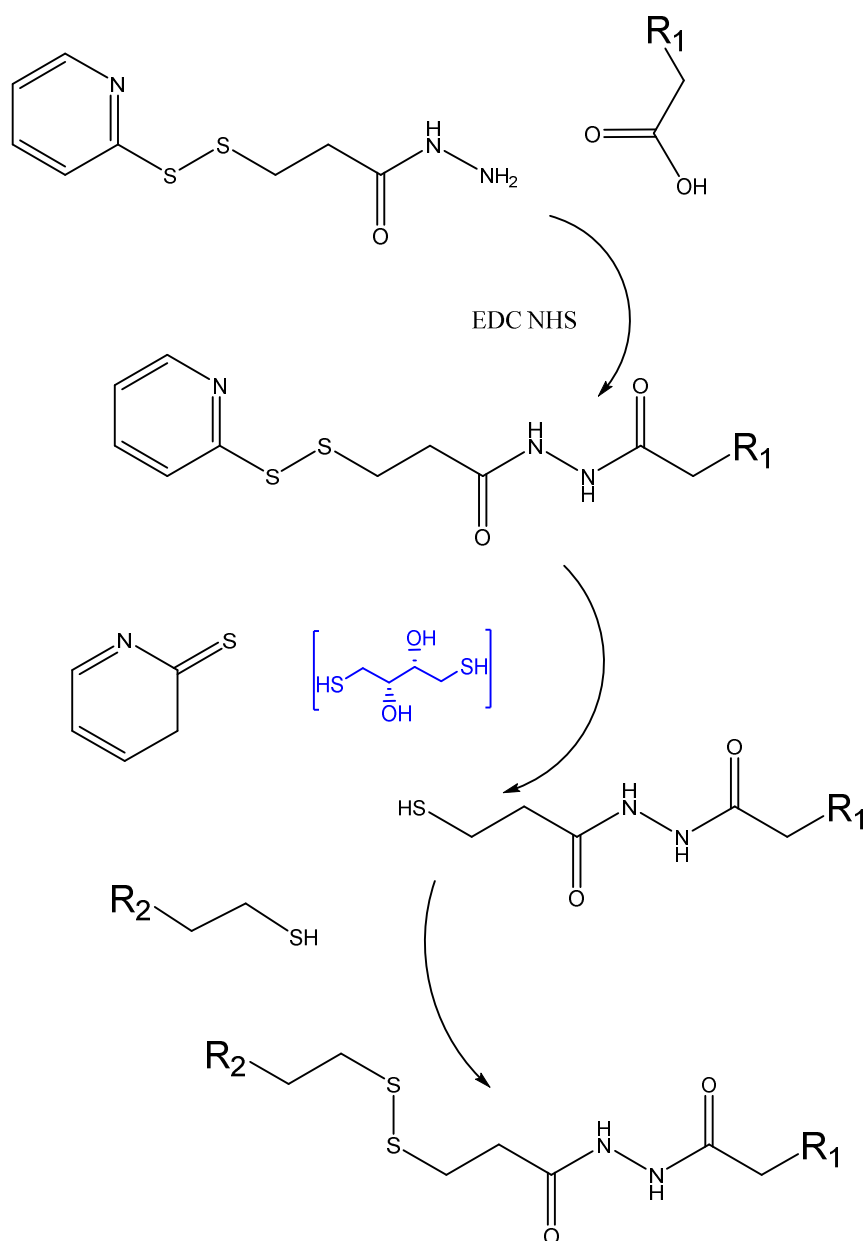


Figure 1-14: The conjugation of a carboxyl moiety to a thiol group using PDPH. In two stages the PDPH is first joined using routine EDC/NHS chemistry before reaction with the thiol group. DTT (blue), may be used to cleave the pyridyl-2-thione leaving group, the thiol group is then introduced by nucleophilic substitution and a covalent bond is shown in blue the spacer arm is ~ 9.2 Å. Adapted from (Hermanson, 2008)

As well as using conjugation routes which have been developed within the organic chemistry field, a number of interactions between proteins and other molecules can be used for constructing biosensors.

1.4.1.1 Biotin - avidin interaction

A commonly exploited high affinity interaction is the biotin-avidin interaction. Biotin vitamin H can be easily tagged onto a biomolecule using previously mentioned pathways. Commonly employed reagents include, biotin-NHS and biotin–maleimide for attachment to NH_2 and SH groups respectively. Avidin is a glycoprotein which is found in eggs; it has a hetro-tetrameric structure where each monomer binds a single molecule of biotin. Overall, the binding sites are arranged as two pairs separated on either side of the avidin complex, as in Figure 1-15. Biotin and avidin bind with an affinity of $K_d = 1.3 \times 10^{-15} \text{ M}^{-1}$, which is approaching the strength of a covalent bond (Hermanson, 2008). Due to the relative orientation of the binding sites, when binding at one of the sites occur it often occludes the other in the pair and it can therefore act as a biomolecular cross-linker.

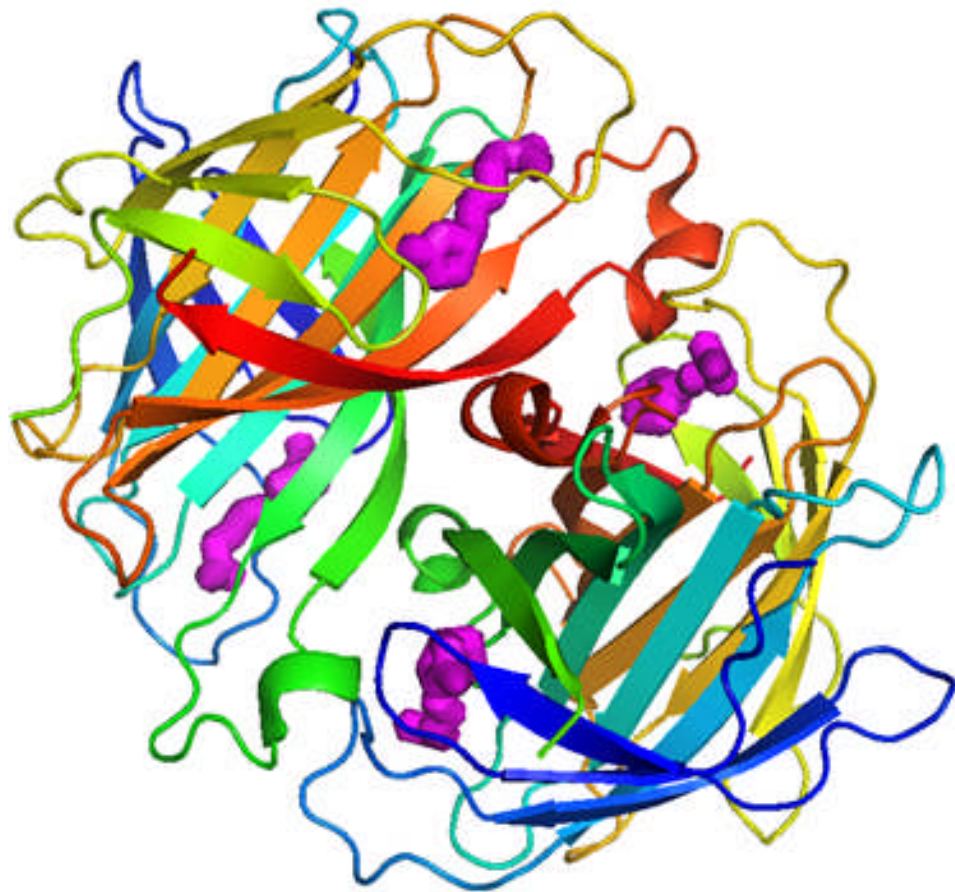


Figure 1-15: The structure of avidin homo tetramer, with 4 molecules of bound biotin (magenta) in two pairs of distally separated sites. Image created using PDB: 2AVI. From RSC PDB (<http://www.rcsb.org/pdb/home/home.do>)

In order to exploit this interaction, a biotin moiety must be tagged onto both antibody and substrate. The biotin group may be introduced by the reaction of an amine group with commercially available reagents such as biotin-N-Hydroxysuccinimide (NHS). As in Figure 1-12, the NHS –carboxy ester is attacked by the amine group on either the antibody or polymer substrate. It is important to note that this is an undirected reaction so any exposed primary amine groups will undergo this chemistry. When biotinylating a protein using biotin-NHS, the location of biotinyl groups will therefore depend on the amino acid sequence of a protein. This leads to uncertainty concerning the orientation of bound proteins on the sensor surface. As mentioned, biotin maleimide can alternatively be used to target the biotin modification towards cysteine sites in an engineered or reduced protein.

1.5 Bioreceptors

Integral to the biosensor is the receptor used. Once again there are a number of parameters which must be considered when choosing the receptor subsystem. Ideally, the receptor should be specific to the biomarker of interest and allow the generation of enough signal to develop a biosensor which is sensitive enough for the given application. Within this thesis a considerable effort has been dedicated to investigating different receptors and assessing ways in which they can be optimised in order to permit the fabrication of improved biosensors. This is an attractive approach as it may improve the quality of the sensor whilst circumventing the need to develop new fabrication techniques for electrodes which would be a more expensive approach to take. This approach also allows the use of tools such as chemical modification and re-engineering of proteins via molecular biology procedures which may again help achieve cheaper, more sensitive biosensors. Within the broad field of biosensor development there are a wide variety of receptors which have been used, the major types are outlined in brief below.

1.5.1 Oligonucleotides

DNA has been used as the bioreceptor in a wide range of electrochemical sensors for a range of analytes, including other oligonucleotides which exploit base pairing between complementary DNA. These sensors can be used to quickly and highly accurately probe for a given sequence and have even been shown able to detect single point mutations along a DNA sequence (Bonanni & del Valle, 2010; Levine et al., 2009; Liu et al., n.d.).

Nucleotide bioreceptors may also be evolved to bind proteins. These are known as RNA or DNA aptamers and exploit the vast range of possible DNA structures. These structures are exceedingly stable as they are self-encoded by the aptamer so may be denatured and reformed many times. The aptamers can be very rapidly evolved using systematic evolution of Ligands by exponential enrichment (SELEX) (Darmostuk et al., n.d.). Aptamers developed in this way have been successfully used for the fabrication of biosensors for a variety of protein analytes including enzymes and cell surface markers (Levine et al., 2009; Queirós et al., 2013; Withey et al., 2008).

As well as being raised to bind to proteins, DNA aptamers may be raised towards small molecule targets including drugs (Hilton et al., 2011; Yun et al., n.d.) and pesticides (Barthelmebs et al., 2011; Chen & Yang, 2015; March et al., 2009). They are advantageous

relative to antibodies which often fail to bind small analytes stringently. A classic example of this is an aptamer raised against theophylline which shows almost no cross reactivity to caffeine which is identical bar the removal of a methyl group (Jiang et al., 2015; Zhao & Yang, 2010). When using antibodies to distinguish between these two analytes, even the best monoclonal antibodies show a cross reactivity of around 15% (Mounié et al., 1990).

An additional benefit of using nucleotide based receptors is that they can be raised to bind toxic compounds. In this case, production of antibodies may not be possible as immunisation using toxins may result in death of the host or cytotoxicity in receptors expressed from. For this reason nucleotides are particularly useful as receptors as they can be screened and enable the creation of stringent binding receptors to otherwise toxic analytes (Castillo et al., 2015; Eissa et al., 2015; Luo et al., 2014). One critical disadvantage of nucleotide receptors is their reliance on charge - charge interactions, as their binding conformation is often held by polar bonds between nucleotides and also charge interactions. This may make their binding conformation very sensitive to change in the environment. This may mean that whilst they are good binders in principle which work well in simple systems such as testing in ground water or simple sample media, testing in more complex and often more relevant sampling matrices such as blood, plasma or urine may render the receptor useless. Limited work has been done to stabilise nucleotide receptors including the inclusion of artificial nucleotides or fluorescent nucleotide moieties which can shield the binding region of the aptamer in more complex chemical environments, this may make them more suitable (Seok Kim et al., n.d.).

1.5.2 Proteins

The other major category of bioreceptors is proteins. This broad category includes some of the most important biosensor systems which are widely used and have been extensively demonstrated.

1.5.2.1 Enzymes

Enzymes are commonly used in the measurement of metabolites and small analytes where an appropriate enzyme may be obtained (Wilson & Turner, 1992). The highly successful glucose biosensor uses glucose oxidase as its receptor (Newman & Turner, 2005; Wilson & Turner, 1992). Enzymes are mostly used in amperometric or potentiometric sensors. In the case of amperometric sensors interaction between the enzyme and the analyte causes a change in current, by either oxidation or reduction (Dzyadevych et al., 2008) which can be quantifiably measured and translated into a signal output. For potentiometric sensors,

the enzyme usually catalyses a reaction which consumes or produces an ion (e.g. NH_4^+) and affects the potential of the electrochemical cell as discussed in section 1.7.3.

Whilst these biosensors may be more easily produced than other types, they can only be achieved for analytes for which a suitable enzyme exists (Scognamiglio, 2013). This practically limits the use of enzymes as bioreceptors for metabolite and small molecule sensors including glucose (Cass et al., 1984; Reiter et al., 2001; Scognamiglio, 2013), ethanol (Manso et al., 2008; Ramanavicius et al., 1999), cholesterol (Vidal et al., 2004), lactate (Hirst et al., 2013; Palmisano et al., 2000) and similar metabolic analytes (Trojanowicz & Krawczyński vel Krawczyk, 1995).

1.5.2.2 Antibodies

Antibodies are the primary agent for the biorecognition of pathogens and toxins in the immune system and have been widely adopted in the development of immunologically based sensors. Antibodies' *in vivo* function is to bind a perceived pathogen which enables the immune system to respond and defend against illness and disease. A diverse binding repertoire is achieved due to gene shuffling in plasma B cells which produce new antibodies after initial infection exposure or immunisation. The binding of the antibody to a selected protein target or biomarker can be used as the interaction for signal generation in a biosensor. Within the structure of the IgG molecule, the Fc, constant region varies very little whereas the Fab region, which is where the binding occurs, has a very variable amino acid sequence. This results in an enormous range of structures and range of charge distributions which is vital for antigen binding. This variety allows the generation of antibodies to a wide range of targets and it is estimated that humans have a library of around 10^{10} distinct antibodies recognising distinct epitope regions (Fanning et al., 1996).

As antibodies are highly versatile and easily sourced they were adopted in the creation of the earliest affinity based biosensors (Bright et al., 1990; Taylor et al., 1991; Vadgama & Crump, 1992; Leech, 1994). Though antibodies are useful, they are not without their drawbacks. They can be unstable, require animal use and show batch to batch variance. Though this can be counteracted to some extent by using monoclonal antibodies which require only one immunisation before the establishment of hybridoma culture and allow for continual expression, the associated methods are very expensive and still rely initially on animals in order to harvest the spleen and isolate B cells for fusion.

1.5.2.3 Modified antibodies

Whilst many biosensors have been constructed using whole IgG as the bioreceptor, a number of studies have modified the antibodies prior to application to the transducer surface. This has enabled the modified antibodies to be deposited in a more oriented manner which has enhanced the function of the overall biosensor (Ahmed et al., 2013; Billah et al., 2010; Makaraviciute & Ramanaviciene, 2013; Spitznagel & Clark, 1993; Tajima et al., 2011).

The IgG molecule consists of 12 immunoglobulin (Ig) fold domains. This fold is a common motif which is largely conserved and found in many proteins. The 12 domains found in the IgG are comprised of 4 polypeptide chains (2 light and 2 heavy chains) which are all held together by disulphide bonds.

There are principally two ways of achieving the modification of whole antibodies, using either chemical cleavage or enzymatic digestion (Zourob, 2009), as summarised in Figure 1-16. Using the chemical approach, disulphide bonds can be selectively reduced using gentle reductants such as either TCEP (Billah et al., 2010) or MEA (Caygill et al., 2012) which break only the disulphide bonds linking Fc domains. Whilst it may be preferable to use the milder TCEP and prevent the complete fragmentation of the protein, some of the disulphide bonds may be partially shielded and thus require the slightly stronger MEA to be used.

When using enzyme based techniques, either pepsin or papain may be used (Harlow & Lane, 1999). In the case of pepsin, the antibody is digested just below the disulphide bonds which hold the two heavy chains together. This results in two Fab' fragments which remain bound. These fragments can then be subsequently cleaved using TCEP to generate Fab' fragments with a basal cysteine residue which is particularly useful for conjugation chemistry (Holford et al., 2012). One drawback of using pepsin, however, is that it is a proteolytic enzyme which has evolved to function in gastric, acidic conditions, and its optimum operational is at pH 3. Such a low pH is typically damaging to antibodies (Kindt et al., 2006). Accordingly there is therefore a trade-off between the extent of digestion and damage caused to the antibody by the acidic environment. The other enzyme which may be used for antibody digestion is papain which is extracted from papaya. Papain is a cysteine protease and when used with antibodies, it digests just above the disulphide bonds holding the two heavy chains together. This generates two individual Fab fragments. The optimal conditions for papain are much milder than those of pepsin,

meaning that antibodies tend to be less damaged during processing. The primary disadvantage of this method is that it leaves no labile cysteine residues for further conjugation as reduction would result in full fragmentation and reduced recognition activity (Gopinath et al., 2014).

The modification of antibodies has been demonstrated in the development of successful, biosensors (Makaraviciute & Ramanaviciene, 2013) including the use of half antibodies (Ahmed et al., 2013; Billah et al., 2010) as well as the use of antibody fragments, both Fab' (Brogan et al., 2003) and Fab (Bonroy et al., 2006) fragments has been demonstrated.

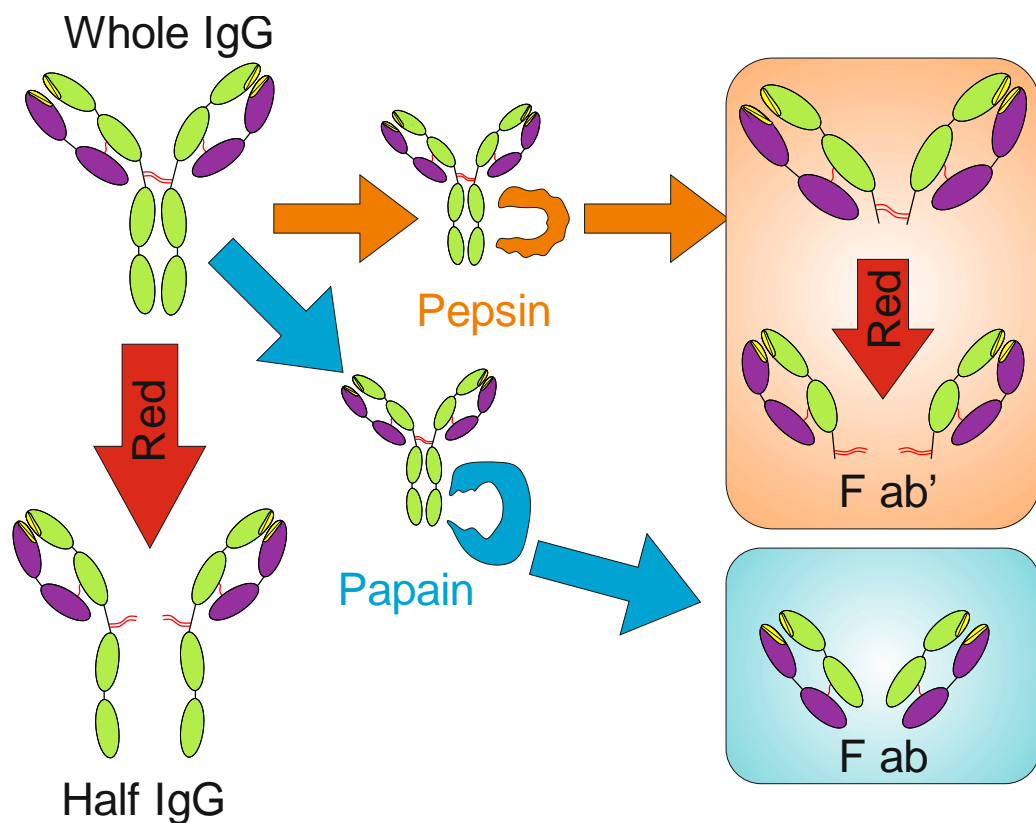


Figure 1-16: Modification of IgG for biosensor applications. The two enzyme based techniques of papain (blue) and pepsin (orange) digestion, generation of half antibodies as well as Fab' fragments is achieved using a reducing agent (red)

1.5.2.4 Antibody mimetics

In a move away from the reliance on animal sources many synthetic proteins have been developed as an alternative. Typically these proteins use a conserved protein scaffold with a separate evolved complementary determining region (CDR). They can often be quickly evolved and screened for binding capacity using standard panning techniques. In Table

1-2, a selection of the main antibody mimics is shown, alongside structural data. This table is far from exhaustive, as there are now over 50 scaffolds that have been demonstrated.

Synthetic binding proteins may be categorised according to their similarities with standard antibodies. Single-chain variable fragment proteins (ScFv's) were initially adopted as an alternative to antibodies. From monoclonal technologies, the two isolated binding domains from heavy and light chains of the antibody are isolated and fused using a small peptide. Once the DNA has been isolated, the proteins can be screened by phage display. Because they are a combination of two Ig domains, ScFv's have limited stability and can be more difficult to express than other antibody mimetics. Another antibody-like binding protein which originated from animal immunisation are nanobodies. These are produced by isolating the single chain antibody mRNA from an immunized camelid, details of which are discussed in more detail below. These two structures are based on the immunoglobulin fold which comprises 2 -four stranded β -sheets which align and present the CDR in the peptide loops between sheets.

Other types of antibody mimetics use protein motifs other than the Ig fold. Another similar protein scaffold has been used to create a β -sheet structure which displays a CDR. In the example of Adnectin[®], which is based on the combination of two four stranded β -sheets, presenting three CDR regions (Lipovsek, 2011). As well as β -sheet based antibody mimetic structures, some structures include α -helices as in the case of Adhirons (Tiede et al., 2014) a scaffold based on a plant phytocystatin which comprises a four stranded β -sheet and a single α -helix. Other antibody mimetics rely more heavily on the presence of alpha helices such as the Anticalin, based on the lipocalin structure which has two-four stranded beta sheets and four- α -helices (Richter et al., 2014; Skerra, 2008). There are also examples of synthetic binding proteins which rely entirely on the α -helix for structure such as the DARPin (Boersma & Plückthun, 2011; Stumpp et al., 2008).

In all of these structures the CDR is located in the non-structural portion of the peptide chain. Whilst in the more antibody-like structures it often forms a binding pocket for a target protein, in the case of DARPins, and structures based on α -helix repeats a binding surface may also be found which increases in size with the number of repeat helix groups.

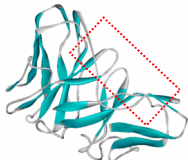
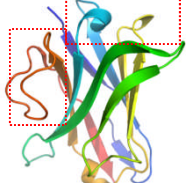
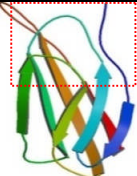
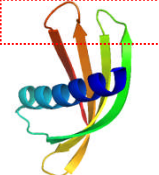
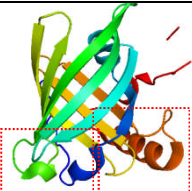
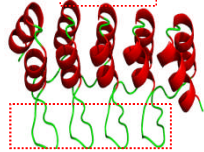
Name	Structure	Parent Protein	Category	Size	Randomisation	PDBid	Ref.
ScFv		Fused heavy and light chain from IgG	Isolated IgG binding domains	30 KDa	25-30 residues	4NKM	(Kalyoncu et al., 2014)
Nanobody		Camelid hclgG antibodies	Isolated Ig binding domain	12-13 KDa	3 CDR regions total 20 residues	1MEL	(Nicholls, 2007)
Adnectin		Human fibronectin	β -sheet structure	10 KDa	3 CDR regions total 20-25 residues	1TTG	(Lipovsek, 2011)
Adhiron		Plant phytocystatin	Mainly β -sheet with 1- α -helix	12-13 KDa	2 CDR regions, 9 residues each	4N6T	(Tiede et al., 2014)
Anticalin		Lipocalin	β -barrel structure with external α -helices	20 KDa	4 CDR regions up to a total of 24 residues	1LNM	(Gebauer et al., 2013)
DARPin		Ankyrin repeat proteins	Repeated α -helix	10-20 KDa	8 residues per repeat	4DUI	(Boersma & Plückthun, 2011; Stumpp et al., 2008)

Table 1-2: Antibody mimetic systems. This list is not exhaustive but shows the variety of protein scaffolds which have been developed. The structures are shown in order of resemblance to conventional IgG or its fragments. CDR position indicated by the red dashed box. PDB reference is to structural data accessed via RCSB Protein data Bank (<http://www.rcsb.org/pdb/home/>)

1.5.2.5 Camelid Nanobodies

Nanobodies are a particularly interesting antibody derivative which are isolated following animal immunisation. As a result of convergent evolution, the families of *Camillidae* (camels, llamas, alpacas, dromedaries etc.) and *Chondrichthyes*, which includes sharks and rays, have both evolved a class of antibodies in addition to the normal mammalian isotypes (Flajnik et al., 2011). These smaller, heavy chain only antibodies appear to have a wider operational temperature and greater molecular stability (De Genst et al., 2006; L. Huang et al., 2010; Vincke & Muyldermans, 2012). In recent years, the isolation of their binding domains has led to the development of nanobody based technologies by companies such as Ablynx (Desmyter et al., 2015; Kolkman & Law, 2010). Nanobodies are very stable small recognition proteins (≤ 13 -KDa) based on a single β -sheet with 3 CDR loops.

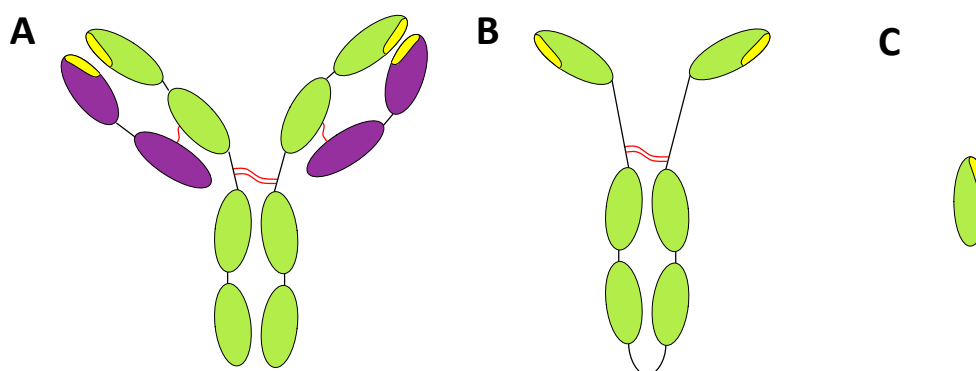


Figure 1-17: A comparison of the domains in IgG antibodies and camelid antibodies, IgG antibodies (A), 150KDa, camelid heavy chain only antibodies (B), 75Kda and the isolated nanobody (C), ~13Kda.

Nanobodies are typically produced by immunising alpacas. After initial immune response, blood is extracted and the lymphocytes are isolated. cDNA from these lymphocytes is then taken (Abbadly et al., 2011; De et al., 2009; Schotte et al., 2012) and a phage display library is constructed in which the displayed protein is the nanobody. This library can then be screened to identify strong binding candidates for nanobody expression. At this stage the binders can also be screened against known cross-reactants to ensure target specificity in a competitive assay. The DNA is then sequenced and subcloned into a stable plasmid (Honda et al., 2003). As this plasmid codes for a monoclonal binder, any batch -to- batch variance is removed and only one immunisation is necessary for a potentially endless source of nanobodies which are proving both cheaper and more reliable in the long term than traditional antibodies (Muyldermans et al., 2009). This approach also dramatically reduces the number of animals required for development of reagents, which is a key goal

of current life science research. Nanobodies are currently being developed for a wide array of immuno-based therapeutic reagents for oncology (Behdani et al., 2013; De Meyer et al., n.d.; Oliveira et al., 2013; De et al., 2009) as well as in the field of diagnostics (Fodey et al., 2011; Hassanzadeh-Ghassabeh et al., 2013; L. Huang et al., 2010)

1.5.2.6 Re-engineered Nanobodies

In this study, recombinant DNA techniques have been employed to generate nanobodies with spatially defined tethering groups as well as a variable length amino acid spacer.

In this thesis, a plasmid was designed to include a His₆-Tag for easy purification, as well as a peptide spacer arm of 5, 10 or 15 amino acids with a cysteine at the N-terminus. The inclusion of the cysteine residue was in order to allow for facile conjugation via its side chain thiol in an oriented manner. Along with orientation, this peptide spacer arm allows for variation of the distance of the bioreceptor from the transducer surface. If the bioreceptor is attached onto or very close to the biosensor interface then steric hindrance may limit analyte binding. By providing a physical spacer, we aimed to minimise the steric hindrance and promote optimum orientation to encourage specific binding of the analyte to the sensor surface. This is an effect which has been previously investigated (Lu et al., 1996; Mitchell, 2010; Piro et al., 2007) and it is hoped that the use of nanobodies will underline the importance of orientation of the bioreceptor. As a comparison to the novel nanobody based biosensors to detect rabbit IgG, data has been collected on traditional antibody systems. The variety of bioreceptors used in this report is shown in Figure 1-18.

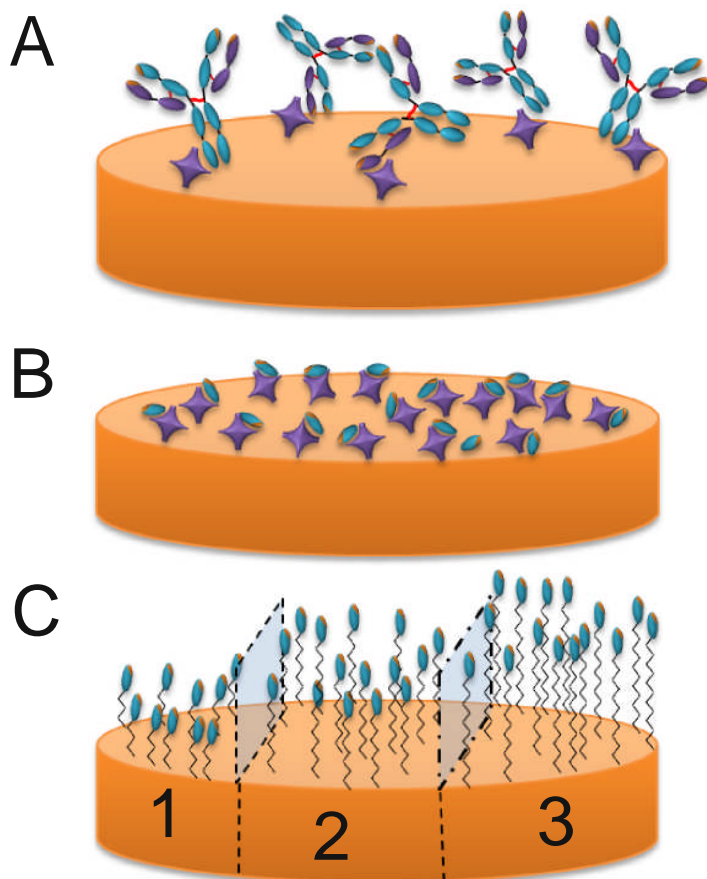


Figure 1-18: An Illustration of different bioreceptors used in impedimetric immunosensors throughout this thesis. (A) non-oriented antibody based biosensors, constructed using biotin avidin crosslinking (B) non-oriented nanobodies, again fabricated using biotin avidin cross-linking and (C) oriented nanobodies with engineered peptide spacer arm of 5, 10 and 15 amino acids, (1,2 and 3 respectively) conjugated using sulfo-SMCC crosslinker

Whilst work in this thesis focuses on the use of nanobodies the lessons learned can hopefully be applied in the application of other similar antibody mimetics. As biosensors are an emergent field there are currently a number of candidate proteins for biosensor development such as darpins (Kummer et al., 2013), Adhirons (Tiede et al., 2014) and affimers (Johnson et al., 2012) the benefits of these systems have been demonstrated mainly using optical biosensor systems (Miranda et al., 2011).

1.5.3 Validating receptors for use in biosensors

To ensure that the receptor to be used in the biosensor will be effective, a range of methods are used to assess crucial binding parameters including K_d , limit of detection and the selectivity to the target analytes by testing the receptor with suspected cross reactants. This can be done using a number of techniques including ELISA, radioisotope tagging and optical methods such as SPR and Biolayer interferometry. In this thesis, biolayer interferometry (BLI) has been used to validate the specificity of nanobodies and assess the effect of peptide spacer inclusion on key binding parameters. A schematic of the Fortebio system used is shown in Figure 1-4.

Though the binding data obtained from BLI experiments is typically expressed in nm, which represents the change in the thickness of the optical layer, it can be analysed using standard binding kinetic equations. In the case of antibodies, the binding model is conventionally considered to be high affinity; fast-on, slow-off, which ideally should be true for receptors in immunosensors where the analyte rapidly binds to the receptor and remains *in-situ* throughout interrogation of the sensor. Using this model, data can be interpreted using one site saturation binding and de-binding equations, shown in Figure 1-19, the principal equations of which are discussed more thoroughly below.

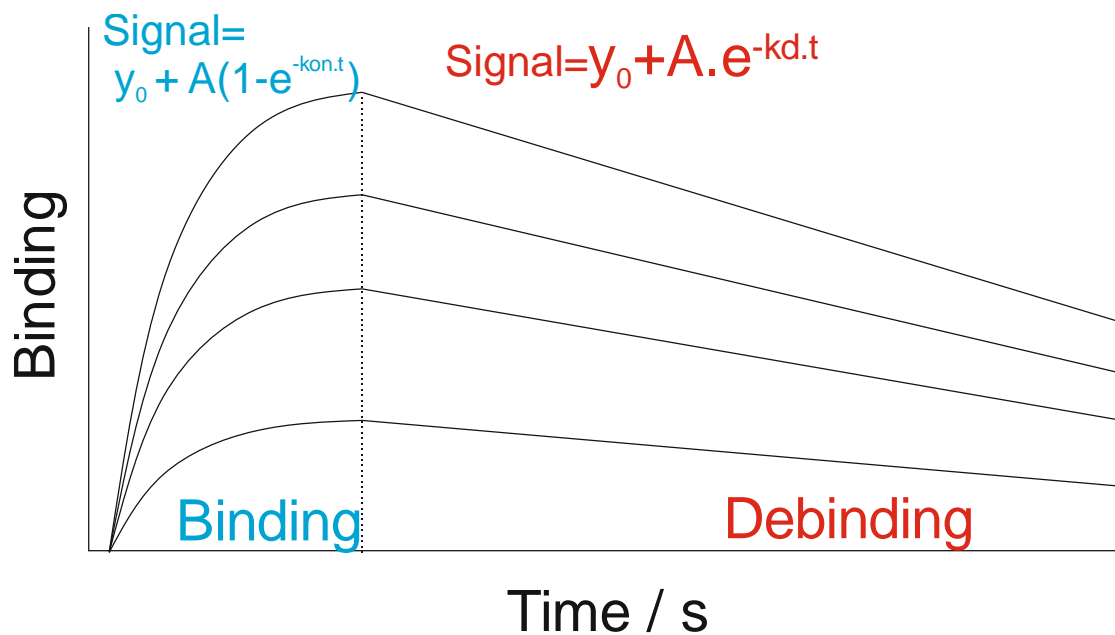


Figure 1-19: Binding data in a typical interferometry experiment. Both binding (blue) and debinding (red) portions of the experiment are displayed.

From these experiments, the measured signal can be used to fit the equations and calculate values for K_{on} and K_{off} . This is achieved by rearranging equations in Figure 1-19 to those below (

Equation 1-2 and Equation 1-3), inputting the measured data.

$$k_a = \frac{\partial [AB]}{\partial t} = \frac{k_{obs} - k_d}{[A]}$$

Equation 1-2: Calculating On rate from one site saturation curve

Where:

k_a = association rate constant ($M \cdot s^{-1}$)

$[AB]$ = concentration of analyte receptor complex (M)

t = time (s)

k_{obs} = Observed linear binding rate. (M)

k_d = dissociation constant. (s^{-1})

$[A]$ = Concentration of analyte (M)

$$k_d = \ln \left(\frac{Y - Y_0}{A} \right) \cdot t^{-1}$$

Equation 1-3: Calculating Off rate from one site binding

Where:

k_d = dissociation rate constant

t = time (s)

y = binding signal at time t (nm)

y_0 = Minimum binding signal achieved (nm)

These two equations can be then used to give the overall binding constant using the relationship:

$$K_D = \frac{K_d}{K_a}$$

Equation 1-4: Calculation of affinity from rate constants

This method has been used to assess the affinity of the nanobodies produced in this thesis and compare them to commercially available antibodies raised against the same targets. It merits noting that whilst antibodies commonly display affinities within the range of $10^{-6} \cdot M^{-1}$ down to $10^{-8} \cdot M^{-1}$ it is however possible to obtain antibodies which can have K_D down to $10^{-12} \cdot M^{-1}$. This may be achieved using techniques such as affinity maturation in which error-prone PCR is used in combination with phage display techniques to slowly refine a population of antibodies and identify the strongest binders (Harlow & Lane, 1999).

1.6 Biosensor regeneration

In theory, regeneration of biosensors enables repeated continual sampling of a given analyte. This is important as it may allow a several fold reduction in the cost associated with consumables, but also it may help to provide higher quality data as it removes sensor-to-sensor variance. The regeneration of the sensor is controlled by the forces which govern analyte binding and these can be categorised into the two competing thermodynamic qualities of enthalpy and entropy.

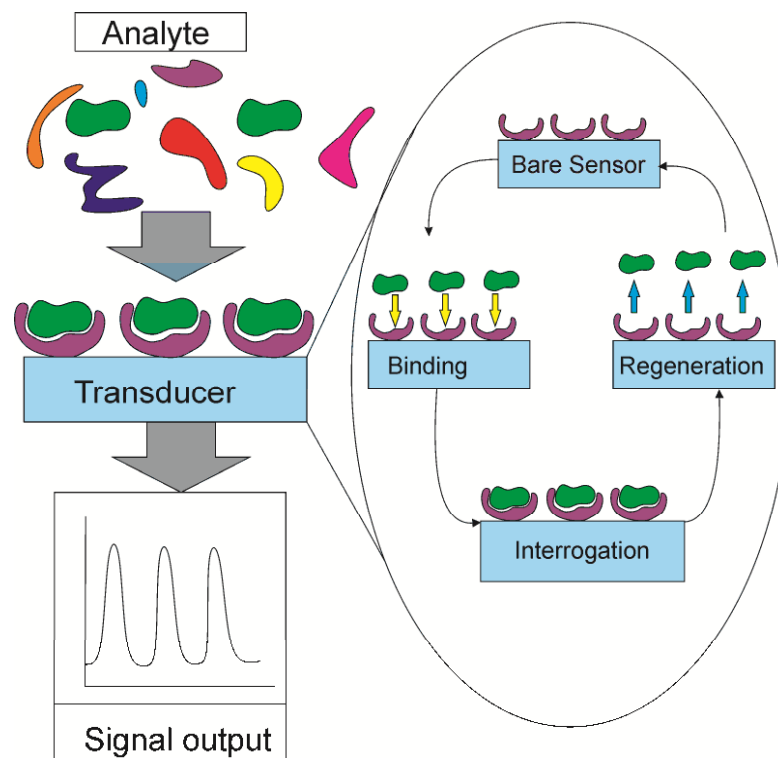


Figure 1-20: A schematic of biosensor regeneration. After exposure to a sample the analyte is bound before interrogation. An active regeneration step is then required in order to return the sensor to its basal state before the cycle can be repeated. (Goode et al., 2014)

1.6.1 Enthalpic interactions

Enthalpy is defined as the total energy of a thermodynamic system (Atkins, 1998). This energy can be distributed in a number of ways including heat (kinetic energy) and potential energy which can take on many forms such as ionic charge or chemical energy. According to the first law of thermodynamics, a system will equilibrate to reduce potential energy.

$$\Delta H = \Delta U - p\Delta V$$

Equation 1-5: Calculation of system enthalpy

Where:

H = Enthalpy (Kj.mol^{-1})

U = Internal Energy (Kj.mol^{-1})

p = pressure (pA)

V = Volume (m^3)

N.B: - in the case of receptor analyte binding pressure and volume will remain constant.

When considering interactions involved in biosensor operation, the differences in potential energy are a crucial force in bioreceptor to analyte binding, which are often mediated by charge-charge interactions. At any pH the various amino acids in solution may be either positively or negatively charged, depending on the iso-electric point (pI) of the amino acid residue. Under physiological conditions e.g. blood at around pH 7.4, there are acidic, negatively charged amino acids such as aspartate and glutamate, as well as corresponding basic or positively charged residues such as lysine, arginine and histidine (Voet, 1998). Interactions between charged side groups may be crucial in forming the tertiary structure of the paratope (Yokota et al., 2003) along with other forces such as hydrogen bonding and Van der Waals interactions (Schwarz et al., 1995). As the charge on each residue is dependent on the solvent environment, factors such as ionic strength, pH and the presence of competitor ions within the solvent can alter the relative strength of the charge interactions to effectively screen enthalpic interactions between the analyte and the bioreceptor which assists in biosensor regeneration (Tsumoto et al., 1996). In the case of antibody - antigen binding, these interactions are often optimised to minimise the potential energy. Typical changes in enthalpy upon antigen binding range from changes as small as -26 kJ.mol^{-1} down to more enthalpically driven interactions where the change may be -130 kJ.mol^{-1} in the most extreme examples (Schwarz et al., 1995). This is a considerable change in enthalpy when compared to typical values for covalent bonds which range from $200\text{-}400 \text{ kJ.mol}^{-1}$ (Atkins, 1998). It is crucial to note that at very low ionic strengths, the binding of an antibody can be promiscuous as any charge differential may mediate binding and lower the stringency of the receptor. Conversely, high ionic strength environments may screen the antigen - antibody interaction to reduce binding entirely (Reverberi & Reverberi, 2007).

1.6.2 Entropic Interactions

Entropy is defined as the inherent chaos or disorder of a system (Atkins, 1998). The second law of thermodynamics states that the entropy of a system will always increase, creating a more disordered system. This acts to lower the potential energy of the system overall, according to Gibb's Law which states that a process will be spontaneous if the Gibb's free energy is negative and where Gibb's free energy is the change in entropy minus the change in enthalpy (Atkins, 1998).

$$\Delta G = \Delta H - T\Delta S$$

Equation 1-6: Calculation of Gibb's free energy

Where:

G = Gibb's free energy (Kj.mol^{-1})

H = Enthalpy (Kj.mol^{-1})

T = Temperature (K)

S = Entropy (Kj.K^{-1})

Though analyte binding may be assumed to cause a decrease in the entropy of a system, there is also entropic compensation by processes such as solvent displacement. To explain this we must consider the role of solvent molecules in the system. In most systems, the unbound state is the high entropy system as the free analyte is highly disordered and although there is a decrease in entropy when the analyte binds, this is outweighed by the change in enthalpy which this contributes negatively, and overall there is a negative Gibb's energy change which explains why this is a spontaneous process. Though this case is the most frequent, there are certain systems in which the entropy is increased upon binding, particularly when dealing with hydrophobic analytes. This is due to the fact that hydrophobic analytes lead to ordered water caging at the solvent interface. Upon binding, these interactions are interrupted and the solvent molecules are then free in solution leading to a rise in entropy overall. Certain amino acids are known for their hydrophobic properties such as tryptophan, valine, leucine, methionine, phenylalanine, cysteine and isoleucine. In some systems, hydrophobic interactions are key to the antibody - antigen interaction and it has been identified that apolar surfaces are often buried at the binding interface and may have a large impact on the analyte binding and subsequent regeneration of a biosensor (Sundberg et al., 2000). At the protein level, biosensors have been developed for the detection of hydrophobic analytes such as fibrin, which have been subsequently regenerated (Choi & Chae, 2009).

In reversing these interactions, entropically driven binding must be reduced by negating the effects of hydrophobic regions; consequently aliphatic detergents are often used. In aqueous solution, this allows the interruption of water caging and minimisation of the hydrophobic effect (Cserháti & Szögyi, 1995) at the interface of the analyte and bioreceptor. A summary of typical approaches for regeneration is shown in Figure 1-21.

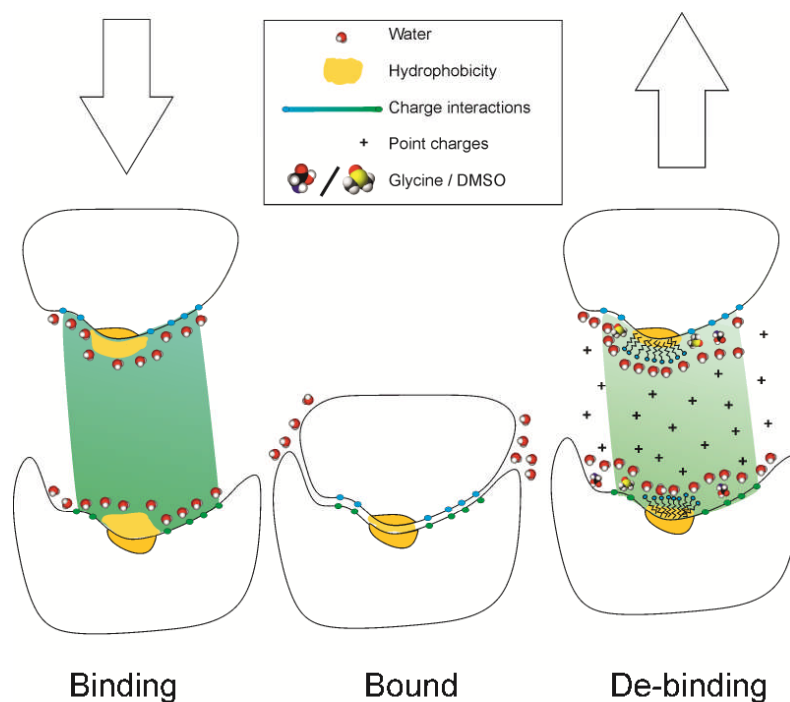


Figure 1-21: Forces governing analyte: receptor binding and regeneration. Electrostatic Interactions (green) along with Hydrophobic regions (yellow) (not to scale) The use of chaotropes, point charges and detergents is also shown (Goode et al., 2014)

1.6.3 Role of pH and electronic environment

As discussed, the solvent environment at a sensor interface is a key determinant for the binding of an analyte to the bioreceptor. It is for this reason that the most widely used approach for regenerating biosensors is to alter the solvent environment. This is easily done by placing the sensor in a regeneration buffer and typically requires common reagents therefore making it a low cost approach to sensor regeneration. Though a crude technique, deployment of regeneration buffers can be easily refined by the use of a fluidic system to bring more precise control of reagent delivery and exposure of the biosensor to regeneration buffer.

1.6.3.1 Acid/Basic Regeneration

In many reports, regeneration has been achieved by the application of high (Michalzik et al., 2005; Steegborn & Skládal, 1997) or low pH (Bright et al., 1990; Lazerges et al., 2006; March et al., 2009; Queirós et al., 2013) buffers to the system. Typically a low pH buffer such as glycine will go no lower than pH 2 in order to prevent irreversible damage to the bioreceptor. Conversely, a high pH buffer will often be employed with a pH around 11 for the same reason (Fortebio, 2007). This has a twofold effect on the system. First, a change in pH alters the enthalpic state of the system by changing the relative charge on the analyte and the bioreceptor. The structural denaturing induced by this effect aids decoupling of the analyte from the bioreceptor (Blanchard et al., 1990). It also contributes to the ionic strength of the environment which screens receptor - analyte interactions (Novotny & Sharp, 1992; Sahin et al., 2010). The ionic strength can also be altered by using strong electrolytes such as Ca^{2+} (Sahin et al., 2010) and NaCl (Radi et al., 2005). If a system is particularly sensitive to a change in pH, this may offer a preferable alternative to prevent irreversible denaturation of components of the sensor such as the bioreceptor or altering the electronic state of the transducer. Though the use of acidic and basic regeneration has been widely reported, one disadvantage is that it can only be used in systems where charge does not affect the baseline signal of the sensor itself.

1.6.3.2 Use of Detergents

Detergents are often used at low concentrations in the regeneration of biosensors (Albrecht et al., 2008; Fortebio, 2007; Mattos et al., 2012). Detergents are hetero-bifunctional molecules which comprise two distinct regions, a polar head which is highly soluble, and an aliphatic non-polar tail. The hydrophobic tails interact with similar regions of the bioreceptor or analyte in an entropically-driven process. The polar head group then extends into the aqueous phase and encourages solubility of the analyte (Giorgos J, 1979). In certain biosensor systems, hydrophobicity may be a key force in the interaction of the bioreceptor with the analyte such as in the detection of hydrophobic analytes including 2-naphthol and 3-isobutyl-2-methoxypyrazin (Cserhádi & Szögyi, 1995; Van Oss, 1995). Typically, mild detergents such as Tween are used for this (Anderson et al., 2007; Fortebio, 2007) although low concentrations of harsher detergents such as SDS have been used (Albrecht et al., 2008; Mattos et al., 2012; Oliveira et al., 2013). Whilst detergents are useful at low concentration and to avoid extremes in pH, they may interrupt systems such as SAMs and so should be used only in systems with a detergent resistant tethering layer.

1.6.4 Electrochemical regeneration

In a limited number of studies, biosensors have been regenerated using direct electrochemical methods. In these studies, reductive desorption of the analyte or receptor has been achieved *via* application of a negative potential to the sensor surface (Bhalla et al., 2010; Choi & Chae, 2009; Choi & Chae, 2009; Liron et al., 2002). Though there are only a few reports of this approach, it is an elegant solution for regeneration as it provides a highly localised environment which can be precisely controlled and requires no further reagents outside of the electrochemical components of the biosensor itself.

1.7 Electrochemistry

Electrochemistry is the study of phenomena caused by charge separation and the flow of charge carriers (Bard & Faulkner, 2001; Brett & Brett, 1998). It is the interface between electronic physics and chemistry. Within this thesis, electrochemical methods have been used to provide an insight into biophysics at the biosensor interface, following the accepted ideas that electrochemistry can be used to monitor changes at the electrode interface (Wang, 2006).

The charge carriers generated or accepted at the sensor are crucial to the generation of electrochemical signal at the interface. Within the electrical system, charge is carried by electrons; this charge is then transferred to chemical carriers at the electrode, in this case, ions in the solution. This generation of ions is mediated by the reduction or oxidation of an ionic species at the sensor interface. The charged ions then move under an applied field, transporting charge through the solution before relinquishing the energy at the opposing electrode. This establishes a flow of both negatively and positively charged ions, both to and away from the respective electrodes in the system.

Electrodes in an electrochemical system tend to be metallic or a conducting metalloid such as carbon (Niu et al., 2012) or a conducting polymer (Barsan et al., 2015; Gerard et al., 2002). It is therefore important to consider the processes that occur when using such electrodes before fabrication of the sensor is approached.

1.7.1 The three-electrode system

By using a three electrode system, the flow of charge between two different electrodes can be measured relative to a third reference electrode. First, there is the working electrode (WE) which is the electrode where any changes are to be monitored. It is often the anode and it is the point of reduction where ions gain an electron before travelling to the cathode. As the surface of this electrode is modified, this may make this process easier or more difficult, allowing a change in signal to be monitored.

The cathode in this system is known as the counter electrode, this electrode is often a large, unreactive, conducting metal electrode which readily oxidises ions causing them to surrender an electron and promoting current flow across the closed circuit,. Because it is

unreactive and large it generates minimal signal itself via reaction with any components in the solution and the charge can transfer easily around the circuit.

To monitor the flow of charge between the working and counter electrodes a reference electrode is also used. This is typically an Ag/AgCl cell in which a stable voltage is established (Scott & Lukehart, 2007). This ensures that any changes in bulk do not affect the signal between working and counter electrode as well as creating a base signal over which the signal from the working electrode can be effectively monitored. Other references such as calomel or mercury electrodes may be used but are not favoured due to instrumental complexity, potential toxicity and the difficulty of incorporating them into a three electrode composite chip as is the case for Ag/AgCl (see Appendix 1).

Since it is possible to monitor the changes in the ability of the working electrode surface to reduce ions and convert from electrical to chemical energy, electronic processes at the surface can be monitored. Changes on an electrode surface may dramatically affect the electrochemical properties of a system. Though this preceding text describes the basic process at the electrochemical interface there are a few key approaches for accurately interrogating the electrochemical process. These can be grouped into amperometry, voltammetry and impedance and will be considered in sections 1.7.2- 1.7.5.

1.7.1 Double layer theory

As the electrode in the electrolyte containing solution interacts with ions, it is important to consider the processes which occur at the interface. Commonly ions are reduced or oxidised at the electrode in a Faradaic process. In order for this to occur, the ions must travel across the solution. This process is mediated by the mass transfer of ions across the bulk electrolyte solution. As ions get closer to the electrode interface, they encounter a number of defined electrochemical regions which are modelled by Guoy-Chapman theory; a schematic of this is shown in Figure 1-22.

Guoy Chapman theory identifies a number of regions encountered by an ion travelling from a bulk solution to the electrode surface where the ion can be oxidised or reduced. The first region encountered is the diffusion layer, where the ion is driven across a concentration gradient. This is due to ion depletion or accumulation at the electrode surface. The ion then encounters a region known as the Debye layer, which is the point of maximum flux between ion concentrations for the respective processes and describes the net electrostatic effect of the ions travelling to or from the electrode.

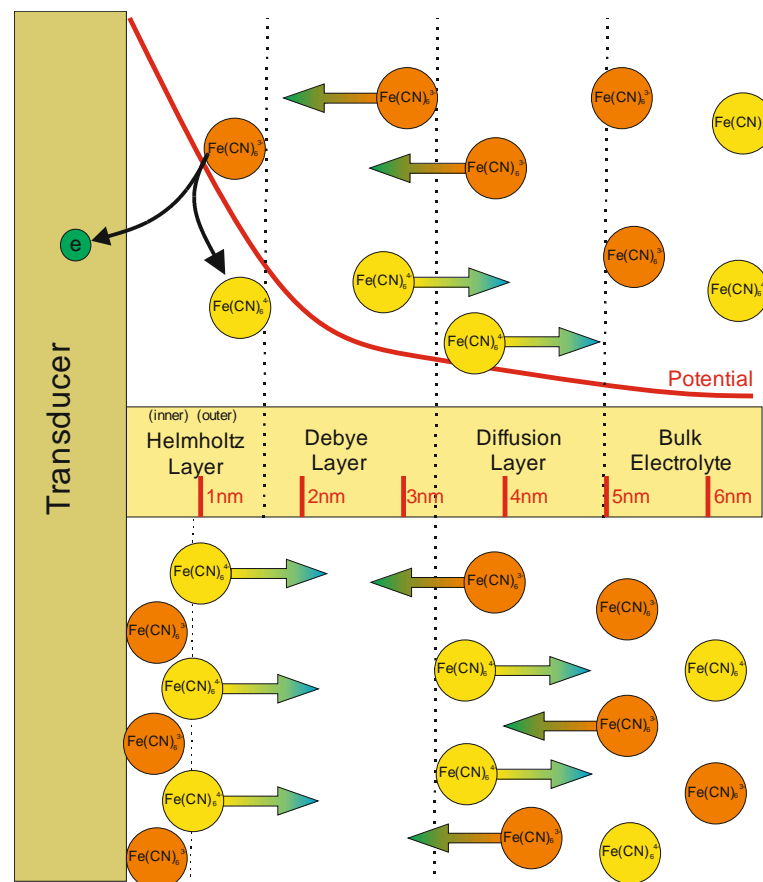


Figure 1-22: A schematic of Guoy-Chapman theory. Showing processes at the electrode interface in a DC system which contains electron mediator, in this case both $\text{Fe}(\text{CN})_6^{-3}$ and $\text{Fe}(\text{CN})_6^{-4}$ ions. Moving away from the transducer surface, the inner and outer Helmholtz layer are followed by the Debye layer in which a depletion of ions can be observed, this is followed by the diffusion layer before the concentration equilibrates and is the same as the bulk electrolyte. N.B. This is a simplified model and the inclusion of tethering layer and the surface roughness mean that there are commonly local variations in the layers observed in a real scenario.

The relative sizes of these two layers is dependent on several factors including temperature, viscosity, surface area, ionic strength and the combination of electrode and electrolyte used. The equations which govern the thickness of these two layers are the following:

$$\kappa^{-1} = \sqrt{\left[\frac{\epsilon_r \cdot \epsilon_0 \cdot RT}{F^2 \cdot \sum c_i \cdot z_i^2} \right]}$$

Equation 1-7: The Debye layer equation

Where:

- κ = Debye layer, normally 0-5 nm
- ϵ_r = Relative dielectric permittivity of the solution
- ϵ_0 = Permittivity of vacuum.
- R = Gas Constant
- T = Temperature
- F = Faraday constant
- c_i = Concentration of charged species 'i'
- z_i = Ionic charge of charged species 'i'

More intimately associated with the electrode interface is the Helmholtz layer which has an inner and outer layer. These two layers are broadly analogous to a plate capacitor where the inner Helmholtz plane is a thin layer of adsorbed reactant species whilst the outer plane is formed of product charge carriers. Their opposing charge causes an immediate spatial separation which leads to the bilayer capacitive properties.

1.7.2 Amperometry

Amperometric biosensors operate by monitoring a change in electron flow or current when the potential is static. These biosensors typically exploit an electroactive enzyme, such as oxidase or reductase which is coupled to the transducer surface. When the substrate is present, the enzyme catalyses the reaction, resulting in a change in electron flow (current) across the surface. This current is proportional to the concentration of the analyte and allows a direct calibration to be performed (Grieshaber et al., 2008; Sapelnikova et al., 2003). This relationship can be determined using Faraday's Law:

$$I = n.F.A.J$$

Equation 1-8: Faraday's Law

Where:

I = current, typically in the nA-mA range

n= number of Electrons transferred at the electrode

F= Faraday constant

A= Area of the electrode

J= Flux coefficient, the transfer of the substrate or analyte to the electrode surface

One drawback of this system is that it requires an enzyme which reduces or oxidises an electroactive analyte specifically, or an enzyme whose catalytic activity can be modulated by incubation with the analyte (Vakurov et al., 2005). This enzyme must be chemically stable to resist processing techniques deployed during the construction of the biosensor. A further problem arising from the use of oxidases is the resulting H₂O₂ generated. Reduction of the H₂O₂ can be achieved on the electrode, however, this occurs at a relatively high potential (+0.7 V) and leads to undesirable side reactions. A common approach is to use an electron mediator such as ferrocene or ferrocyanide as in the case of Prussian blue (Hirst et al., 2013; Pchelintsev et al., 2009; Ricci & Palleschi, 2005) which catalyses the reduction of H₂O₂ at 0 V.

In spite of these technical difficulties, the most widely known electrochemical biosensor, the glucose sensor, is amperometric and uses glucose oxidase (Newman & Turner, 2005; Reiter et al., 2001; Scognamiglio, 2013; Wilson & Turner, 1992). This allows glucose levels to be easily measured in diabetic patients and it currently account for ~85% market share in the biosensor industry (Newman & Turner, 2005). As well as the glucose sensor a number of other amperometric biosensors have been developed for similar molecules/ metabolites where a suitable enzyme is readily available. These include sensors for lactate (Hirst et al., 2013; Palmisano et al., 2000), cholesterol (Vidal et al., 2004) and ethanol (Manso et al., 2008).

1.7.3 Potentiometry

Potentiometric sensors operate by monitoring the voltage when no current is passed through the system. This technique may be used to measure specific ion concentration by using ion selective membranes; this is the theoretical basis for modern pH probes which operate using a H⁺ permeable membrane. The first potentiometric sensor measured the

change in potential resulting from a similar change in the concentration of protons (H⁺). The principle equation which determines operation for a potentiometric sensor is the Nernst equation:

$$E = E^0 - \left(\frac{2.302 RT}{n.F} \right) \cdot \log_{10} \frac{[Red]^b}{[Ox]^a}$$

Equation 1-9: The Nernst equation

Where:

R = Gas constant

n= number of electrons transferred at the electrode

F= Faraday constant

T= Temperature

It can be seen from this equation that as the ionic concentration of either reduced or oxidised species changes, so will the potential (E) of the system. Again these sensors rely on the availability of a robust enzyme, often a hydrolase which limits their applicability for many analytes. Voltammetric interrogation can also be carried out using potentiometry. In this case, the interrogation is passive as it is the generation of potential is measured. As an enzyme reaction occurs ions are produced, typically H⁺ or NH₄⁺ which establishes a measureable potential across the system and allows a signal to be calibrated (Tang et al., 2010), successful sensors have been constructed for analytes including cholesterol (Israr et al., 2010) and urea (Dhawan et al., 2009; Ramesh et al., 2015).

1.7.4 Voltammetry

Voltammetry is the investigation of monitoring current when an applied potential (V) is varied. Voltammetry can be additionally used in the construction of biosensor systems as it allows for the initiation of chemical reactions including reductive cleaning of electrodes or polymer deposition by electropolymerisation (Barlett & Cooper, 1993; Choi & Chae, 2009; Lacroix et al., 2000). Within the field of voltammetry, three commonly used techniques are potential step, linear sweep and cyclic voltammetry. In potential step voltammetry the applied potential (voltage) is suddenly switched between two predetermined points and the corresponding change in current is monitored. In linear sweep voltammetry, the potential is applied over a range which moves in one direction only and the current is measured over time as the potential is changed.

Cyclic voltammetry is the most commonly used technique, where the linear potential sweep is reversed when a set potential is reached and again, current is monitored over time. This application of increasing and decreasing potential can be cycled multiple times and generates meaningful data on the properties of both solution and electrode as well as any changes which occur at the interface. By sweeping the potential in both directions data can be generated on both reduction and oxidation (Fisher, 1996). The flow of current across the electrochemical cell is the signal that is measured. This is dependent on the mass transfer of charge carrying species to the electrode surface. For applications in this study, the redox change of $\text{Fe}(\text{CN})_6^{-3/4}$ was measured using cyclic voltammetry, which is described more fully in Chapter Three.

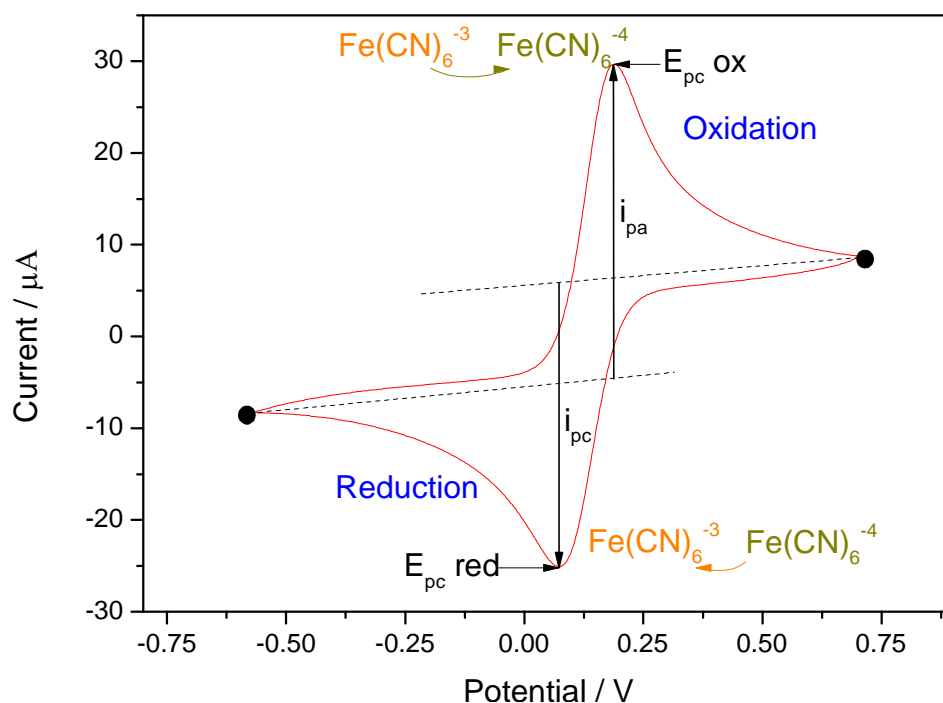


Figure 1-23: CV obtained in the ferri-ferrocyanide system. This sample data is labelled with the key information that can be given from a CV, where the potential has been cycled between the two points (●) at -0.6 V and +0.75 V. Both oxidation (upper) and reduction (lower) of electrolyte species is shown. Each process has a potential (E_{pc} Ox and E_{pc} Red, respectively) at which it occurs most readily and the peak current (i_{pa} and i_{pc} , respectively) is observed. The processes of reduction / oxidation are shown alongside and these are the reactions which occur at the peak cathodic (reduction) and peak anodic(oxidation) voltages.

When $\text{Fe}(\text{CN})_6^{-4}$ ions donate an electron, $\text{Fe}(\text{CN})_6^{-3}$ is generated at the sensor surface, the increased concentration around the electrode establishes a concentration gradient between $\text{Fe}(\text{CN})_6^{-3}$ ions at the interface and in the bulk. Thus diffusion occurs between the electrode and the bulk solution. This gradient will continue until generation of $\text{Fe}(\text{CN})_6^{-3}$ is reduced at the surface and eventually will reach a stage where the concentration of $\text{Fe}(\text{CN})_6^{-4}$ ions will be lower at the interface than at the bulk, so diffusion will occur in the opposite direction.

For both reduction and oxidation processes, there is an associated potential at which either process is favoured and the diffusion of the relevant carrier is at a maximum for the given system. At this potential, a corresponding peak current is observed. A peak is observed for the oxidation, (i_{pa}) as well as reduction (i_{pc}). As the reaction is reversible, the size of the peaks for both reduction and oxidation should be the same.

Cyclic voltammetry is the most popular method by which redox processes are studied as it allows a direct, quantitative correlation of the data and redox phenomena. For systems the ferri/ferrocyanide system used, the electron transfer is quick and current flow is limited only by the diffusion of the species to the electrode surface. We can therefore monitor the presence of any surface coatings which may slow current flow across the surface or have their own associated redox peaks.

The resulting concentration gradient as well as the mass transfer processes which occur during CV are described by Fick's Law, which states that the current is a quantitative measure of how rapidly a species is reduced or oxidised at the electrode: electrolyte interface. Using data obtained from voltammetric experiments, a vast wealth of data can be obtained regarding the surface and processes which occur at the electrode: electrolyte interface. As well as providing qualitative data, values can be used to calculate important parameters such as the effective surface area. As it is uncommon to find electrodes which are perfectly flat, their effective surface area may be much larger than their geometric surface area. The difference can be calculated using the Randles Sevcik, Equation 1-10.

$$i_p = 0.4463 n.F.A.C \sqrt{\frac{nFvD}{RT}}$$

Equation 1-10: The Randle's- Sevcik equation

Where:

i_p = current maximum in amps

n = number of electrons transferred in the redox event (usually 1)

A = electrode area in cm^2

F = Faraday constant in C.mol^{-1}

D = diffusion coefficient in $\text{cm}^2.\text{s}^{-1}$

C = concentration in mol.cm^{-3}

v = scan rate in V.s^{-1}

R = Gas constant in $\text{V.C.K}^{-1}.\text{mol}^{-1}$

T = temperature in K

This under standard conditions simplifies to:

$$i_p = 2.688 \times 10^5 3\sqrt{n}.A.\sqrt{D}.C\sqrt{v}$$

Equation 1-11: Simplified Randle's-Sevcik equation

And this equation can subsequently be rearranged to give:

$$A = \frac{2.688 \times 10^5 3\sqrt{n}.A.\sqrt{D}.C\sqrt{v}}{i_p}$$

Equation 1-12: Calculating area from Randle's Sevcik equation

Using Equation 1-11, typical values give a larger electrode area than by physically measuring the electrodes, for screen printed electrodes the actual surface area may be 5-10 times larger than the geometric surface area a phenomenon explained by surface porosity in addition to superficial roughness of the interface (Alonso-Lomillo et al., 2010; Niu et al., 2012; van Noort & Mandenius, 2000).

1.7.5 Impedance

Impedimetric biosensors directly exploit the binding of the analyte to the bioreceptor by observing the difference in conductivity across the electrode: electrolyte interface. Impedance is the ratio between changes in measured current when a changing voltage is applied. In electrochemical impedance spectroscopy (EIS), the current is measured when an oscillating AC voltage is applied. In the example of Immunosensors, analyte binding at the sensor interface results in addition of matter to the electrode surface; it is this that affects its resistive and capacitive properties. This is a more suitable approach for many analytes as it is often much easier to obtain binding proteins for a wide variety of analytes than an electroactive enzyme. For these reasons IgG has traditionally been used as their wide availability and well-defined binding kinetics and reasonable chemical stability make them particularly attractive for the development of biosensors (Barton et al., 2009; Billah et al., 2010; Conroy et al., 2009; Joseph, 2006; Kaláb & Skládál, 1997; Konstantinov et al., 2009; Millner et al., 2009). Impedimetric immunosensors have also been demonstrated using other types of binding proteins (Conroy et al., 2010; Rodgers et al., 2010) as well as oligonucleotides (Queirós et al., 2013; Yun et al., n.d.) and lectins (Hu et al., 2013).

When the electrode is interrogated in an impedimetric sensor, both capacitive and resistive data is generated giving bulk Impedance $|Z|$. This bulk impedance can be deconvoluted into real (resistive, Z') and imaginary (capacitive, $-Z''$) components.

It is important to consider the mechanistic origins of this signal at the interface. The resistance is generated by the interface opposing the flow of current and effectively slowing down charge carriers at the interface. The capacitance is the ability of the system to store up charge after the initial application of the potential. Usually, both components are affected upon analyte binding although either may dominate. The way these processes are investigated, is by subjecting the electrochemical cell to an alternating oscillating wave of potential, this is usually a small perturbation (typically $\sim\pm 10\text{mV}$) around a set potential at which the electrochemical system may be active. The electrode is subjected to a wide range of frequencies to fully characterise processes which occur at the electrode: electrolyte interface. Impedance is calculated from the ratio between the applied voltage and the measured current across the electrochemical cell. As seen in Figure 1-24 impedance takes account of changes in both modulus and phase shift of the measured current.

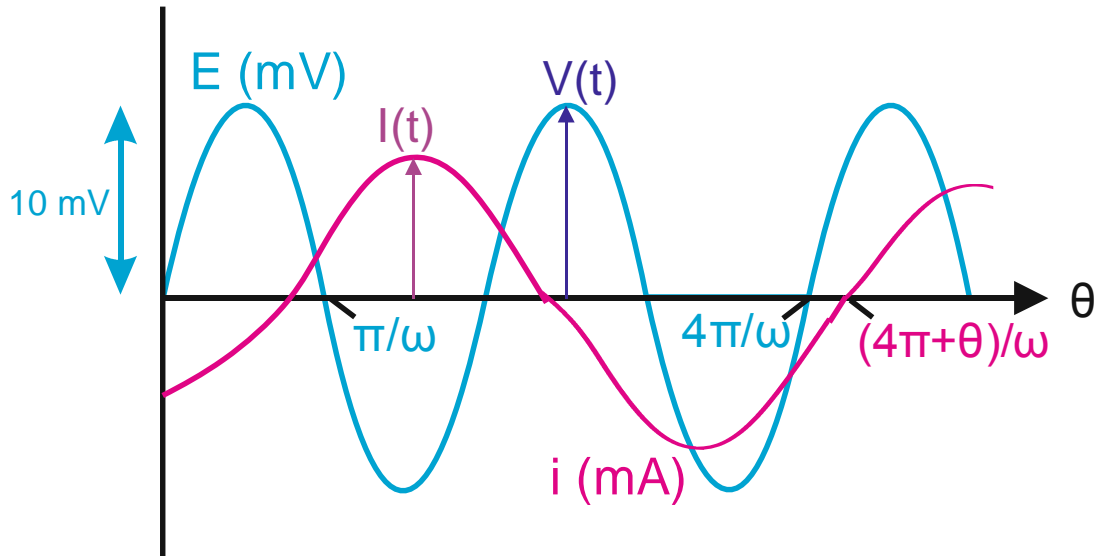


Figure 1-24: Phase shift in complex impedance. Applied oscillating voltage (blue) is modulated by a small perturbation voltage ($\pm 10\text{mV}$ is typical) and the change in current (magenta) is then measured. The current will be different in both, phase angle ($\pi+\theta$) and amplitude. This change forms the basis for impedance measurements. Figure adapted from (Bard & Faulkner, 2001)

By assessing the change in current through the cell, the impedance can be calculated using Ohms Law. In its normal format, this law states:

$$R = \frac{V}{I}$$

Equation 1-13: Ohm's Law

In order to use this equation, we must consider the voltage and the current measured when in AC. The voltage at a given time can be calculated using the equation:

$$V_t = V_m \sin \omega t$$

Equation 1-14: Calculating voltage in an AC circuit

Where:

t=time in sec

ω = angular frequency, rad.sec-1

This is equal to $2\pi f$

f= frequency in Hz

V_m = amplitude

V= voltage at time t

As well as potential, the current can be calculated using the equation:

$$I = I_m \sin(\omega t + \theta)$$

Equation 1-15: Calculating current from phase shift

Where:

t=time in sec

ω = angular frequency, rad.sec-1

This is equal to $2\pi f$

where f= frequency in Hz

I_m = maximum current

θ = Phase angle, rad

V= current at time t

By using Ohm's Law with the identities established for both resistance and impedance, the total impedance can be calculated using the following equation:

$$Z = \frac{V(t)}{I(t)} = \frac{V_m \sin \omega t}{I_m \sin(\omega t + \theta)}$$

Equation 1-16: Total impedance from potential and current

Where Z= total Impedance

If the system is considered in both extremes, where it either behaves as a capacitor or a resistor we can see the origin of both real and imaginary components of impedance respectively. In a resistor system Ohm's Law states that:

$$I = \frac{V}{R} = \frac{V_m \sin \omega t}{R} = I_m \sin \omega t \left[I_m = \frac{V_M}{R} \right]$$

Equation 1-17: Ohms Law in a resistor subject to oscillating potential

Whilst in a pure capacitor, there is no current (**I**) and the capacitance is the ratio of charge to voltage which can be rearranged to give Equation 1-18, when considering the wave diagram, a pure capacitor would lead to a phase shift of $\pi/2$ rad, explained below:

$$Q = C.V = C.V_m \sin \omega t$$

Equation 1-18: Calculating charge from capacitance and potential

If this is then integrated with respect to time:

$$\begin{aligned} I &= \frac{\delta Q}{\delta t} = \frac{\delta(C.V_m \sin \omega t)}{\delta t} = C.V_M \frac{\delta}{\delta t}(\sin \omega t) = C.V_M \omega \cos \omega t \\ &= \frac{V_m}{1/\omega.C} \sin\left(\omega t + \frac{\pi}{2}\right) \end{aligned}$$

Equation 1-19: Integrating charge with respect to time

As $1/\omega.C$ is known as capacitive reactance (often expressed in Ohms) in the case of a resistor:

$$I = I_m \sin\left(\omega t + \frac{\pi}{2}\right)$$

Equation 1-20: Emergence of capacitance in observed current

From Equation 1-20, we can see that in the case of a pure capacitor the phase shift (θ) has been replaced by $\pi/2$.

Alternatively, the wave can be considered as a combination of sine & cosine functions, which are analogous to the resistive and capacitive properties respectively (with cosine being $(\pi/2)$ phase shifted with respect to the sine wave). Using Euler's relationship, the combination of these two waves can be used to derive the phase angle as well as total impedance using Equation 1-23 which is equivalent to "gain" or signal. This allows the output at each frequency to be represented on a Nyquist plot.

$$e^{i\theta} = \cos \theta + i\sin \theta$$

Equation 1-21: Euler's identity

$$\theta = \text{Arctan} \left(\frac{i\sin \theta}{\cos \theta} \right) = \text{Arctan} \left(\frac{-z''}{z'} \right)$$

Equation 1-22: Calculation of phase angle

$$|Z| = \sqrt{(z')^2 + (-z'')^2}$$

Equation 1-23: Calculation of total impedance

The Nyquist plot is a commonly used method to represent impedance data from a range of frequencies. In the Nyquist plot (Figure 1-25) the different frequencies to which the electrode has been subjected are displayed as different data points on axis of a real and imaginary parts of impedance (Z' and $-Z''$ respectively). The coordinates of each point are a product of real and imaginary parts which correspond to the phase shift (θ) and change in amplitude between potential and current. This means that over a range of frequencies points can be plotted and the Nyquist plot is constructed.

From this plot, the relationship between real and imaginary components of impedance can be shown across a range of frequencies. This provides data about the electrified interface and the charge transfer across the electrode. In a typical metal electrode system, there are a number of features of the Nyquist plot of particular interest.

At high frequencies, signal is mainly generated by kinetic processes whereby the change in charge direction occurs faster than the solution can compensate. In the ferri/ferrocyanide system used in work within this thesis, i.e. $\text{Fe}(\text{CN})_6^{-3} \leftrightarrow \text{Fe}(\text{CN})_6^{-4}$, there is an intrinsic limit to the speed at which species can be generated and reduced at the surface. If the direction of current through an electrochemical system is switching very rapidly, this speed becomes the limiting factor and slows charge transfer across the electrode. This is the basis for solution resistance (R_s) in an electrochemical cell.

At marginally lower frequencies, the input potential matches the responsive capabilities of the electrode: electrolyte system in question and resistance is minimised. This generally leads to a flattening of the curve. It is in this frequency range that data on the capacitance of the system can be obtained; as there is negligible resistance, any change between applied and measured signal originates from associated double layer capacitance at the electrode (C_{DL}). In some models, this element can be replaced with a constant phase

element (C_{PE}) which is similar to capacitance, but accounts for non-ideal behaviour, when the capacitor shows partially resistive properties. When considering the normal electrochemical model of capacitance based on ideal-surface plate capacitors, this deviation can be explained by differences in surface texture or charge distributions on the electrode surface.

At lower frequencies still, information on the charge transfer resistance (R_{CT}) is obtained. At these frequencies, the transfer of charge across the electrochemical cell is slowed only by surface species e.g. bound analyte or polymer. This frequency range (typically 0.1 Hz-10Hz) therefore often generates the most interesting data in binding events at a biosensor interface.

In other cases, particularly when using clean metal surfaces which have a very thin diffusion layer, Warburg Impedance is seen as a large linear tail on the arc Figure 1-25. This signal is generated by the diffusional limitations of the system which occurs at low frequencies (Lvovich, 2012). The signal generated by Warburg Impedance is its own complex impedance of capacitance in parallel with a resistive element. This is a result of a depletion of charge carriers close to the electrode, often when wavelength of the perturbation signal is larger than the diffusion layer. This establishes a diffusion gradient meaning that more charge carriers must travel to the electrode in order to permit further charge transfer across the cell, as the diffusion speed of the species concerned limits the process, the effect becomes more pronounced at lower frequencies and thus more signal is generated resulting in the increasing linear trace.

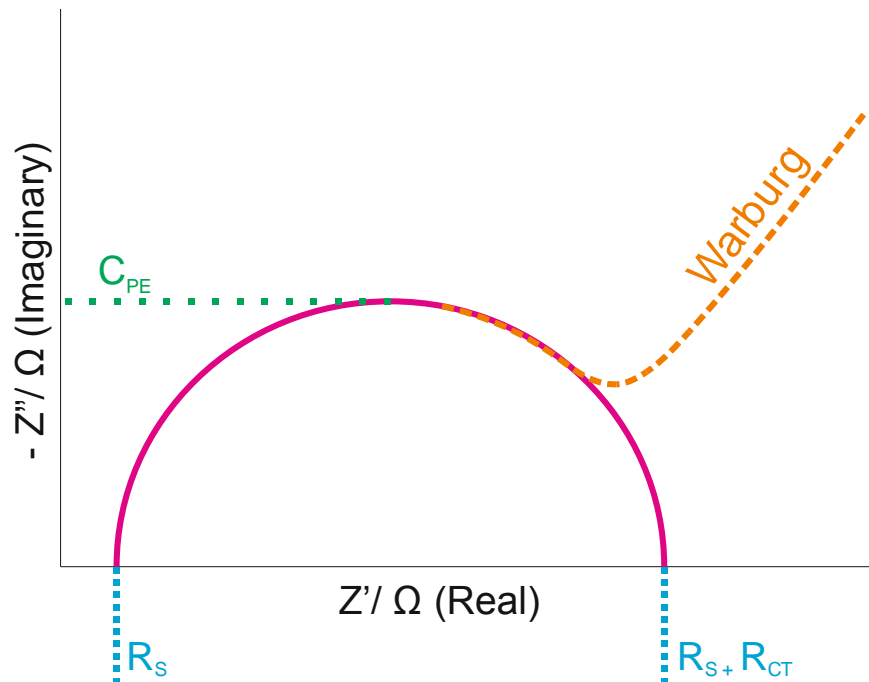


Figure 1-25: The Nyquist plot schematic. The overall plot is a combination of real (Z') and imaginary ($-Z''$) impedance and allows us to interpret the vital parameters of the system, charge transfer resistance (R_{CT}), solution resistance (R_s) and the constant phase element (C_{PE}) which in turn may permit the calculation of the double layer capacitance (C_{DL}). Warburg impedance (W) is also included for illustrative purposes.

In order to obtain values for these essential electrochemical parameters, often the measured data is simulated using an equivalent electrochemical cell model. For impedance on metal electrodes, this is commonly based on the Randle's circuit (Figure 1-26). From this circuit, the individual components can be seen to contribute to the overall impedance and signal observed when interrogating the electrode impedimetrically.

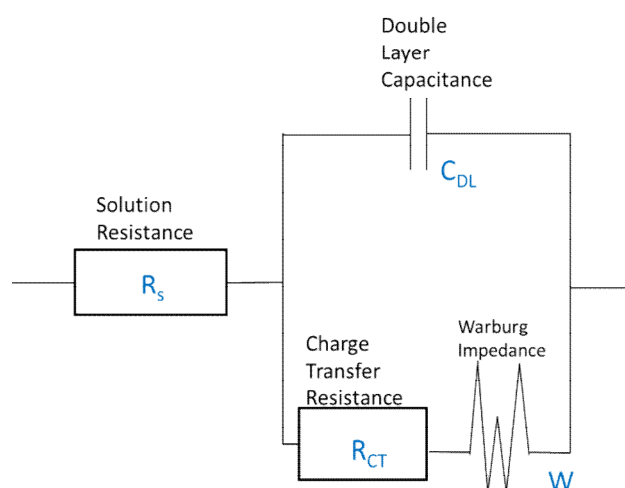


Figure 1-26: The Randles' equivalent cell, key sources of impedance signal for a metal electrode in an electrolyte solution; R_s , solution resistance generated by movement of charge carriers through the solution; C_{DL} double layer capacitance experienced at the electrochemical double layer around the electrode; R_{CT} charge transfer resistance encountered by charge carriers at the electrode interface and Warburg impedance which is a frequency dependent effect

Another way which in data may be displayed from impedimetric interrogation of an electrode is the Bode plot in which the signal is plotted as a function of the log of the interrogation frequency. The Bode plot provides useful data about the behaviour of the electrode and can help to identify frequencies at which the surface behaves more as a capacitor or a resistor. This may help in the development of a biosensor as it can help identify the optimum frequency with which to interrogate which would reduce data acquisition time. One way of ascertaining the optimum frequency at which to analyse a binding event is to interpret the impedance data using a Bode plot as in Figure 1-27. The Bode plot is constructed of two individual plots, both analysing the change in total impedance ($|Z|$) and phase angle shift ($\delta\theta$) as a log of frequency.

If the plot for phase angle is first considered, the Bode plot can very easily display the frequencies at which the electrode surface is behaving as a capacitor. As previously shown from mathematical principles, this is when there is the maximum phase shift ($\delta\theta = \pi/2$). In the Bode plot a peak is commonly seen at a distinct frequency.

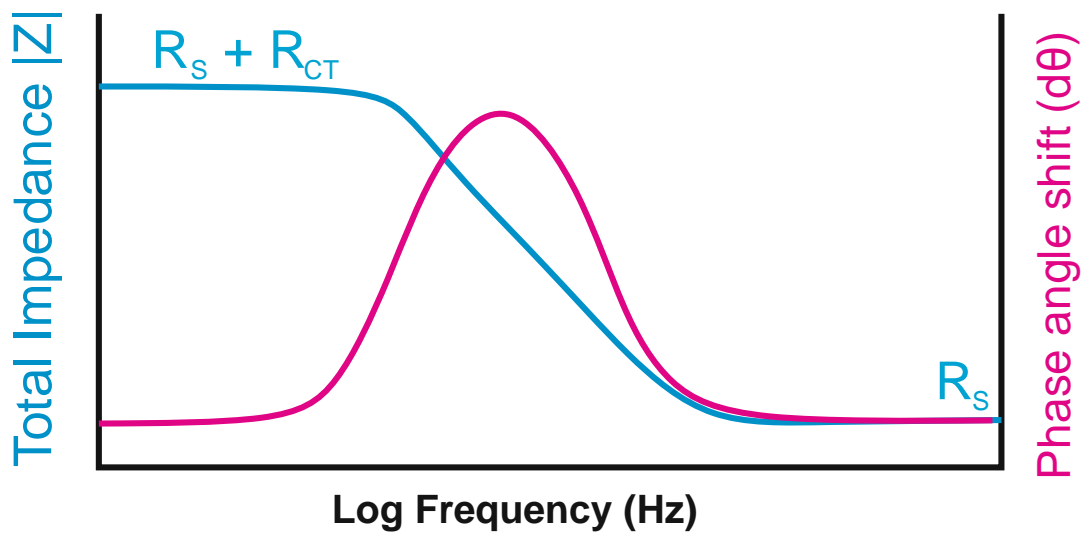


Figure 1-27: A sample Bode plot. The phase angle shift (magenta) can be seen to peak around a maximum value where the surface behaves as a capacitor. When considering the total impedance (blue), the regions where it is horizontal correspond to frequencies where the surface is behaving as a resistor.

Of more use practically are the regions of the plot where the surface behaves as a resistor. As previously discussed at the high frequencies this resistance is generated by limitations in the electrolytic solution which will not be altered by analyte binding.

The Bode plot therefore isolates the frequencies at which the impedance data gives information primarily on the charge transfer resistance across the sensor. This is useful in the generation of a commercial biosensor as it allows for much more simple instrumentation to be employed and fixed frequency analysis to be used. In order for this to be used however the system interrogated must be reliable to the point where any change in signal is due to analyte binding fixed frequency analysis is therefore rarely used.

1.8 Project aims

The main aim of this project is to progress the understanding and development of biosensor function. Biosensor regeneration will be investigated using a previously developed myoglobin sensor. This will demonstrate the possibility of re-using impedimetric immunosensors which could be a critical step in lowering the cost per test and promote their wider adoption.

A further aim is to develop a novel biosensor system using nanobodies as bioreceptor. This will enable investigation of alternative receptor type and will enable comparison between traditional antibody based sensors and smaller binding proteins.

The use of the small recombinant binding proteins will enable investigation of receptor spacing phenomena at the biosensor interface with the aim of improving the reproducibility and sensitivity of sensors. In principle, spacing can be varied in the X-Y plane by varying the concentration at which the receptor is loaded. In addition, the spacing of the receptors in the Z-plane is proposed by re-engineering the receptors to possess a variable length peptide spacer.

This study will aid the understanding of processes at the biosensor interface and inform the fabrication of nanobody based immunosensors as well as those fabricated using other antibody mimetics.

2 | Chapter Two: Materials & Methods

2.1 Materials

2.1.1 Inorganic materials

$K_3Fe(CN)_6$, $(K_4Fe(CN)_6 \cdot 3H_2O)$ and H_2O_2 were purchased from Sigma Aldrich (Poole, UK). H_2SO_4 (95% v/v) was purchased from Merck (Hoddeson, UK). All other inorganic chemicals were purchased from BDH laboratory supplies (Poole, UK).

2.1.2 Organic materials

Biotin-N-Hydroxysuccinimide, mercaptohexanol, mercaptohexadecanoic acid, aniline and 2-ABA were purchased from Sigma Aldrich (Poole, UK). 1,2 dipalmitoyl-*sn*-glycero-3-phosphoethylamine-N- (Sodium salt) was purchased from Avanti Lipids Inc. (Alabaster, USA). NeutrAvidin was purchased from Pierce biotechnology (Rockford, USA). All other organic chemicals were purchased from BDH laboratory supplies (Poole, UK).

2.1.3 Antibodies

Antibodies used in the project were sourced as outlined in Table 2-1.

Antibody	Origin	Source
Anti- Myoglobin	Rabbit polyclonal IgG	GenScript Ltd.
Anti-Digoxin	Sheep polyclonal IgG	Therapeutic Antibodies UK Ltd.
Anti- Rabbit-HRP	Mouse polyclonal IgG	AbCam Plc.
Immunised Sera	Immunised rabbit sera	Cocalico Ltd.
Naïve Sera	Non-immunised rabbit	Biogenes GmbH
Anti –Sox9	Rabbit Polyclonal IgG	AbCam Plc.
Anti – Rabbit	Sheep Polyclonal	Abcam Plc.

Table 2-1 : Sources for antibodies and sera for purification studies. Antibodies were purchased pre purified from these companies

2.1.4 Plasmids for nanobodies

Nanobodies were sourced from AbCam Plc, under licence from Ablynx GmbH. P8D8 Vectors (screened against rabbit IgG) were ligated into pHEN6 Vectors using Novablue *E.Coli* cells from Merck Millipore. This enabled the use of restriction enzymes *BstII* and *PstI* to be used, both purchased from New England Biolabs Ltd.

2.1.5 Agarose gels

Oligonucleotide fragments were isolated using 2% w/v agarose E-gels, containing Sybr® Green and purchased from Invitrogen.

2.1.6 Bacterial strains

Novablue *E.Coli* strains were purchased from Merck Millipore for plasmid amplification and WK6 *E.Coli* cells were purchased from New England Biosciences Ltd for protein expression.

2.1.7 Growth media for bacteria

Bacteria were cultured in LB (Luria-Bertani) media for transformation. This media contained tryptone (10 mg.ml⁻¹), NaCl (10 mg.ml⁻¹) and yeast extract (5 mg.ml⁻¹). For the production of agar plates, agar (15 mg.ml⁻¹) was added to LB medium as well as ampicillin at 50 µg.ml⁻¹ to inoculate non transformed cultures. TB (Terrific Broth) media was used for expression of nanobodies, it contained tryptone (12 mg.ml⁻¹), yeast extract (24 mg.ml⁻¹), glycerol (0.4% v/v) and TB salts (0.17M KH₂PO₄ and 0.72M K₂HPO₄).

2.1.8 Buffers and solutions

A full summary of buffers used throughout can be found in Appendix 2.

2.1.8.1 SDS-PAGE

10 x Tris-Glycine SDS-PAGE running buffer was purchased from National Diagnostics and Coomassie Instant blue was purchased from Generon. PBS was made up from 1x PBS tablets (100 ml.⁻¹) purchased from Fisher Scientific. Pre-cast gels were purchased from Invitrogen®. Broad range protein markers were purchased from Bio-Rad and other inorganic buffers were made from salts purchased from Sigma Aldrich (Poole, UK).

2.1.8.2 Western blot

The Western blotting transfer buffer used was 25 mM Tris, 92 mM Glycine, 20 % (v/v) methanol. Nitrocellulose membrane, Ponceau stain and 20x transfer buffer was bought from Invitrogen®.

2.1.8.3 TES buffer

Periplasmic extraction was done using TES buffer (0.2 M Tris-HCL, 0.5 M Sucrose, and 0.5 mM EDTA pH 8)

2.1.9 Consumables

Slide-a Lyse dialysis units and PD-10 columns were purchased from Thermo Scientific.

2.1.9.1 Electrodes

A variety of transducers were investigated (Appendix 1-1). P3 silicon based electrodes were purchased from Tyndall Institute (Cork, Ireland). 12 WE electrodes were purchased from Phillips N.V., Netherlands. CX2220AT dual electrodes were purchased from Dropsens (Oviedo, Spain). 8 and 12 WE electrodes were purchased from Kanichi Ltd (Manchester, UK). AC9C.W1.R1 electrodes were purchased from BVT (Brno, Czech Rep.). Transducers, with their respective electrode geometries are shown in Appendix 1.

2.2 Methods

2.2.1 Synthesis of nanobodies

In this project, Nanobodies were synthesised from existing stable 'P8D8' plasmids. The plasmid was coded for a nanobody top rabbit IgG which had been isolated from the lymphocytes of an immunised alpaca. Isolation and panning was done by Abcam Plc.

2.2.1.1 Ligation of DNA into P8D8 containing PHEN6 vector

Initially, 15 µl of the plasmid was thawed before adding 2.5 µl 10x Cut Smart buffer (New England Biolabs) as well as the 2.5 µl *Pst*I 20,000 U.ml⁻¹ (New England Biolabs) and 5 µl *Bst*EII, 10,000 U.ml⁻¹ (New England Biolabs) restriction enzymes. This was incubated at 37 °C for 1 hr before adding 1µl 'FastAP' 1 U.ml⁻¹ (Thermo) alkaline phosphatase to prevent recombination. Fragment identity was confirmed and fragments were isolated by running a 2% (w/v) agarose gel. This was achieved using E-gels cartridges (Thermo) for 8 min at 200 V. The desired insert was then removed from the gel before being incubated with the vector overnight at 4 °C in the presence of 1 µl T4 Ligase. 3,000 U.ml⁻¹(New England Biolabs). The stable plasmid was then stored at -20 °C.

This ligation allowed the same restriction enzymes as above (the *Pst*I and *Bst*EII) to be used to ligate the insert into the vector. The *pHEN6* Vector also conferred ampicillin resistance allowing for selection of the transformed *E.Coli*.

2.2.1.2 Transformation of E.coli using heat shock treatment

The Novablue® cells were gently thawed on ice and aliquotted into 50 µl samples before being mixed with 3µl of the plasmid at 100 ng.ml⁻¹. After a further 30 min on ice, the cells were exposed to a heat block for 45 s at 42 °C before being returned to the ice for 1 min. The Cells were then added to 500 µl SOC Media and incubated at 37 °C in an Infors® HT Multitron shaking incubator (220 rpm) for 1 hr. To select successfully transformed plasmids 200 µl of the cell suspensions were spread on LB: ampicillin plates (100 µg.ml⁻¹) and grown overnight.

2.2.1.3 Plasmid isolation & nanobody synthesis

Colonies were selected and grown up the following day in 5 ml LB: ampicillin (100 µg.ml⁻¹). Qiagen® Miniprep kits were used according to the manufacturer's protocols in order to isolate the plasmid and the concentration of the plasmid was assayed using a Nanodrop (Thermo). The plasmid, 10 µl at ~100ng.ml⁻¹ was then sent to Source Bioscience® for sequencing to ensure the plasmid contained the nanobody, spacer arm and the terminal

cysteine. M13 primer was used in both F and R directions to ensure complete sequencing of the linker region. Nanobodies were then produced by transforming *E.coli* cells as above into competent WK6 cells. Cells were plated onto TB-ampicillin plates incubated at 37 °C overnight. The following day, colonies were selected and added to 5ml LB+ ampicillin which were incubated at 37 °C overnight. These were then added to 500 ml LB+ ampicillin. Once optical density had reached 0.6 cultures were induced using IPTG (100 mM) and incubated at 37 °C overnight in an Infors® HT Multitron shaking incubator (220 rpm).

2.2.1.4 Extraction of periplasm & purification

The periplasm was extracted by decanting cells into centrifuge flasks and collected by centrifugation at 3,000 xg for 30 min. Supernatant media was discarded and cells were re-suspended using TES Buffer which had been stored at 4 °C. After mixing on a shaker for 30 min on ice, a further 75 ml TES buffer was added and shaking on ice was continued for a further 30 min. Samples were then split into 50ml falcon® tubes and centrifuged at 6,800 xg for 3 min to separate the periplasm extract from the cell bodies. The periplasm extract was then ready for purification in order to isolate the nanobodies.

Owing to the engineered His₆-tag, the nanobodies could be easily purified. This was achieved using an Akta explorer fitted with a GE Histrap® Ni⁺ chelating column. Periplasm was run through the column at a rate of 1 ml.min⁻¹ followed by copious rinsing with wash buffer containing 10 mM imidazole, 20 mM Tris base and 0.5 M NaCl. This was immediately followed with 5 ml elution buffer comprising 0.3 M imidazole, 20mM Tris base and 0.5 M NaCl, A₂₈₀ was monitored using an in-line spectrophotometer and fractions containing eluted protein were pooled before dialysis.

2.2.1.5 Dialysis of proteins

Buffer exchange was then carried out to remove excess imidazole against DW Buffer (PBS + 50 mM NaCl). This was achieved using Thermo Scientific Slide-A-Lyze® chambers according to manufacturer's instructions. 1000x volume of buffer was changed three times over a 15 hour period.

2.2.2 SDS- PAGE and western blots

The SDS-PAGE gel was run with MOPS, MES or TA buffer (Table 2.2) systems depending on the molecular weight of the target protein. Gels (3-8% Tris Bis, (v/v) Nu-Page for MES and MOPS and 5% (v/v) Tris-Acetate for TA) were removed from their packaging and rinsed with the correct buffer before being placed into an electrophoresis tank. The buffer was

then added to the tank at 1x concentration and 500 μ l antioxidant (Sigma PCG3007) was added to the core tank.

To confirm the identity of protein present in the eluates from immunoprecipitation experiments, the fractions were subjected to gel electrophoresis using non-reducing SDS-PAGE. Pre-cast gels (4-12% MES) were purchased from Invitrogen to which 8 μ l Sample Buffer (50 mM Tris-HCl pH 6.8, 2% SDS, 10% glycerol, 1% β -mercaptoethanol 12.5 mM EDTA, 0.02 % bromophenol blue) containing approximately 1 μ g of the protein of interest was added into each well and electrophoresis was continued at 200 V for 50 min under constant voltage. Gels were then either stained using Instant Blue Coomassie stain according to manufacturer's instruction or used for western blotting. For western blots, the gel was carefully placed between felt pads and a nitrocellulose membrane in a transfer cassette before being closed tightly and placed back into the electrophoresis tank. The cassette was then soaked in transfer buffer (25 mM Bicine, 25 mM Bis-Tris, 1 mM EDTA 20% Methanol (v/v), pH 7.2) before being subjected to 30 V for 70 min. Proteins were imaged by soaking the membrane for two minutes in Ponceau stain (1 g.l⁻¹ in 5% acetic acid (v/v)).

After the protein transfer had been confirmed, the Ponceau was rinsed off using 1x TBST Buffer until the pink colour had faded. Membranes were then blocked using 5%(w/v) BSA in TBST (50 mM Tris, 150 mM NaCl, 0.05% (v/v) Tween 20, pH 7.6) for 30 min and probed with the appropriate antibody conjugates (1:10,000) in blocking buffer and left to incubate for 1 h. Membranes were then washed thoroughly (2x 15 min PBST-T plus 1x 15 min PBS) before adding ECL HRP-Substrate and imaging using a Syngene G:Box System to record the chemiluminescent signal. Blots were then analysed using GeneSnap software (Syngene).

2.2.3 Immunoprecipitation experiments

N-Hydroxysuccinimide (NHS) and Sulfolink[®] sepharose beads were purchased from GE and Sigma respectively and proteins were conjugated according to manufacturers' protocols. The standard nanobody was conjugated to NHS beads and all of the modified spacer containing nanobodies were conjugated to Sulfolink beads using the labile cysteine residue. A negative control was varied out by conjugating the amino acid cysteine only from a cysteine containing buffer (50mM cysteine in 50 mM Tris-Hydroxymethylaminomethane plus 5 mM EDTA). Beads were incubated with 100 μ l diluted rabbit sera (10% Sera: PBS) for two hours. After binding, a mild acid wash was completed using pH 4 100 mM sodium citrate and a final RIPA Buffer (50 mM NaCl, 1%

(v/v) IGEPAL CA-630®, 0.5% (w/v) sodium deoxycholate, 0.1% (w/v) SDS and 50 mM Tris, pH 8.0) in order to remove any non-specifically bound protein from the beads.

For elution, a two stage procedure was adopted .Firstly, a 100 mM glycine elution buffer at pH 2 was used in order to interrupt nanobody: antigen binding. A second elution was performed using PBS plus 100 mM DTT to investigate cleavage of the nanobody form the Sulfolink beads.

2.2.4 Biotinylation of antibodies

Antibodies were produced to a concentration of 1 mg.ml⁻¹ in PBS. Any azide was removed via dialysis to prevent interference with conjugation chemistry. Then 1 mg.ml⁻¹ biotin NHS in DMSO:PBS solution was prepared as per the previous section. The two were combined and allowed to react for 30 min. The bound and unbound biotin was then separated by centrifugal filtration.

Millex centrifuge separation tubes with a molecular weight cut off of 10 KDa were used; 2 ml of the biotin: antibody mixture was added and the tubes were centrifuged at 8,900 *xg* for 3 min. Biotin-containing buffer was then discarded and 300 µl fresh PBS was added. This process was repeated five times to remove the unbound biotin from the mixture. The biotinylated antibodies were then pipetted onto the NeutrAvidin containing electrode surface, and left for 1 h to react. The electrode was then rinsed thoroughly using PBS to complete biosensor fabrication.

2.2.5 Reduction of nanobody dimers

Nanobody dimers, were treated with 50 mM 2-mercaptoethylamine (2-MEA), in degassed PBS buffer plus 10 mM EDTA for 90 min at 37 °C. The reduced proteins were then applied, to Amicon filters (3,000 MWCO) and centrifuged at 16,000 *xg* to remove excess MEA. Buffer was replaced with previously degassed 1×PBS plus 10 mM EDTA three times. The proteins were then used immediately to prevent recombination by disulphide bond formation between the reduced proteins.

2.2.6 Electrode preparation

2.2.6.1 mSAM construction

Some electrodes allowed self-assembled monolayers to be created. This was achieved by dissolving 10 mg mercaptohexadecanoic acid (MHDA) in 1 ml chloroform then aliquotting 144 µl into 10 ml EtOH. Then 52 µl of biotin-capryol-DPPE (Supplied by Avanti Polar Lipids

Inc. at 10 mg.ml^{-1} in chloroform) was added to create a 1:1 molar ratio of MHDA: Lipid. Electrodes were submerged for 24 hours to create the mSAM (Billah et al., 2010; Conroy et al., 2010).

2.2.6.2 Polymer deposition

For some electrodes, electrodeposition of polymer was employed. This was achieved by connecting the electrodes to an Autolab electrochemical workstation running GPES software (with a separate counter & reference where necessary).

For deposition of PANI:2-ABA copolymer, the electrochemical cell was set up and CVs were run for 20 scans between 0 and 1 V at a scan rate of 0.05 V.s^{-1} in a 1:1 mixture of 50 mM of aniline and 2-ABA in 50 ml 1 M HCl.

In the case of Polytyramine deposition, two scans were executed from 0 to 1.6 V at a scan rate of 0.2 V.s^{-1} in a solution of 25 mM tyramine dissolved in methanol plus 0.3M NaOH to serve as a counter ion.

2.2.6.3 Bioconjugation of the receptor to the sensor surface

Biotinylation of the sensor surface

1 mg Biotin-NHS was dissolved in 100 μl dimethyl sulphoxide (DMSO) and added to 900 μl PBS, 10 μl of which was then pipetted onto the electrodes. This enabled biotinylation of primary amines, the electrodes were incubated for 1 hr in a moist environment to prevent drying, before being thoroughly rinsed in PBS to remove unlinked biotin.

Addition of NeutrAvidin

NeutrAvidin at $4 \mu\text{g.ml}^{-1}$ in PBS was pipetted onto the electrodes. This was left for 1 h in a moist atmosphere to react before being thoroughly washed.

Oriented conjugation using Sulfo-SMCC

The polymer-modified electrodes were incubated with 5 mM sulfosuccinimidyl 4-[N-maleimidomethyl cyclohexane-1-carboxylate (Sulfo-SMCC) solution in 10 mM PBS-EDTA pH 7.2 for 1 h, as described previously (Billah et al., 2010; Bonroy et al., 2006; Lu et al., 1996). The freshly reduced proteins, either half antibody or nanobodies, were then added to the sulfo-SMCC modified electrode and incubated for 1 h. These electrodes were incubated for 30 min in PBS to rinse away any non-specifically bound proteins and ensure baseline signal stability. The sensors were interrogated electrochemically prior to analyte detection to obtain a baseline sensor signal.

2.2.1 Electrochemical instrumentation

All electrochemistry experiments were based on a three electrode system in an electrochemical cell. This was true for both early experiments involving external reference and counter electrodes to the working electrode and later experiments using transducers that integrated all three onto one sensing chip. The working electrode used was always gold, the external reference was Ag/AgCl (Metrohm AG, Herisau, Germany) and the external counter electrode was a platinum rod. The three electrode system was controlled by an EcoChemie μ Autolab Type III with a frequency response analyser (FRA-2) potentiostat (Windsor Scientific Limited, Slough, Berkshire, UK). was used to apply a current to the electrochemical cell through the counter electrode. The voltage difference between the working electrode and the reference electrode was then measured. The Autolab measured the difference between the cell voltage and the desired voltage and completed a feedback loop, causing an amplifier to drive current into the cell to maintain the voltages. Autolab software was used to acquire electrochemical measurements and for further data analysis. All electrochemical interrogation was done at room temperature and in a Faraday cage.

2.2.1.1 Working electrodes

Gold

Gold was chosen as the working electrode material due to its availability, ease of preparation (electrodeposition, sputtering and physical vapour deposition) and patterning using screen printing. This is advantageous as fabrication does not require clean room m so is comparatively cheaper.

Electrode design and production

The Working electrodes used were screen printed gold electrodes designed and produced by Dropsens (Asturias, Spain). These comprised of two gold working electrodes fired onto a ceramic base (Appendix 1). The counter and the Ag/AgCl reference electrode were also printed on the same transducer base.

2.2.1.2 Reference electrode

An Ag/AgCl reference was integrated into the transducer chip. Reference electrodes are chosen due to their ability to maintain a stable double layer, and therefore potential, against which other potentials may be compared. Typically, a reference will measure the potential difference between the working electrode and the counter electrode. This allows the system to maintain a controlled applied voltage to the

working electrode throughout experiments (Bard and Faulkner 2001; Wang 2006). Ag/AgCl electrodes are commonly used in electrochemistry due to their well-studied and highly efficient redox mechanism and low toxicity.

2.2.1.3 Counter electrode

The counter or auxiliary electrode is the final electrode in the three electrode system. Its purpose is to complete the circuit by providing current to the working and reference electrodes and should be comprised of an inert conductor. The counter electrode must be at least ten times the surface area of the working electrode to allow efficient exchange of electrons such that the electrochemistry is not limited (Brett & Brett, 1998). For some experiments an external counter electrode was provided, comprising a platinum rod. In most experiments, a gold counter was integrated on the Dropsens chip.

2.2.2 Interrogation of sensors

The sensors were incubated with a given concentration of analyte for 30 min, starting with the lowest concentration before sequential increase. The sensors were electrochemically interrogated with an Autolab III Module (Eco Chemie B.V.) Electrodes were placed in a cell containing 10 mM $K_3Fe(CN)_6$, $K_4Fe(CN)_6$ and 10 mM PBS, pH 7.2.

2.2.2.1 Cyclic voltammetry

For CV, GPES software was used, the electrodes were scanned either from -1 V to +1 V or -0.4 V to +0.7 V, the wider range representing a full analysis of the chemical nature of the electrodes at strongly reductive and oxidative potentials respectively.

2.2.2.2 Electrochemical impedance spectroscopy

After sensor assembly, electrochemical impedance spectroscopy (EIS) was used to monitor analyte recognition using NOVA software on a FRA-2 AUTOLAB type III electrochemical workstation. The impedance analysis was performed over a frequency range from 0.25 Hz to 25 kHz using a modulation voltage of 10 mV at an applied voltage of 0.0 V with respect to Ag/AgCl₂. All impedance experiments were performed in an electrolyte solution of 10 mM $K_3[Fe(CN)_6]$ / $K_4[Fe(CN)_6]$ (1:1 ratio) in 1×PBS, pH 7.4. Fully fabricated immunosensors were incubated with 10 µl analyte for 30 min prior to copious rinsing in PBS and electrochemical interrogation.

2.2.2.3 Data handling

Using Autolab NOVA Software, the biosensor was modelled using a modified Randles' Circuit in which the pure capacitor was replaced with a constant-phase element to more closely simulate the non-ideal nature of capacitance at the biosensor surface (Bard & Faulkner, 2001). As the effects of Warburg impedance were not observed in the data, this component was also excluded from the model. This model allowed statistical estimation of the solution resistance (R_s), charge transfer resistance (R_{CT}) and constant-phase element (Q). Using this analysis, the error of the data fit was found to have an average deviation of $2.887\% \pm 0.096$ ($n=64$). For calibration, of the biosensor R_{CT} is used as it is the most sensitive to analyte binding and hence the most widely used measure for impedimetric analysis of biosensors (Ahmed et al., 2013; Caygill et al., 2012; Lillie et al., 2001; Prodromidis, 2010).

2.2.3 Regeneration of electrodes

To investigate the regeneration of biosensor electrodes, myoglobin sensors were constructed on polymer substrates and a standard concentration of 10^{-8} M was tested.

2.2.3.1 Electroreduction of nitrate

To achieve localised alkali concentrations around working electrodes, the electroreduction of nitrate ions was executed. Using 100 mM PBS with 100 mM sodium nitrate, electrodes were connected to an Autolab electrochemical workstation running GPES software. Chrono-amperometric methods were used, with a voltage ≤ 2.0 V, time was modulated by the software.

2.2.3.2 Regeneration buffers

All acidic buffers were based on a 100 mM glycine solution with pH altered using HCl within the range pH 2-4. For later incubations a fluidics chamber, designed by Dropsens (DRP-CFLWCL-TG) was included. This allowed incubation parameters to be controlled as the flow rate was set at $1 \text{ ml}\cdot\text{min}^{-1}$, allowing exposure of the sensor to the de-binding buffer to be controlled precisely. The final buffer used was 100 mM glycine in 50% propylene glycol at pH 2.75 with 1% DMSO.

2.2.4 Octet studies

To analyse the binding parameters of the nanobodies, kinetic analysis was executed using a ForteBio® Octet Red system. For analysis of the basic nanobody and IgG, receptors were bound to amine reactive probes (AGRP2) following manufacturers protocols using EDC/NHS chemistry.

For sulfhydryl conjugation of freshly reduced nanobodies, EDC/NHS conjugation was initially followed by incubation with 10 mM PDPH in DMSO for 10 min. The PDPH activated probe was then exposed to the reduced nanobody for 10 min before a 5 min wash in PBS and baseline measurement. Binding data was then obtained, allowing 10 minutes for binding and 1 h for debinding data to be collected.

2.2.4.1 Data handling

Initial analysis was undertaken, fitting a one site binding profile and global fitting to derive initial values for the binding parameters for each of the bioreceptors. The equations which govern this fast on slow off binding kinetics interaction:

$$y = y_0 + A(1 - e^{k_a \cdot t})$$

Equation 2-1: One site saturation signal

Where the variables are as in

Equation 1-2.

$$y = y_0 + A \cdot e^{-k_d \cdot t}$$

Equation 2-2: One Site desaturation signal

These two equations contribute to give the overall binding constant:

$$KD = \frac{K_d}{K_a}$$

Equation 2-3: Binding affinity

However due to inadequate simulation between the above equations and the measured data the data was reanalysed, to obtain more accurate rates. . In the modelling of this data, two distinct rates were used to modify the previous equations to:

$$\text{binding Signal} = y_0 + A(1 - e^{k_{a1} \cdot t}) + B(1 - e^{k_{a2} \cdot t})$$

Where $A + B = 1$

Equation 2-4: Two site saturation signal

$$\text{debinding Signal} = y_0 + (A \cdot e^{-k_{d1} \cdot t}) + (B \cdot e^{-k_{d2} \cdot t})$$

$$\text{Where } A + B = 1$$

Equation 2-5: Two site desaturation signal

3 Chapter Three:

Fabrication and Regeneration of Immunosensors

3.1 Introduction

As described in Chapter Two, biosensors were fabricated on Dropsens composite electrodes. This was achieved by electropolymerising a polyaniline (PANI) 2-aminobenzylamine (ABA) copolymer onto the working electrode. Polyaniline has been widely used in biosensors as a conducting polymer. However, by itself polyaniline does not contain sufficient tethering groups for efficient conjugation chemistry. ABA was therefore included to incorporate the necessary amine groups for conjugation of the bioreceptor.

This tethering layer was then used to conjugate the bioreceptor to the surface using one of two mechanisms either Biotin NHS in order to permit the cross linking with a biotinylated receptor using NeutrAvidin[®], the second approach used Sulfo SMCC to introduce a maleimide group and enable oriented conjugation between the crosslinker and the thiol moiety. Once biosensors had been fabricated and interrogated, regeneration of impedimetric Immunosensors was approached.

As antibodies are a key tool across many fields, there has been intense research into the bio-physics of antibody binding and its reversibility. The binding interactions for which antibodies are used have different rate constants for both association and dissociation (K_a and K_b , respectively). These can be very different; typically K_a is very fast whilst K_b is much slower. These constants describe the “fast on/slow off” model of antibody binding. It is often therefore necessary to partially denature the antibody to induce dissociation. Partial denaturation and sensor regeneration is usually accomplished using pH alteration, a detergent, or chaotropic agents (Blanchard et al., 1990; Giorgos J, 1979). This causes the non-covalent forces between antigen and antibody to be screened and the enthalpic interactions are reduced, additionally a slight distortion of the antibody structure may occur, which allows the antigen to separate from the antibody. For biosensors, this may allow the development of reusable sensors for both research and commercial applications. Regeneration of antibodies used in non-electrochemical biosensors has been successfully achieved (Kandimalla et al., 2004; Wijesuriya et al., 1994) including systems using flow cells (Choi & Chae, 2009; Drake & Klakamp, 2011). Currently, there have been only limited reports of the regeneration of electrochemical biosensors (Bhalla et al., 2010).

It has been reported that optical immunosensors can be regenerated up to ten times with only a minimal loss in signal before a sudden loss in subsequent cycles (Wijesuriya et al.,

1994). This is an important finding and one which must be considered in the development of new biosensors. The effect of pH shifts on the electrochemical properties of the system may cause charging or degradation of the baselayer which may interfere with subsequent sensor operation.

3.1.1 Chemical regeneration

The most widely reported approach to regeneration uses chemical regeneration buffers, where a low pH buffer such as glycine or a high pH solution such as NaOH is used. This often has other components such as DMSO, Tween-20 or Ethylene glycol incorporated at low concentration.

3.1.2 Electro-reduction of nitrate

Another proposed method of regenerating antibodies is by using electro-reduction. By applying a negative voltage to the electrode, ions can be selectively reduced. One particularly powerful instance of electroreduction is the reduction of nitrate ions. In this process the ion gains electrons, which results in the generation of hydroxyl ions. This causes a rapid and highly localised increase in the pH. The reduction of nitrate ions into various species is described in Figure 3-1 along with the quantity of generated hydroxyl ions.

As nitrogen has many oxidation states available, when electro-reduction is initiated there is an abundance of electrons provided at the interface, the nitrate present is then available to undergo a number of reduction stages which result in the release of hydroxyl groups. The number of hydroxyl groups directly matches the number of electrons with which the nitrate reacts, and, the change in oxidation number of the Nitrogen in the ion.

It can be seen therefore that by electrochemically providing a ready source of electrons a very alkali region can be quickly generated at the electrode interface. This method can therefore be used to provide transient pulses which may induce localised regeneration of the biosensor interface.

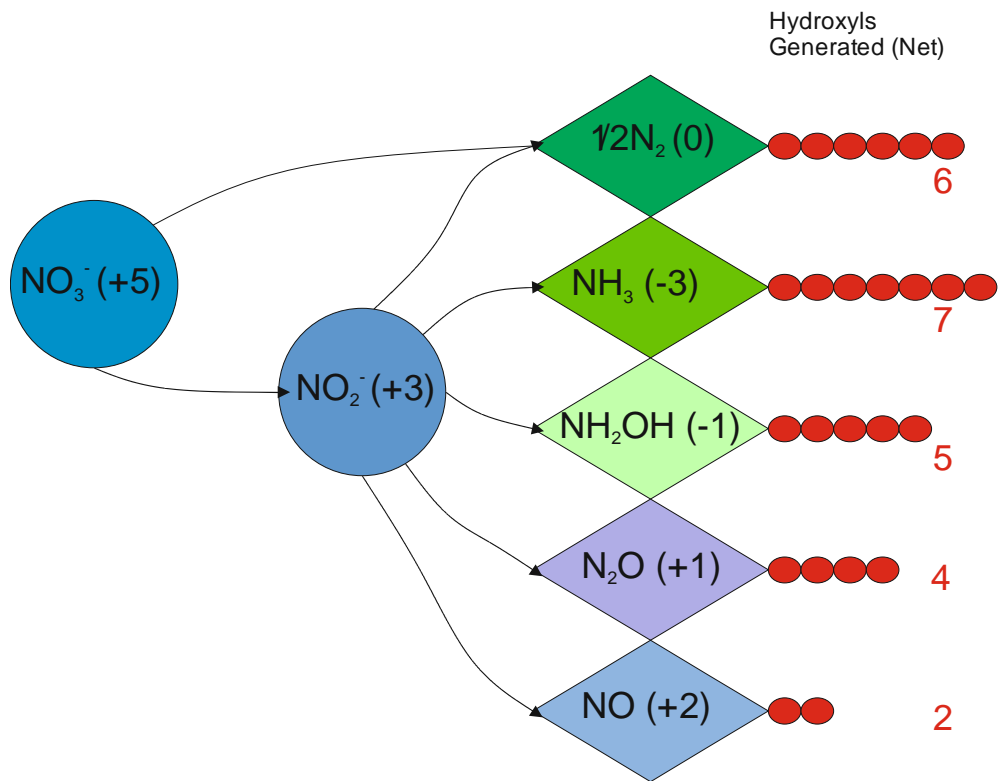


Figure 3-1: Electroreduction of nitrate ions. Upon the reduction of nitrate, many species are produced owing to the many oxidation states of nitrogen (shown). The reduction of nitrate into of each of these ions results in the generation of a vast quantity of Hydroxyl ions (red)

3.2 Results

3.2.1 Fabrication of myoglobin sensors

In order to fabricate myoglobin sensors, PANI 2-ABA copolymer was electropolymerised onto the working electrode. This resulted in the gradual deposition of an electro-conductive species which was gradually deposited over 20 scans. This polymer is not soluble and is a more robust alternative to SAMs. Another reason for using conducting polymer was that the electrodes used have significant surface roughness, meaning that they were unsuitable for tethering layers such as SAMs which would possess defects.

For the fabrication of the tethering layer; a 1:1 monomer ratio of aniline:2-ABA was made to 100 Mm with respect to each species in 1 M HCl. This was then electropolymerised onto screen printed gold electrodes (DRP-CX2220AT) using cyclic voltammetry. Twenty scans were run from 1.0 V to 0.0 V at a scan rate of 50 mV.s^{-1} . The resulting CVs (vs. Ag/AgCl reference electrode) are shown overlaid in Figure 3-2. The increase in peak heights with corresponding scan number showed the increasing conductivity of deposited polymer as each potential cycle was applied and more polymer was deposited. This is characteristic of PANI as the polymer is deposited and molecular orbitals overlap to create conduction pathways between the electrode and the bulk solution (Gerard et al., 2002).

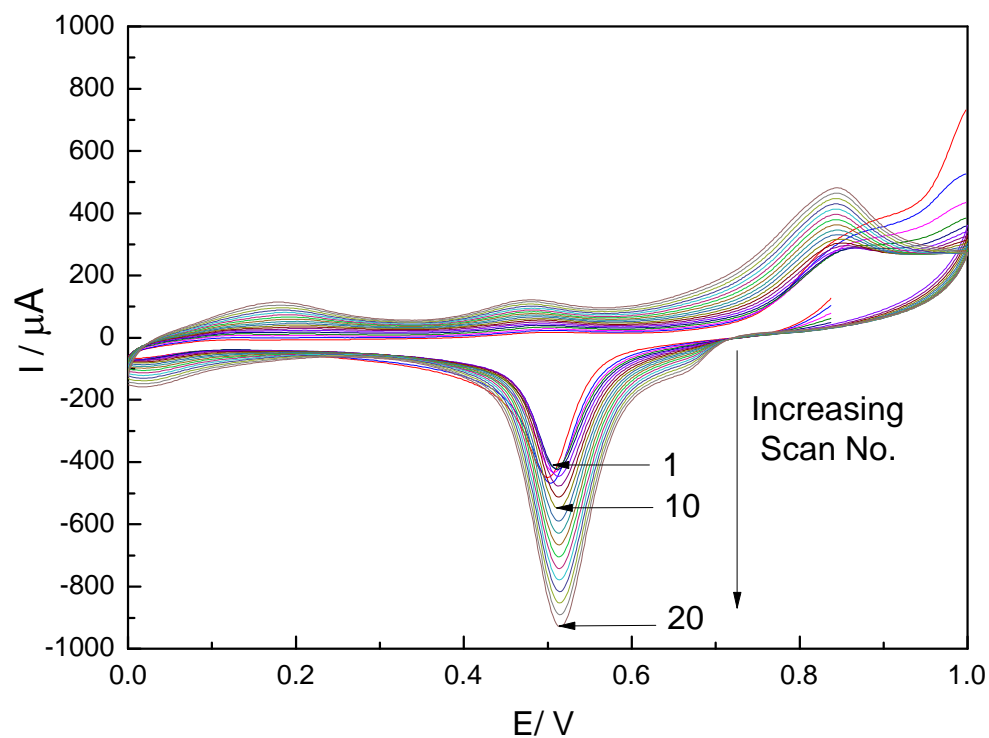


Figure 3-2: Electropolymerisation of PANI 2-ABA copolymer onto a gold electrode. 20 consecutive CV scans were conducted resulting in an increasing size of the plotted current, this shows the deposition of polymer across scans as each repeat shows the greater oxidation and reduction signal generated by a larger quantity of polymer on the electrode surface.

After polymer deposition, the sensor was constructed using biotin- NeutrAvidin crosslinker as described in chapter 2. Resulting impedance scans of each construction step can be observed in Figure 3-3.

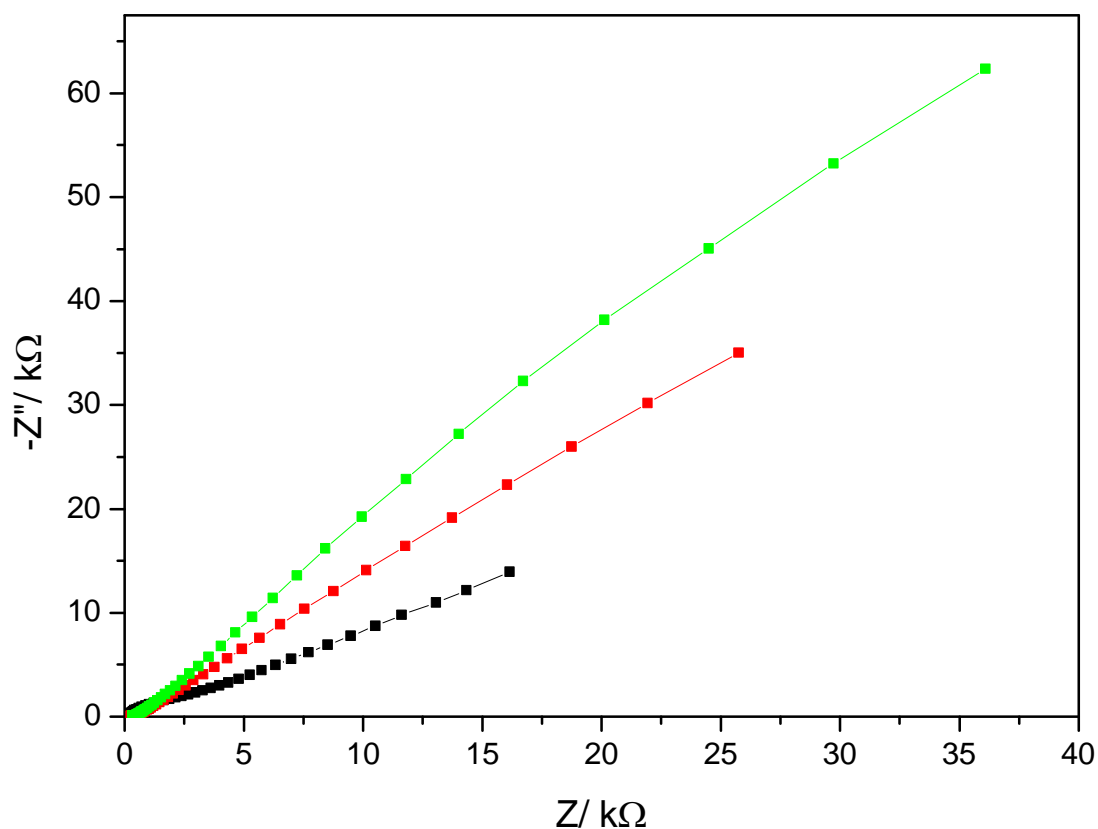


Figure 3-3: Impedance scans of consecutive construction steps. Bare gold electrode (—■—). Deposited PANI:2-ABA (—■—) and fully constructed myoglobin sensor (—■—)

3.2.2 Interrogation of myoglobin sensors

After successful deposition of the PANI:2-ABA copolymer and attachment of both biotin and Avidin, biotinylated myoglobin antibodies were conjugated to the transducer surface. Non-specific sensors were also constructed using another biotinylated antibody, in this case the anti-lysyl oxidase antibody.

Both specific and non-specific sensors were exposed to increasing concentrations of myoglobin for 30 min duration before being rinsed and interrogated using electrochemical impedance spectroscopy.

Interrogation was achieved by immersing the electrode in the mediator solution containing $\text{Fe}(\text{CN})_6^{-3/4}$, at an applied voltage of 0V with respect to a Ag/AgCl reference electrode. Data was taken at 51 frequencies between 0.25 Hz to 25 kHz as described in Chapter Two.

Data shown in Figure 3-4 shows the Nyquist plots of both specific signal and non-specific signal. It can be observed that increasing analyte resulted in a larger Nyquist plot. This corresponds to a larger resistance and capacitance across the sensor surface.

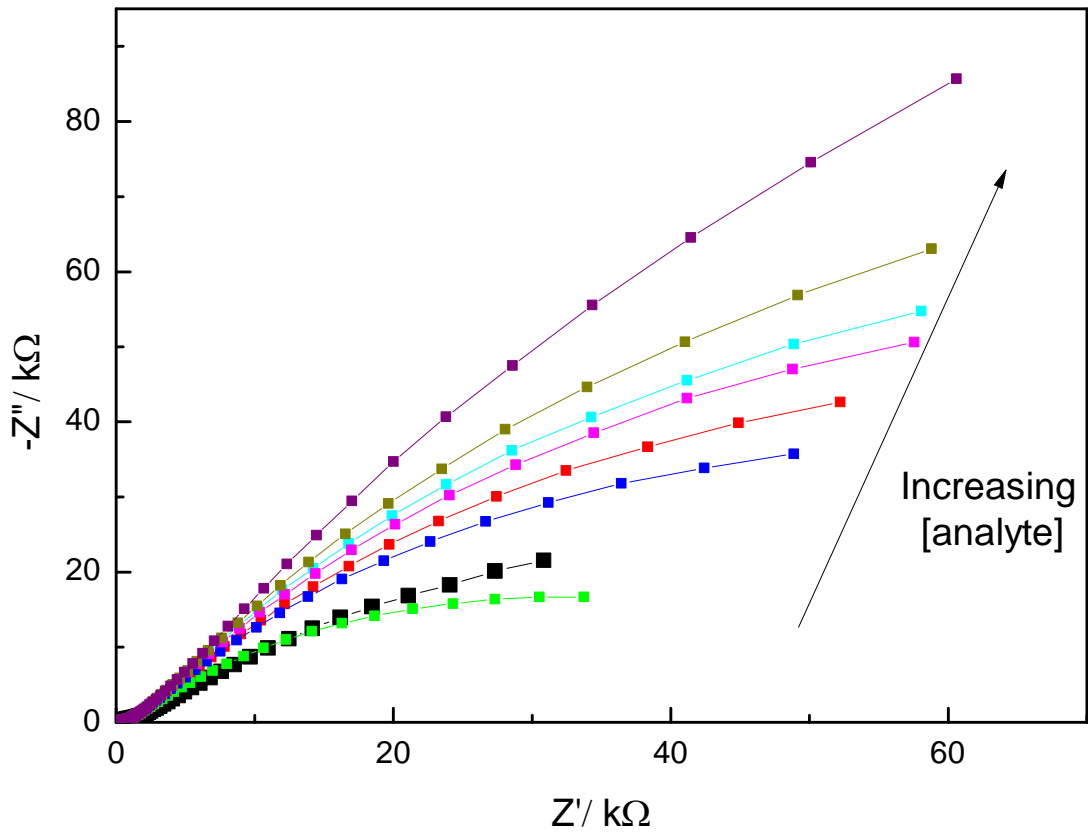


Figure 3-4: Nyquist Plots of a PANI-2-ABA myoglobin sensor. Bare sensor (—■—), increasing analyte concentration; 10^{-11} M (—■—), 10^{-10} M (—■—), 10^{-9} M (—■—), 10^{-8} M (—■—), 10^{-7} M (—■—), 10^{-6} M (—■—), 10^{-5} M (—■—).

This change in resistance was assessed by obtaining values for the charge transfer resistance (R_{CT}), using Nova software as described in Chapter Two. This allowed a calibration of the concentration of myoglobin vs. R_{CT} as shown in Figure 3-5. There is a clear signal generated by binding of the analyte to the biotinylated antibody.

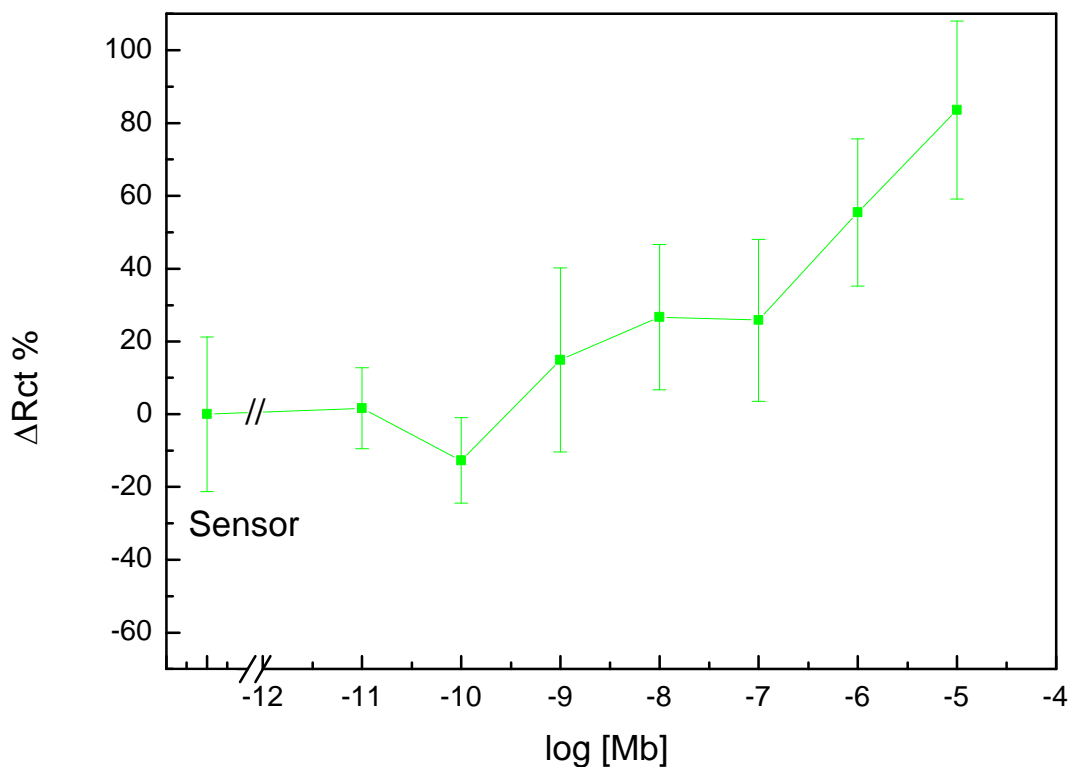


Figure 3-5: Charge transfer resistance of a myoglobin biosensor on PANI-2ABA. ($n=5 \pm SE$)

This data has demonstrated that copolymer based immunosensors to Myoglobin were successful at specific detection of the analyte and that R_{CT} increased with concentration of Myoglobin due to the binding of the antibody and analyte. Data from Non-specific sensors has shown minimal binding.

3.2.3 Chemical Regeneration of myoglobin sensors

Initially regeneration was investigated using 100 mM Glycine buffered at a range of pH values. After an initial 30 min binding with 10^{-6} M Myoglobin, the sensor was interrogated using EIS. The sensor was then incubated with regeneration buffer for 15 s before allowing rebinding, again with 10^{-6} M myoglobin for 30 min. The sensor was again interrogated using EIS to monitor signal over a number of regeneration cycles. Values for the change in R_{CT} after consecutive incubations are shown in Figure 3-6.

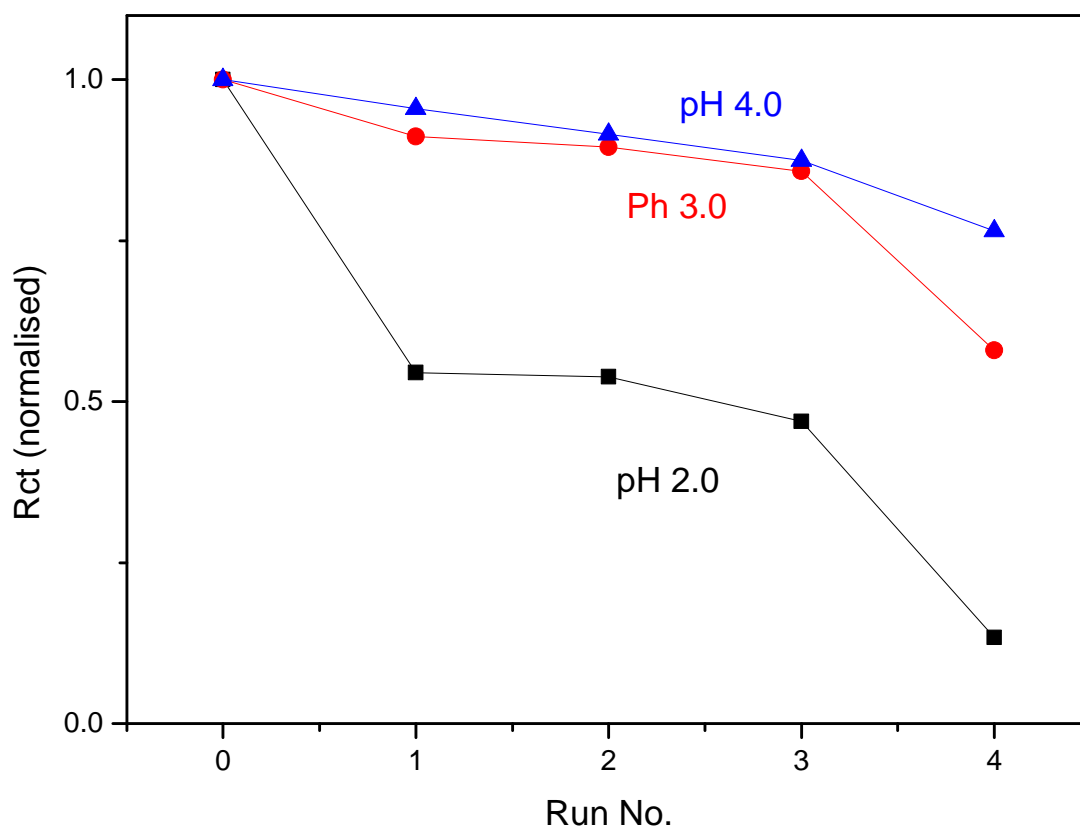


Figure 3-6: pH study of myoglobin biosensor regeneration. R_{CT} was normalised to original sensor readings (run 0). After analyte binding and initial interrogation, samples were incubated with 100 mM glycine buffer for 15 s before repeating analyte incubation and repeating interrogation steps. Regeneration buffers used were 100 mM glycine at pH 4.0 (—■—), pH 3.0 (—■—) and pH 2.0 (—■—).

From this data, regeneration at pH 2.0 showed a rapid decrease in the signal yield from successive interrogations. Where pH 3.0 and 4.0 were used, a steady but much slower decrease in the signal yielded could be observed. Following a substantial consideration of the literature, a common candidate identified was pH 2.75. This literature survey resulted in the publication of a review paper (Goode et al., 2014), and work was continued using the pH 2.75. After pH had been established, a study into incubation times was carried out. Data was obtained by incubating sensors in 100 mM glycine at pH 2.75 for a range of incubation times from 10 s to 90 s (Figure 3-7).

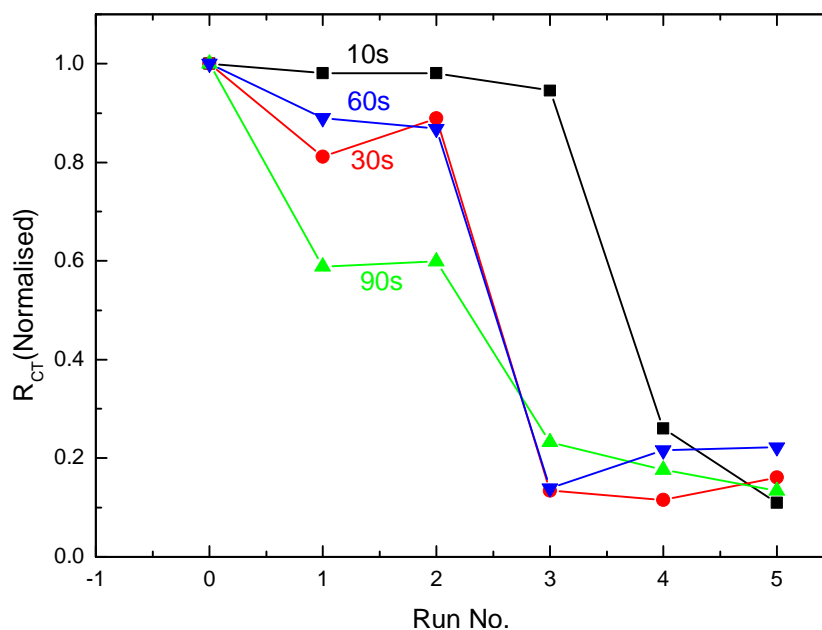


Figure 3-7: Time study of myoglobin biosensor regeneration. After analyte binding and initial interrogation, samples were incubated in 100 mM glycine at pH 2.75 for a range of time before repeating analyte binding and interrogation. Times of incubation were: 10 s (—■—); 30 s (—●—); 60 s (—▼—); 90 s (—▲—).

From this data, it can be seen that when incubating the biosensor with 100 mM glycine at pH 2.75 for 10 s the signal does not decrease dramatically as in previous experiments. When increasing the incubation time beyond 10 s however, the signal quickly decays upon regeneration. By the time a 90 s incubation with the low pH glycine was used, the signal had decreased by ~45% after only one regeneration cycle. This demonstrates that although the chosen pH of 2.75, near to previously successful pH 3.0 was suitably mild, after an extended incubation the sensor does become damaged. This highlights the fact that time is an important parameter which must be controlled precisely.

3.2.3.1 Use of Fluidics

In order to more stringently control the exposure of the sensor to the regeneration buffer, immunosensors were mounted into a flow cell system as shown in Figure 3-8 to allow the regeneration process to be controlled more accurately. By using the same pH 2.75 buffer with a flow rate of 1 ml.min⁻¹, the working electrode was exposed for 15 seconds, to allow for lag, results are shown in Figure 3-9.

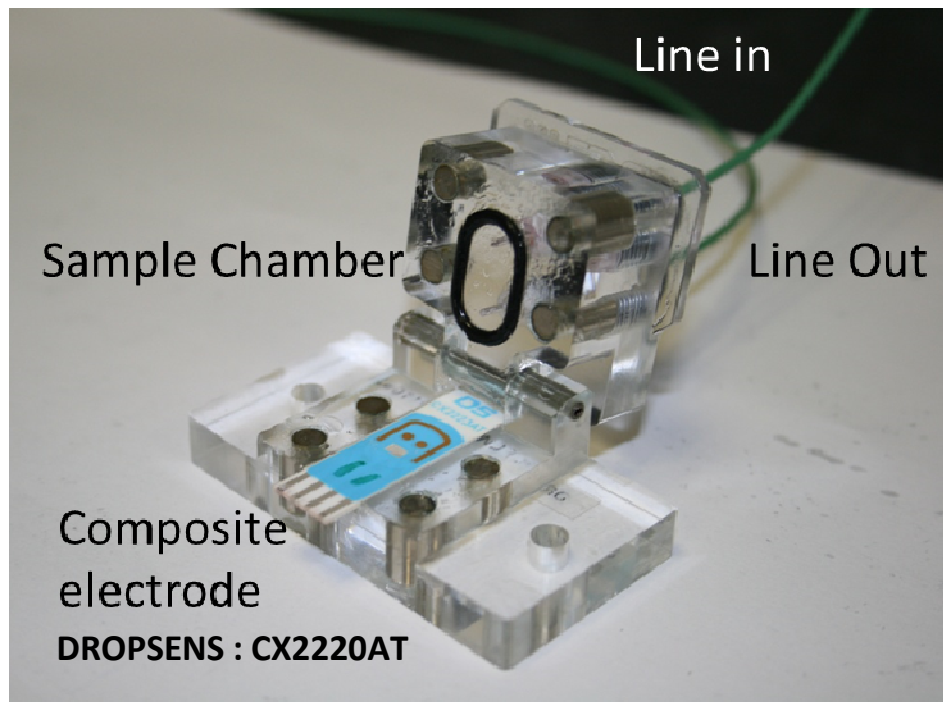


Figure 3-8: The Dropsens microfluidics rig, which was used in order to control regeneration of the sensor more precisely the oval gasket defines the flow chamber with lines in and out which were used to change between electrochemical interrogation buffer and regeneration buffer.

It is important to note that this data displays Z' , due to the large amounts of noise encountered. Data obtained using R_{CT} showed limited success in regeneration studies and in addition, the reproducibility was unacceptable in this sensor system. By monitoring the Z' (real) component of the impedance, this gives us an approximation of the resistive properties across the biosensor surface. Figure 3-9 demonstrates that when analysing at individual frequencies, biosensors could be reused. By enabling regeneration, it may be possible to reduce the variability between different interrogations as they could be executed on the same sensor. It is also a good development when considering economic factors in the biosensor market as would likely reduce the cost per test.

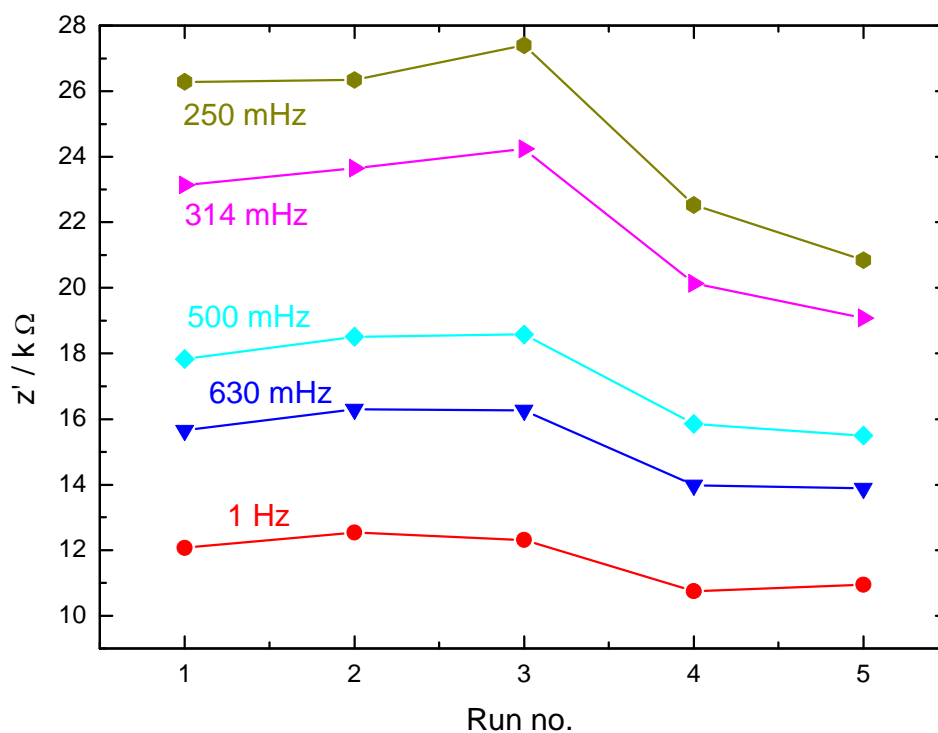


Figure 3-9: Monitoring myoglobin biosensor regeneration across frequencies. Real impedance (resistive element) was monitored over a range of regeneration cycles at the following frequencies: 1 Hz (—■—), 630 mHz (—■—), 500 mHz (—■—), 314 mHz (—■—), 250 mHz (—■—).

3.2.3.2 Electronic Polymorphism of PANI

The highly variable nature of regeneration data on the sensors which had been constructed using the pani:2-ABA polymer lead to an inspection of the literature (Hwang et al., 2001; Kennedy et al., 2007; Lacroix et al., 2000; Raffa et al., 2006; Sergeyeva et al., 1996) on the chemistry of poly aniline. It became apparent that the polymer in question had a number of electronic states: the fully reduced form (pernigraniline), the mixed reduced/ oxidised form (emeraldine) and the oxidised form (leucoemeraldine). It was also discovered that by terminating electrodeposition at various potentials, the copolymer could be observed in each of these three states. This was investigated and a number of EIS scans of the polymer deposited at each electronic state were reviewed to assess the electronic stability of the copolymer itself, data shown in Figure 3-10.

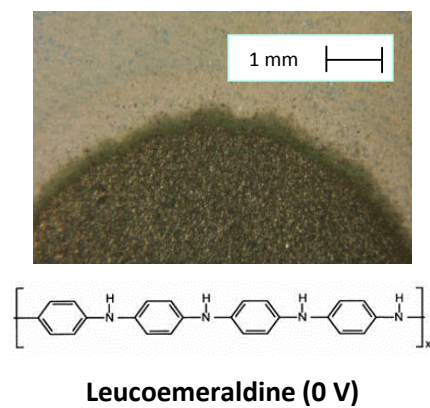
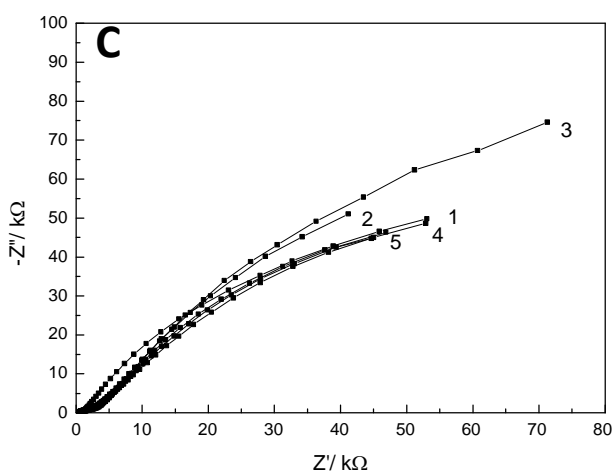
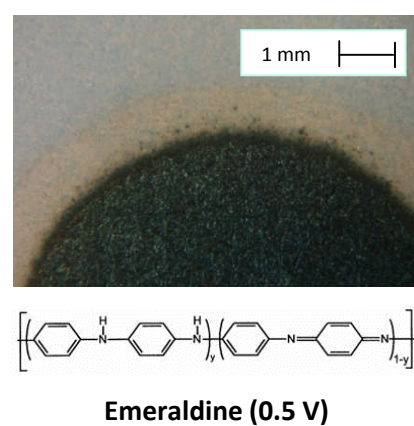
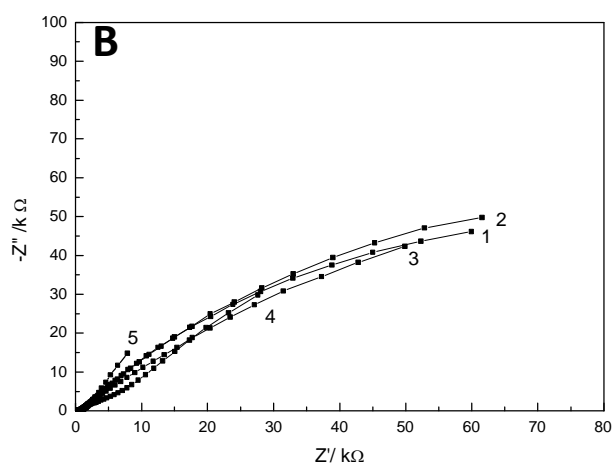
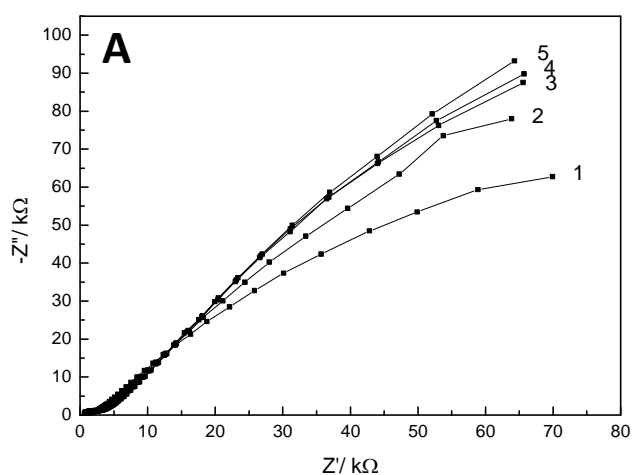


Figure 3-10: Different electronic configurations of PANI: 2ABA copolymer. A, B and C were subjected to 20 CV cycles as described in methods. The end potential was set at; A= 1 V, B= 0.5 V and C= 0 V. In order to ensure that the polymer was in a defined electronic state.

Following this consecutive EIS scans were run, Nyquist plots are shown alongside photographs of the surface and schematics of each of the three electronic structures.

This data highlighted the variability of the polymer layer and showed the change in signal generated from the polymer alone. It was due to this that a new polymer needed to be chosen. Given the need for accessible moieties for conjugation and a stable signal in a wide variety of chemical environments, there were only a few candidate polymers. From these polytyramine was chosen as it had been previously demonstrated useful for biosensor applications (Ahmed et al., 2013; Ates, 2013; Gerard et al., 2002; Labib et al., 2010; Pournaras et al., 2008).

3.2.3.3 Operational stability of polytyramine vs. polyaniline

By exposing PANI:2-ABA to different pH buffers, the electronic variability of the polymer could be compared between the inferior PANI:2-ABA and the PTyr. This was observed clearly in both the Nyquist plots (Figure 3-11, Figure 3-14) and derived data For R_{CT} (Figure 3-12, Figure 3-15).

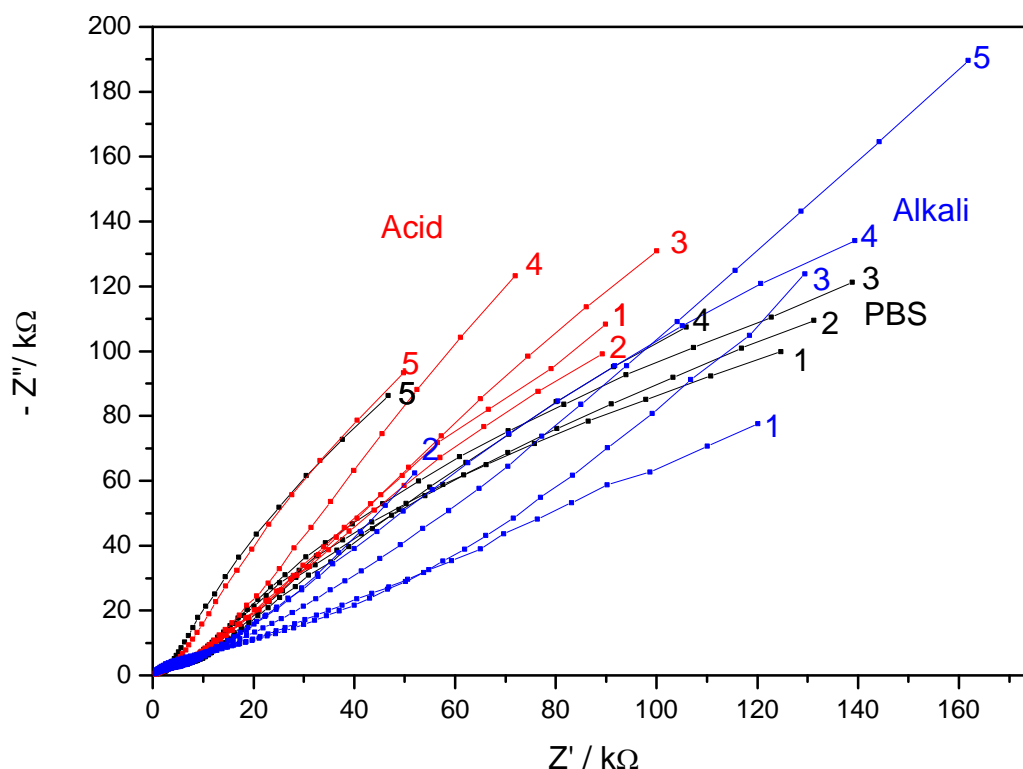


Figure 3-11: The stability of PANI:2-ABA. After electropolymerisation three separate experiments were run to investigate electronic stability of the polymer. Consecutive EIS scans (1-5) were run following sequential 10 s incubations in the following buffers: **acid** 100 mM glycine pH2.0 (—■—), **Alkali** 10 mM NaOH :N₂HPO₄ Buffer pH 12.0(—■—) and 10 mM PBS pH 7.4 (—■—)

When considering the Nyquist plots of consecutive incubations in a range of environments, the Pani was observed to display poor reproducibility. In particular in acidic environments, where continual incubation in pH 2.0 buffer resulted in an arc which consistently became steeper, this property of increasing signal in the imaginary component of impedance is analogous to an increase in the capacitive properties of the interface. It is therefore hypothesised that as the PANI polymer is soaked in acid, it becomes charged which causes interference in R_{CT} rendering sensor calibration impossible. Whilst capacitance is not generally used in biosensor calibration, it is an important property of electrochemical biosensors, in particular impedimetric ones where R_{CT} is modelled using a Randle's cell as the large change in capacitance may cause an artefact when trying to simulate data.

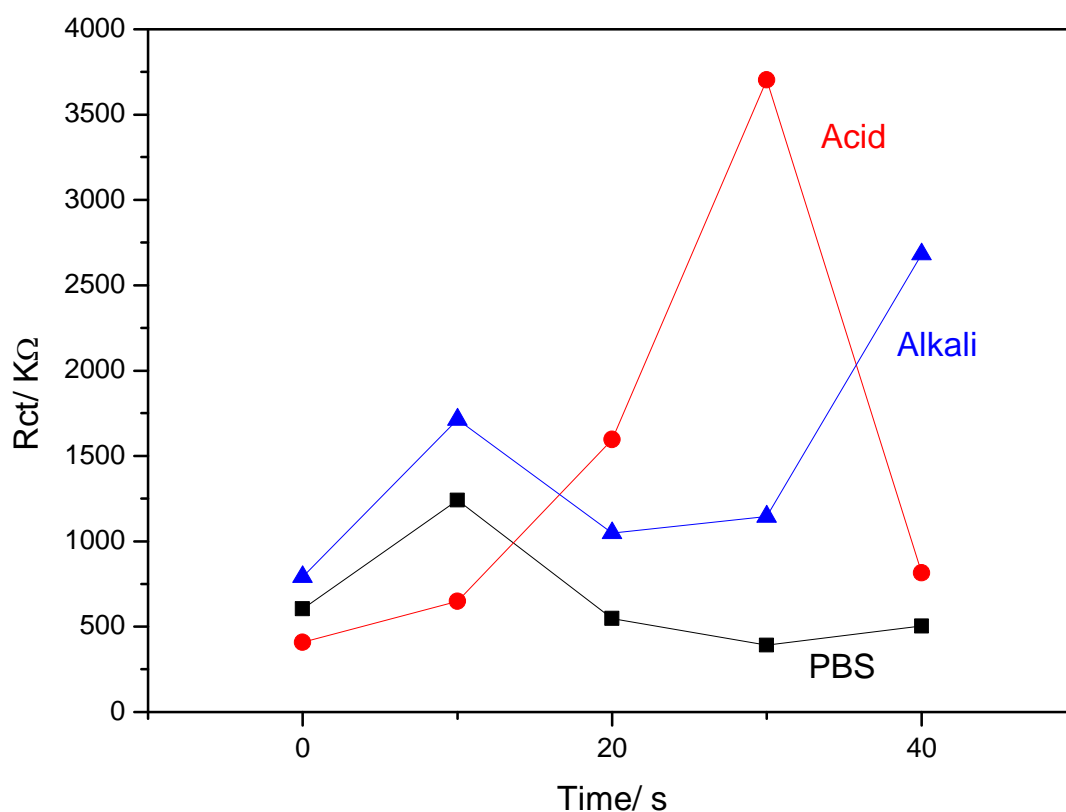


Figure 3-12: Analysed R_{CT} on stability of PANI:2-ABA. The polymer coated electrode was exposed to different conditions for increasing incubation times, acid 100 mM glycine pH2.0 (—●—), Alkali 10 mM NaOH : N_2HPO_4 Buffer pH 12.0(—▲—)and 10 mM PBS pH 7.4 (—■—)

Since this change is on an electrode with only polymer deposited and not a fully constructed biosensor, this may be a great hindrance to the calibration of a successful biosensor. As acidic regeneration had been previously pursued, these data may help explain the limited degree of reproducibility observed. Polytyramine had been identified as a strong candidate for replacing PANI due to its superior stability, therefore electrodes were cleaned and deposition of PTyr was executed as outlined in Chapter Two, the results of which are shown in Figure 3-13. In this trace, after initial oxidation of tyramine at around 0.5 V in the first scan, a smaller scan was observed for the second scan. This implies that tyramine is oxidised onto the electrode surface, forming an insulating film, a property which has been previously identified (Pournaras et al., 2008; Tsuji et al., 1990).

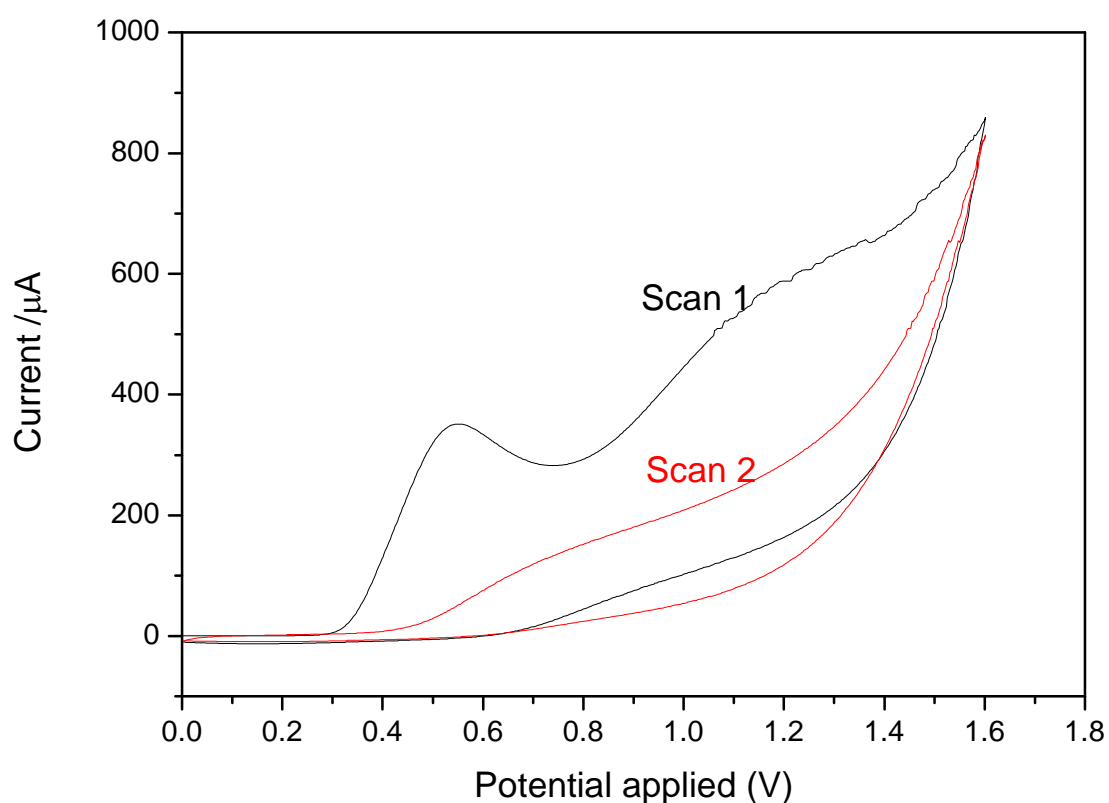


Figure 3-13: Electropolymerisation of polytyramine film. Tyramine was dissolved in methanol with 0.3M NaOH to act as a counter ion consecutive CV scans are shown Scan 1 (black) and scan 2 (red).

The stability of Polytyramine (PTyr) was then assessed and compared with previous data from PANI: 2-ABA Copolymer. As previously, incubation of a polymer coated electrode in a variety of different buffers was followed with consecutive EIS scans (Figure 3-14).

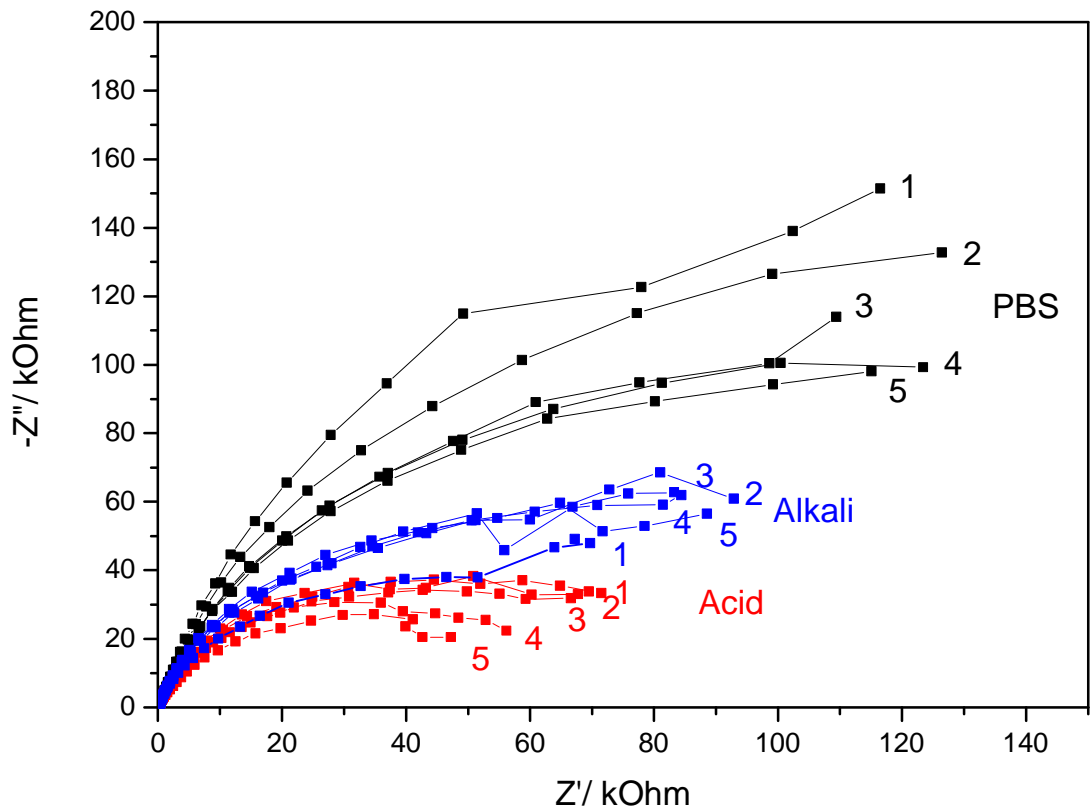


Figure 3-14: The stability of PTyr. Stability of the polymer was assessed as in figure 3-12, EIS scans were run with consecutive 10 s incubations in the following buffer: acid 100 mM glycine pH2.0 (—■—), Alkali 10 mM NaOH :N₂HPO₄ Buffer pH 12.0(—■—)and 10 mM PBS pH 7.4 (—■—)

From these data it can be seen that the three electrodes interrogated formed distinct datasets with a clear distinction between those exposed to acid, alkali and PBS. Though there is a difference between the electrodes themselves, for the purposes of this experiment it is really the change occurring at each electrode which is critical.

In order to investigate this factor in isolation, the change in charge transfer resistance was calculated (Figure 3-15) to assess the effect of the various environments on the polymer. From the figure, it can be observed that PTyr is a much more stable polymer than PANI. This suggested that PTyr was a more viable choice for of biosensor regeneration across the pH range used with acidic glycine regeneration.

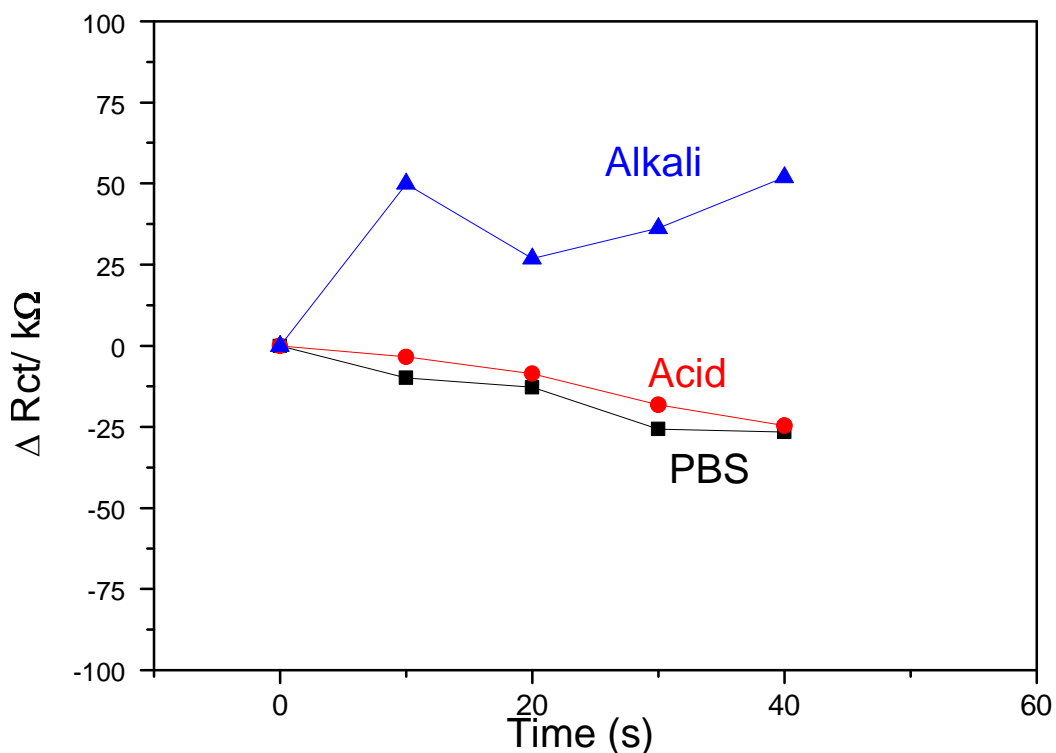


Figure 3-15: Analysed R_{CT} on the stability of PTyr. Polymer coated electrode was exposed to different conditions for increasing incubation times, acid 100 mM glycine pH 2.0 (—■—), Alkali 10 mM NaOH : N_2HPO_4 Buffer pH 12.0 (—▲—) and 10 mM PBS pH 7.4 (—■—)

Considering the data shown in Figure 3-15, it was observed that whilst there was a minor change in the R_{CT} when exposing the PTyr to an acidic buffer. This helped to confirm the improvement in stability that had been achieved by changing the polymer layer.

3.2.3.4 Electroregeneration of Myoglobin sensors

As polytyramine had been proven a more stable electropolymer, its suitability for use in electro-reductive regeneration was assessed. Literature values for the electro-reduction of nitrate ions state that a potential of -2.8 V causes optimal reduction of nitrate ions. After one ten second interval of electro-reduction, the PTyr appears to have been stripped. This can be observed in the Nyquist plot (Figure 3-16) where after the first electro-reductive cycle the Nyquist plot dramatically drops to resemble data similar to a bare gold electrode.

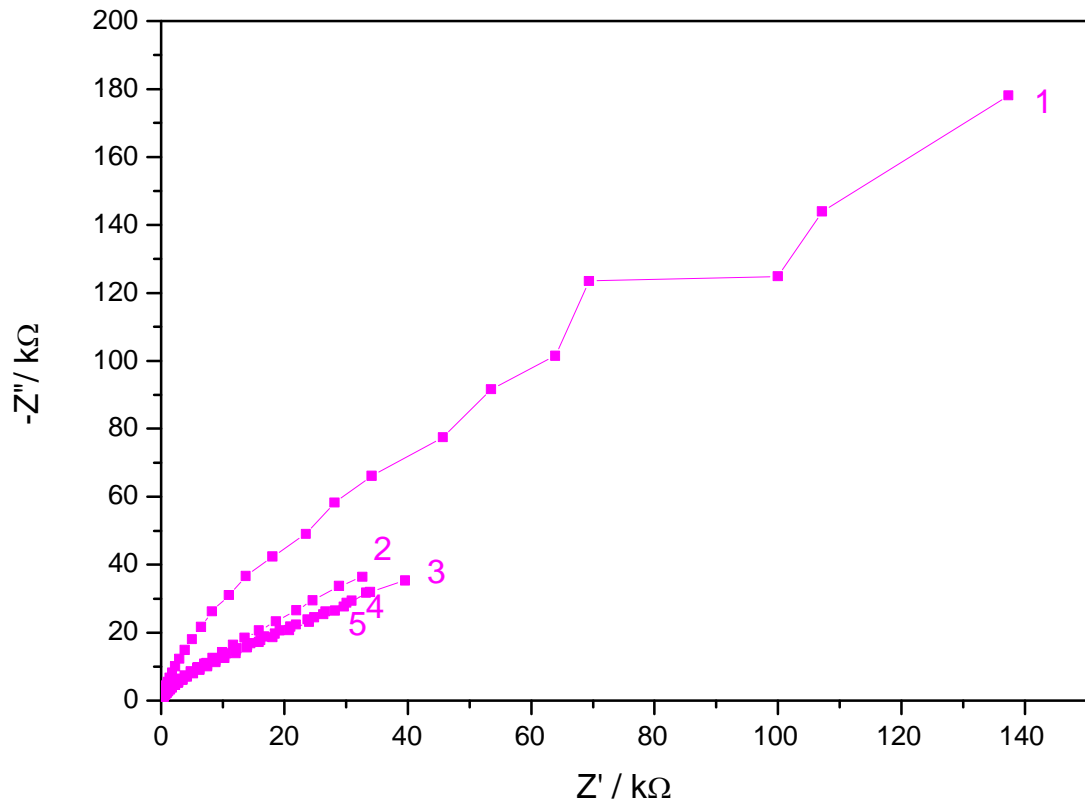


Figure 3-16: Stability of PTyr after 10s periods of electroreduction of nitrate. After initial reading (1), the electrodes were subjected to consecutive electroreductive cycles.

The data was again analysed to assess the change in charge transfer resistance and again the dramatic decrease in resistance after one 10 s electroreductive cycle was clearly visible (Figure 3-17).

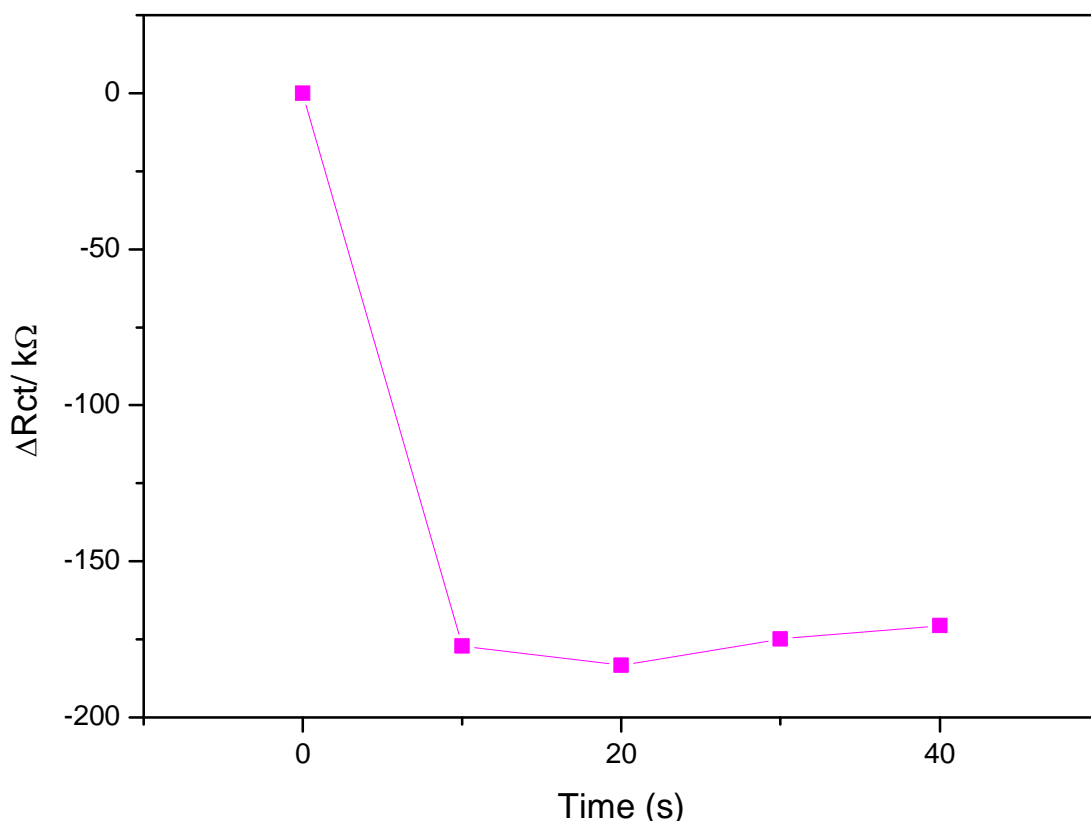


Figure 3-17: Analysed R_{CT} of PTyr film after electroreduction of nitrate. The polytyramine coated electrode was exposed to 10s pulses of electroreductive current before consecutive EIS interrogations.

As the negative potential of -2.8 V was found to be too aggressive, electro-reduction of nitrate over a wide potential range was assessed to ascertain whether it could be modulated. A cyclic voltammogram was taken to monitor this reduction process in isolation (Figure 3-18). The reduction peak was observed to begin at around -1.7 V. By moderating the reduction voltage to -2.0 V, it was hoped that a more gentle reduction could be achieved and perhaps a milder alkali pulse generated which could in turn prevent stripping of the electrode and the resultant drop in resistance which had been previously observed.

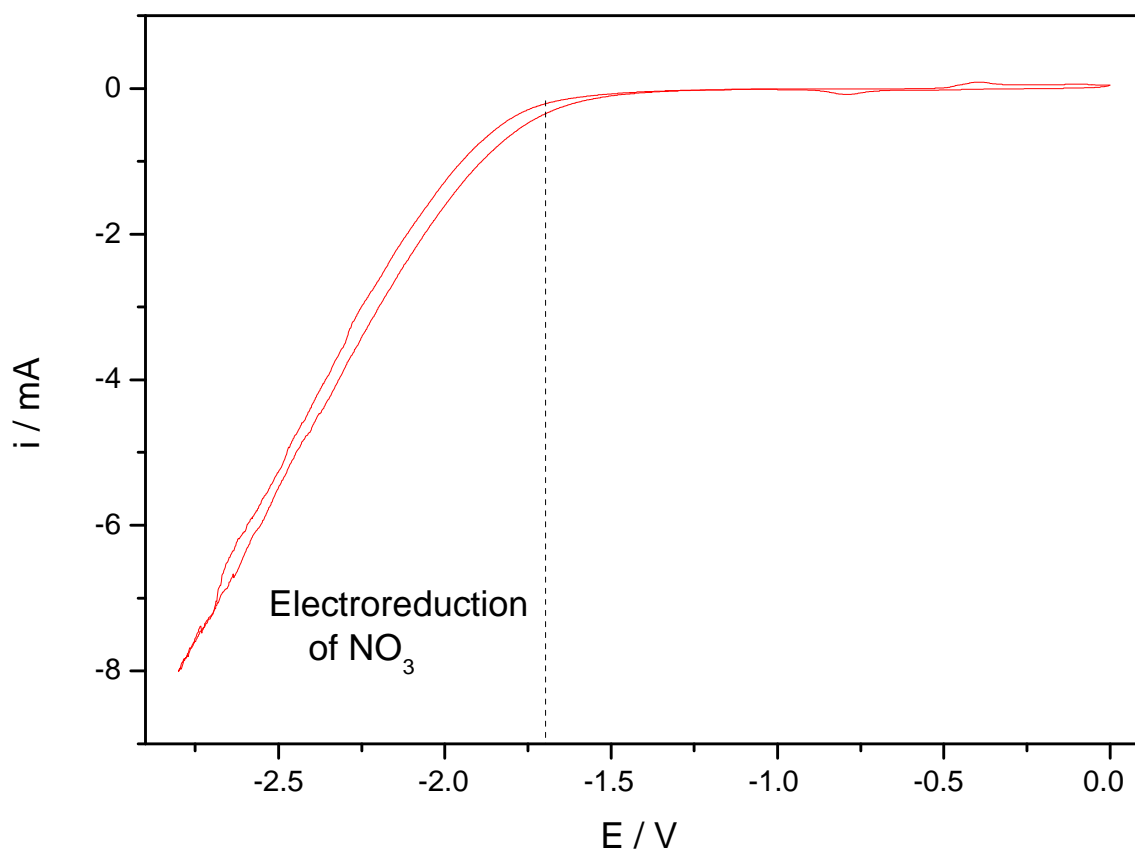


Figure 3-18: Monitoring the electroreduction of nitrate. CV was done from 0 down to -2.8 V reduction can be observed at all voltages lower than a \sim -1.7V.

By exposing a polytyramine coated electrode to the less aggressive electro-reduction regime, at a potential of only -2.0 V and monitoring after a 5 s reductive pulse it was expected that the tyramine might remain on the surface. However, as can be seen in Figure 3-19, even after 5 s there was considerable stripping of the polymer from the electrode.

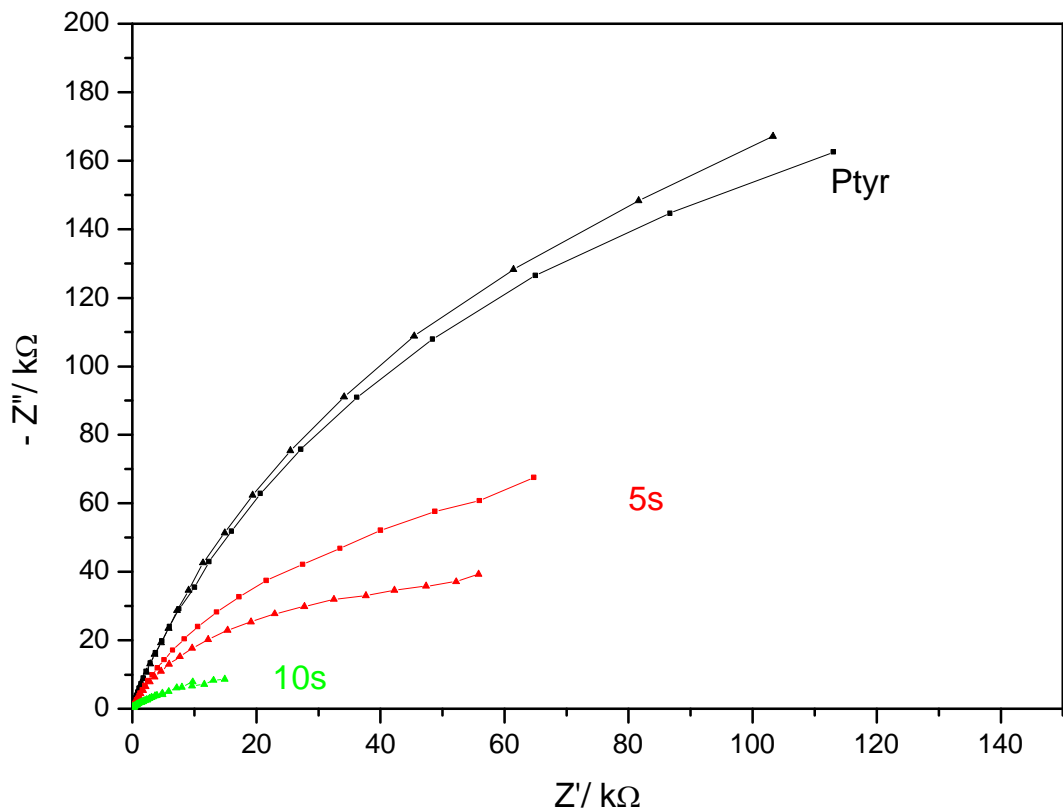


Figure 3-19: Electro-reduction of nitrate at -2.0 V. Consecutive Nyquist plots of a Polytyramine coated electrode after deposition of Polytyramine film (—■—) and then following 5 s (—●—) and 10 s (—▲—) electroreduction of Nitrate at -2V, the two plots show data collected from each working electrode of a dual sensor Dropsens electrode.

Since it was clear that even by limiting the reduction of nitrate by both the potential and the time, this method was too harsh, this approach was abandoned. Though it has been proven in certain biosensor systems (Abbady et al., 2011; Bhalla et al., 2010; Choi & Chae, 2009; Liron et al., 2002), it remains unsuitable for the type of transducers and tethering layers attempted here.

3.2.3.5 Fabrication of sensors using PTyr

Once the stability of PTyr had been confirmed, a myoglobin biosensor was constructed as with the previous PANI:2-ABA sensor used. This was again constructed using biotinylated anti-myoglobin antibodies following the functionalization of the amine containing surface with Biotin-NHS and the addition of NeutrAvidin. Similarly to previous work in Figure 3-3, construction of the sensor was monitored using EIS (data shown in Figure 3-20). From this data it is noted that the polytyramine layer deposited has an increased resistance and capacitance, thus supporting previous findings that an insulating layer is deposited.

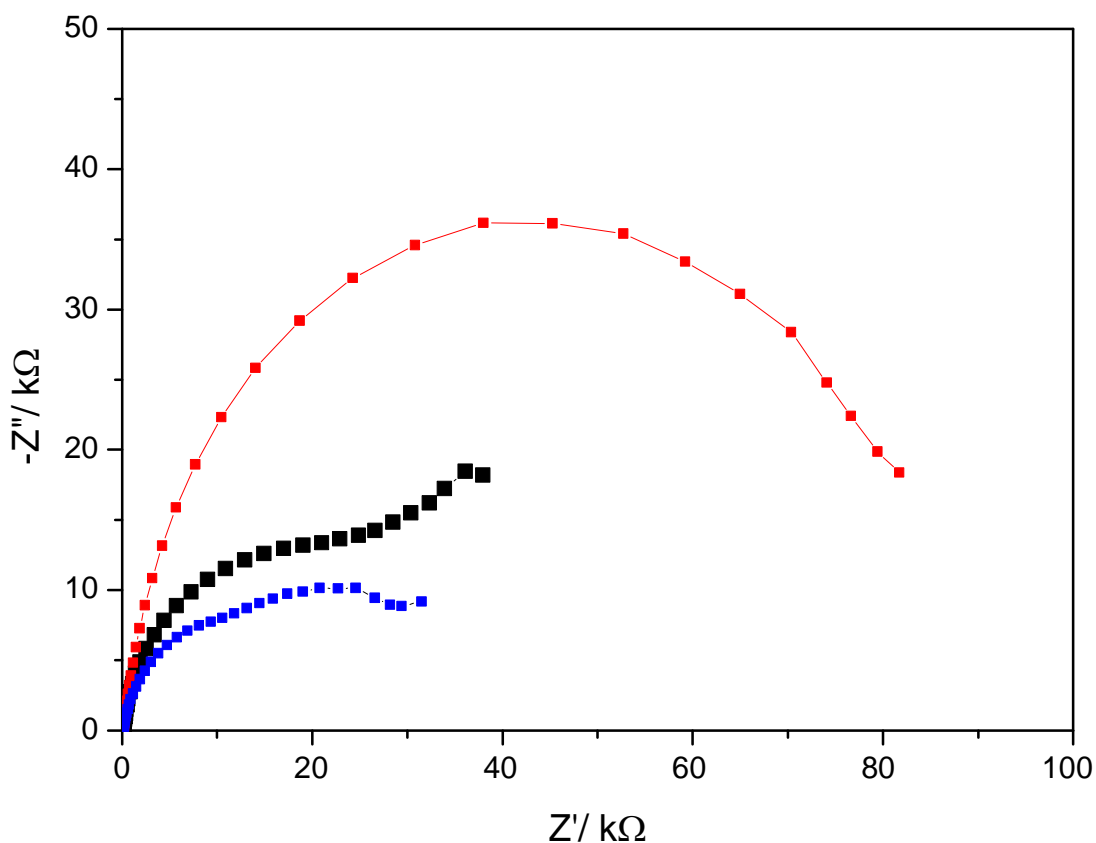


Figure 3-20: Nyquist plots of PTyr based sensor construction. EIS Scans were conducted for Bare gold electrode (—■—), deposited PTyr film(—■—) and fully constructed myoglobin sensor(—■—).

Once constructed, the myoglobin sensor was calibrated by incubating the sensor with consecutive concentrations (10^{-11} - 10^{-5} M myoglobin) and interrogating the sensor using EIS. From the Nyquist plots (data not shown) the change in R_{CT} was used to calibrate the sensor. It can be seen from the data in Figure 3-21 that the signal of the sensor is

comparable to that of the PANI sensor, with a slightly higher signal generated for the same concentration of analyte.

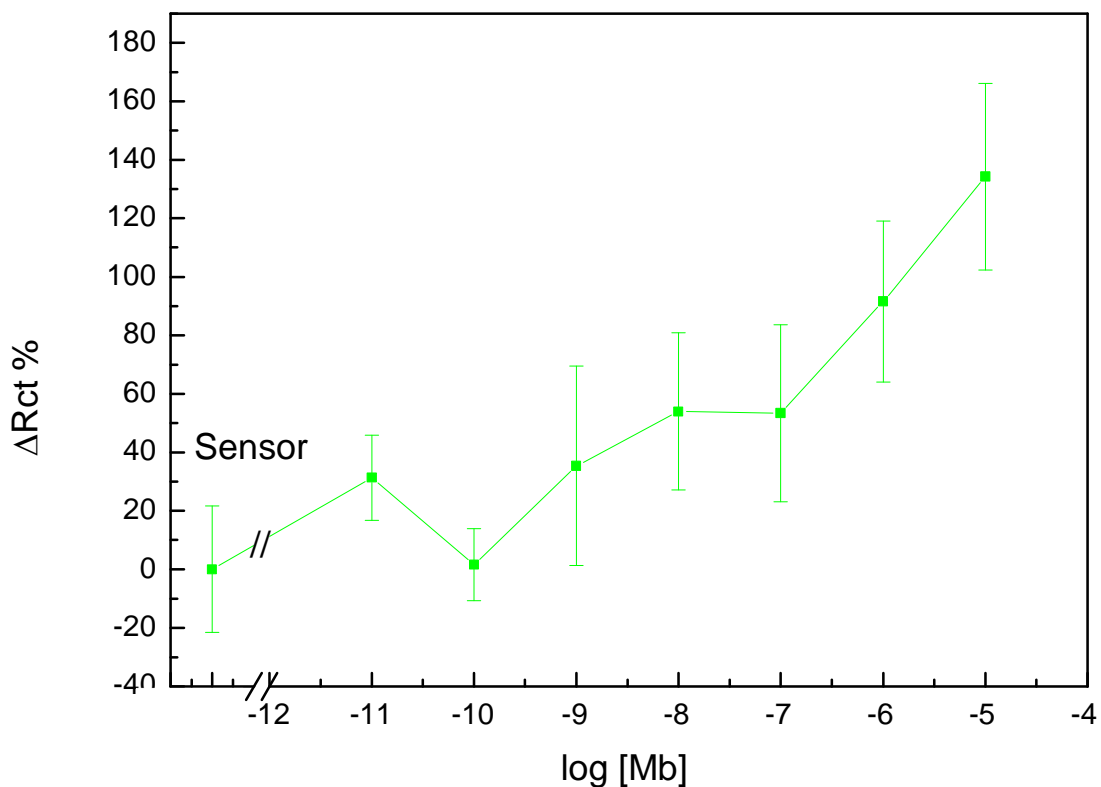


Figure 3-21: Calibration of a PTyr based immunosensor for myoglobin. R_{CT} was generated using the modified Randle's cell, ($n=8 \pm SE$)

3.2.4 Return to chemical approach using a complex regeneration buffer

When returning to a chemical buffer based approach to regeneration, the literature was re-assessed and the buffer composition was altered to include other components in order to satisfy the needs of regeneration and minimise alteration of the transducer surface. As discussed in Chapter One, regeneration involves altering the thermodynamic state at the biosensor interface to overcome the thermodynamic interactions and induce de-binding of the two.

To achieve this, the chaotrope DMSO was included as well as propylene glycol to reduce the effect of Van der Waals forces between the analyte and the receptor. A low level of the detergent SDS was also included to promote solvation of the analyte receptor interface. Using this improved buffer at pH 2.75 as before, regeneration as repeated using the fluidics cell, the overall composition of the regeneration buffer was therefore 100 mM glycine in 50% propylene glycol pH 2.75 1%DMSO .

3.2.5 Verification of incubation times, using fluidics.

Using the above regeneration buffer, a study was executed with an initial incubation time of 20 s. After PTyr was deposited a myoglobin biosensor was constructed and interrogated using EIS to obtain a baseline signal. The sensor was then incubated with 10^{-6} M myoglobin and interacted before being exposed to regeneration buffer for 20 s and rinsed in PBS. EIS interrogation was then repeated to assess the level of regeneration, this process was repeated 8 times to investigate the success of repeat regeneration cycles. In Figure 3-22, a clear difference between the "On" and "Off" signal can be seen though the off signal rapidly decreases and positive signal from the binding of analyte can only be seen for 3 cycles.

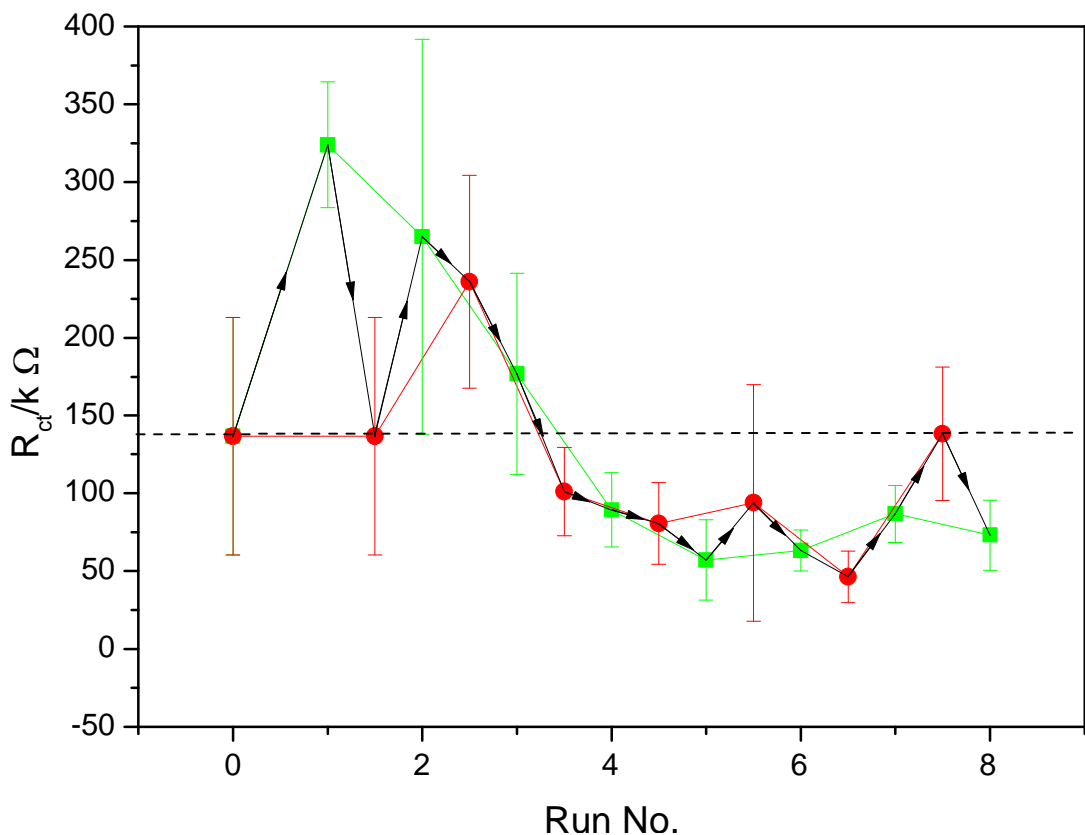


Figure 3-22: Regeneration of a myoglobin sensor using complex regeneration buffer. Regeneration was executed with 20s incubation in 100 mM Glycine in 50% propylene glycol pH 2.75 1%DMSO data shows Binding (—■—) and Debinding(—●—) ($n=8 \pm SE$)

The incubation time of the sensor in the regeneration buffer was decreased to 10 s in order to provide milder regeneration conditions and see if the number of successful cycles could be extended. From the Nyquist data (Figure 3-23), a clear difference can be seen between interrogations made when the analyte was bound vs. unbound interrogations following biosensor regeneration. This difference was observed for the first five repeats before additional repeats yielded no signal change.

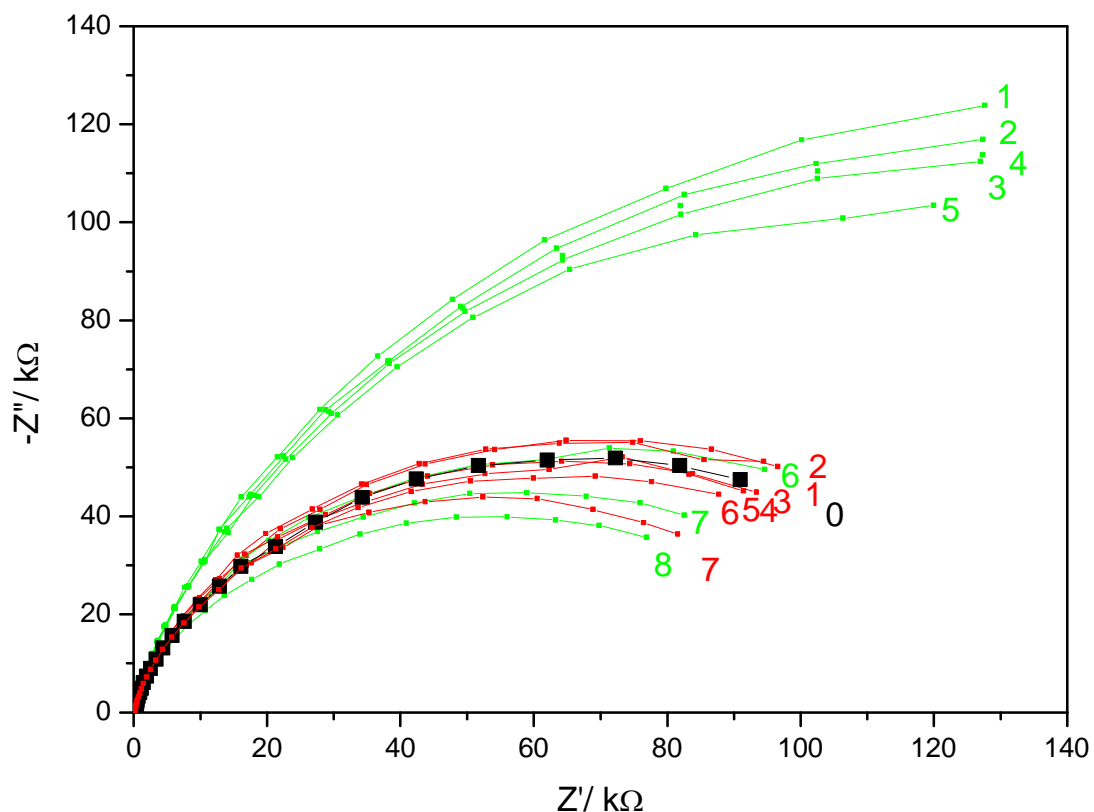


Figure 3-23: Nyquist plots of the successful regeneration of a myoglobin sensor. 5 successful cycles were observed. After baseline sensor signal acquisition (—■—) regeneration was executed with 10s incubation in 100 mM glycine in 50% propylene glycol pH 2.75 1% DMSO data shows data obtained after consecutive analyte exposure (—■—) as well as those obtained after regeneration(—■—).

This trend was also observed when analysing the change in charge transfer resistance (Figure 3-24). As in Figure 3-22, the difference signal acquired after analyte binding and after regeneration can be clearly seen. In Figure 3-24 however the decay of the signal between successive regeneration cycles is much less pronounced. In this experiment, a total of five regeneration cycles were achieved before the signal collapsed.

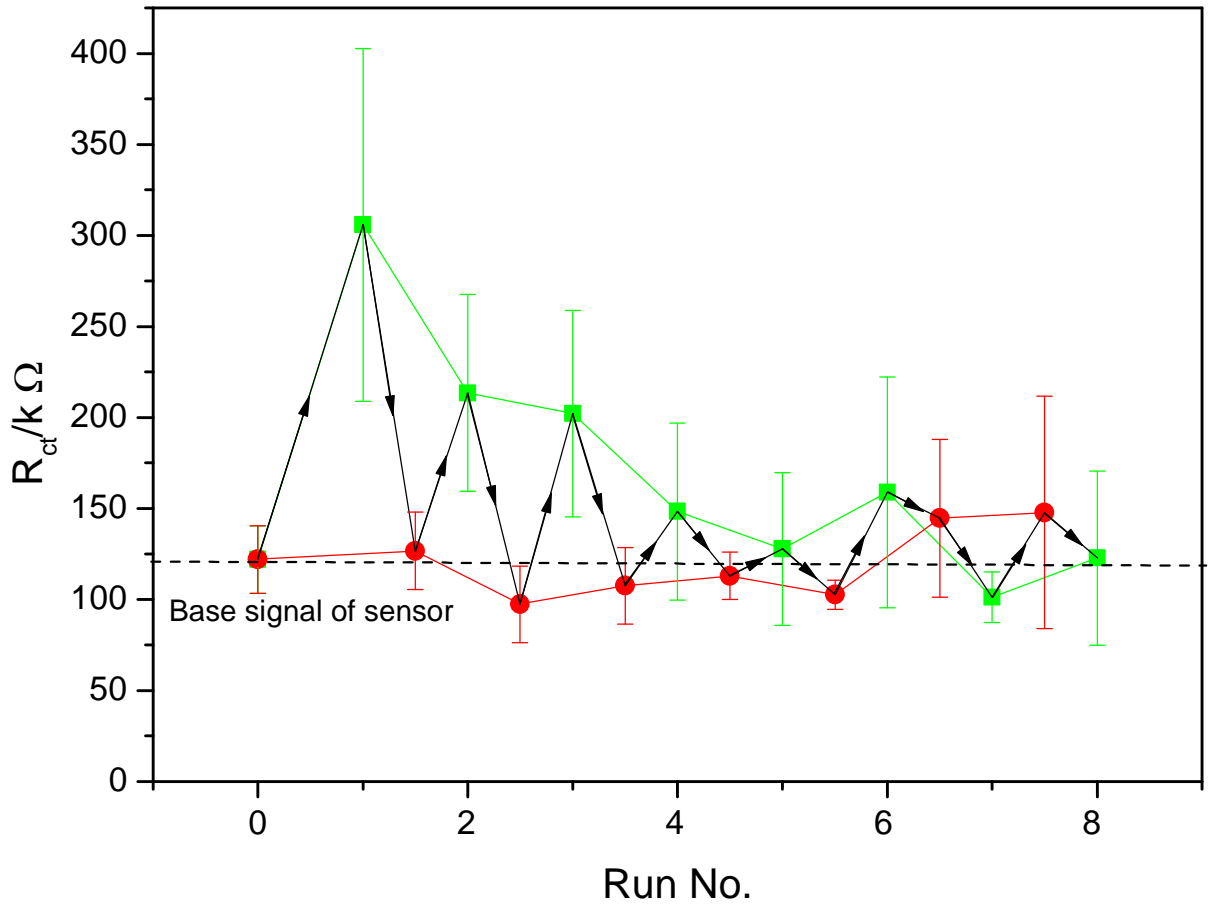


Figure 3-24: Successful regeneration of a myoglobin biosensor. Regeneration was executed with 20s incubation in 100 mM glycine in 50% propylene glycol pH 2.75 1%DMSO data shows binding (—■—) and debinding(—■—), ($n=8 \pm SE$)

3.3 Discussion

Based on observations made at AbCam, the re-folding of antibodies after binding to an immunogen was routinely achieved. It was shown that these methods can be used to successfully regenerate an electrochemical biosensor. Though previous work had shown that antibodies could be successfully regenerated in other types of biosensor (Drake & Klakamp, 2011) such as optical sensors (Wijesuriya et al., 1994) and in non-antibody electrochemical biosensors (Bhalla et al., 2010; Choi & Chae, 2009). This work has demonstrated the successful regeneration of an electrochemical immunosensor. This was achieved using 100 mM glycine at pH 2.75 in 50% propylene glycol pH 2.75 1% DMSO for 10 seconds which in a controlled fluidics setup this could be effectively extended to five repeats. Although the current protocol showed poor reproducibility, this work remains a good proof of concept and worth of further investigation because if a reliable method could be established, it would be of great interest for both research and commercial work. A crucial factor in the use of electrochemical sensors is the electronic state of the baselayer, particularly in the case of polymer based electrodes. Although acid conditions may be effective at de-binding antigens from the sensory antibodies, they may cause a charging effect of the surface and cause a large non-specific signal.

A microfluidics study which could enable parameters to be controlled much more tightly. When considering the incubation time in acid and rinsing, automatic control could assist in improving the reliability of results and increase the number of regenerated cycles which can be achieved. Automatic control may also help in the development of a point of use system, where computer controlled microfluidic packaging may be preferable for reducing the need for user expertise and ensuring consistency.

Polyaniline is a poor substrate for regeneration in electrochemical sensors as it has multiple electronic states. Though the regeneration of optical sensors on this substrate had been previously demonstrated (Nakamura et al., 2013), its multiple states lead to a change in its signal and interference with interrogation techniques. This reinforces the fact that the choice of substrate is a key consideration for electrochemical sensors if we aim to fabricate re-useable sensors.

Electro-reduction of NO_3^- was successful as shown from cyclic voltammetry experiments. However, the process proved too harsh and led to the stripping of PTyr. Electro-reduction is an elegant solution for the generation of localised regions of high pH but has been shown to require very stable surfaces so may not be appropriate for many biosensor

tethering layers. In a limited number of studies, this approach has been used to strip the electrode permitting reconstruction of the sensor entirely (Choi & Chae, 2009).

After an in-depth literature review a more complex buffer achieved regeneration. This allowed the transient denaturation of the antibodies on the biosensor to achieve five regeneration cycles. The recipe of the regeneration buffer was; 100mM glycine in 50%propylene glycol +1% DMSO at pH 2.75. If we assess the thermodynamic activity of the individual ingredients of this buffer it can help underline their active role in the regeneration process. First, glycine was used to enable a buffered low pH solution to be created, in this case pH 2.75. As discussed in 1.6.3 the shift of the pH away from the isoelectric point of the receptor protein may help denature the protein and induce decoupling of the analyte from the receptor. The next component, propylene glycol is a miscible diol, carbohydrate, its carbon basis and the negative charges associated with the alcohol moieties mean that it can behave as a very weak detergent enabling the screening of Van-der-vaals forces and compensate for any positive charges in a system. Dimethyl sulphoxide was included as a strong aprotic solvent which also behaves as a kosmotrope, this means that in an aqueous solution the DMSO will preferentially interface with biomolecules and restore interactions between water molecules. As hydration caging can be a vital component of antigen antibody interaction, DMSO provides a method of interrupting this process and assists in the decoupling of the analyte from the receptor. Through action of these different components there is an overall net shift in the thermodynamic state of the system in which the change in Gibb's energy favours the unbound state of the analyte which results in debinding at the sensor interface consequently allowing the regeneration and reuse of the biosensors.

Though there was a gradual signal loss, for instances where positive: negative signal determination is large, this provides a more than adequate solution as it would still allow for measurement. Another solution would be to have a calibration reading taken in parallel to ensure that any loss in signal could be accounted for and accurate measurements could continue to be taken.

4 Chapter Four: Results: Nanobody production, optimisation and characterisation

4.1 Antibodies

Work in this chapter focuses on the development of novel bioreceptors to detect rabbit IgG. The analyte IgG was selected due to the availability of bioreceptors for detection and the commercial needs of AbCam Plc. As well as providing a useful tool for quality control and process management the development of this sensor would represent a valuable tool for use in research environments as well as a sensor to assist in the management of various immunological disorders. Throughout this chapter, conventional antibodies against rabbit IgG, a goat anti rabbit polyclonal IgG, was used as the benchmark by which to compare other bioreceptors. A summary of the receptors used in both this chapter and the next is shown in Figure 4-1

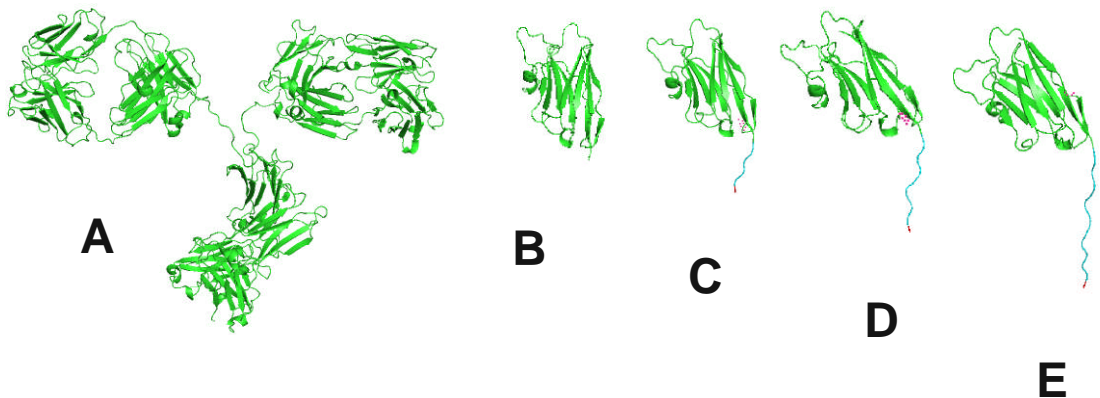


Figure 4-1: Schematic of different bioreceptor constructs used. Including (A) full IgG (1IgG), and nanobody (B)(1MEL) with 5, 10 and 15 amino acid linker arm, respectively (C,D and E). Alongside complete camelid single domain antibody (F) (for comparison).

4.2 Nanobodies.

Nanobodies to rabbit IgG were used as a novel bioreceptor. Previous work at Abcam had isolated the DNA sequence coding for the P8D8 nanobody which binds rabbit IgG. This DNA had been isolated following immunisation of an alpaca and panning using rabbit IgG in phage display as outlined in Chapter One. During panning the binders showed no cross-reactivity when tested against IgG from other animals (sheep, goat, mouse and others) an improvement of antibody technology where this cannot be assessed until after the production of the antibody.

Once the DNA had been isolated, its sequence was ligated into a plasmid using T4 ligation as detailed in Chapter Two. The *pHEN6* vector used has sites for the restriction enzymes *PstI* and *BstEII* at either side of the nanobody coding region. In addition there is an *EcoRII* site in which the coding sequence for a His₆-Tag is commonly ligated in order to simplify purification of the resultant nanobodies. A summary of the plasmid sequence is shown in Figure 4-2. *pHEN6* is useful as it also codes for ampicillin resistance and so allows downstream selection of colonies when expressing protein.

4.2.1 Vector selection and recombinant molecular biology.

Alongside the *pHEN6* vector coding for the P8D8 anti-rabbit IgG (referred to hereafter as the insert), separate *PHEN6* vectors were synthesised by replacing the His-tag region with a polynucleotide coding for the peptide spacer arm (5, 10 or 15 aa based on a GGGGS repeating motif) followed by a His-tag again in order to simplify purification. A summary of the plasmids used can be seen in Figure 4-2.

Plasmids were digested as described in Chapter Two and an Agarose gel cartridge (E-gel[®]) was run to confirm digestion and well as isolate the fragments. The gel was imaged before removal of the DNA, Data shown in Figure 4-3. The running of the gel was continued to enable collection of the Vector in the lower well. The times taken to retrieve the DNA Fragments were 10 min for the nanobody insert and approx. 40 min for the vectors.

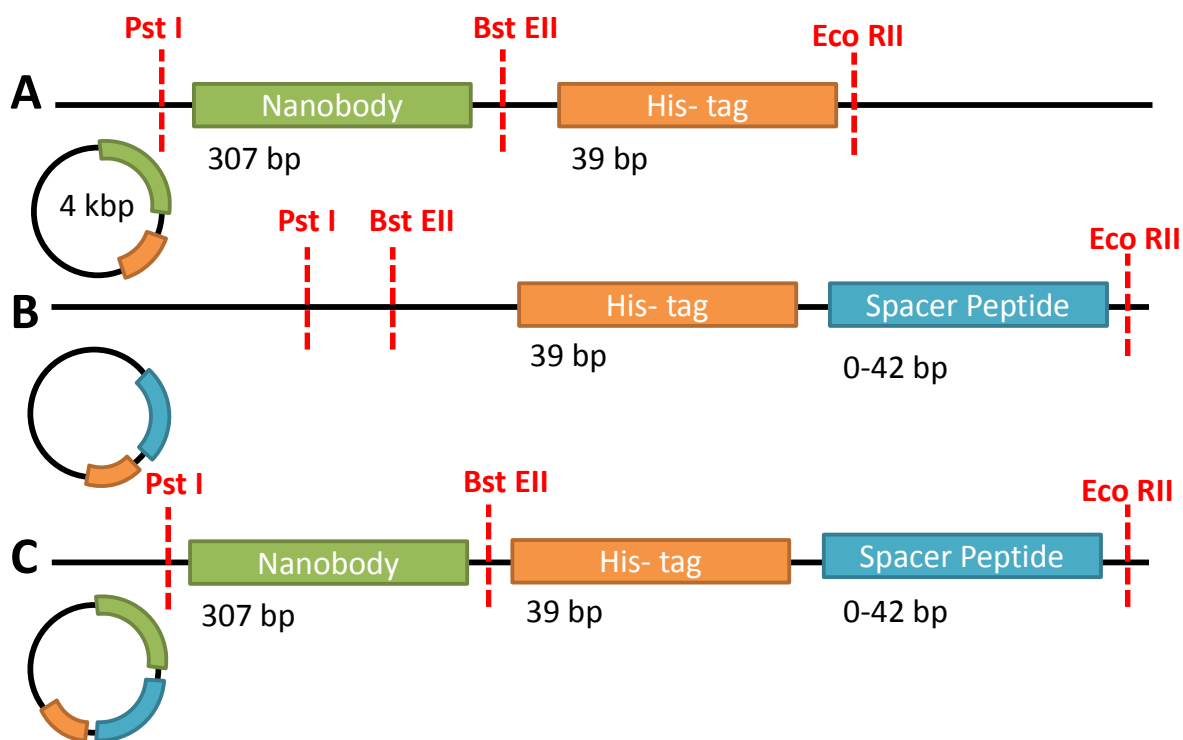


Figure 4-2: Map of *pHEN6* vector used for expression of nanobodies in *E.Coli*. (A) *pHEN6* containing the nanobody insert (green) with restriction sites displayed, (B) Modified *pHEN6* with spacer arm (blue) and his tag (orange), (C) successfully transformed plasmid containing both P8D8 coding vector and insert coding for nanobody with spacer arm.

Upon removal from the gel, the vectors were eluted sequentially, in order of ascending base pair length. The unmodified *pHEN6* vector coding for the P8D8 nanobody with only a his₆-tag between *BstEII* and *EcoRII* sites was removed the first. The Modified *pHEN6* vectors coding for P8D8 nanobodies with spacer arms were sequentially removed from the gel with a gradual increase in the time taken for the DNA to reach the collection well up to the final vector, coding for a 15 amino acid spacer. By the time that the vectors were collected from the agarose gel, some lateral shift could be seen in the lanes as the vector DNA progressed through the agarose gel. This may be due to heating of the gel or depletion of ions (Wilson & Walker, 2010).

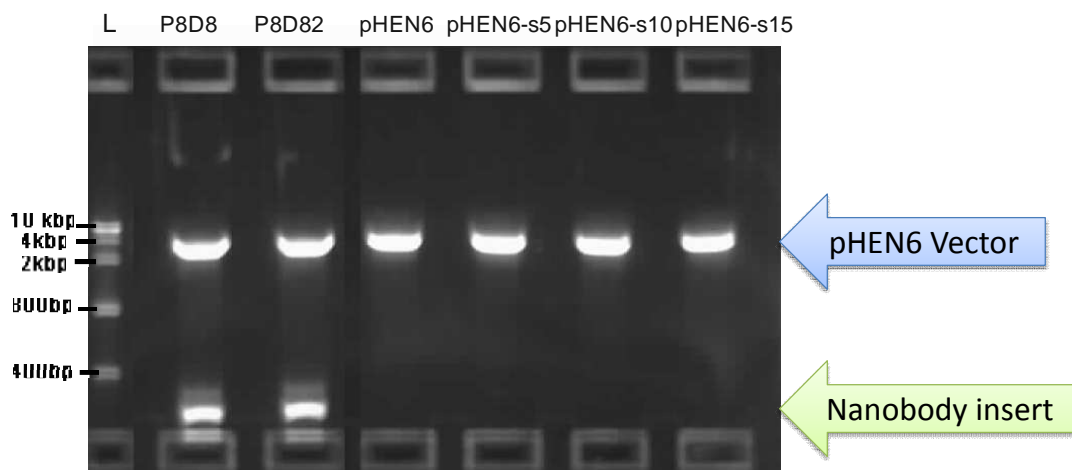


Figure 4-3: E-gel image of vectors after digestion. The gel was run to remove nanobody insert and check for contaminants. Lanes show: P8D8, control *pHEN6* vector coding for 'P8D8' nanobody from Abcam verified stock; P8D82, *pHEN6* vector digested from new stocks; B vector, vector coding for his tag only, P8D8-S5 coding for nanobody with 5 aa spacer; P8D8-S10 coding for nanobody with 10 aa spacer P8D8-S15 coding for nanobody with 15 aa spacer.

After removal from the gel (Figure 4-3), plasmids were then ligated according to methods in Chapter Two. Stable plasmids were then quantified using a Nanodrop® micro spectrophotometer to ensure sufficient yield had been achieved, the plasmids were then stored at -20 °C before use. To confirm successful plasmid ligation, transformation of *E. Coli* was performed using the heat shock technique with competent Nova blue cells, in order to increase plasmid yield. The resulting cells were then plated onto ampicillin plates and allowed to grow under antibiotic selection. Colonies were then selected and grown in TB media with ampicillin ready for miniprep. Plasmid DNA was extracted using a Qiagen Miniprep kit according to manufacturer's protocols and the yielded DNA concentration was verified using a Nanodrop micro spectrophotometer before being sent for sequencing.

4.2.2 Sequencing data

Plasmids were sent to Source Bioscience for sequencing, full sequence data confirmed the inclusion of peptide spacer and successful ligation of the nanobody scaffold with correct CDR sequences. DNA and amino acid sequence data have been omitted due to commercial sensitivity. Access can however be applied for by contacting Abcam Plc.

4.2.3 Expression of nanobody peptide.

Once plasmid identity had been confirmed, plasmids were transformed into competent WK6 cells using the heat shock technique and cultured as described in Chapter Two. The periplasm was then extracted and nanobodies were purified as outlined.

To assess the purity of the extracted proteins, aliquots of the peak concentration were run on a MES gel under both reducing and non-reducing conditions. Results are shown in

Figure 4-4. Not only can the overall purity of the samples be observed but it can be seen that the nanobodies with peptide spacers had formed dimers which were reduced when the gel was run under reducing conditions.

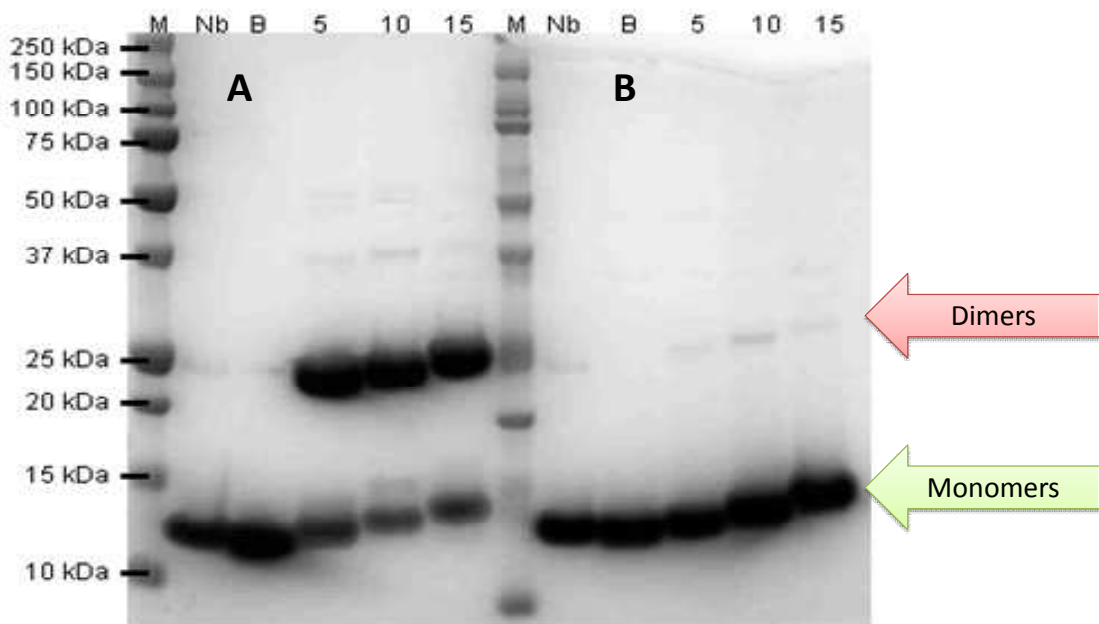


Figure 4-4: SDS-PAGE of nanobodies. Under both non-reducing (A) and reducing (B) conditions. M= marker, Nb= control P8D8D nanobody, B= basic P8D8D nanobody (spacer), 5, 10 and 15 =P8D8D nanobody with respective amino acid linker. On the left panel the formation of dimers can be observed. Whereas the inclusion of 10 mM DTT led to their almost complete removal b reduction (right hand panel).

The presence of these native dimers meant that to enable any directed sulfhydryl chemistry, e.g. for conjugation at a biosensor interface the dimers had to be reduced. If we consider the sequences obtained, it is also crucial to note that there is another pair of cysteines within the structure of the nanobody scaffold itself. Though the DTT may be

good for the reduction of dimers, its aggressive nature may mean that it could reduce this disulphide bond too and affect the function of the nanobody.

4.2.4 Disulphide cleavage using TCEP beads

Using previous protocols from the Millner lab (Ahmed et al., 2013; Billah et al., 2010; Caygill et al., 2012) tris(2-carboxyethyl)phosphine (TCEP) was initially investigated as method of disulphide reduction. By incubating the nanobody dimers with TCEP beads separation was simplified as simple centrifugation was permitted as an adequate method for separation of the TCEP, a necessary step for the downstream use of reduced monomers. After 90 min incubation with 10 mM TCEP beads in degassed PBS-EDTA, the samples were immediately placed in a non-reducing SDS-PAGE sample buffer along with untreated nanobodies and nanobodies which had been incubated with DTT to ensure reduction. Data from this is shown in Figure 4-5.

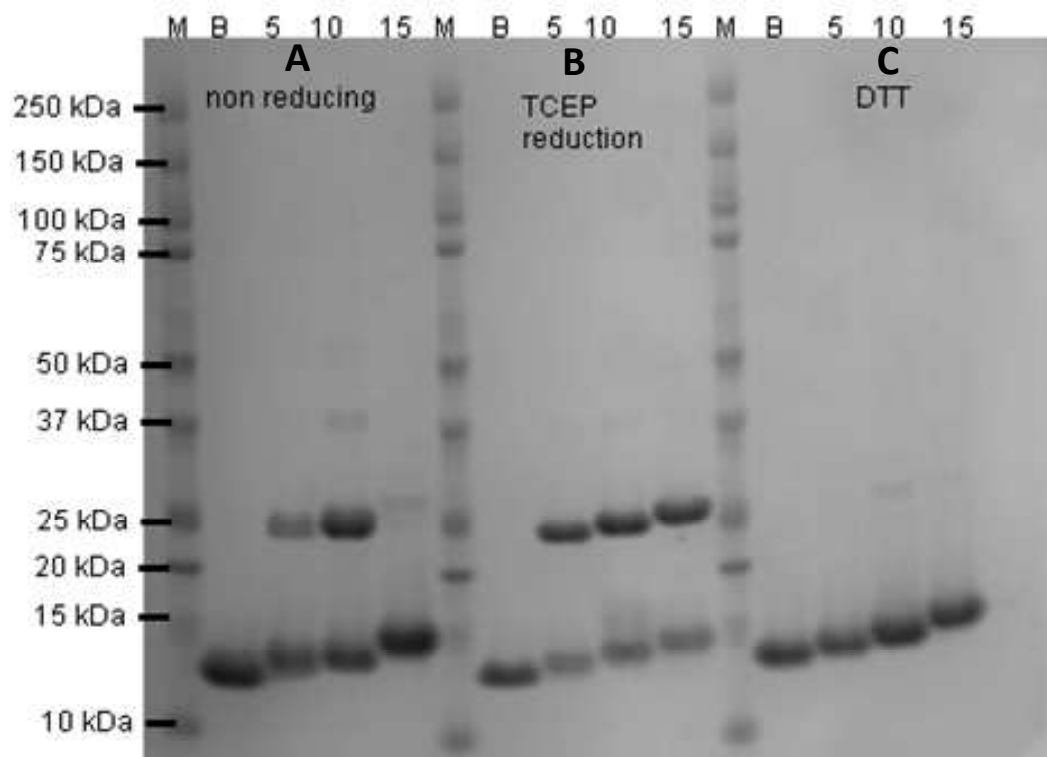


Figure 4-5: SDS-PAGE of nanobodies subjected to TCEP reduction. SDS-PAGE was conducted using non reducing conditions after TCEP Reduction (B). This was compared to non-reducing SDS-PAGE (A) and Reducing SDS-PAGE (C), M= Marker, B= basic P8D8D nanobody (no spacer), 5, 10 and 15 = P8D8D nanobody with respective amino acid linker. On the left panel the formation of dimers can be observed. Whereas the inclusion of 10 mM DTT led to their almost complete removal by reduction (right hand panel).

From this data, it can be seen that though TCEP had been proven to be a strong enough reducing agent in similar studies, in the case of nanobodies there is still a significant proportion of dimers present in the sample. Densitometry analysis was done on the gel from Figure 4-5 and whilst in the positive control it can be seen that over 90% of dimers had been reduced when DTT was used, in the case of TCEP only 30% of dimers were successfully reduced.

4.2.5 Disulphide cleavage using β -MEA

In order to provide effective reduction of nanobody dimers, a stronger reducing agent β -mercaptoethylamine (also known as cysteamine or 2-MEA) was selected. As with previous protocols, buffers were degassed and EDTA was included to minimise the reformation of dimers after separation from residual MEA. Again, a non-reducing SDS PAGE gel was run to assess the reduction of nanobody dimers, Samples were compared with untreated nanobodies and those incubated with DTT. Data from these experiments are displayed in Figure 4-6.

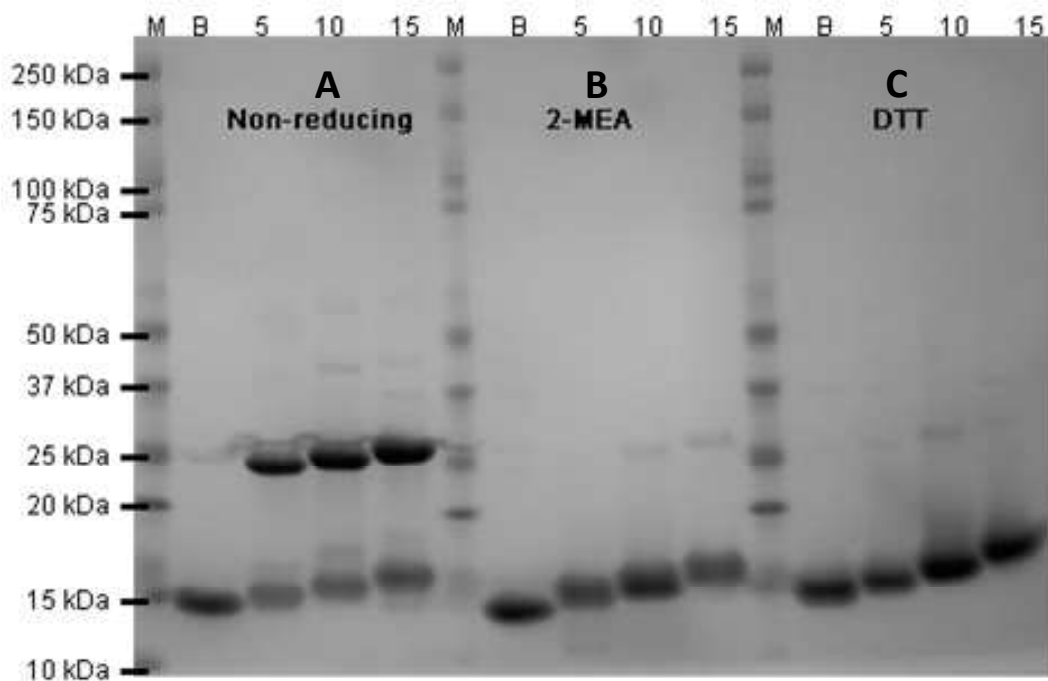


Figure 4-6: SDS-PAGE of nanobodies subjected to 2-MEA reduction. SDS-PAGE was conducted using non reducing conditions after 2-MEA Reduction (B). This was compared to non-reducing SDS-PAGE (A) and Reducing SDS-PAGE (C), M= Marker, B= basic P8D8D nanobody (no spacer), 5, 10 and 15 = P8D8D nanobody with respective amino acid linker. On the left panel the formation of dimers can be observed. Whereas the inclusion of 10 mM DTT led to their almost complete removal by reduction (right hand panel).

From Figure 4-6 we can see that the 2-MEA has been much more successful in the reduction of nanobody dimers, with results comparable to reduction using DTT, a strong reducing agent. Again, taking densitometric data 2-MEA reduced between 100-80 % of dimers. Interestingly, dimer reduction was slightly less successful (~80%) when studying nanobodies with the longest peptide spacer. This trend was observed in nanobodies treated with both DTT and 2-MEA. Percentage cleavage can be seen below in Table 4-1.

Conditions	Receptor	B	5	10	15
No Treatment	Monomer	100	24	30	29
	Dimer	0	76	70	71
2-MEA	Monomer	100	100	85	80
	Dimer	0	0	15	20
DTT	Monomer	100	100	87	97
	Dimer	0	0	13	3

Table 4-1: Densitometry data from 2-MEA reduction of nanobody dimers.

In order to understand this phenomenon a higher resolution approach was taken to investigate the reduction of nanobody dimers using 2-MEA. After incubation with 2-MEA at 37 °C for 90 min, samples were subjected to size exclusion chromatography, by running on a Superdex® column, in an Akta® Explorer HPLC system. Running samples at 1ml.min⁻¹ absorbance at both 280 nm and 220 nm was monitored in order to allow more accurate quantification than previous densitometry experiments. Absorbance data at both 280 nm (for aromatic residues) and 220 nm (for peptide bonds) is shown in Figure 4-7

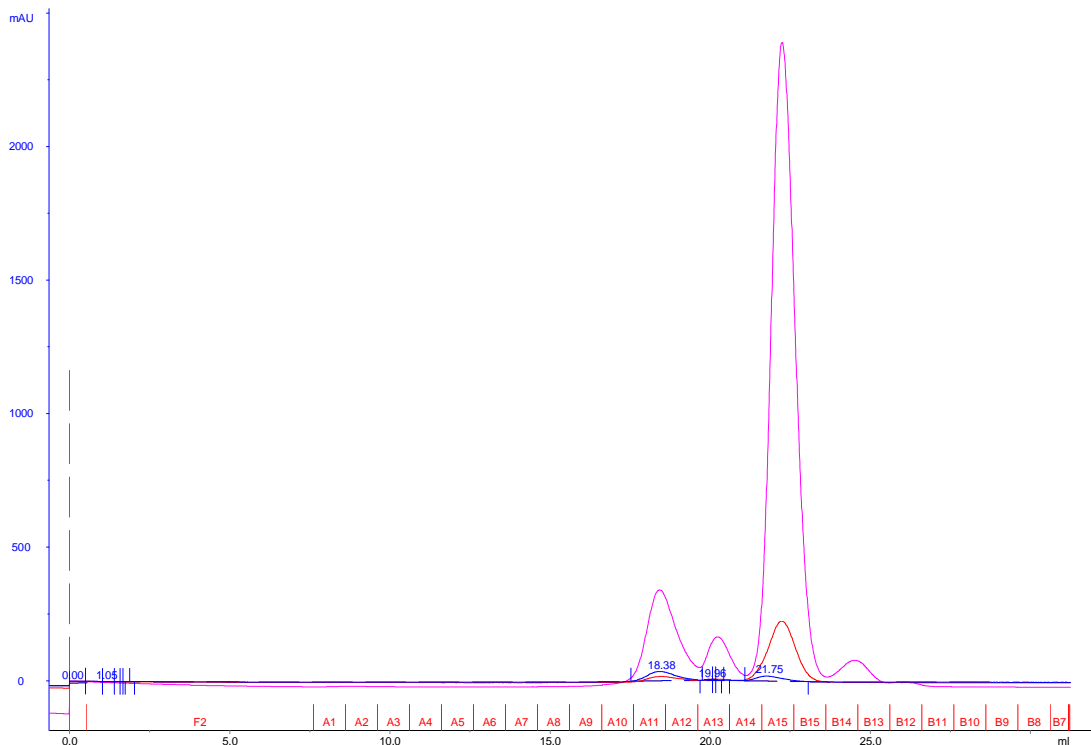


Figure 4-7: Size exclusion chromatography of reduced nanobody dimers. The absorbance over an 30 ml injection course (collected 1ml fractions, red) is shown, absorbance was measured at, 280 nm (), 260 nm() and 220 () nm. Dimers eluted first at 10-12ml with monomers eluting later. The larger monomer peak was observed between 14-16 ml fractions and the overall purity observed in Figures 4-5 – 4-7 indicate that these peaks can only be due to the presence of nanobodies.

This data supports previous studies and confirms the successful reduction of nanobody dimers using MEA. From calculations, the reduction of monomers was 80% successful. Therefore when considering the nanobody concentration on a sensor surface, 120% of the required concentration was used to account for the unreactive nanobody (i.e. that in dimeric form). It is important to remember however that this was time dependant and that once monomers were separated from the 2-MEA, given enough time will reform dimers. This highlights the importance of working quickly to ensure the receptor concentration can be effectively controlled.

4.2.6 Immunoprecipitation of rabbit IgG from serum.

As reduction comparable to that of DTT was observed in the previous investigations, it was essential to confirm that the reduction has not irreparably damaged the nanobody or that analyte recognition has been interrupted, particularly when considering the presence of a disulphide bond in the nanobody scaffold structure. In order to do this, a two-elution step Immunoprecipitation experiment was planned, in which eluates could be interrogated

using immunoblotting. A schematic of the experimental approach can be seen in Figure 4-8. Western Blot was not attempted as by using immunoprecipitation, sulfolink chemistry could be easily employed to ensure both cysteine residues of the spacer arm were functional for conjugation as well as the immunogenicity of the nanobody.

Beads used for immunoprecipitation were either NHS carboxy ester tagged (for basic nanobody) or Sulfolink® (for nanobodies with peptide spacer arms) allowing amine containing or cysteine residues to be exploited respectively. The nanobodies were conjugated to the beads using the appropriate chemistries, in the case of Sulfolink beads, dimers were reduced using 2-MEA as above before being applied to the beads. An outline of the methods used is given in Chapter Two.

After the nanobodies had been conjugated to the beads, they were incubated with 10% (v/v) rabbit serum in PBS containing rabbit IgG. After appropriate and multiple washing steps (as outlined in Chapter Two), a first acid elution was conducted in order to elute immunogenically bound rabbit IgG, Fractions were immediately neutralised in Tris to prevent damage to the IgG. After a brief wash step, a DTT elution was executed in order to reverse the Sulfolink binding and release bound nanobodies from the beads.

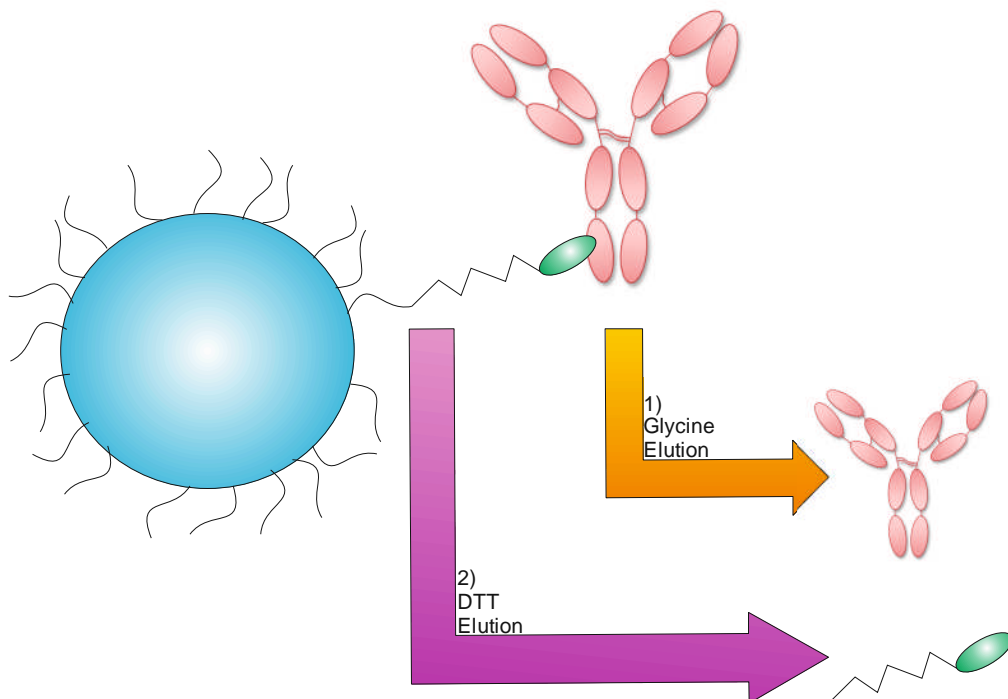


Figure 4-8: Schematic for immunoprecipitation experiments. After Sulfolink conjugation of the bead with the modified nanobody construct, rabbit serum was applied and unbound proteins were washed away. A two-step elution was then executed with (1) primary acidic glycine elution pH 2.0 (orange) to liberate bound IgG and then (2) a DTT elution (magenta) to release Nanobody bound by Sulfolink chemistry.

The fractions of these different eluates were collected and analysed by running on an SDS-PAGE gel which was stained using Coomassie blue Figure 4-9 (A). Alongside the elutions, rabbit serum was run to enable comparison between eluted samples and sera proteins. This helped to confirm the presence of rabbit IgG in the glycine elution lane and confirm that the lower band seen (12-15KDa) was the nanobody as it was absent in rabbit sera samples. In addition to a Coomassie staining, proteins were further identified by western blotting. Fractions which had been run on an SDS-PAGE gel were transferred to a nitrocellulose membrane and interrogated in one of two ways. Either a goat anti rabbit – HRP conjugate was used to interrogate the membrane as in Figure 4-9 (B) or an anti his-tag –HRP Conjugate was used Figure 4-9(C). When interrogating using the anti-rabbit HRP, it was observed that signal was generated in both sera lanes and lanes for the glycine elution this confirms that rabbit IgG had eluted using an acidic buffer and therefore that the rabbit IgG had successfully bound to the nanobody which had been attached to the bead.

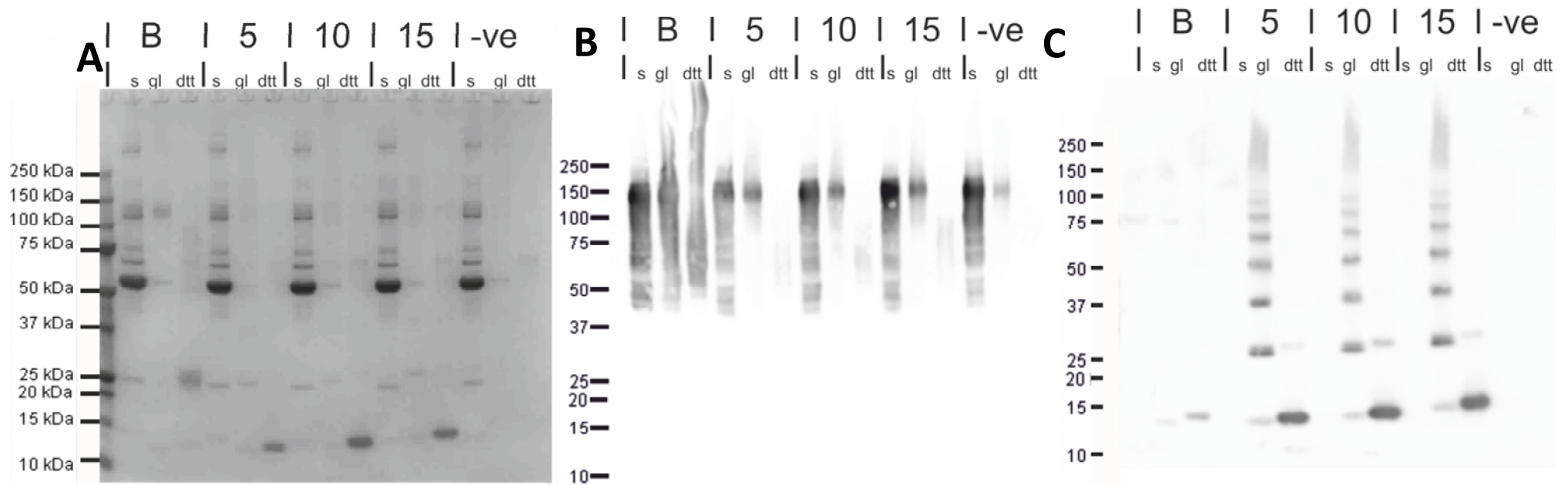


Figure 4-9: Blotting experiments from immunoprecipitation fractions. Coomassie stain (A) and immunoblot using anti rabbit IgG secondary Dako cat# P0448 (B) and anti His₆-tag secondary Abcam ab1187 (C). Across all panels diluted sera (s) are compared with fractions yielded from immunoprecipitation elutions, both glycine (gl) and DTT (dtt) respectively. In each panel B, 5,10, 15 are the respective nanobody constructs with 5,10 and 15 amino acid spacer respectively alongside a non-specific (C) control where Sulfolink[®] beads were blocked with buffer containing cysteine as a negative control (-ve)

In the second immunoblot experiment, the nanobody was identified using an anti-His₆-HRP conjugated secondary antibody (Figure 4-9 (C)). In the lanes where DTT Elution had been executed, a clear band can be seen (12-15Kda) along with weaker bands corresponding to nanobodies which have reformed dimers upon elution (24-50KDa); this clearly shows the elution of the Sulfolink conjugated nanobodies in the presence of DTT. In addition to the bands indicative of nanobody elution a regular ladder of proteins is observed in the lanes associated with glycine elution of the bound IgG. These bands do not adequately correspond to the mass of IgG fragments so must be protein of another source. As these bands cannot be observed on the Coomassie stain however they may represent low concentrations of protein which have bound the Anti-His₆ – HRP Conjugated antibody. As signal generated using an enzyme reporter amplifies the signal generated by the protein this may explain their presence as visible bands in the immunoblot.

It is important to highlight the presence of other bands in this blot; this is possibly due to the use of an anti-His₆- HRP antibody which may bind to other negatively charged sera proteins present in the glycine elution which have co eluted with the antibodies. It is likely that they are at very low analyte concentrations as the directly quantitate method of Coomassie staining has failed to generate a signal at these molecular weights. As this signal in western blot is developed by the action of the HRP conjugated antibody the signal is amplified rather than directly proportional so even low levels of bounding can generate a signal. This would indicate that the proteins eluted are at a much lower concentration than the nanobodies which reflected in the signal intensity from. The band for these contaminants is much lower than the Band observed for the eluted nanobodies in the DTT elusion lanes.

The data obtained so far in this chapter has confirmed that nanobodies can be produced with a peptide spacer arm allowing for oriented conjugation. Whilst dimers of these nanobodies form natively, they can be selectively reduced and this does not negatively impact upon their binding capacity.

4.3 Analysis of binding parameters using BLI

In order to assess the binding parameters of the nanobodies which had been expressed and compare the different binding constructs an optical biosensor system was used. All of this work was done using a Fortebio Blitz system in which binding is assessed in terms of change in the optical thickness at the biosensor interface as explained in chapter one. The Fortebio® Octet system uses interferometry with the bioreceptor immobilised at the end of a fibre optic probe. As well as comparative data for later electrochemical studies this allowed an investigation into key binding parameters of both the antibody and the nanobody). As a control, the goat anti-rabbit IgG antibody receptor was first conjugated to Forte Bio amine reactive probes (ARP2) using EDC-NHS conjugation chemistry, following manufacturer's protocols. Real time binding data from this experiment is shown Figure 4-10. From this data we can see the steep association curve followed by a much shallower dissociation curve. When comparing specific to non-specific signal (i.e. using sheep IgG for analyte) the difference can clearly be seen.

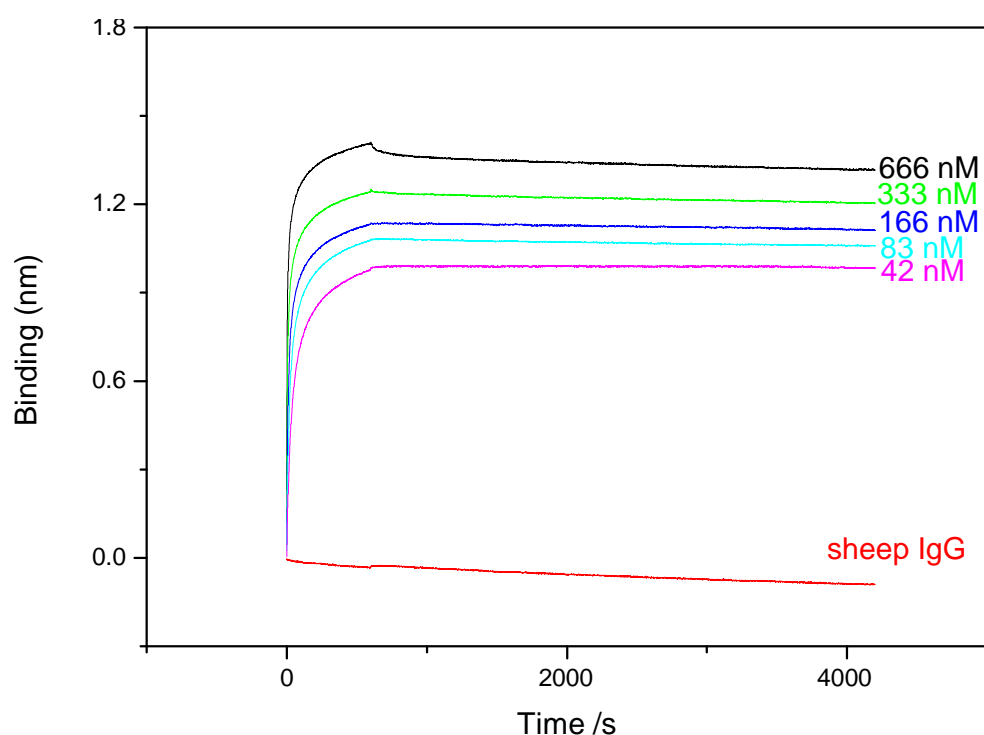


Figure 4-10: Real time binding data for an antibody based rabbit IgG sensor. A Fortebio probe was functionalised with goat anti rabbit IgG antibody. Association data was collected for 600 s before allowing 3600 s for dissociation data to be collected. After receptor conjugation and baseline measurement probes were incubated with rabbit IgG at: 666 nM (), 333 nM (), 166 nM (), 83 nM (), 42 nM (), as well as Sheep IgG at 666 nM ().

As the control used was sheep IgG, this confirms that the antibody used shows no cross reactivity to the sheep IgG. Another feature of the data is that is important to observe is the binding signal reached at every concentration. Using this data it is possible to calibrate a sensor and compare the signal yield from each bioreceptor used. Using this technique with data obtained from the previous figure, Figure 4-11 was generated.

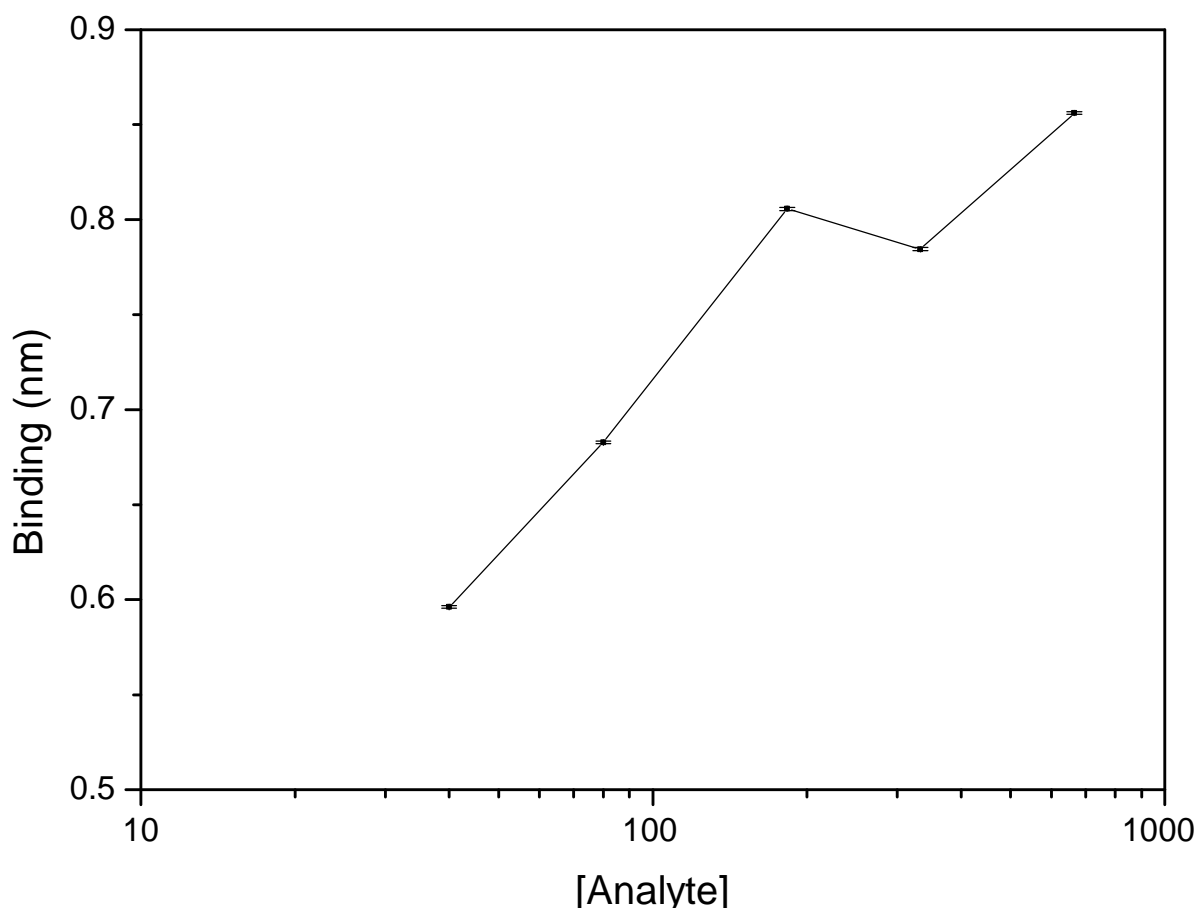


Figure 4-11: Calibration using R_{\max} data from the Octet. Maximum binding signal was taken from the association curve and plotted against the concentration of analyte for that given experiment. As can be observed a positive correlation was achieved, Error bars represent Δ error [R_{\max}] a figure which is generated in the Fortebio analysis software.

The same experiment as before was repeated for each of the nanobody. P8D8 nanobodies were attached to the probe surface using the same amine to carboxyl conjugation chemistry as when using IgG as the receptor (EDC-NHS). After initial scoping work, the concentration of the nanobody was optimised on the probe surface to minimise artefacts from nanobody aggregation on the surface of the probe which could be observed as a distinct curvature in the dissociation curve. The nanobody concentration was therefore optimised at 60 nM. A full analyte concentration range was run using 60nM P8D8

nanobody in the conjugation step. The sensor to rabbit IgG was then run using amine reactive probes in the Fortebio Octet as before. Data from these experiments are shown in Figure 4-12.

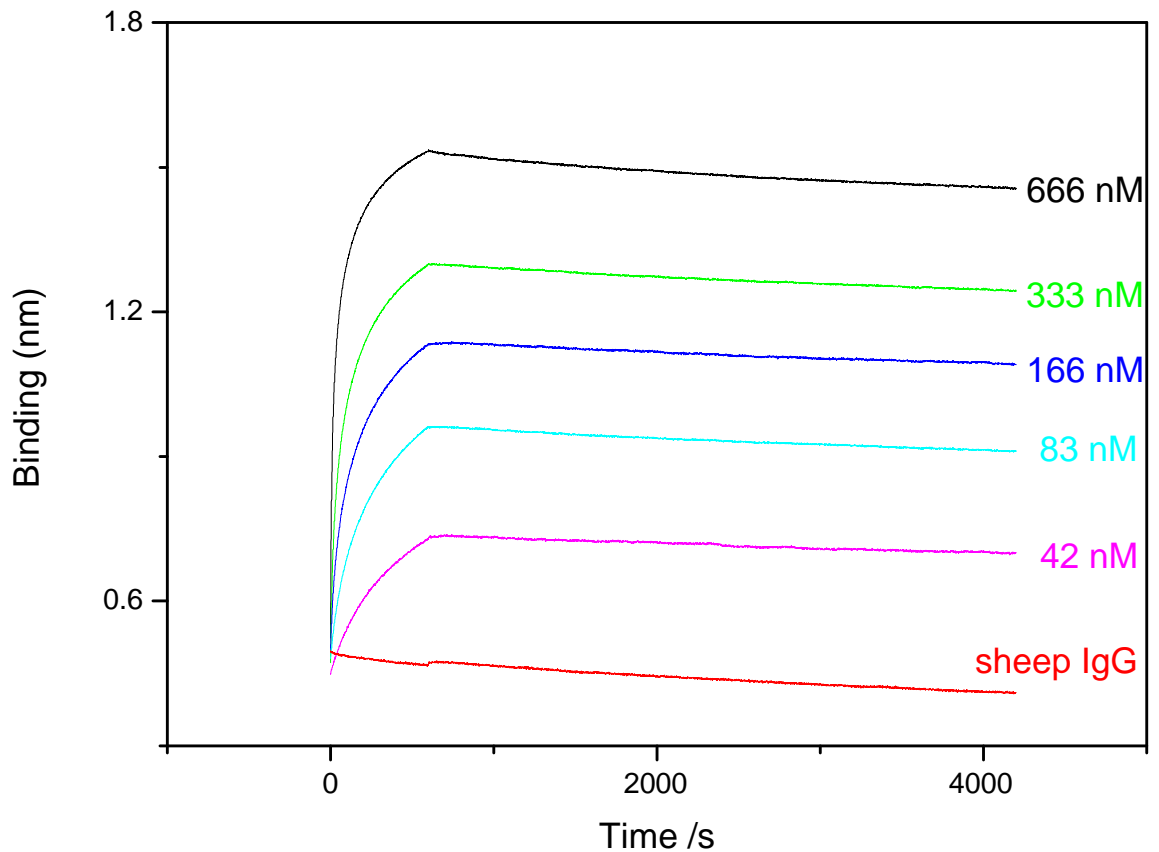


Figure 4-12: Real time binding data from a full titration of nanobody based sensor. Association data was collected for 600 s before allowing 3600 s for dissociation data to be collected. After receptor conjugation and baseline measurement probes were incubated with rabbit IgG at: 666 nM (), 333 nM (), 166 nM (), 83 nM (), 42 nM (), as well as Sheep IgG at 666 nM ().

Again from this data a clear difference could be seen between non-specific and -specific analytes as well as a gradual increase in the level of signal reached at each concentration. The total size of the signal generated was also broadly comparable to that observed when using IgG as the receptor. The signal obtained in both nanobody and antibody receptor systems was then compared shown in Figure 4-13.

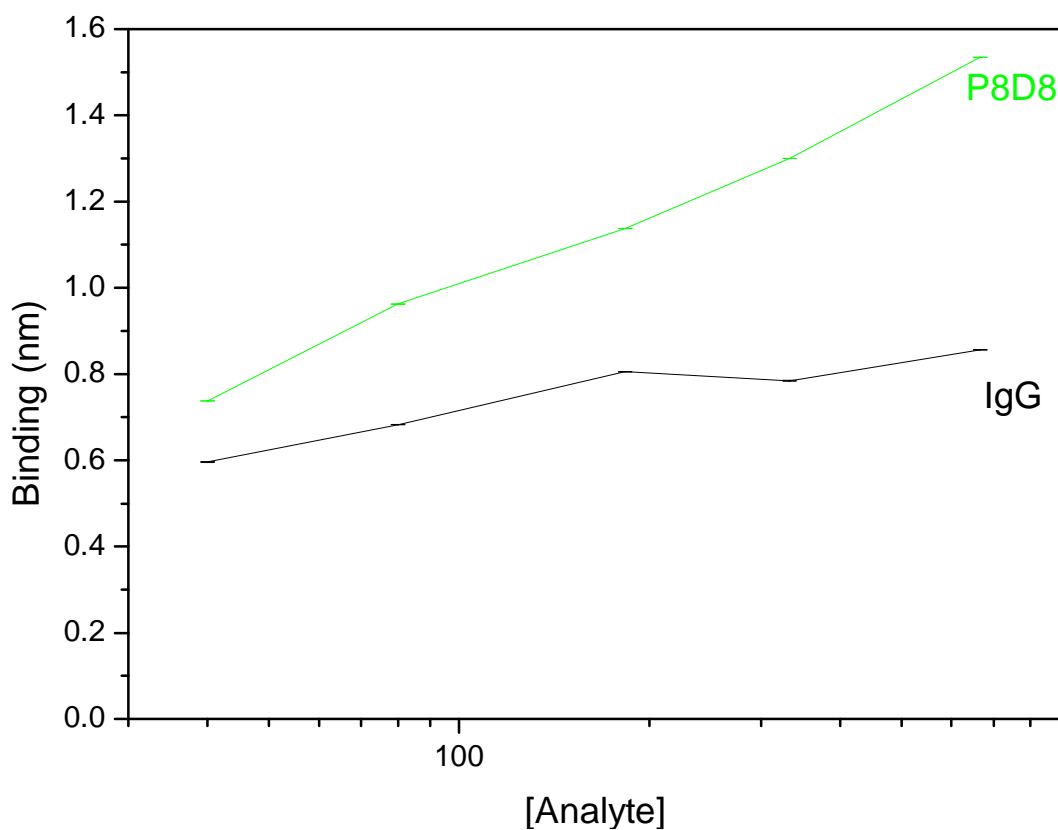


Figure 4-13: A comparison of R_{\max} for the detection of IgG using various receptors. Probes were all interrogated with the same analyte range the receptors used were IgG (), P8D8 (), R_{\max} was obtained using ForteBio software

From this data, it was observed that when using IgG and P8D8, both attached using EDC-NHS chemistry to couple the receptor using the amine moiety a relatively large amount of signal was generated. In the particular case of nanobody, the size of signal generated exceeded that of IgG at every concentration which may indicate that a more sensitive IgG biosensor was achieved.

4.4 Bioreceptor parameters

The binding data can also be used to assess binding parameters (K_a , K_b and eventually K_D). In calculating these figures we can compare the different bioreceptors used. By looking at both the association and dissociation data which was obtained in the Fortebio system it was possible to calculate these values and eventually the K_D , for each receptor system.

As introduced in chapter one, the binding of an analyte to an antibody, in particular a monoclonal antibody should follow a one-site binding saturation model. As the nanobodies we have used are monoclonal with respect to the CDR sequence this should be a valid model to use.

However it was also discussed, in Chapter One how true one-site binding vary rarely occurs in biological samples, this is due to heterogeneity within protein samples. Whilst 100% homogeneity is always the aim, in practise proteins are labile and even the best samples contain a small proportion of damaged protein. For this reason, a two-site binding model was adopted where essentially the binding parameters for the second site reflect the binding parameters of the damaged receptors. As there is only one binding site it therefore perhaps more convenient to refer to this binding model as a two-stage binding process, the equations for this process have been outlined in Chapter One.

The allocation of two binding constants allows for the model to account for both optimal and sub optimal binding mechanisms which are simulated by each of the two binding sites in the model. By modelling the data from the kinetic experiment using nanobodies conjugated directly to the amine reactive probes (using EDC-NHS chemistry) the difference between measured and simulated data using either the One site binding or two stage binding models could be assessed, this data is shown in Figure 4-14. By changing the model used, the χ^2 value decreased from 7.367 down to 0.01 and r^2 increased from 0.554 to 0.998.

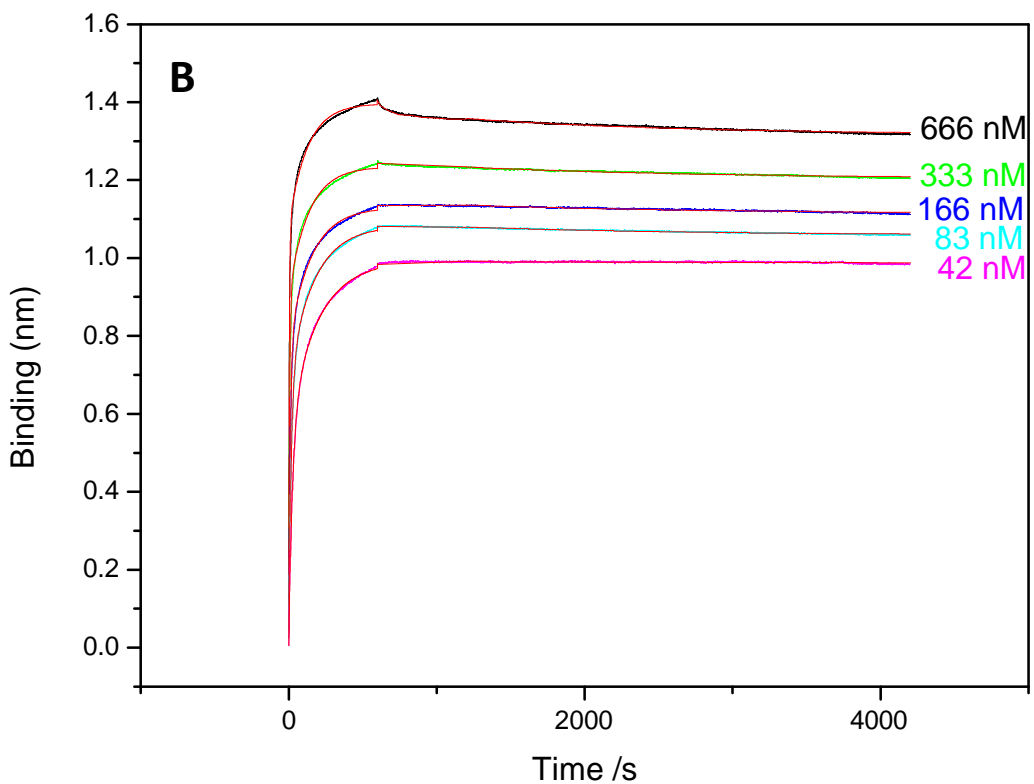
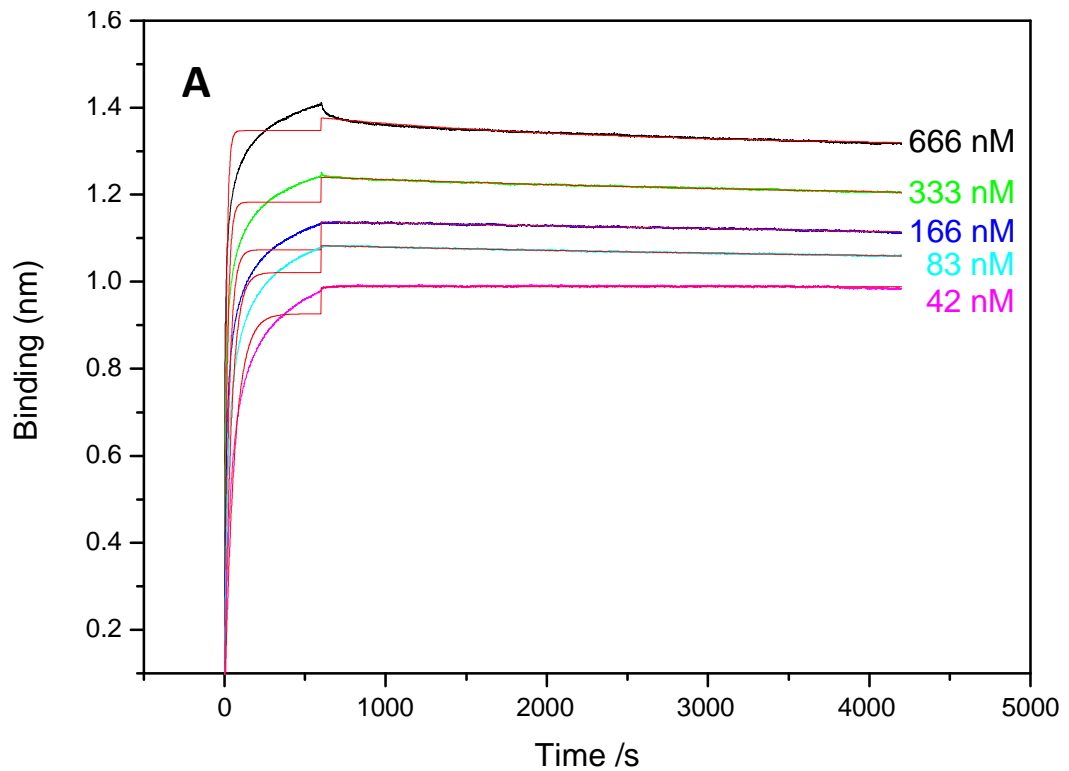


Figure 4-14: Comparison of one-site and two stage binding model to fit data. Using both One site (A) in which the analysis gave statistical values of $R^2 = 0.554$ and $\chi^2 = 7.367$. In the Two stage binding (B) Statistical values were $R^2 = 0.998$ and $\chi^2 = 0.001$. Data modelled was from unmodified P8D8 nanobody conjugated to the probe surface using EDC-NHS chemistry In both panels. Sensors were incubated with rabbit IgG at: 666 nM (), 333 nM (), 166 nM (), 83 nM (), 42 nM (), non-specific data was subtracted before fitting, fitted data is shown overlaid ().

As well as providing a better simulation, when extracting values for K_a and K_b , it allowed the identification of values for each parameter which described the 'fast-on, slow-off' model of antibody antigen binding. Numbers for K_a were $2-6 \cdot 10^5$ and K_b were $2 \cdot 10^{-5}-7 \cdot 10^{-6}$. Comprehensive data is given in

Table 4-2 and Table 4-3. From the data fitting which is modelled by equation in Chapter Two, the output also included a percentage function describing the weighting of each site towards the overall K_d value, these are also shown.

From these tables we can see that whilst the model is fitted with a weighting of 85-99% towards optimal binding, by including sub optimal binding the data can be much more accurately fitted.

Receptor	One site binding			R ²	χ ²
	K _a	K _b	K _d		
IgG	1.71 × 10 ⁵	4.46 × 10 ⁻⁶	2.70 × 10 ⁻¹¹	0.657	3.217
P8D8	1.82 × 10 ⁵	3.15 × 10 ⁻⁶	3.61 × 10 ⁻¹¹	0.554	7.367

Table 4-2: Data from one site binding model. Using the one site binding model, the R² and χ² values reflected the poor fit seen in Figure 4-14. After initial comparison of IgG receptor and P8D8 nanobody, one-site binding was abandoned

Table 4-3: Data from two site binding model. Using the two site binding model both R² and χ² values were improved. The parameters for optimal (site 1) and sub optimal (site 2) binding can be seen along with the relative percentages which weight the total binding constant K_d.

Receptor	Binding site 1			Binding site 2			Global parameters				
	K _{a1}	K _{b1}	K _{d1}	K _{a2}	K _{b2}	K _{d2}	x, % site 1	y, % site 2	K _d total	R ²	χ ²
IgG	5.95 × 10 ⁵	5.42 × 10 ⁻⁴	9.12 × 10 ⁻¹⁰	1.65 × 10 ⁵	1.10 × 10 ⁻¹	6.67 × 10 ⁻⁷	96.6	3.4	2.32 × 10 ⁻⁸	0.996	0.035
P8D8	1.35 × 10 ⁵	7.45 × 10 ⁻⁵	4.61 × 10 ⁻¹⁰	7.46 × 10 ⁴	4.99 × 10 ⁻³	6.69 × 10 ⁻⁸	92.4	7.6	5.52 × 10 ⁻¹⁰	0.989	0.084

Using the two –site binding model, the overall affinity constant K_D was calculated for each receptor. Values are compared in Figure 4-15 alongside the K_D derived using one site binding, it can be seen that this value is much lower and highlights the potential pitfalls of using one site binding to model kinetic data.

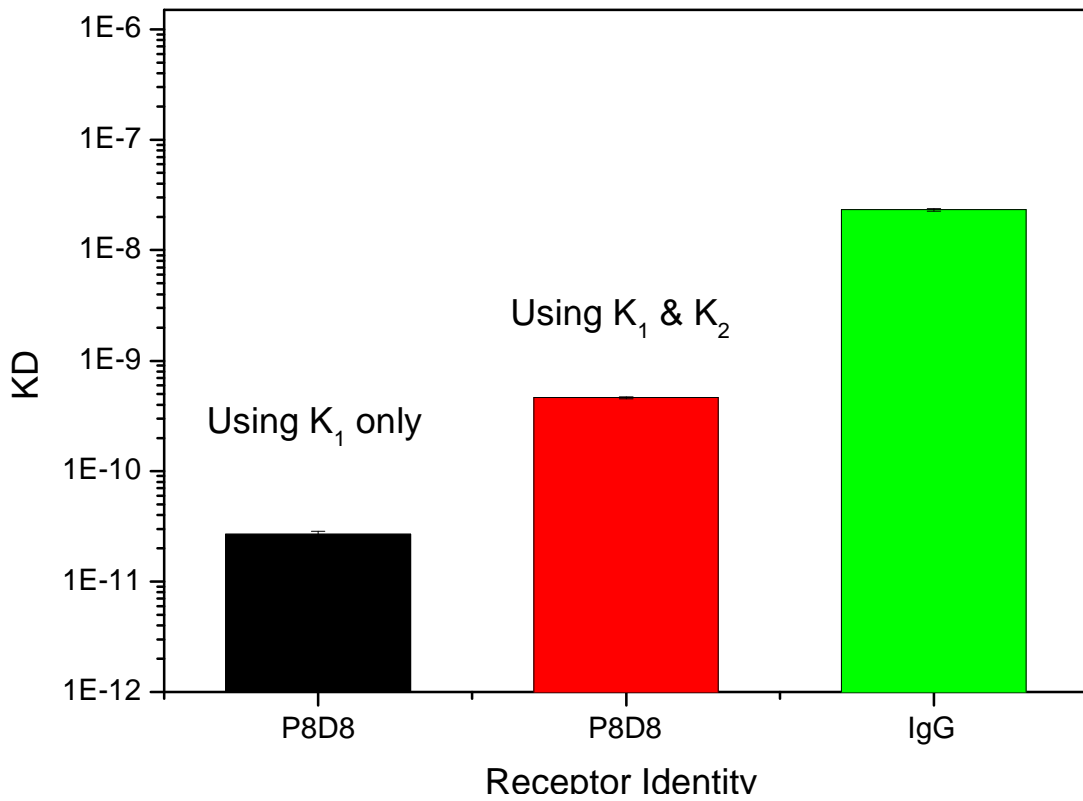


Figure 4-15: Comparison of binding constants of different bioreceptor systems. Data has been included for both one site binding model () and two site binding model () for the P8D8. Alongside two mode binding data for IgG ().

4.5 Discussion

When producing nanobodies it is important to consider the impact that any modifications may have for a given application. Whilst work in this chapter has focussed on the characterisation of nanobodies it has highlighted some issues which arose from modification at the molecular level.

Primarily there was the formation of dimers. Whilst this introduction of the cysteine residue is particularly useful for allowing a variety of conjugation routes, the formation of the disulphide bond was thermodynamically favoured and led to the formation of dimers. As the sequencing data confirmed the presence of a separate integral cysteine pair, it was necessary to reduce the disulphide bond between nanobodies whilst leaving the disulphide bonds within the nanobody undamaged. It is likely that the internal disulphide was more stable due its internal location and shielding from the buffer (Hagihara & Saerens, 2014). This meant that a less aggressive reducing agent, 2-MEA could be used to semi-selectively reduce nanobody dimers Figure 4-6. By incubating for 90 min at 37 °C a rate of around 80% reduction was achieved, though DTT was found to reduce almost 100% of dimers it is also likely that such a strong reductant would cleave the internal disulphide bond which could cause unfolding of the nanobody and a loss in biological activity.

Immunoprecipitation experiments were executed to ensure the immunogenicity of the nanobodies remained after the reduction of dimers as well as confirming that the engineered cysteine could be used as a conjugation route for the protein.

When the unmodified nanobodies were assessed using interferometry, the signal that they generated was considerably higher (in terms of signal per unit analyte) than when using IgG as the receptor. This may be due to the smaller size of the nanobody which may allow a higher packing density of receptors on the surface. When this is exposed to the analyte it can therefore bind a much higher number of analyte molecules and generate a higher signal.

When characterising the receptors by their binding affinities, a clear difference was seen between the K_d for IgG and those measured for nanobody systems, as the antibody is a polyclonal and the nanobody was previously panned using phage display and the optimum binder was selected this result is not surprising. The values for both antibody (2×10^{-8}) and

nanobody (4.7×10^{-10}) fall within the typical values which are commonly observed (Abbady et al., 2011; Conroy et al., 2009; Harlow & Lane, 1999). It is particularly important to note the difference in data fits achieved when using one-site and two-site binding models. By using the two-site binding fit although the second-sub optimal binding accommodated for only a small percentage of the population a much better fit was achieved and a more representative K_d value could be obtained for each receptor.

5 Chapter Five: Results: Using nanobodies in electrochemical biosensors

5.1 Introduction

Once nanobodies had been successfully synthesised from bacteria and reengineered to possess the variable length peptide spacer arm, they were applied to impedimetric biosensors. The nanobody based sensors were constructed similarly to sensors in Chapter Three, based on an electropolymerised thin film of tyramine. As in previous work in Chapter Three, sensor signal is represented as a change in the charge transfer resistance upon addition of increasing analyte concentration. Resistances were calculated using the modified Randles' Cell in Figure 5-1 and modelled to Nyquist plots for each concentration (data not shown).

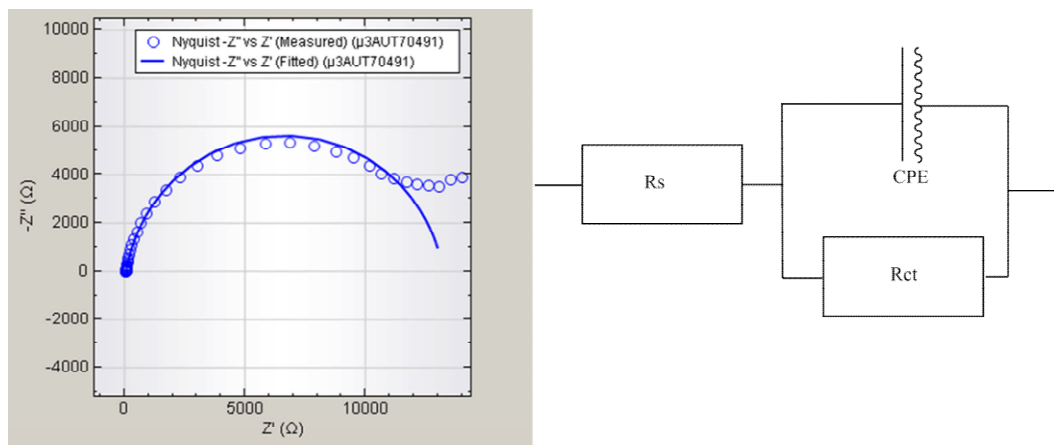


Figure 5-1: Sample Nyquist Plot, measured data (points) with simulated data overlaid (Arc) (left) using the modified Randles' cell (Right) Note: Left is a screen capture from Nova Software by Autolab®

In this Chapter, the nanobodies raised against rabbit IgG were again used. This was driven by the needs of the commercial sponsor for a rapid test for rabbit IgG. It may also have implications in the testing of various immunosuppressive conditions such as the assessment of immunodeficiency in HIV or monitoring of a patient during chemotherapy.

5.2 Antibody based sensors

As a comparator, an immunosensor was constructed using a goat – anti rabbit IgG polyclonal IgG receptor. To save confusion throughout this chapter the ‘analyte’ will refer to rabbit IgG unless otherwise stated. By first looking at the Nyquist plots measured upon increasing analyte concentration a clear and sequential increasing arc upon analyte addition can be observed as in Figure 5-2.

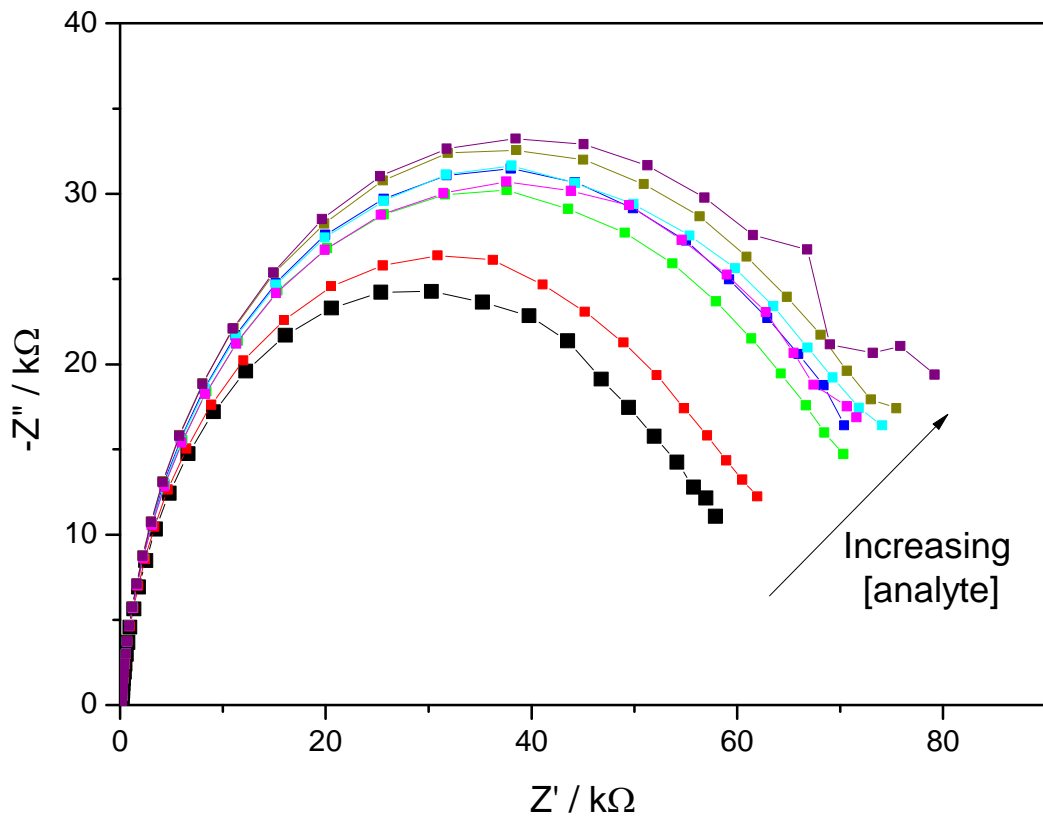


Figure 5-2: Nyquist plot of antibody based sensor for rabbit IgG. Sensor (—■—), increasing analyte concentration; 10^{-13} M (—■—), 10^{-12} M (—■—), 10^{-11} M (—■—), 10^{-10} M (—■—), 10^{-9} M (—■—), 10^{-8} M (—■—), 10^{-7} M (—■—).

The change in charge transfer resistance of this sensor can be observed in Figure 5-3. As is commonly seen, the recognition of the analyte by the receptor causes an increase in the resistance across the biosensor interface.

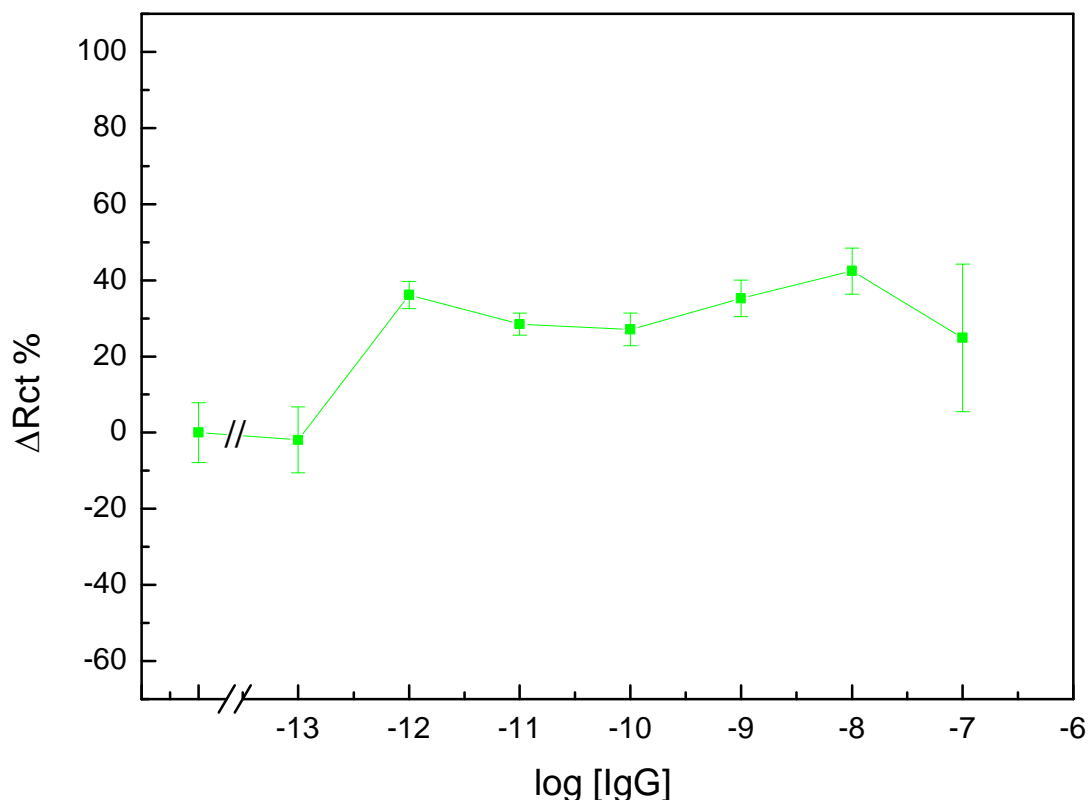


Figure 5-3: The calibration of a rabbit IgG sensor using IgG receptor. Signal is displayed as a % change in R_{CT} from the bare sensor ($n=8 \pm SE$). Fabricated sensor was incubated with analyte for 30 min prior to EIS interrogation as outlined in Chapter 2.

This increase in resistance/impedance corresponds to a physical slowing of the transport of charge carriers across the electrolyte and to the electrode. This slowing is caused by the presence of the analyte protein which impedes the free path of charge carriers when it is bound. This feature is a common theme in the literature covering impedimetric immunosensors (Guan et al., 2004; Lvovich, 2012; Prodromidis, 2010; Teles, 2011).

5.2.1 Control data

To ensure that signal measured was specific to rabbit IgG and to measure the sensitivity of the biosensor, a negative control was run. This time, sheep IgG, a structurally very similar protein to rabbit IgG, was used as the analyte. IgG is known to have a sticky tendency and this experiment helped to eliminate the possibility of non-specific protein aggregation on the interface generating an increase in resistance. The clear difference between specific signal generated by rabbit IgG and non-specific signal, when the sensor is incubated with the same concentration of Sheep IgG can be seen in Figure 5-4.

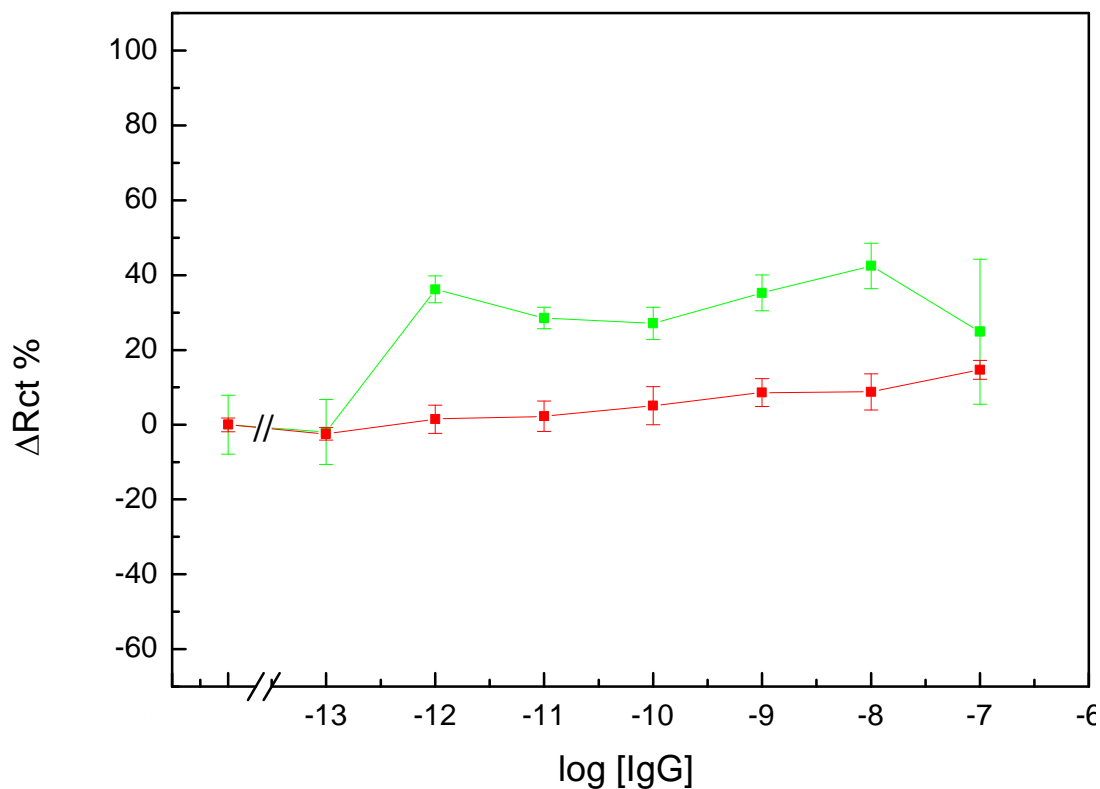


Figure 5-4: Calibration of a rabbit IgG biosensor constructed using IgG receptor. Specific, rabbit IgG (—■—), sheep IgG non-specific (—■—), (n=8 ±SE). Fabricated sensor was incubated with analyte for 30 min prior to EIS interrogation as outlined in chapter 2.

These experiments gave an idea of what was possible using standard immunosensor construction techniques with the standard receptor system, IgG. This data serves as a baseline to compare sensors fabricated with novel bioreceptors (nanobodies) reported in this thesis.

5.3 Nanobody based biosensor

As discussed in Chapter One there are currently many alternative bioreceptors emerging for use in biosensor fields. As orientation has previously been demonstrated as a key performance parameter (Billah et al., 2010; Makaraviciute & Ramanaviciene, 2013), existing conjugation techniques were used to assess the nanobody when used in a non-oriented manner. Nanobodies were biotinylated following the protocols in Chapter Two. The smaller molecular weight of the nanobodies meant that there were fewer amine groups for biotinylation which in itself may bring a degree more order to the system by restricting the number of potential orientations of the nanobody on the sensor surface.

After nanobody biotinylation and separation, biotinylation was confirmed using a dot blot and the sensors were fabricated, again on a polytyramine matrix using biotin NeutrAvidin® crosslinking.

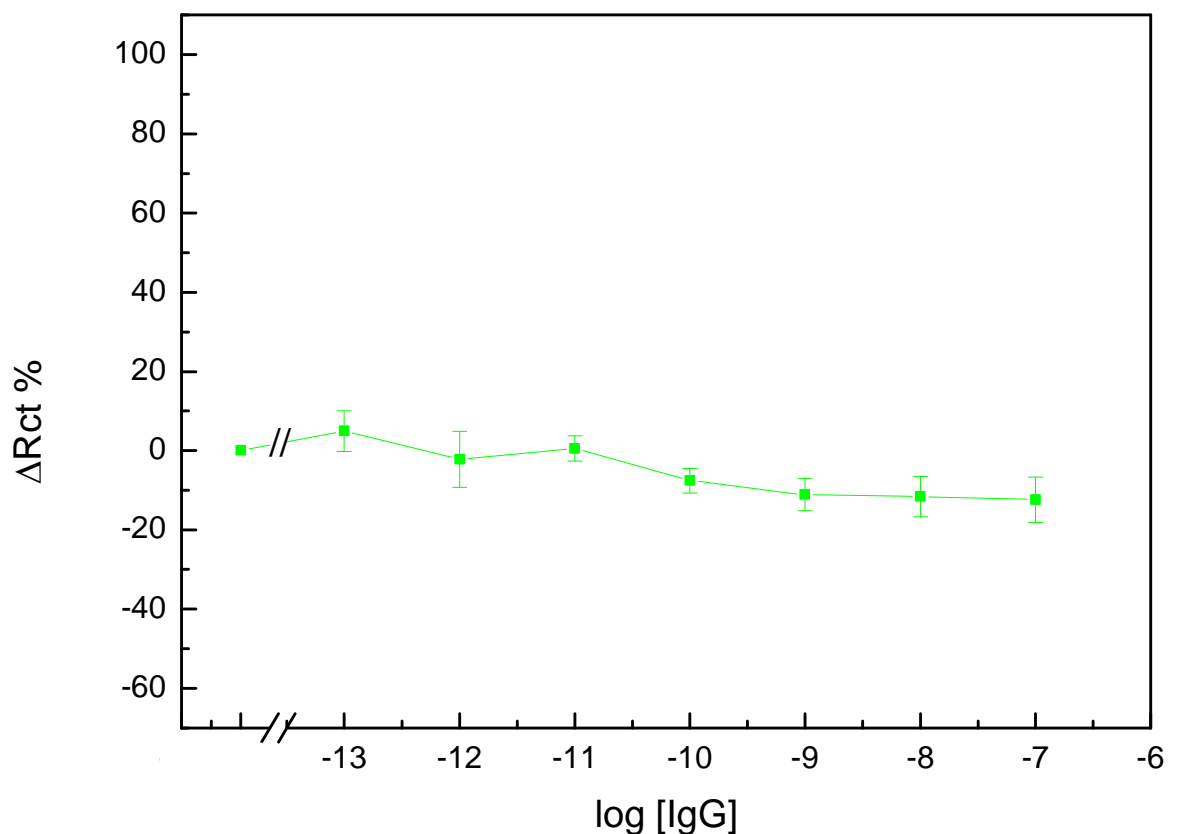


Figure 5-5: Initial calibration of a nanobody based sensor for rabbit IgG ($n=8 \pm SE$). Fabricated sensor was constructed using 600 nM receptor which was then incubated with analyte for 30 min prior to EIS interrogation as outlined in Chapter 2.

The first experiments were executed to assess if using standard approaches could lead to the simple creation of a biosensor for rabbit IgG. Using identical protocols for the fabrication of an IgG sensor but only changing the receptor resulted in a sensor which displayed no significant change in signal over a wide concentration range as in Figure 5-5.

5.3.1 Optimisation

As has been previously demonstrated, receptor concentration is a critical parameter which determines the successful generation of signal by a biosensor (Zourob, 2009). Therefore sensors were made using serial dilutions to optimise the concentration of receptor used on the biosensor. Data from these experiments can be seen in Figure 5-6.

From Figure 5-6, a receptor concentration of 6 nM was chosen as the optimum concentration. This was due to the improved reproducibility and reasonable sensitivity of R_{CT} Measured. Though data obtained using 60 nM showed a larger change in signal at 10^{-8} M analyte, the calibration was less linear and the reproducibility was lower.

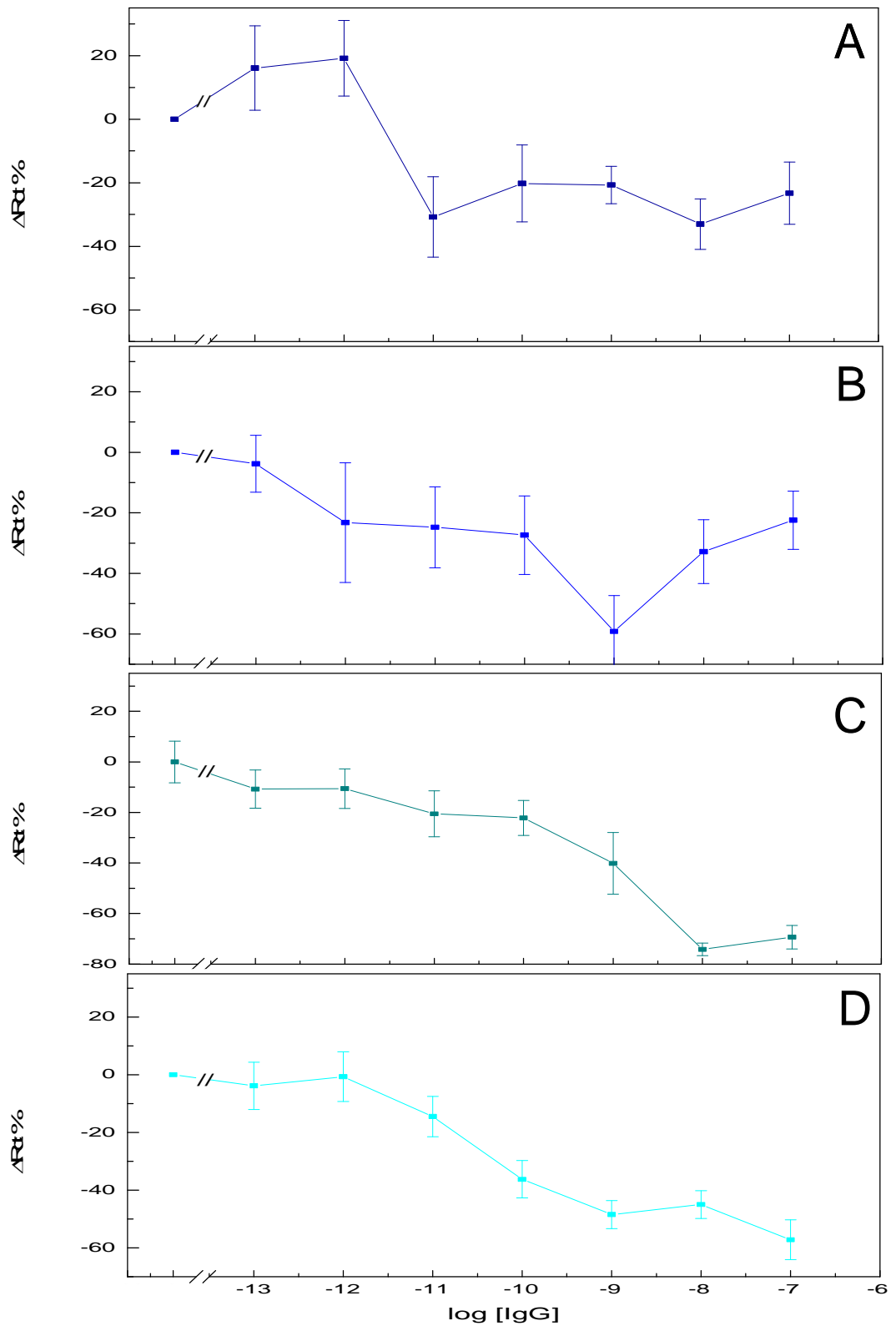


Figure 5-6: Optimising nanobody concentration. In the development of nanobody based sensor for rabbit IgG, initial studies (A) were conducted using 6 μM receptor, the experiment was then repeated using 600 nM (B), 60 nM (C) and 6 nM (D) receptor (n=8 \pm SE)

5.3.2 Controls

After having optimised the receptor concentration, it was clear that this was a primary determinant of the sensor signal. It can be observed that the reducing resistance was not an artefact, this was confirmed by looking at the Nyquist plot as shown in Figure 5-7. Here, it can be seen that after sensor construction, sequential addition of the analyte resulted in a decreasing arc which corresponds to the lower resistances previously observed.

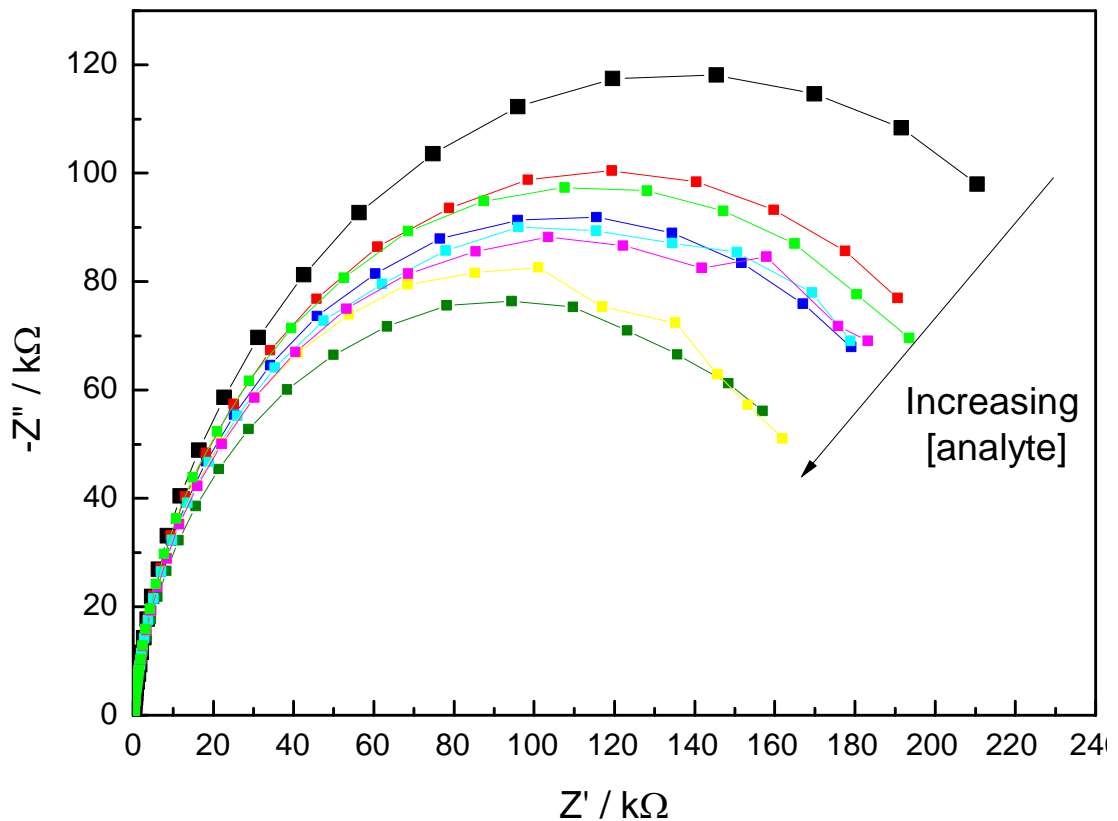


Figure 5-7: Nyquist plots of a nanobody based sensor with increasing analyte. Bare sensor (—■—), increasing analyte concentration; 10^{-13} M (—■—), 10^{-12} M (—■—), 10^{-11} M (—■—), 10^{-10} M (—■—), 10^{-9} M (—■—), 10^{-8} M (—■—), 10^{-7} M (—■—).

To confirm that this negative trend was indicative of the specific binding of analyte, non-specific controls were performed, again using sheep IgG. The results of these experiments can be seen in Figure 5-8 . There was a clear difference between specific and nonspecific signal and the negative trend is analyte dependant.

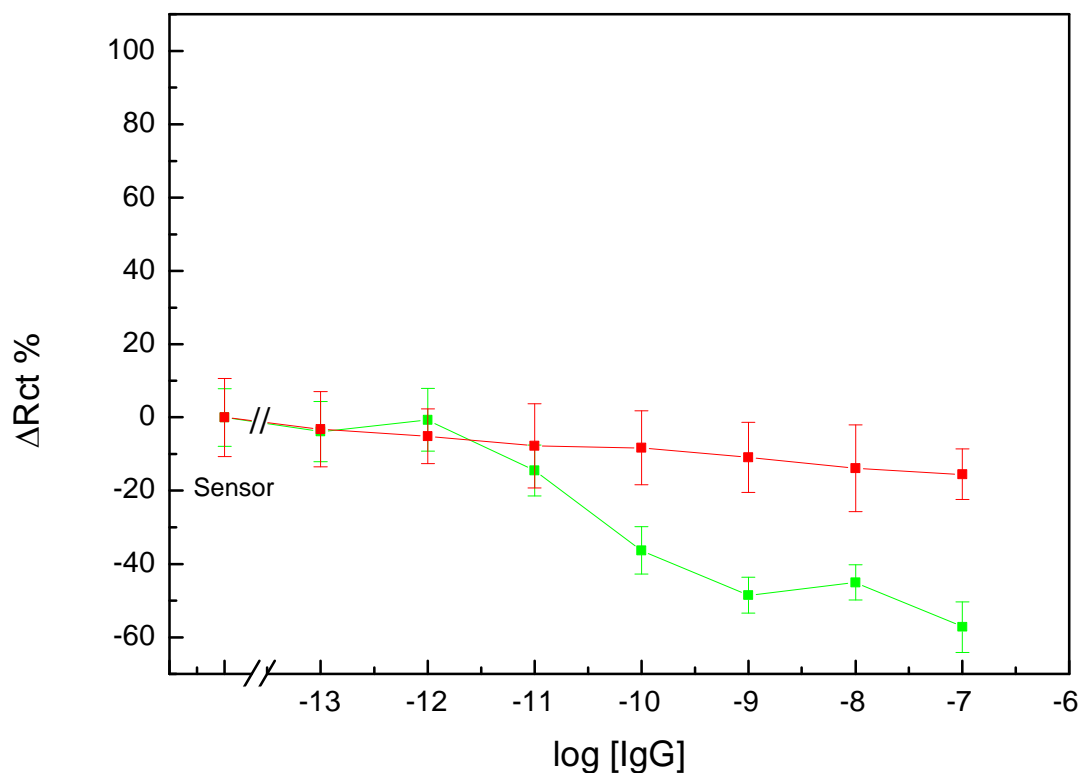


Figure 5-8: Calibration of a rabbit IgG biosensor using biotinylated P8D8 nanobodies. Specific, rabbit IgG (—■—), sheep IgG non-specific (—■—), (n=8 ±SE). Fabricated sensor was incubated with analyte for 30 min prior to EIS interrogation as outlined in chapter 2.

This work confirmed that the decrease in signal was specific to the analyte. Whilst a valid measure for calibrating a sensor, the result seemed counter intuitive. Work was therefore done to identify if this was a feature which could be seen across other biosensors fabricated using nanobody as the bioreceptor.

Nanobodies raised against green fluorescent protein(GFP) were kindly supplied by commercial sponsors, Abcam plc. These were then used to fabricate a similar sensor. For the positive control, GFP was added at a comparable molarity to that of the IgG to ensure that any effects observed were not due to a drastic change in the sampling concentration of the analyte. Meanwhile for the negative control, rabbit IgG was used. As the specific analyte for the original sensor this allowed investigation of whether the rabbit IgG may have been binding non-specifically to any other component of the biosensor. The results of the GFP sensor experiments can be seen in Figure 5-9.

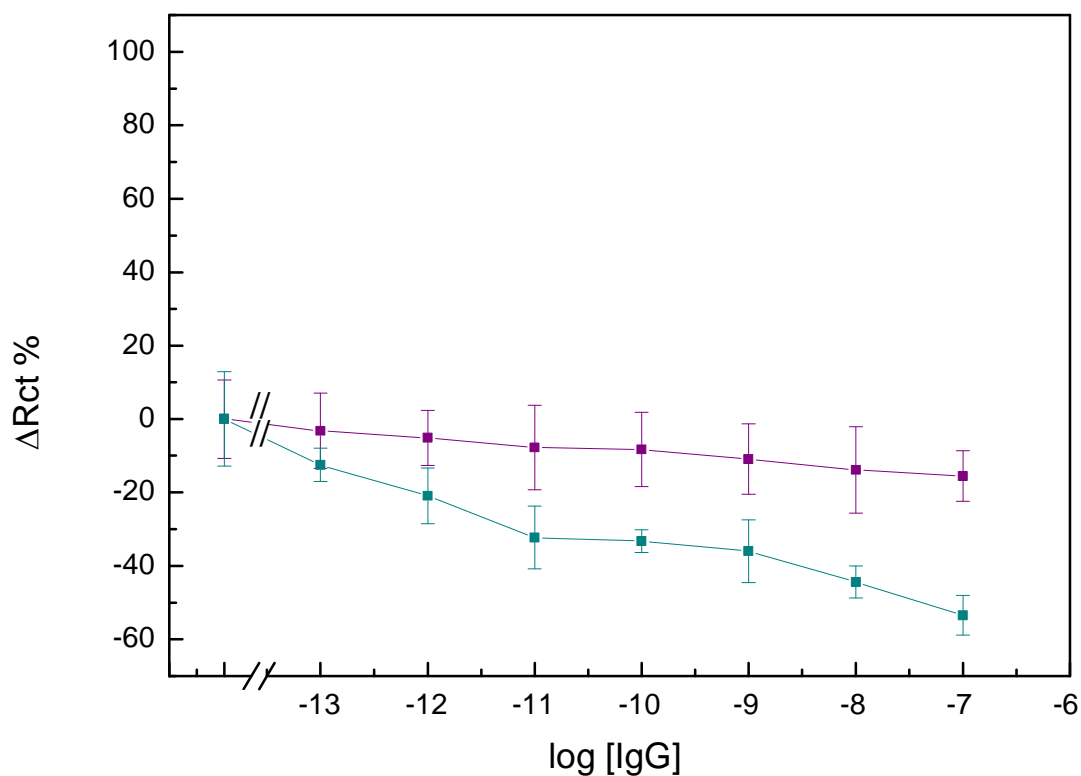


Figure 5-9: Comparison of specific and nonspecific signal for a GFP biosensor. Sensor was constructed using nanobodies screened against GFP. Specific, GFP (—■—), rabbit IgG nonspecific (—■—), (n=8 ±SE). Fabricated sensor was incubated with analyte for 30 min prior to EIS interrogation as outlined in chapter 2.

Again, this decrease in the charge transfer resistance was observed, the initial hypothesis was that it was due to a change in the Tyramine tethering layer, a concept discussed in depth later on however initial experiments were executed using self-assembled monolayer based sensors to see if this could be confirmed. A 4-aminothiophenol layer was deposited on an electrode to enable conjugation of the nanobody to the surface in a manner which could not permit its movement upon binding. As this could not be done on the Dropsens electrodes, owing to their uneven surface and the inherent unsuitability for self-assembled monolayer deposition (as outlined in Chapter One), these sensors were made on bespoke gold wire electrodes. Due to electrode variability and poor quality of manufacture however these results were inconclusive so sensors could not be meaningfully calibrated.

5.4 Oriented nanobody biosensors

The use of nanobodies with a peptide spacer was then investigated as a method of rectifying the reduction in resistance observed when tethering nanobodies on the biosensor using more traditional approaches. It was hypothesised that not only would orientation improve signal generation a concept which has been widely demonstrated (Spitznagel & Clark, 1993; Bonroy et al., 2006; Makaraviciute & Ramanaviciene, 2013), but also that by providing a degree of freedom away from the electrode surface that any disruption in the tethering layer could be minimised and the optimal sensor configuration could be achieved.

Accordingly nanobodies were re-engineered to possess a 5, 10 or 15 amino acid spacer arm (based on a GGGGS motif, repeating respectively with a terminal cysteine. Effectively this allows the nanobody to be positioned approximately 2, 4 or 6 nanometres above the electrode surface. The relevance of these dimensions will be discussed accordingly. Following data from Figure 5-6, the concentration of nanobody was maintained at 6 nM, as the nanobodies required reduction, the quantity applied to the surface was greater, to ensure that 6nM was the effective concentration. This was achieved using data from Chapter Four in which the relative concentration of monomer and dimer were obtained via chromatography experiments.

5.4.1 P8D8-S5 Based biosensor interrogation

Native nanobody dimers were reduced using 2-MEA and conjugated to a polytyramine tethering layer following protocols from Chapter Two. The resulting biosensors were incubated with either specific rabbit IgG analyte or non-specific sheep IgG as previously described. The first nanobody receptor to be investigated had a five amino acid spacer as described in Chapter Three. Results from interrogation of the impedimetric immunosensors are shown in Figure 5-10.

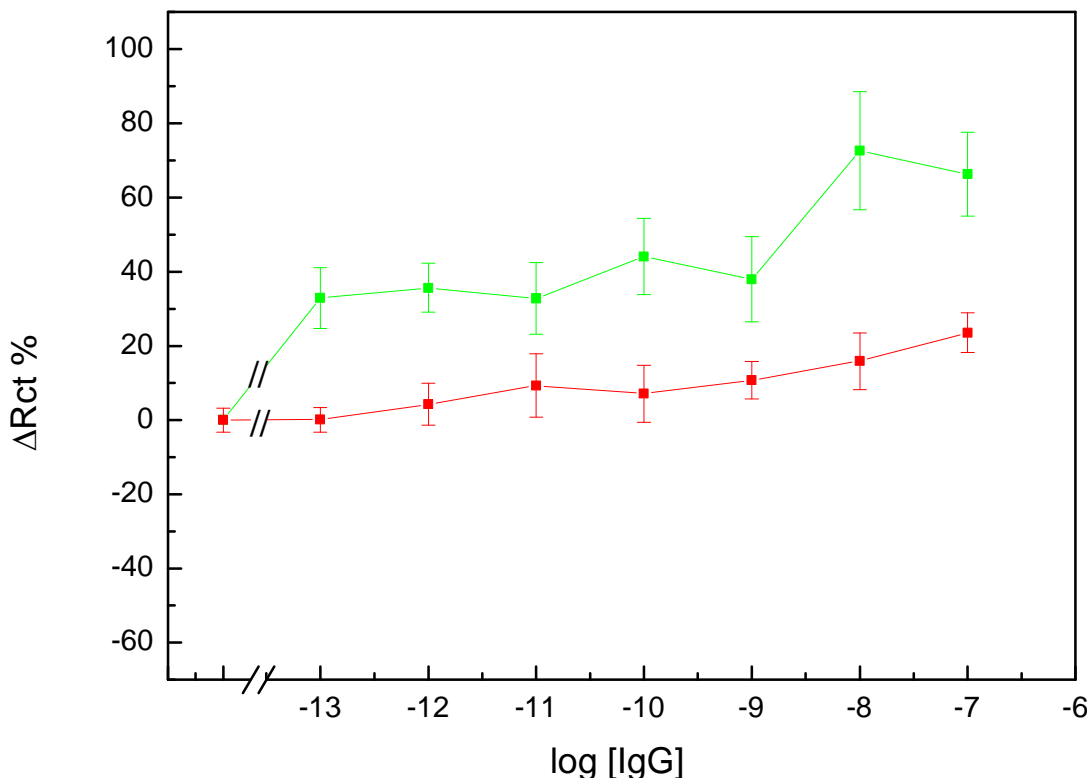


Figure 5-10: Calibration of a sensor using P8D8-S5 nanobody. Specific, rabbit IgG (—■—), sheep IgG nonspecific (—■—), (n=8 ±SE). fabricated sensor was incubated with analyte for 30 min prior to EIS interrogation as outlined in chapter 2.

From this graph it can be observed that the decrease in resistance is reversed when using a peptide spacer arm and that R_{CT} increased, with a maximum of ~70% greater than that observed when using standard antibody as the receptor as in Figure 5-4. This data in Figure 5-10 shows that by allowing a degree of freedom and some physical spacing away from the surface, a large impedimetric signal maybe generated. If we consider the spacer arm length, calculated to be 2 nm above the transducer surface this places the antibody binding at a distance which roughly corresponds to the Debye layer as set out in Figure 5-15.

5.4.2 P8D8-S10 Based biosensor interrogation

A repeat of the approach used for the five amino acid spacer nanobody was performed replacing the receptor for a nanobody with a ten amino acid spacer to investigate the role of spacer length from the biosensor interface. It was thought that by allowing more spacer freedom binding may be more easily mediated so a longer spacer arm was therefore used. Data from this experiment is shown in Figure 5-11.

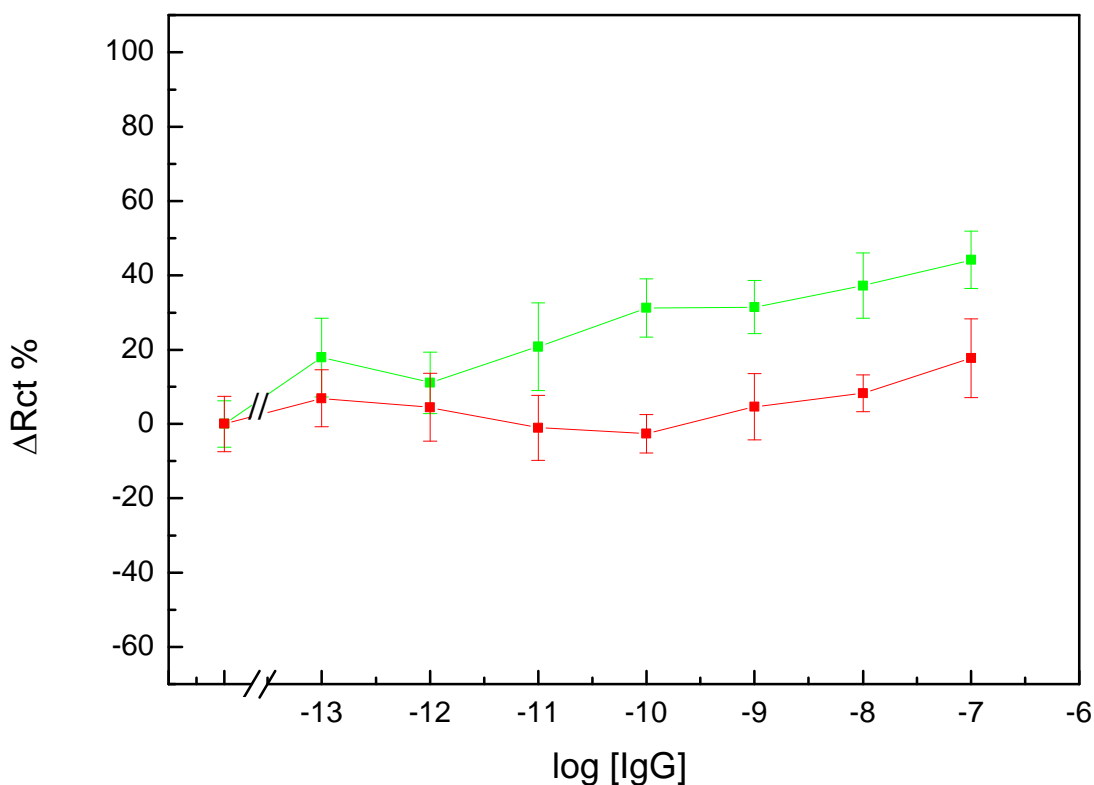


Figure 5-11: Calibration of a sensor using P8D8-S10 nanobody. Specific, rabbit IgG (—■—), sheep IgG nonspecific (—■—), (n=8 ±SE). Fabricated sensor was incubated with analyte for 30 min prior to EIS interrogation as outlined in chapter 2.

From Figure 5-11 we can see that whilst an operational sensor has been successfully produced, the size of the signal was significantly lower than when using the bioreceptor with a five amino acid spacer. Along with this observation, it can also be seen that the size of the non-specific signal was also larger.

5.4.3 P8D8-S15 Based biosensor interrogation

The investigation into the distance away from the biosensor interface that the nanobody was placed was continued by investigating sensors where the nanobody had a fifteen amino acid spacer arm. Data from this experiment, as shown in Figure 5-12 shows that the signal generated by the sensor was negligible when compared to the non-specific control.

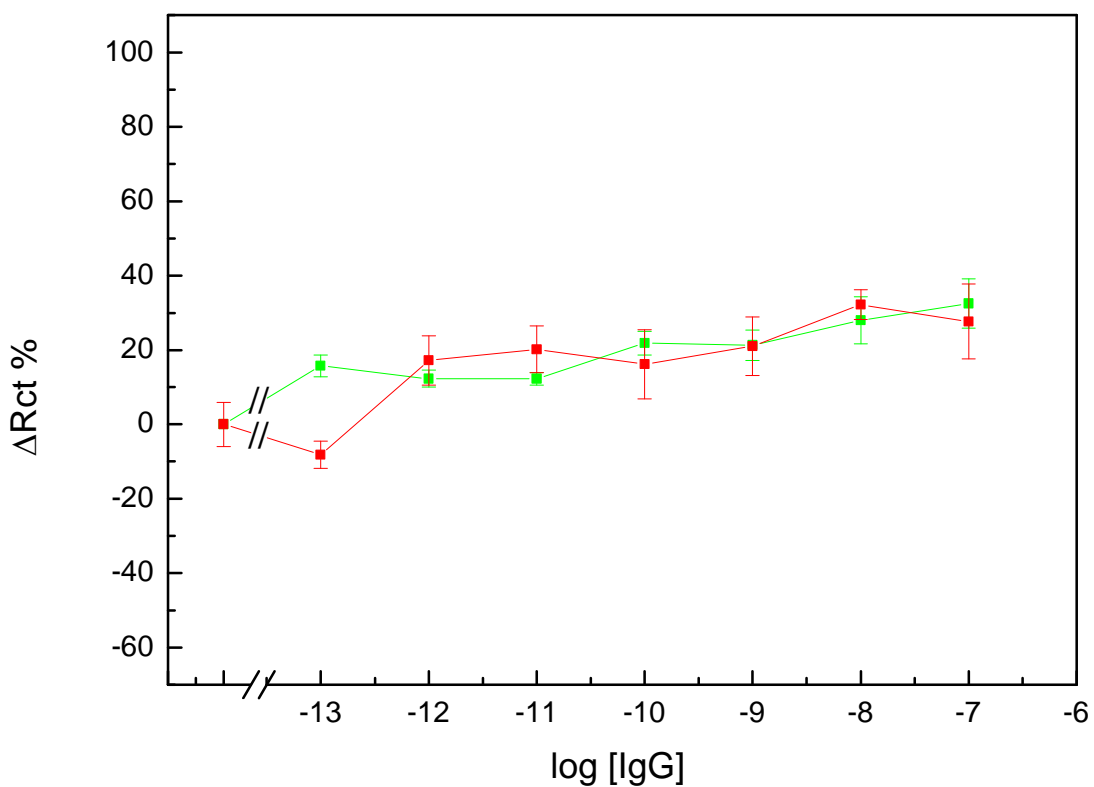


Figure 5-12: Calibration of a sensor using P8D8-S15 a nanobody. Specific, rabbit IgG (—■—), sheep IgG nonspecific (—■—), (n=8 ±SE). Fabricated sensor was incubated with analyte for 30 min prior to EIS interrogation as outlined in chapter 2.

Data from Chapter Four showed that this receptor is functional and successfully binds the analyte protein when it has been conjugated using similar chemistry. It is therefore unexpected to see such a low increase in signal. One feature which is unique to this data set is the relatively large signal generated by the non-specific analyte.

5.5 Comparison of bioreceptor systems

By combining much of the data present within this Chapter a direct comparison of bioreceptor systems can be achieved. In Figure 5-13, signal has been displayed as a result of total binding minus non-specific binding, in each case using the sheep IgG control to assess this.

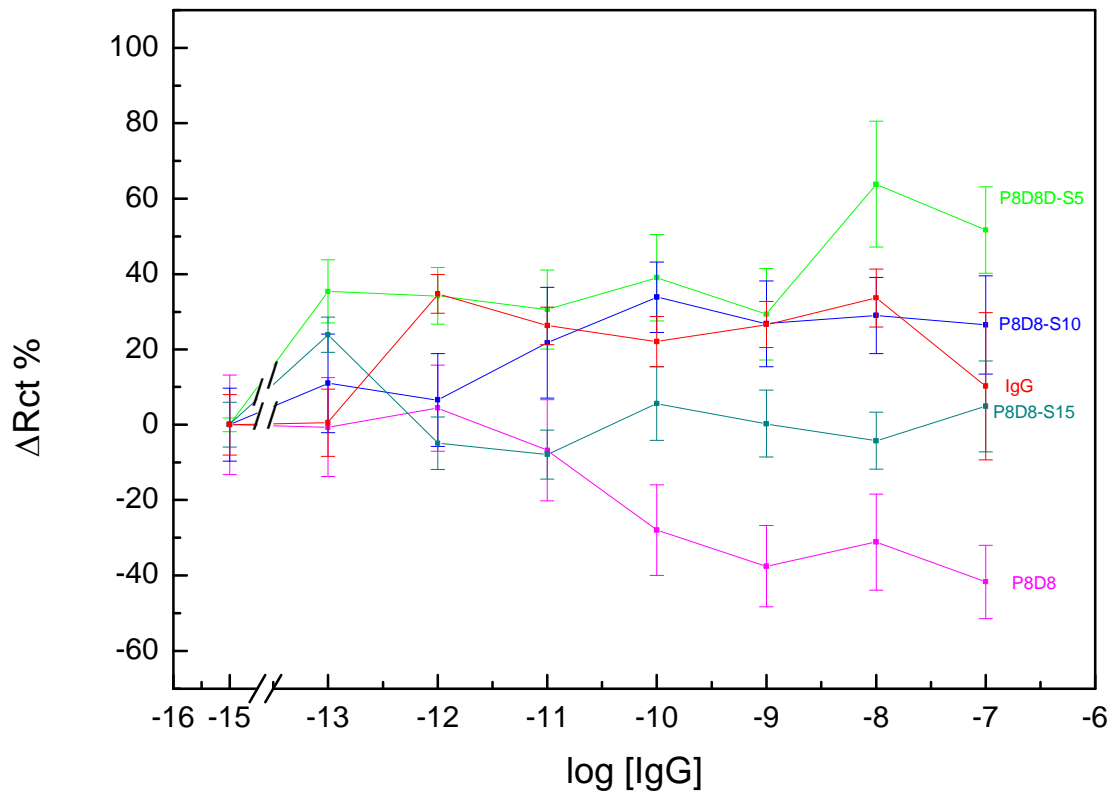


Figure 5-13: Comparison of the specific signal generated different receptors. Biotinylated P8D8 sensor (—■—), Biotinylated IgG (—■—), P8D8-S5 (—■—), P8D8-S10 (—■—), P8D8-S15 (—■—), data generated from figures 4, 8, 11-13 ($n=8 \pm SE$).

This figure shows the clear difference between biotinylated IgG and biotinylated nanobody as the receptor which highlights the unpredictable nature of signal generation at the biosensor interface. When comparing the receptors with different peptide spacer arms the 5 amino acid proved to generate more analyte specific signal than when using IgG however as the peptide spacer arm length was increased this advantage rapidly disappeared. By the time the spacer arm was increased to a length of 6 nm (15 amino acid spacer) the sensor provided no significant signal change upon analyte addition. Though the data from Figure 5-12 indicated an increase in charge transfer resistance, it was no longer analyte dependant.

5.6 Testing of optimised nanobody biosensor

After having confirmed that the biosensor constructed using a two nanometre or five amino acid spacer was the optimal configuration, the biosensor was tested in the presence of serum, a medically relevant sample matrix. For these experiments, screened human sera was used as it would contain no residual rabbit IgG. The sera was then either used undiluted, spiked with rabbit IgG or diluted 10% (v/v) in PBS, before being spiked with rabbit IgG and interrogated. The data from these experiments is shown in Figure 5-14 alongside non-specific controls of sheep IgG in PBS (as in Figure 5-10) and additionally serum which contained no rabbit IgG due to its human origin. The latter of these two controls confirmed the specificity of the sensor and the lack of cross reactivity with other serum proteins.

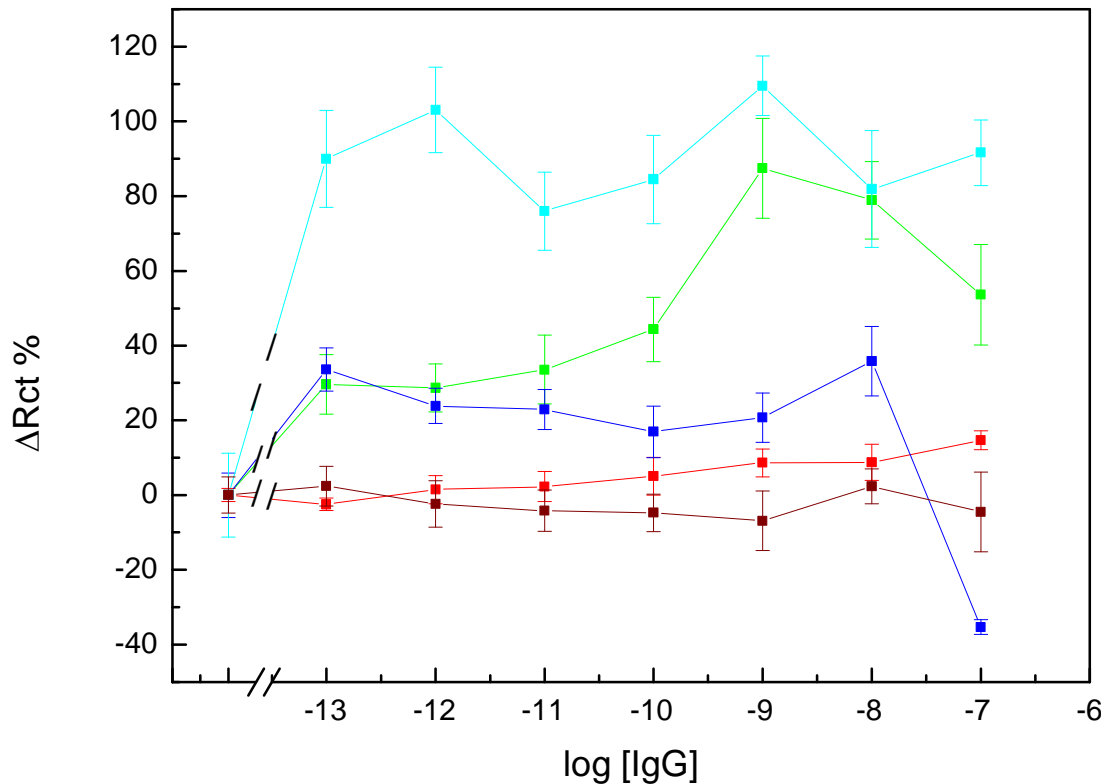


Figure 5-14: Testing of the P8D8-S5 biosensor in serum; rabbit IgG in PBS (—■—), rabbit IgG in 100% human sera (—■—), rabbit IgG in 10% human sera (—■—), sheep IgG in PBS (—■—), human sera with no rabbit IgG (—■—), note: in this case consecutive runs do not correspond to a direct concentration of IgG and merely represent sequential interrogation cycles with a 30 min incubation in sera between readings. ($n=8 \pm SE$).

From this range of controls we can see that the biosensor constructed using the bioreceptor with five amino acid spacer was sensitive down to pM levels, and though a linear calibration was not obtained within the sample size (n=8) there was a significant trend across the data. The lack of reactivity with negative controls is also a key goal in biosensor development and from this data in Figure 5-14 we can see there was a significant difference between all negative and positive control experiments.

5.7 Discussion

Data presented in this Chapter has highlighted the importance of controlling the spatial orientation of the bioreceptor at the interface of a biosensor. Whilst there is a push towards the use of non-antibody binding proteins and other small receptor systems the data has shown the caution with which such approaches should be taken.

The unexpected decrease in charge transfer resistance may be explained by the relative sizes of the receptor and analyte. As the receptors are very much smaller than their target analyte proteins. This may lead to a high packing density of receptor which cannot be maintained upon analyte recognition. Though commonly the transducer and tethering layer are seen as solid/ semi –solid they are potentially quite mobile (Barlett & Cooper, 1993) and more akin to a spongy matrix. This means that when the relatively large analyte (IgG) binds, the polymer also shifts on the sensor surface. It is believed that it is this process of stretching and shifting of the polymer which becomes the primary source of signal generation at the interface. In the development of biosensors, particularly those based on self-assembled monolayers (Campuzano et al., 2006; Rodgers et al., 2010) this process has previously been describes as a ‘pinholing’ effect. This effect is observed when rather than the charge carriers having to give up their electrons which then continue to tunnel though the tethering, conducting polymer layer, channels are opened up and the charge carriers can directly interface with the underlying gold substrate (Bharathi et al., 2001). This process reduces the kinetic barriers to charge transfer across the biosensor interface which corresponds to a lower resistance. In the work presented within this chapter a similar effect has been observed; however rather than the partial destruction of a monolayer it has occurred due to the flexing of a semi rigid polymer layer much like the flexing of wire wool.

By including the oriented spacer arm, a degree of freedom was afforded to the receptor. This meant that though it was still bound covalently to the transducer layer, the arm itself could shift without causing the same distortion in the tethering layer. This mechanism meant that in this instance the decrease in R_{CT} was not observed as there was no shift in the polymer layer. Instead, the binding caused the normal kinetic barrier to influx of the charge carriers at the electrode interface, this kinetic barrier can be seen again as the resistance, R_{CT} which corresponds to an overall reduction in speed of charge transport across the interface. As is often observed in many biosensor systems, this resistance

increased proportionally with the analyte concentration and allowed a calibration to be constructed.

Though the use of the spacer afforded a higher degree of freedom to the receptor, its use beyond 2 nm showed limited success. According to Guoy-Chapman theory it can be seen that at 2 nm is at the Debye layer. At this region there is the maximum flux between the different species of charge carrier (ions). In the $\text{Fe}(\text{CN})_6^{-3}|\text{Fe}(\text{CN})_6^{-4}$ system used this corresponds to a region of maximal flux between the different forms. As it is this flux and the subsequent charge carriers that get through this layer which cause current flow and charge to be transported around the electrochemical circuit it is hypothesised that binding in this region contributes to a greater signal yield from the biosensor overall. It is for this reason that the signal decrease is observed when using the greater spacer arm length of four and six nm, though some signal is still generated owing to the flexible nature of the peptide spacer and the fact that some receptors may still be located closer to the interface as is displayed on the lower portion of Figure 5-15.

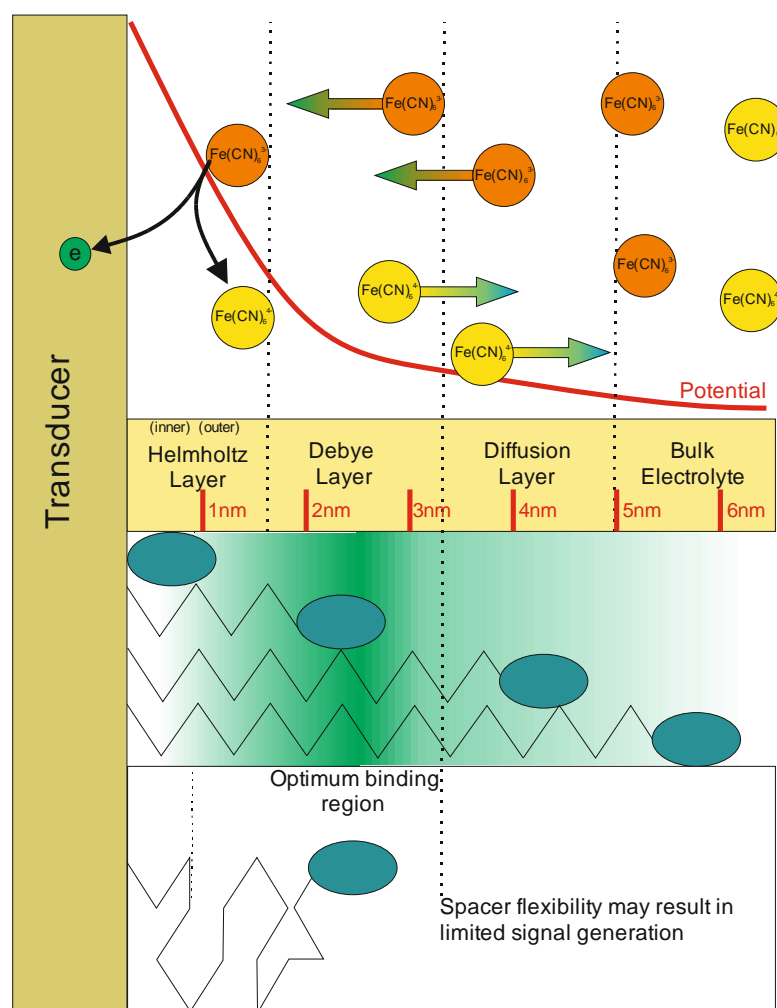


Figure 5-15: Guoy-Chapman theory in nanobody based sensors. The different layers which are critical for generation of signal at an electrode interface are shown alongside the nanobody with peptide spacer.

It is interesting to note that when using the larger spacer arms is the increase in non-specific signal size. This may be due to the slightly sticky nature of the IgG analyte which has been previously identified (Fanning et al., 1996; Harlow & Lane, 1999). If we compare the size of specific and non-specific signal in both the ten and fifteen amino acid spaced receptor, the correlating increasing non-specific signal of this would seem to support this hypothesis. Another explanation could be obtained again, by considering the role of the Debye layer, as, if the length of the spacer arm is at 6 though the binding may still occur, it does not generate any meaningful electrochemical signal and there is no perceived change in R_{CT} . Limited signal may also be generated closer to the Debye layer also; this may be due to the flexibility of the glycine serine spacer as illustrated in Figure 5-15.

6 | Chapter Six: Discussion

6.1 General Discussion

The limited progress achieved in bringing sensitive, low cost sensors to market is a widely documented disappointment in a field which has a good track record at the proof of concept level. This project was aimed at gaining an understanding of the processes needed to enable eventual commercialisation of reagentless impedimetric immunosensors.

Following previous studies, the receptor was identified as one of the critical components which determines the output of the sensor (Baniukevicius et al., 2013; Bonroy et al., 2006; Makaraviciute & Ramanaviciene, 2013; Tajima et al., 2011) and in this thesis the majority of work has concerned investigation of the bioreceptor component.

This was achieved by pursuing two principal areas of investigation. The first area examined was the regeneration of previously developed biosensors. The second area was the production and optimisation of nanobodies and their eventual application in impedimetric immunosensors. In this chapter, a discussion of these two principle areas is provided alongside an outline of the opportunities and issues which exist in the field of impedimetric immunosensors.

6.2 Binding biophysics and regeneration

Whilst the successful regeneration of biosensors had been demonstrated in other systems (Goode et al., 2014), the work in this thesis has demonstrated the potential for regeneration in impedimetric immunosensors by exploiting thermodynamic processes of analyte: receptor binding. Previous studies have shown success in both optical and mechanical systems but true regeneration has had only limited demonstration in impedimetric immunosensors (Goode et al., 2014; J. Huang et al., 2010; Queirós et al., 2013; Yun et al., n.d.). Within the broader category of electrochemical sensors, previous work had widely demonstrated re-use (Manoso et al., 2008; Vidal et al., 2004). The distinction made between re-use and regeneration is a crucial one which needs to be more clearly defined within the literature (Goode et al., 2014). For many reported studies on the 'regeneration' of amperometric biosensors, sensor signal was monitored until there was a return to baseline signal, caused by the gradual catalysis of all of the analyte which then permitted re-use of the sensor. For active regeneration, a regeneration buffer must be used to return the sensor to baseline signal in a controlled manner. Though this had been demonstrated in one enzyme based sensor for heart disease biomarkers (Lu et al., 2011), it has been most widely demonstrated in immunosensor systems where binding of the analyte to an antibody or other receptor was reversed (Bryan et al., 2013; Xu et al., 2013; Yun et al., n.d.). The work done in this thesis demonstrated the possibility of regenerating impedimetric immunosensors by assessing the on and off signal between regenerative steps and consideration of the thermodynamic processes governing this was used to inform, choice of the regeneration buffers.

Through work presented here, the unstable nature of the PANI:2-ABA copolymer was shown, corroborating evidence from previous studies (Caygill et al., 2012). The use of low pH to induce regeneration highlighted the effect of the multiple oxidation states of the polymer on the signal generated. This led to a re-selection of the base polymer. PTyr was used as, it has been previously ascertained that by polymerising from alkali-methanol, a stable, thin insulating film is deposited (Cosnier, 2005) which also bears pendant amine moieties. This thin film allowed conjugation and subsequent calibration of the previously demonstrated myoglobin biosensor.

This polytyramine based biosensor generated a signal that was much less sensitive to its chemical environment, thus allowing for the use of regeneration buffers that could decouple the receptor from analyte allowing its reuse. By optimising both pH and

exposure time, as well as including other constituents to assist regeneration by taking into account both the enthalpy, and entropy state of the biosensor. In this way, five regeneration cycles were achieved. Whilst this is fairly limited compared to the number of regeneration cycles claimed in optical sensors, where up to 200 cycles have been reported (Drake & Klakamp, 2011), this proof of concept already points towards considerable cost savings. If this technique could be further refined using automated control, further regeneration may be possible, lowering the cost of testing using impedimetric immunosensors. The more robust nature of nanobodies (Nicholls, 2007) and purely artificial receptors such as Adhirons (Tiede et al., 2014) may also enhance the possibility of regeneration owing to their stability.

Though the realisation of biosensor regeneration may be of clear benefit, it may not be a practical advantage in certain applications, examples include medical settings where the use of single-use items is often required in order to minimise clinician exposure to pathogens (Wilson & Jugner, 1968). Examples where regeneration may be of particular use are in environmental protection and process sampling where remote monitoring may be desired as well as home monitoring of a medical condition over a time course. In this example, the sensor could be used by only one patient ensuring there is no cross contamination or infection.

6.3 Nanobodies in reagentless immunosensors

Though reagents such as half antibodies and fragmented antibodies have been used frequently there had been almost no work published using the novel nanobody binding protein in impedimetric sensors. Their use had been previously proposed (Hassanzadeh-Ghassabeh et al., 2013; L. Huang et al., 2010) and to date they have been applied to optical and amperometric sensor systems (Campuzano et al., 2014). Only recently, a study was published on their use in impedimetric immunosensors for the detection of apolipoprotein (Li et al., 2015).

Unique to this project was the development of the peptide spacer arms with engineered cysteine residues to permit oriented conjugation. Whilst these could be successfully expressed from *E.Coli*, they formed disulphide linked dimers when expressed. By following similar approaches used for the reduction of antibodies (Ahmed et al., 2013; Billah et al., 2010; Caygill et al., 2012; Harlow & Lane, 1999) it was possible to reduce the nanobody dimers and then conjugate them to the transducer using the engineered cysteine residue. When the reduced P8D8 nanobody with spacer was attached to the insulating polytyramine film using SMCC, an increased resistance was observed upon analyte binding. This was in contrast to the non-engineered P8D8 nanobodies directly attached to the polytyramine film using biotin NeutrAvidin cross-linking where a decrease in resistance was observed with increasing analyte concentration..

As described in Chapter Five, this difference in impedance response is believed to be due to the distortion of the insulating polytyramine tethering layer. Indeed in the work by Li et al reporting the use of nanobodies in impedimetric immunosensors (Li et al., 2015), an increase in resistance was observed. The reduction in R_{CT} has been previously observed in other systems where a small receptor has been binding something much larger on a polytyramine surface (Rushworth, Ahmed, et al., 2014). In another study by the Millner group a similar sensor was constructed in which a small peptide bound a much large amyloid protein. This lead to the decrease in resistance upon analyte binding (Rushworth, Ahmed, et al., 2014).

Another key parameter affecting sensor performance identified is optimisation of the receptor concentration on the sensor surface. This is frequently unreported within the literature, but is an easy step which could help in the replication and adaptation of reported work. One issue that merits further investigation is how the optimal receptor

concentration may be different when detecting different analyte species. It may be that there is a relationship between the optimum loading of receptors and the size of both the receptors themselves and the analyte molecules. Though true investigation of this would require a number of receptor analyte pairs to be investigated, a meta-analysis could be carried out.

6.4 Discovered opportunities

The use of peptide spacer technology for oriented conjugation on the biosensor surface was novel in this project. Given the increasingly prolific nature of patents in the field of antibody mimetics, the work presented may provide a commercially and technologically useful application in the field.

Whilst other patents have focussed on the use of a spacer for functionalization, e.g. introduction of a glycan region (Aivazian et al., 2012) or the development of heterodimers for bivalent antibody mimetics (Revets & Hoogenboom, 2010) there have to date been no patents which protect the concept of varying the length of a peptide spacer arm for use in biosensor applications; and specifically nothing that discusses the use of a spacer for increasing the efficacy of the nanobody in a given application. This study illustrates that the length of this peptide spacer arm may be a critical parameter in the fabrication of biosensors as well potentially in other applications. Whist work in this project has focussed on nanobodies; similar effects may be seen when using different small antibody mimetics. The use of variable length peptide spacer arms could therefore have a far-reaching impact in the development, adoption and application of antibody mimetic binding proteins in a variety of systems.

6.5 Requirements for sensor commercialisation

Whilst the discoveries made within this thesis may increase fundamental understanding of operation, a range of factors must be considered for the ultimate commercialisation of any point of care impedimetric immunosensors.

The first consideration is the electrode used; commonly the maximum cost of single use electrodes is considered to be around \$1 (Alocilja & Radke, 2003; Luong et al., 2008). The gold Dropsens electrodes used in this thesis were €4 ea. (\$4.40) and so would be prohibitively expensive for single use sensors except perhaps for use in critical medicine. Though the work in Chapter Three has proven the ability to reuse these sensors up to five times, theoretically reducing the electrode cost per test to 88¢, this would require fluidics apparatus in order to ensure practical deployment and as discussed may not be suitable for applications such as multi-patient sampling. Other costs which must be considered are the cost of materials and human resources for biosensor fabrication. These costs are likely to fall if mass production can be deployed. For polymerisation this may require connectors which permit many electrodes to undergo CV in parallel and perhaps custom tanks to be designed for monomer solutions. It may also require large scale application of cross linkers and receptors using a robotic system such as a BioDot® or similar (Pataky & Brugger, 2014).

The cross linkers used are another source of expense. Sulfo-SMCC costs £3 .mg⁻¹ so this may represent a significant cost when scaling up production processes. Similarly, for receptors conjugated using biotin-NHS, this costs £1.mg⁻¹. One way in which the issues of production costs have been negated in this thesis is the use of nanobodies which enable large scale bacterial expression. This could mean that in large scale production, the cost of receptor used is greatly reduced. As data from Chapter Five has shown, biosensors can be constructed using a minimal quantity of nanobody, ensuring that the costs represented with the bioreceptor can be minimised.

Once the cost of biosensor fabrication of has been minimised and assuming that it reaches an acceptable level, its implementation to point of care for field use must be considered. As previously outlined the use of fixed frequency analysis would greatly reduce the instrumentation required. Not only would this permit miniaturisation and lower the cost but it could also reduce the time taken to interrogate sensors as it removes the need for a full frequency scan to be taken.

For any diagnostic device, the newly developed sensor must provide detection equal to the current gold standard test for the given analyte. For many analytes the gold standard is an enzyme linked immuno sorbent assay (ELISA) which can commonly identify a target biomolecule down to the nanomolar range. Though the ELISA is typically performed in a 96-well plate, representing a comparatively low materials cost as samples can be batched, the real expense is associated in the human resource as it requires a skilled operator and complex clinical analyses which, all of which take a substantial amount of time and therefore may represent a significant cost. Another drawback of such systems is the need to run them in centralised locations, this therefore relies on the collection of samples that must be sent to a central testing facility such as a pathology lab, adding greater logistic burden.

Another significant hurdle to the commercial launch of an impedimetric immunosensor is regulatory approval. Once a sensor has been developed and can be justified both practically and commercially regulatory approval must be obtained. FDA approval is commonly seen as the global standard under which biosensors are a category 2 medical device (excepting category 3 implanted biosensors). For approval, the biosensor must be compared to existing alternatives, where applicable, to demonstrate its efficacy and applicability (Liotta & Petricoin, 2012). Within Europe similar regulation is enforced by the European Medicines Agency (EMA) and work must be done which conforms to ISO 11.100.10: *in-vitro* diagnostic test systems (ISO, 2010). It is only once approval has been granted that marketing for point of care diagnostics can begin. This lengthy and costly process therefore still represents a major hurdle for the translation of proof of concept work to field or point of care deployment.

6.6 Future Work

Investigations from this work have indicated that the location of the binding event of the analyte should be placed within the Debye Layer in a given system to ensure maximum signal generation. This could be investigated by repeating experiments from Chapter Five with a different electron mediator solution e.g. hexa-amine ruthenium chloride, or the same mediator at a different ionic strength where the diffusion layer and accordingly the Debye layer thickness would be altered.

From these experiments it would be possible to identify whether the nanobody with five amino acid spacers would still be the optimal binder or whether by changing the Debye layer thickness another spacer arm became optimal. This would demonstrate the relationship between the binding location and signal generated in impedimetric sensors.

Throughout the field, there is limited consensus on the interpretation of impedimetric data. Whilst for many sensors the change in resistance is monitored, for some analytes capacitance is monitored as the output. Ideally total impedance (Z) at a given frequency could be used and would allow for fixed frequency analysis. In order to achieve this, experiments could be conducted in which fixed frequency analysis was conducted to investigate viability and compatibility with current biosensor instrumentation.

Another avenue which merits further investigation is the use of the anti-GFP nanobodies from Chapter Five which were used for control experiments. With the development of a GFP sensor and the binding of GFP analyte to the sensor surface, it may be possible using super resolution optical microscopy capable of sub 20 nm resolution (e.g. STORM) to image the GFP directly on the surface of the electrode. As each nanobody binds one molecule of GFP this could enable direct quantification of the amount of nanobody which successfully conjugates to the sensor interface and also a way of investigating the real spacing of receptors at the biosensor surface.

These suggestions would all focus on gaining a clearer picture of the physical parameters at the biosensor surface and may help inform subsequent biosensor fabrication.

6.6.1 Limitations within the field

As has been illustrated throughout this thesis, the promising work which has been done across the field of impedimetric immunosensors is still very far from realising its potential and from commercial application. One of the complexities is the wide variety of transducer systems used. Indeed work in this thesis has shown that even within a fairly specific biosensor assembly, the nature of a polymer film to be a particular source of signal generation and analysis. It is therefore necessary for a standard approach to be taken across the field to permit the comparison of different studies. In order to do this a number of requisite steps must be taken, all of which may be relatively easy to address in terms of commercialising tools for research.

The primary consideration would be the development of highly reproducible electrodes with a predetermined geometry, regular surface chemistry and reasonably flat surfaces which could be used for either SAM construction or the attachment of a more robust tethering layer. Though many of the commercially available electrodes have reasonable characteristics for techniques such as amperometry and potentiometry, for the more demanding technique of impedance, measurement variability is still an issue (laneselli et al., 2014). Another shortcoming in the literature is the propensity for authors to report a trend in changing resistance or capacitance which is rarely accompanied with a mechanism to explain the observed trend. Without a consideration of the origins of the signal it becomes difficult to establish a set of rules by which to measure and compare different sensors. This shortcoming has been previously identified (Daniels & Pourmand, 2007), however, there is little evidence of a concerted effort within the field to improve reporting in this area. The work in this thesis led to the development of a hypothesis on the shifting of the insulating polymer tethering layer, which may explain the same trend of decreasing resistance upon analyte addition as has been observed in a similar system (Rushworth, Ahmed, et al., 2014).

By looking individually at the electrodes and the electrochemical system used as well as fabrication steps such as the tethering layer used, the conjugation chemistry and the sizes of both receptor and analyte, it may be possible to establish a framework to more fully describe the processes which generates the impedance signal. If this could be done across the field, it could help to explain many of the observed phenomena and streamline the development process.

The aim of developing such a framework would be that it could allow the identification of certain systems which outperform others, assisting in the selection of a standard approach across the field. This approach has previously been achieved in other methods such as SPR leading to the emergence of market leaders (e.g. Biacore). However, due to the relative infancy of reagentless electrochemical techniques, it is unclear whether sufficient data is yet available to form a field-wide consensus.

Another benefit of standardization of electrodes, and assembly approaches for different analytes is that it would enable fixed frequency analysis (FFA). Work in this thesis has focussed on the analysis of a wide frequency range which has enabled the generation of Nyquist curves and the calculation of R_{CT} values. However, this is an instrumentally and computationally intensive method, which, whilst superior in a research environment due to the breadth and robustness of data generated, is unsuitable for point of care or field use. If the variability of fabricated sensors could be reduced to an appropriate level then use of FFA could permit a one data point analysis of the impedimetric signal, lowering the instrumental costs and acquisition time required. Indeed sensors for parathyroid hormone (Özcan et al., 2014) and of bitter taste molecules (Hui et al., 2013) has demonstrated proof of concept in this area which may be more widely adopted.

7 | References

- Abbadly, A.Q. et al. 2011. Evaluation of a nanobody phage display library constructed from a Brucella-immunised camel. *Veterinary Immunology and Immunopathology*. **142**(1–2),pp.49–56.
- Abbas, A. et al. 2011. New trends in instrumental design for surface plasmon resonance-based biosensors. *Biosensors and Bioelectronics*. **26**(5),pp.1815–1824.
- Ahmed, A. et al. 2013. Novel Impedimetric Immunosensor for Detection of Pathogenic Bacteria *Streptococcus pyogenes* in Human Saliva. *Analytical Chemistry* [online]. Available from: <http://pubs.acs.org/doi/abs/10.1021/ac403253j> [Accessed December 11, 2013].
- Aivazian, T.D. et al. 2012. Linker peptides and polypeptides comprising same. Available from: <http://www.google.co.uk/patents/WO2012088461A2> [Accessed July 31, 2015].
- Albert et al. 2002. Optical Sensor Arrays for Medical Diagnostics *In: Biomedical Diagnostic Science* [online]. CRC Press. Available from: <http://www.crcnetbase.com/doi/abs/10.1201/b14042.pt2> [Accessed July 16, 2015].
- Albrecht, C. et al. 2008. Two immunoassay formats for fully automated CRP detection in human serum. *Anal Bioanal Chem*. **391**(5),pp.1845–52.
- Alocilja, E.C. and Radke, S.M. 2003. Market analysis of biosensors for food safety. *Biosensors and Bioelectronics*. **18**(5–6),pp.841–846.
- Alonso-Lomillo, M.A. et al. 2010. Screen-printed biosensors in microbiology; a review. *Talanta*. **82**(5),pp.1629–1636.
- Anderson, H. et al. 2007. Quartz crystal microbalance sensor design: I. Experimental study of sensor response and performance. *Sensors and Actuators B: Chemical*. **123**(1),pp.27–34.
- Arya, S.K. et al. 2009. Recent advances in self-assembled monolayers based biomolecular electronic devices. *Biosensors and Bioelectronics*. **24**(9),pp.2810–2817.
- Ates, M. 2013. A review study of (bio)sensor systems based on conducting polymers. *Materials Science and Engineering: C*. **33**(4),pp.1853–1859.
- Atkins 1998. Physical Chemistry. *Oxford Press*.
- Bain, C.D. et al. 1989. Formation of monolayer films by the spontaneous assembly of organic thiols from solution onto gold. *Journal of the American Chemical Society*. **111**(1),pp.321–335.
- Bally, M. et al. 2006. Optical microarray biosensing techniques. *Surface and Interface Analysis*. **38**(11),pp.1442–1458.
- Baniukeyvic, J. et al. 2013. Application of oriented and random antibody immobilization methods in immunosensor design. *Sensors and Actuators B: Chemical*. **189**(0),pp.217–223.

- Bard, A.J. and Faulkner, L.R. 2001. *Electrochemical Methods*. John Wiley & Sons.
- Barlett, P.N. and Cooper, J.M. 1993. A review of the immobilization of enzymes in electropolymerized films. *Journal of Electroanalytical Chemistry*. **362**(1–2),pp.1–12.
- Barnes, W.L. et al. 2003. Surface plasmon subwavelength optics. *Nature*. **424**(6950),pp.824–830.
- Barsan, M.M. et al. 2015. Electrochemical sensors and biosensors based on redox polymer/carbon nanotube modified electrodes: A review. *Analytica Chimica Acta*. **881**,pp.1–23.
- Barthelmebs, L. et al. 2011. Electrochemical DNA aptamer-based biosensor for OTA detection, using superparamagnetic nanoparticles. *Sensors and Actuators B: Chemical*. **156**(2),pp.932–937.
- Barton, A.C. et al. 2009. Labelless AC impedimetric antibody-based sensors with pg ml⁻¹ sensitivities for point-of-care biomedical applications. *Biosensors and Bioelectronics*. **24**(5),pp.1090–1095.
- Behdani, M. et al. 2013. Development of VEGFR2-specific Nanobody Pseudomonas exotoxin A conjugated to provide efficient inhibition of tumor cell growth. *New Biotechnology*. **30**(2),pp.205–209.
- Bhalla, V. et al. 2010. Chip cleaning and regeneration for electrochemical sensor arrays. *Thin Solid Films*. **518**(12),pp.3360–3366.
- Bharathi, S. et al. 2001. Novel Electrochemical Interfaces with a Tunable Kinetic Barrier by Self-Assembling Organically Modified Silica Gel and Gold Nanoparticles. *Langmuir*. **17**(1),pp.1–4.
- Bhatia, S.K. et al. 1989. Use of thiol-terminal silanes and heterobifunctional crosslinkers for immobilization of antibodies on silica surfaces. *Analytical Biochemistry*. **178**(2),pp.408–413.
- Billah, M.M. et al. 2010. Directed immobilization of reduced antibody fragments onto a novel SAM on gold for myoglobin impedance immunosensing. *Bioelectrochemistry*. **80**(1),pp.49–54.
- Blanchard, G.C. et al. 1990. Regeneration of immunosorbent surfaces used in clinical, industrial and environmental biosensors: Role of covalent and non-covalent interactions. *Journal of Immunological Methods*. **130**(2),pp.263–275.
- Boero, C. et al. 2011. Targeting of multiple metabolites in neural cells monitored by using protein-based carbon nanotubes. *Sensors and Actuators B: Chemical*. **157**(1),pp.216–224.
- Boersma, Y.L. and Plückthun, A. 2011. DARPins and other repeat protein scaffolds: advances in engineering and applications. *Current Opinion in Biotechnology*. **22**(6),pp.849–857.

- Bombarová, K. et al. 2015. Surface Plasmon Resonance Ellipsometry Based Biosensor for the Investigation of Biomolecular Interactions. *Materials Today: Proceedings*. **2**(1),pp.70–76.
- Bonanni, A. and del Valle, M. 2010. Use of nanomaterials for impedimetric DNA sensors: A review. *Analytica Chimica Acta*. **678**(1),pp.7–17.
- Bonroy, K. et al. 2006. Comparison of random and oriented immobilisation of antibody fragments on mixed self-assembled monolayers. *Journal of Immunological Methods*. **312**(1–2),pp.167–181.
- Boujtita, M. 2014. 1 - Chemical and biological sensing with carbon nanotubes (CNTs) In: K. C. HONEYCHURCH, ed. *Nanosensors for Chemical and Biological Applications* [online]. Woodhead Publishing, pp. 3–27. Available from: <http://www.sciencedirect.com/science/article/pii/B9780857096609500011> [Accessed July 16, 2015].
- Brett, C.M.A. and Brett, A.M.O. 1998. *Electroanalysis*.
- Bright, F.V. et al. 1990. Regenerable fiber-optic-based immunosensor. *Analytical Chemistry*. **62**(10),pp.1065–1069.
- Brogan, K.L. et al. 2003. Direct oriented immobilization of F(ab') antibody fragments on gold. *Analytica Chimica Acta*. **496**(1–2),pp.73–80.
- Bryan, T. et al. 2013. An optimised electrochemical biosensor for the label-free detection of C-reactive protein in blood. *Biosensors and Bioelectronics*. **39**(1),pp.94–98.
- del Campo, F.J. 2014. Miniaturization of electrochemical flow devices: A mini-review. *Electrochemistry Communications*. **45**,pp.91–94.
- Campuzano, S. et al. 2006. Characterization of alkanethiol-self-assembled monolayers-modified gold electrodes by electrochemical impedance spectroscopy. *Journal of Electroanalytical Chemistry*. **586**(1),pp.112–121.
- Campuzano, S. et al. 2014. Disposable amperometric magnetoimmunosensors using nanobodies as biorecognition element. Determination of fibrinogen in plasma. *Biosensors and Bioelectronics*. **52**(0),pp.255–260.
- Cass, A.E. et al. 1984. Ferrocene-mediated enzyme electrode for amperometric determination of glucose. *Anal Chem*. **56**(4),pp.667–71.
- Cass, A.E.G. et al. 1985. Ferricinium ion as an electron acceptor for oxido-reductases. *Journal of Electroanalytical Chemistry and Interfacial Electrochemistry*. **190**(1–2),pp.117–127.
- Castillo, G. et al. 2015. Detection of aflatoxin B1 by aptamer-based biosensor using PAMAM dendrimers as immobilization platform. *Food Control*. **52**,pp.9–18.
- Caygill, R.L. et al. 2010. A review on viral biosensors to detect human pathogens. *Analytica Chimica Acta*. **681**(1–2),pp.8–15.

- Caygill, R.L. et al. 2012. Novel impedimetric immunosensor for the detection and quantitation of Adenovirus using reduced antibody fragments immobilized onto a conducting copolymer surface. *Biosensors and Bioelectronics*. **32**(1),pp.104–110.
- Chawla, S. et al. 2011. Fabrication of polyphenol biosensor based on laccase immobilized on copper nanoparticles/chitosan/multiwalled carbon nanotubes/polyaniline-modified gold electrode. *Journal of Biotechnology*. **156**(1),pp.39–45.
- Chen, A. and Yang, S. 2015. Replacing antibodies with aptamers in lateral flow immunoassay. *Biosensors and Bioelectronics*. **71**,pp.230–242.
- Chirizzi, D. and Malitesta, C. 2011. Potentiometric urea biosensor based on urease immobilized by an electrosynthesized poly(o-phenylenediamine) film with buffering capability. *Sensors and Actuators B: Chemical*. **157**(1),pp.211–215.
- Choi, S. and Chae, J. 2009. Reusable biosensors via in situ electrochemical surface regeneration in microfluidic applications. *Biosensors and Bioelectronics*. **25**(2),pp.527–531.
- Clark, L.C. and Lyons, C. 1962. Electrode systems for continuous monitoring in cardiovascular surgery. *Annals of the New York Academy of Sciences*. **102**,pp.29–45.
- Cole, L.A. 2015. 31 - The future and a new generation of pregnancy tests In: L. A. C. A. BUTLER, ed. *Human Chorionic Gonadotropin (HGC) (Second Edition)* [online]. San Diego: Elsevier, pp. 335–339. Available from: <http://www.sciencedirect.com/science/article/pii/B9780128007495000316> [Accessed September 25, 2015].
- commons, W. 2014. Glucose Meters. Available from: http://en.wikipedia.org/wiki/File:Glucose_meters.jpg.
- Conroy, D.J.R. et al. 2010. Biosensing for the Environment and Defence: Aqueous Uranyl Detection Using Bacterial Surface Layer Proteins. *Sensors*. **10**(5),pp.4739–4755.
- Conroy, P.J. et al. 2009. Antibody production, design and use for biosensor-based applications. *Seminars in Cell & Developmental Biology*. **20**(1),pp.10–26.
- Cosnier, S. 2005. Affinity Biosensors Based on Electropolymerized Films. *Electroanalysis*. **17**(19),pp.1701–1715.
- Cserhádi, T. and Szögyi, M. 1995. Role of hydrophobic and hydrophilic forces in peptide-protein interaction: New advances. *Peptides*. **16**(1),pp.165–173.
- Daniels, J.S. and Pourmand, N. 2007. Label-Free Impedance Biosensors: Opportunities and Challenges. *Electroanalysis*. **19**(12),pp.1239–1257.
- Darain, F. et al. 2003. Disposable amperometric immunosensor system for rabbit IgG using a conducting polymer modified screen-printed electrode. *Biosensors and Bioelectronics*. **18**(5–6),pp.773–780.
- Darmostuk, M. et al. n.d. Current approaches in SELEX: An update to aptamer selection technology. *Biotechnology Advances* [online]. Available from:

<http://www.sciencedirect.com/science/article/pii/S0734975015000336> [Accessed July 17, 2015].

- Davis, F. and Higson, S.P.J. 2005. Structured thin films as functional components within biosensors. *Biosensors and Bioelectronics*. **21**(1),pp.1–20.
- De Genst, E. et al. 2006. Antibody repertoire development in camelids. *Developmental & Comparative Immunology*. **30**(1–2),pp.187–198.
- De, H.J.J.W. et al. 2009. Anti-fc-receptor single domain antibodies (nanobodies-tm) and therapeutic use. Available from:
<https://www.google.com/patents/EP2102243A2?cl=en>.
- Delong America n.d. *CNT Surface* [online]. Available from: <http://www.lv-em.com/sem-organic-carbon-nanotubes>.
- De Meyer, T. et al. n.d. Nanobody-based products as research and diagnostic tools. *Trends in Biotechnology* [online]. (0). Available from:
<http://www.sciencedirect.com/science/article/pii/S0167779914000419>.
- Demirel, G. et al. 2008. A novel DNA biosensor based on ellipsometry. *Surface Science*. **602**(4),pp.952–959.
- Desmyter, A. et al. 2015. Camelid nanobodies: killing two birds with one stone. *Current Opinion in Structural Biology*. **32**,pp.1–8.
- Dhawan, G. et al. 2009. Recent developments in urea biosensors. *Biochemical Engineering Journal*. **44**(1),pp.42–52.
- Drake, A.W. and Klakamp, S.L. 2011. A strategic and systematic approach for the determination of biosensor regeneration conditions. *Journal of Immunological Methods*. **371**(1–2),pp.165–169.
- Dzyadevych, S.V. et al. 2008. Amperometric enzyme biosensors: Past, present and future. *Irbm*. **29**(2-3),pp.171–180.
- Eissa, S. et al. 2015. Aptamer-based competitive electrochemical biosensor for brevetoxin-2. *Biosensors and Bioelectronics*. **69**,pp.148–154.
- Evans, S.D. and Ulman, A. 1990. Surface potential studies of alkyl-thiol monolayers adsorbed on gold. *Chemical Physics Letters*. **170**(5–6),pp.462–466.
- Ewels, C. n.d. *CNT graphic* [online]. Available from:
<http://www.ewels.info/img/science/nanotubes/tube.angled.jpg>.
- Fanning, L.J. et al. 1996. Development of the Immunoglobulin Repertoire. *Clinical Immunology and Immunopathology*. **79**(1),pp.1–14.
- Fisher, A.C. 1996. *Electrode Dynamics*. Oxford ; New York: OUP Oxford.
- Flajnik, M.F. et al. 2011. A Case Of Convergence: Why Did a Simple Alternative to Canonical Antibodies Arise in Sharks and Camels? *PLoS Biol*. **9**(8),p.e1001120.

- Fodey, T. et al. 2011. Developments in the production of biological and synthetic binders for immunoassay and sensor-based detection of small molecules. *TrAC Trends in Analytical Chemistry*. **30**(2),pp.254–269.
- ForteBio, I. 2007. Regeneration Strategies for Amine reactive Biosensors on the Octet System, Technical note 8. ,p.11.
- Gebauer, M. et al. 2013. Combinatorial Design of an Anticalin Directed against the Extra-Domain B for the Specific Targeting of Oncofetal Fibronectin. *Journal of Molecular Biology*. **425**(4),pp.780–802.
- Gerard, M. et al. 2002. Application of conducting polymers to biosensors. *Biosensors and Bioelectronics*. **17**(5),pp.345–359.
- Ghindilis, A.L. et al. 2009. Sensor Array: Impedimetric Label-Free Sensing of DNA Hybridization in Real Time for Rapid, PCR-Based Detection of Microorganisms. *Electroanalysis*. **21**(13),pp.1459–1468.
- Giannetto, M. et al. 2006. New selective gas sensor based on piezoelectric quartz crystal modified by electropolymerization of a molecular receptor functionalised with 2,2'-bithiophene. *Sensors and Actuators B: Chemical*. **115**(1),pp.62–68.
- Giepmans, B.N.G. et al. 2006. Review - The fluorescent toolbox for assessing protein location and function. *Science*. **312**(5771),pp.217–224.
- Gilbreth, R.N. and Koide, S. 2012. Structural insights for engineering binding proteins based on non-antibody scaffolds. *Current Opinion in Structural Biology*. **22**(4),pp.413–420.
- Giorgos J, D. 1979. Effect of detergents on antibody-antigen interaction. *Analytical Biochemistry*. **98**(2),pp.445–451.
- Gonzalez-Martinez, M.A. et al. 2007. Optical immunosensors for environmental monitoring: How far have we come? *Analytical and Bioanalytical Chemistry*. **387**(1),pp.205–218.
- Goode, J.A. et al. 2014. Biosensor Regeneration: A Review of Common Techniques and Outcomes. *Langmuir* [online]. Available from: <http://dx.doi.org/10.1021/la503533g> [Accessed February 24, 2015].
- Göpel, W. and Heiduschka, P. 1995. Interface analysis in biosensor design. *Biosensors and Bioelectronics*. **10**(9–10),pp.853–883.
- Gopinath, S.C.B. et al. 2014. Current aspects in immunosensors. *Biosensors and Bioelectronics*. **57**,pp.292–302.
- Grieshaber, D. et al. 2008. Electrochemical Biosensors - Sensor Principles and Architectures. *Sensors*. **8**(3),pp.1400–1458.
- Grönwall, C. and Ståhl, S. 2009. Engineered affinity proteins—Generation and applications. *Journal of Biotechnology*. **140**(3–4),pp.254–269.

- Guan, J.G. et al. 2004. Impedimetric biosensors. *Journal of Bioscience and Bioengineering*. **97**(4),pp.219–226.
- Habermüller, K. et al. 2000. Electron-transfer mechanisms in amperometric biosensors. *Fresenius' Journal of Analytical Chemistry*. **366**(6-7),pp.560–568.
- Hagihara, Y. and Saerens, D. 2014. Engineering disulfide bonds within an antibody. *Biochimica et Biophysica Acta (BBA) - Proteins and Proteomics*. **1844**(11),pp.2016–2023.
- Haleyur Giri Setty, M.K. and Hewlett, I.K. 2014. Point of Care Technologies for HIV. *AIDS Research and Treatment*. **2014**,p.20.
- Harlow, E. and Lane, D. 1999. *Using Antibodies: A Laboratory Manual*. CSHL Press.
- Hassanzadeh-Ghassabeh, G. et al. 2013. Nanobodies and their potential applications. *Nanomedicine (Lond)*. **8**(6),pp.1013–26.
- Hays, H.C.W. et al. 2006. Development of capacitance based immunosensors on mixed self-assembled monolayers. *Sensors and Actuators B: Chemical*. **114**(2),pp.1064–1070.
- Hermanson, G.T. 2008. *Bioconjugate Techniques*. Academic Press.
- Hilton, J.P. et al. 2011. A microfluidic affinity sensor for the detection of cocaine. *Sensors and Actuators A: Physical*. **166**(2),pp.241–246.
- Hirst, N.A. et al. 2013. An amperometric lactate biosensor using H₂O₂ reduction via a Prussian Blue impregnated poly(ethyleneimine) surface on screen printed carbon electrodes to detect anastomotic leak and sepsis. *Sensors and Actuators B: Chemical*. **186**(0),pp.674–680.
- Holford, T.R.J. et al. 2012. Recent trends in antibody based sensors. *Biosensors and Bioelectronics*. **34**(1),pp.12–24.
- Homola, J. et al. 1999. Surface plasmon resonance sensors: review. *Sensors and Actuators B-Chemical*. **54**(1-2),pp.3–15.
- Honda, T. et al. 2003. Method of constructing camel antibody library. Available from: <https://www.google.com/patents/WO2003025020A1?cl=en>.
- Huang, J. et al. 2010. An electrochemical impedimetric immunosensor for label-free detection of *Campylobacter jejuni* in diarrhea patients' stool based on O-carboxymethylchitosan surface modified Fe₃O₄ nanoparticles. *Biosensors and Bioelectronics*. **25**(5),pp.1204–1211.
- Huang, L. et al. 2010. Nanobodies®: proficient tools in diagnostics. *Expert Review of Molecular Diagnostics*. **10**(6),pp.777–785.
- Hui, G.-H. et al. 2013. Electrochemical impedance spectrum frequency optimization of bitter taste cell-based sensors. *Biosensors and Bioelectronics*. **47**,pp.164–170.

- Hu, Y. et al. 2013. Label-free electrochemical impedance spectroscopy biosensor for direct detection of cancer cells based on the interaction between carbohydrate and lectin. *Biosensors and Bioelectronics*. **43**(0),pp.79–83.
- Hwang, B.-J. et al. 2001. Nucleation and Growth Mechanism of Electropolymerization of Aniline on Highly Oriented Pyrolytic Graphite at a Low Potential. *Electroanalysis*. **13**(1),pp.37–44.
- Ianeselli, L. et al. 2014. Development of stable and reproducible biosensors based on electrochemical impedance spectroscopy: Three-electrode versus two-electrode setup. *Biosensors and Bioelectronics*. **55**,pp.1–6.
- ISO 2010. ISO 11.100.10 in-vitro diagnostic test systems. *ISO 11.100.10 in-vitro diagnostic test systems* [online]. Available from: http://www.iso.org/iso/home/store/catalogue_ics/catalogue_ics_browse.htm?ICS1=11&ICS2=100&ICS3=10 [Accessed April 8, 2015].
- Israr, M.Q. et al. 2010. Potentiometric cholesterol biosensor based on ZnO nanorods chemically grown on Ag wire. *Thin Solid Films*. **519**(3),pp.1106–1109.
- Jiang, H. et al. 2015. Theophylline detection in serum using a self-assembling RNA aptamer-based gold nanoparticle sensor. *Biosensors and Bioelectronics*. **70**,pp.299–303.
- Jin, Z. et al. 2001. Development of a polyaniline-based optical ammonia sensor. *Sensors and Actuators B: Chemical*. **72**(1),pp.75–79.
- Johnson, A. et al. 2012. Sensitive Affimer and Antibody Based Impedimetric Label-Free Assays for C-Reactive Protein. *Analytical Chemistry*. **84**(15),pp.6553–6560.
- Joseph, W. 2006. Electrochemical biosensors: Towards point-of-care cancer diagnostics. *Biosensors and Bioelectronics*. **21**(10),pp.1887–1892.
- Kaláb, T. and Skládal, P. 1997. Disposable multichannel immunosensors for 2,4-dichlorophenoxyacetic acid using acetylcholinesterase as an enzyme label. *Electroanalysis*. **9**(4),pp.293–297.
- Kalyoncu, S. et al. 2014. Effects of protein engineering and rational mutagenesis on crystal lattice of single chain antibody fragments. *Proteins: Structure, Function, and Bioinformatics*. **82**(9),pp.1884–1895.
- Kandimalla, V.B. et al. 2004. Regeneration of ethyl parathion antibodies for repeated use in immunosensor: a study on dissociation of antigens from antibodies. *Biosensors and Bioelectronics*. **20**(4),pp.903–906.
- Kankare, J. 2002. Sauerbrey Equation of Quartz Crystal Microbalance in Liquid Medium. *Langmuir*. **18**(18),pp.7092–7094.
- Karlsson, R. 2004. SPR for molecular interaction analysis: a review of emerging application areas. *Journal of Molecular Recognition*. **17**(3),pp.151–161.

- Kennedy, B. et al. 2007. A study of the oxidation and polymerisation of meta substituted phenol and aniline derivatives. *Journal of Electroanalytical Chemistry*. **608**(1),pp.22–30.
- Kindt, T.J. et al. 2006. *Kuby Immunology* 6Rev Ed edition. New York: W.H.Freeman & Co Ltd.
- Kolkman, J.A. and Law, D.A. 2010. Nanobodies – from llamas to therapeutic proteins. *Drug Discovery Today: Technologies*. **7**(2),pp.e139–e146.
- Konstantinov, K.N. et al. 2009. Rapid detection of anti-chromatin autoantibodies in human serum using a portable electrochemical biosensor. *Biosensors and Bioelectronics*. **24**(7),pp.1949–1954.
- Kulys, J.J. et al. 1980. Electron exchange between the enzyme active center and organic metal. *FEBS Letters*. **114**(1),pp.7–10.
- Kummer, L. et al. 2013. Knowledge-Based Design of a Biosensor to Quantify Localized ERK Activation in Living Cells. *Chemistry & Biology*. **20**(6),pp.847–856.
- Labib, M. et al. 2010. A novel competitive capacitive glucose biosensor based on concanavalin A-labeled nanogold colloids assembled on a polytyramine-modified gold electrode. *Analytica Chimica Acta*. **659**(1–2),pp.194–200.
- Lacroix, J.C. et al. 2000. Aniline electropolymerization on mild steel and zinc in a two-step process. *Journal of Electroanalytical Chemistry*. **481**(1),pp.76–81.
- Laschi, S. and Mascini, M. 2006. Planar electrochemical sensors for biomedical applications. *Medical Engineering & Physics*. **28**(10),pp.934–943.
- Lawal, A.T. and Adeloju, S.B. 2013. Polypyrrole based amperometric and potentiometric phosphate biosensors: A comparative study B. *Biosensors and Bioelectronics*. **40**(1),pp.377–384.
- Lazcka, O. et al. 2007. Pathogen detection: A perspective of traditional methods and biosensors. *Biosensors and Bioelectronics*. **22**(7),pp.1205–1217.
- Lazerges, M. et al. 2006. In situ QCM DNA-biosensor probe modification. *Sensors and Actuators B: Chemical*. **120**(1),pp.329–337.
- Leech, D. 1994. Affinity biosensors. *Chemical Society Reviews*. **23**(3),pp.205–213.
- Levine, P.M. et al. 2009. Real-time, multiplexed electrochemical DNA detection using an active complementary metal-oxide-semiconductor biosensor array with integrated sensor electronics. *Biosensors and Bioelectronics*. **24**(7),pp.1995–2001.
- Li, H. et al. 2015. Construction of a biotinylated cameloid-like antibody for label-free detection of apolipoprotein B-100. *Biosensors and Bioelectronics*. **64**,pp.111–118.
- Lillie, G. et al. 2001. Electrochemical impedance spectroscopy as a platform for reagentless bioaffinity sensing. *Sensors and Actuators B-Chemical*. **78**(1-3),pp.249–256.

- Li, M. et al. 2012. Recent developments and applications of screen-printed electrodes in environmental assays—A review. *Analytica Chimica Acta*. **734**(0),pp.31–44.
- Liotta, L.A. and Petricoin, E.F. 2012. Regulatory approval pathways for molecular diagnostic technology. *Methods in Molecular Biology (Clifton, N.J.)*. **823**,pp.409–420.
- Lipovsek, D. 2011. Adnectins: engineered target-binding protein therapeutics. *Protein engineering, design & selection: PEDS*. **24**(1-2),pp.3–9.
- Liron, Z. et al. 2002. Voltage-induced inhibition of antigen-antibody binding at conducting optical waveguides. *Biosensors and Bioelectronics*. **17**(6–7),pp.489–494.
- Liu, G. et al. n.d. Single-nucleotide polymorphism genotyping using a novel multiplexed electrochemical biosensor with nonfouling surface. *Biosensors and Bioelectronics* [online]. (0). Available from: <http://www.sciencedirect.com/science/article/pii/S095656631200797X>.
- Losic, D. et al. 2001. Influence of surface topography on alkanethiol SAMs assembled from solution and by microcontact printing. *Langmuir*. **17**(11),pp.3307–3316.
- Lu, B. et al. 1996. Oriented immobilization of antibodies and its applications in immunoassays and immunosensors. *Analyst*. **121**(3),p.29R–32R.
- Lu, L. et al. 2011. Improved electrochemical immunosensor for myeloperoxidase in human serum based on nanogold/cerium dioxide-BMIMPF₆/l-Cysteine composite film. *Colloids and Surfaces B: Biointerfaces*. **86**(2),pp.339–344.
- Luong, J.H.T. et al. 2008. Biosensor technology: Technology push versus market pull. *Biotechnology Advances*. **26**(5),pp.492–500.
- Luo, P. et al. 2014. Aptamer biosensor for sensitive detection of toxin A of *Clostridium difficile* using gold nanoparticles synthesized by *Bacillus stearothermophilus*. *Biosensors and Bioelectronics*. **54**,pp.217–221.
- Luppa, P.B. et al. 2001. Immunosensors - principles and applications to clinical chemistry. *Clinica Chimica Acta*. **314**(1-2),pp.1–26.
- Lvovich, V.F. 2012. *Impedance Spectroscopy*. Wiley.
- Makaraviciute, A. and Ramanaviciene, A. 2013. Site-directed antibody immobilization techniques for immunosensors. *Biosensors and Bioelectronics*. **50**(0),pp.460–471.
- Manso, J. et al. 2008. Alcohol dehydrogenase amperometric biosensor based on a colloidal gold–carbon nanotubes composite electrode. *Electrochimica Acta*. **53**(11),pp.4007–4012.
- March, C. et al. 2009. A piezoelectric immunosensor for the determination of pesticide residues and metabolites in fruit juices. *Talanta*. **78**(3),pp.827–833.
- Mattos, A.B. et al. 2012. A dual quartz crystal microbalance for human cardiac troponin T in real time detection. *Sensors and Actuators B: Chemical*. **161**(1),pp.439–446.

- Michalzik, M. et al. 2005. Development and application of a miniaturised quartz crystal microbalance (QCM) as immunosensor for bone morphogenetic protein-2. *Sensors and Actuators B: Chemical*. **105**(2),pp.508–515.
- Millner, P.A. et al. 2009. Nanostructured transducer surfaces for electrochemical biosensor construction—Interfacing the sensing component with the electrode. *Seminars in Cell & Developmental Biology*. **20**(1),pp.34–40.
- Miranda, F.F. et al. 2011. Reagentless fluorescent biosensors from artificial families of antigen binding proteins. *Biosensors and Bioelectronics*. **26**(10),pp.4184–4190.
- Mitchell, J. 2010. Small Molecule Immunosensing Using Surface Plasmon Resonance. *Sensors*. **10**(8),pp.7323–7346.
- Mounié, J. et al. 1990. Methods of theophylline assay and therapeutic monitoring of this drug. *Annales De Biologie Clinique*. **48**(5),pp.287–293.
- Mustafa, M.K. et al. 2010. Detection of β -amyloid peptide (1–16) and amyloid precursor protein (APP770) using spectroscopic ellipsometry and QCM techniques: A step forward towards Alzheimers disease diagnostics. *Biosensors and Bioelectronics*. **26**(4),pp.1332–1336.
- Muyldermans, S. et al. 2009. Camelid immunoglobulins and nanobody technology. *Veterinary Immunology and Immunopathology*. **128**(1–3),pp.178–183.
- Nabok, A. et al. 2011. Detection of low molecular weight toxins using an optical phase method of ellipsometry. *Sensors and Actuators B: Chemical*. **154**(2),pp.232–237.
- Nakamura, K. et al. 2013. *Electro-enzymology Coenzyme Regeneration*. Springer Science & Business Media.
- Neuman, K.C. and Nagy, A. 2008. Single-molecule force spectroscopy: optical tweezers, magnetic tweezers and atomic force microscopy. *Nature Methods*. **5**(6),pp.491–505.
- Newman, J.D. and Turner, A.P.F. 2005. Home blood glucose biosensors: a commercial perspective. *Biosensors and Bioelectronics*. **20**(12),pp.2435–2453.
- Nicholls, H. 2007. Nanobodies: The ultrasmall antibodies. *New Scientist*. **196**(2624),pp.50–53.
- Nien, P.-C. et al. 2009. Fabricating an Amperometric Cholesterol Biosensor by a Covalent Linkage between Poly(3-thiopheneacetic acid) and Cholesterol Oxidase. *Sensors*. **9**(3),pp.1794–1806.
- Niu, X. et al. 2012. Porous screen-printed carbon electrode. *Electrochemistry Communications*. **22**(0),pp.170–173.
- van Noort, D. and Mandenius, C.-F. 2000. Porous gold surfaces for biosensor applications. *Biosensors and Bioelectronics*. **15**(3–4),pp.203–209.
- Novotny, J. and Sharp, K. 1992. Electrostatic fields in antibodies and antibody/antigen complexes. *Progress in Biophysics and Molecular Biology*. **58**(3),pp.203–224.

- Oliveira, S. et al. 2013. Targeting tumors with nanobodies for cancer imaging and therapy. *Journal of Controlled Release*. **172**(3),pp.607–617.
- O'Sullivan, C.K. and Guilbault, G.G. 1999. Commercial quartz crystal microbalances - theory and applications. *Biosensors & Bioelectronics*. **14**(8-9),pp.663–670.
- Özcan, B. et al. 2014. Introducing a new method for evaluation of the interaction between an antigen and an antibody: Single frequency impedance analysis for biosensing systems. *Talanta*. **125**,pp.7–13.
- Palmisano, F. et al. 2000. Simultaneous monitoring of glucose and lactate by an interference and cross-talk free dual electrode amperometric biosensor based on electropolymerized thin films. *Biosensors and Bioelectronics*. **15**(9-10),pp.531–539.
- Pataky, K. and Brugger, J. 2014. 3 - Rapid prototyping techniques for the fabrication of biosensors. In: R. NARAYAN, ed. *Rapid Prototyping of Biomaterials* [online]. Woodhead Publishing, pp. 75–96. Available from: <http://www.sciencedirect.com/science/article/pii/B9780857095992500039> [Accessed August 13, 2015].
- Pchelintsev, N.A. et al. 2009. Simultaneous deposition of Prussian Blue and creation of an electrostatic surface for rapid biosensor construction. *Sensors and Actuators B: Chemical*. **138**(2),pp.461–466.
- Piro, B. et al. 2007. Investigations of the steric effect on electrochemical transduction in a quinone-based DNA sensor. *Biosensors and Bioelectronics*. **22**(12),pp.3126–3131.
- Pohanka, M. 2008. Electrochemical biosensors – principles and applications. *J. Appl. Biomed.* **6**,p.8.
- Pournaras, A.V. et al. 2008. Development of an impedimetric immunosensor based on electropolymerized polytyramine films for the direct detection of Salmonella typhimurium in pure cultures of type strains and inoculated real samples. *Analytica Chimica Acta*. **624**(2),pp.301–307.
- Prodromidis, M.I. 2010. Impedimetric immunosensors—A review. *Electrochimica Acta*. **55**(14),pp.4227–4233.
- Queirós, R.B. et al. 2013. A label-free DNA aptamer-based impedance biosensor for the detection of E. coli outer membrane proteins. *Sensors and Actuators B: Chemical*. **181**(0),pp.766–772.
- Radi, A.-E. et al. 2005. Reusable Impedimetric Aptasensor. *Analytical Chemistry*. **77**(19),pp.6320–6323.
- Raffa, D.L. et al. 2006. Electrochemical copolymerization of aniline and ortho-aminobenzylamine. Studies on its conductivity and chemical derivatization. *Journal of Electroanalytical Chemistry*. **587**(1),pp.60–66.
- Ramanavicius, A. et al. 1999. Polypyrrole-Entrapped Quinohemoprotein Alcohol Dehydrogenase. Evidence for Direct Electron Transfer via Conducting-Polymer Chains. *Analytical Chemistry*. **71**(16),pp.3581–3586.

- Ramesh, R. et al. 2015. Potentiometric biosensor for determination of urea in milk using immobilized *Arthrobacter creatinolyticus* urease. *Materials Science and Engineering: C*. **49**,pp.786–792.
- Reiter, S. et al. 2001. A reagentless glucose biosensor based on glucose oxidase entrapped into osmium-complex modified polypyrrole films. *Sensors and Actuators B: Chemical*. **79**(2–3),pp.150–156.
- Reverberi, R. and Reverberi, L. 2007. Factors affecting the antigen-antibody reaction. *Blood Transfus.* **5**(4),pp.227–40.
- Reverts, H. and Hoogenboom, H.R.J.M. 2010. Method for obtaining polypeptide constructs comprising two or more single domain antibodies. Available from: <http://www.google.co.uk/patents/EP2215125A1> [Accessed July 31, 2015].
- Ricci, F. and Palleschi, G. 2005. Sensor and biosensor preparation, optimisation and applications of Prussian Blue modified electrodes. *Biosensors and Bioelectronics*. **21**(3),pp.389–407.
- Richter, A. et al. 2014. Anticalins: Exploiting a non-Ig scaffold with hypervariable loops for the engineering of binding proteins. *FEBS Letters*. **588**(2),pp.213–218.
- Rodgers, M.A. et al. 2010. Lipocalin based biosensors for low mass hydrophobic analytes; development of a novel SAM for polyhistidine tagged proteins. *Sensors and Actuators B: Chemical*. **150**(1),pp.12–18.
- Rushworth, J.V., Ahmed, A., et al. 2014. A label-free electrical impedimetric biosensor for the specific detection of Alzheimer's amyloid-beta oligomers. *Biosensors and Bioelectronics*. **56**,pp.83–90.
- Rushworth, J.V., Goode, J.A., et al. 2014. *Impedimetric Biosensors for Medical Applications: Current Progress and Challenges*. Not Avail.
- Sahin, E. et al. 2010. Comparative effects of pH and ionic strength on protein–protein interactions, unfolding, and aggregation for IgG1 antibodies. *Journal of Pharmaceutical Sciences*. **99**(12),pp.4830–4848.
- Sapelnikova, S. et al. 2003. Amperometric sensors based on tyro sinase-modified screenprinted arrays. *Talanta*. **61**(4),pp.473–483.
- Schotte, P. et al. 2012. Method for the production of domain antibodies. Available from: <https://www.google.com/patents/US20120157664>.
- Schuhmann, W. et al. 2000. Electron-transfer pathways between redox enzymes and electrode surfaces: reagentless biosensors based on thiol-monolayer-bound and polypyrrole-entrapped enzymes. *Faraday Discuss.* (116),pp.245–55; discussion 257–68.
- Schwarz, F.P. et al. 1995. Thermodynamics of Antigen-antibody Binding using Specific Anti-lysozyme Antibodies. *European Journal of Biochemistry*. **228**(2),pp.388–394.
- Scognamiglio, V. 2013. Nanotechnology in glucose monitoring: Advances and challenges in the last 10 years. *Biosensors and Bioelectronics*. **47**(0),pp.12–25.

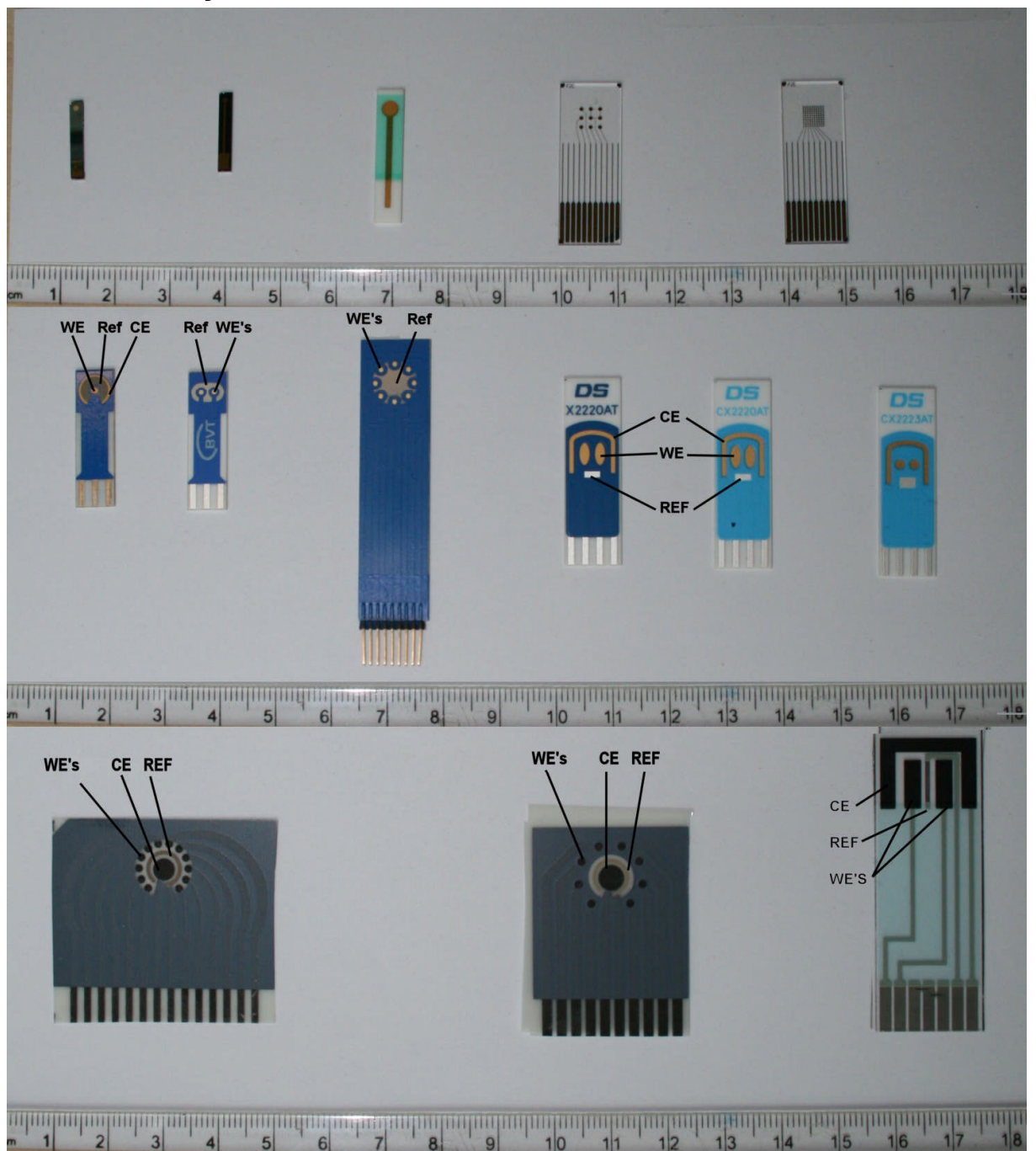
- Scott, R.A. and Lukehart, C.M. (eds.). 2007. *Applications of physical methods to inorganic and bioinorganic chemistry*. Hoboken, NJ: Wiley.
- Seok Kim, Y. et al. n.d. Aptamer-based nanobiosensors. *Biosensors and Bioelectronics* [online]. Available from: <http://www.sciencedirect.com/science/article/pii/S0956566315302086> [Accessed October 6, 2015].
- Sergeyeva, T.A. et al. 1996. Polyaniline label-based conductometric sensor for IgG detection. *Sensors and Actuators B: Chemical*. **34**(1–3),pp.283–288.
- Singh, R. et al. 2014. Biosensors for pathogen detection: A smart approach towards clinical diagnosis. *Sensors and Actuators B: Chemical*. **197**,pp.385–404.
- Skerra, A. 2008. Alternative binding proteins: Anticalins – harnessing the structural plasticity of the lipocalin ligand pocket to engineer novel binding activities. *FEBS Journal*. **275**(11),pp.2677–2683.
- Skottrup, P.D. 2010. Small biomolecular scaffolds for improved biosensor performance. *Analytical Biochemistry*. **406**(1),pp.1–7.
- Song, M.-J. et al. 2007. Electrochemical biosensor array for liver diagnosis using silanization technique on nanoporous silicon electrode. *Journal of Bioscience and Bioengineering*. **103**(1),pp.32–37.
- Spitznagel, T.M. and Clark, D.S. 1993. Surface-Density and Orientation Effects on Immobilized Antibodies and Antibody Fragments. *Nat Biotech*. **11**(7),pp.825–829.
- Steegborn, C. and Skládal, P. 1997. Construction and characterization of the direct piezoelectric immunosensor for atrazine operating in solution. *Biosensors and Bioelectronics*. **12**(1),pp.19–27.
- Stumpp, M.T. et al. 2008. DARPins: A new generation of protein therapeutics. *Drug Discovery Today*. **13**(15–16),pp.695–701.
- Sundberg, E.J. et al. 2000. Estimation of the Hydrophobic Effect in an Antigen–Antibody Protein–Protein Interface†,‡. *Biochemistry*. **39**(50),pp.15375–15387.
- Suzuki, M. et al. 2008. Surface Plasmon Resonance Array Devices *In: Handbook of Biosensors and Biochips* [online]. John Wiley & Sons, Ltd. Available from: <http://onlinelibrary.wiley.com/doi/10.1002/9780470061565.hbb097/abstract> [Accessed July 16, 2015].
- Tajima, N. et al. 2011. Significance of Antibody Orientation Unraveled: Well-Oriented Antibodies Recorded High Binding Affinity. *Analytical Chemistry*. **83**(6),pp.1969–1976.
- Tang, D. et al. 2010. Simultaneous determination of five-type hepatitis virus antigens in 5 min using an integrated automatic electrochemical immunosensor array. *Biosensors and Bioelectronics*. **25**(7),pp.1658–1662.
- Taylor, R.F. et al. 1991. Antibody- and receptor-based biosensors for detection and process control. *Analytica Chimica Acta*. **249**(1),pp.67–70.

- Teles, F.S.R.R. 2011. Biosensors and rapid diagnostic tests on the frontier between analytical and clinical chemistry for biomolecular diagnosis of dengue disease: A review. *Analytica Chimica Acta*. **687**(1),pp.28–42.
- Tiede, C. et al. 2014. Adhiron: a stable and versatile peptide display scaffold for molecular recognition applications. *Protein Eng Des Sel*. **27**(5),pp.145–55.
- Trojanowicz, M. and Krawczyński vel Krawczyk, T. 1995. Electrochemical biosensors based on enzymes immobilized in electropolymerized films. *Microchimica Acta*. **121**(1-4),pp.167–181.
- Tsuji, I. et al. 1990. Enzyme immunosensors based on electropolymerized polytyramine modified electrodes. *Biosensors & Bioelectronics*. **5**(2),pp.87–101.
- Tsumoto, K. et al. 1996. Role of salt bridge formation in antigen-antibody interaction - Entropic contribution to the complex between hen egg white lysozyme and its monoclonal antibody HyHEL10. *Journal of Biological Chemistry*. **271**(51),pp.32612–32616.
- Vadgama, P. and Crump, P.W. 1992. Biosensors: recent trends. A review. *Analyst*. **117**(11),pp.1657–1670.
- Vakurov, A. et al. 2005. Acetylcholinesterase-based biosensor electrodes for organophosphate pesticide detection: II. Immobilization and stabilization of acetylcholinesterase. *Biosensors and Bioelectronics*. **20**(11),pp.2324–2329.
- Vakurov, A. et al. 2009. The preparation of size-controlled functionalized polymeric nanoparticles in micelles. *Nanotechnology* [online]. **20**(29). Available from: [://WOS:000267612700017](http://www.ncbi.nlm.nih.gov/pubmed/19411177).
- Van Oss, C.J. 1995. Hydrophobic, hydrophilic and other interactions in epitope-paratope binding. *Molecular Immunology*. **32**(3),pp.199–211.
- Vidal, J.-C. et al. 2004. Amperometric cholesterol biosensor based on in situ reconstituted cholesterol oxidase on an immobilized monolayer of flavin adenine dinucleotide cofactor. *Analytical Biochemistry*. **333**(1),pp.88–98.
- Vincke, C. and Muyldermans, S. 2012. Introduction to heavy chain antibodies and derived Nanobodies. *Methods Mol Biol*. **911**,pp.15–26.
- Voet, V. Pratt 1998. Fundamentals of Biochemistry. *Wiley*.
- Wang, J. 2006. Analytical Electrochemistry, 3rd Edition - Joseph Wang. Available from: <http://eu.wiley.com/WileyCDA/WileyTitle/productCd-0471678791.html> [Accessed July 15, 2015].
- Wan, Y. et al. 2011. Carbon nanotube-based ultrasensitive multiplexing electrochemical immunosensor for cancer biomarkers. *Biosensors and Bioelectronics*. **30**(1),pp.93–99.
- Warriner, K. et al. 1997. Stability of dodecyl sulphate-doped poly (pyrrole)/glucose oxidase modified electrodes exposed in human blood serum. *Materials Science and Engineering: C*. **5**(2),pp.81–90.

- Wijesuriya, D. et al. 1994. Regeneration of immobilized antibodies on fiber optic probes. *Biosensors and Bioelectronics*. **9**(8),pp.585–592.
- Willamson, c n.d. *CNT Forest* [online]. Available from: <http://www.ifm.eng.cam.ac.uk/research/cip/current/cim-up/cnt-fab/>.
- Wilson, J.M.G. and Jugner, J. 1968. Principles and Practice of Screening for Disease. *World Health Organisation - Public Health Papers*. **34**,p.162.
- Wilson, K. and Walker, J. 2010. *Principles and Techniques of Biochemistry and Molecular Biology*. Cambridge University Press.
- Wilson, R. and Turner, A.P.F. 1992. GLUCOSE-OXIDASE - AN IDEAL ENZYME. *Biosensors & Bioelectronics*. **7**(3),pp.165–185.
- Windmiller, J.R. et al. 2011. Bicomponent Microneedle Array Biosensor for Minimally-Invasive Glutamate Monitoring. *Electroanalysis*. **23**(10),pp.2302–2309.
- Withey, G.D. et al. 2008. DNA-programmable multiplexing for scalable, renewable redox protein bio-nanoelectronics. *Bioelectrochemistry*. **74**(1),pp.111–117.
- Xu, M. et al. 2013. The label free picomolar detection of insulin in blood serum. *Biosensors and Bioelectronics*. **39**(1),pp.21–25.
- Yang, N. et al. 2015. Carbon nanotube based biosensors. *Sensors and Actuators B: Chemical*. **207, Part A**,pp.690–715.
- Yokota, A. et al. 2003. The role of hydrogen bonding via interfacial water molecules in antigen-antibody complexation - The HyHEL-10-HEL interaction. *Journal of Biological Chemistry*. **278**(7),pp.5410–5418.
- Yun, C. et al. n.d. An Electrochemical Impedimetric Immunosensor for Ultrasensitive Determination of Ketamine Hydrochloride. *Sensors and Actuators B: Chemical* [online]. (0). Available from: <http://www.sciencedirect.com/science/article/pii/S0925400513004115>.
- Zain, Z.M. et al. 2010. Development of an implantable D-serine biosensor for in vivo monitoring using mammalian D-amino acid oxidase on a poly (o-phenylenediamine) and Nafion-modified platinum-iridium disk electrode. *Biosensors & Bioelectronics*. **25**(6),pp.1454–1459.
- Zhao, G.-C. and Yang, X. 2010. A label-free electrochemical RNA aptamer for selective detection of theophylline. *Electrochemistry Communications*. **12**(2),pp.300–302.
- Zhu, Z.G. et al. 2013. Enzyme-free glucose biosensor based on low density CNT forest grown directly on a Si/SiO₂ substrate. *Sensors and Actuators B: Chemical*. **178**,pp.586–592.
- Zourob, M. 2009. Recognition Receptors in Biosensors.

8 | Appendices

8.1 Variety of electrodes used



8.2 Buffers Used

<u>Name</u>	<u>Ingredients</u>	<u>pH</u>	<u>Application</u>
PBS	137 mM NaCl, 2.7 mM KCl, 4.3 mM Na ₂ HPO ₄ , 1.47 mM KH ₂ PO ₄	7.4	General Use
LB	Tryptone (10 mg.ml ⁻¹), NaCl (10 mg.ml ⁻¹), yeast extract (5 mg.ml ⁻¹)	7.5	Cell culture
TB	Tryptone (12 mg.ml ⁻¹), yeast extract (24 mg.ml ⁻¹), glycerol (0.4% v/v), TB salts (0.17M KH ₂ PO ₄ and 0.72M K ₂ HPO ₄).	7.5	Cell culture
TES	0.2 M Tris-HCL, 0.5 M Sucrose, 0.5 mM EDTA	8	Protein Extraction
Imidazole Elution Buffer	0.3 M imidazole, 20mM Tris base and 0.5 M NaCl	7.9	Ni+ column
Imidazole Wash Buffer	10 mM imidazole, 20mM Tris base and 0.5 M NaCl	7.9	Ni+ column
DW	PBS + 50 mM NaCl	7.4	Dialysis
Tris-Glycine Running	25 mM Tris, 192 mM Glycine 0.1 % SDS	8.6	PAGE
MES	50 mM MES, 50 mM Tris base, 0.1% SDS, 1 mM EDTA	7.3	PAGE
TA	50 mM Tricine, 50 mM Tris base, 0.1% SDS	8.2	PAGE
MOPS	50 mM MOPS, 50 mM Tris base, 0.1% SDS, 1 mM EDTA	7.7	PAGE
TBST	50 mM Tris, 150 mM NaCl, 0.05% (v/v) Tween 20 [®]	7.6	PAGE
Transfer	25 mM Tris, 192 mM Glycine, 20 % (v/v) methanol	8.3	Western Blot
Ponceau stain	Ponceau 1 g.l ⁻¹ in 5% acetic acid (v/v)	5	Western Blot
PBS-T	PBS + 0.5% Tween 20 [®]	7.4	Western Blot
Coupling Buffer	120 ml, 50 mM Tris, 5 mM EDTA-Na;	8.5	IP
RIPA	50 mM NaCl, 1% (v/v) IGEPAL CA-630 [®] , 0.5% (w/v) sodium deoxycholate, 0.1% (w/v) SDS and 50 mM Tris	8	IP
Glycine elution Buffer	100 mM Glycine	2.0	IP
DTT Elution Buffer	PBS + 100 mM DTT	7.4	IP
Regeneration Buffer	100 mM Glycine, 50% Propylene Glycol (v/v), 1% DMSO (v/v)	2.75	EIS
Interrogation Buffer	PBS +10 mM K ₃ Fe(CN ₆), K ₄ Fe(CN ₆)	7.2	EIS

8.3 Sequencing data for P8D8 nanobody

P8D8 Sequence:

- Redacted due to commercial sensitivity at the request of AbCam Plc.
Sequence data may be provided upon application to Abcam Plc.

His₆-tag Sequence:

ACCACCATCANCATCACGGTTCA

Spacer:

(CAG GTG GTG GTG GTA)_n GCG

M13 Primer Sequence :

Forward:

5'-d(GTTTTCCCAGTCACGAC)-3'

Reverse:

5'-d(CAGGAAACAGCTATGAC)-3'

8.4 Poster presented at BBI 2013

Regeneration of impedimetric immunosensors: Working towards reusable biosensors to increase cost effectiveness

Jack A. Goode^{1,2}, Prof. Paul A. Millner¹
¹Leeds Institute of Genetics, Health & Therapeutics,
 University of Leeds, UK
²Abcam Plc. Cambridge, UK
 *Email: sm07 jag@leeds.ac.uk



Introduction

A reusable biosensor offers key advantages such as low cost and reduced variance. Although regeneration of biosensor systems has been shown¹, this has not yet been achieved for electrochemical immunosensors.

Aims

1. To explore different polymer substrates.
2. To investigate different methods of regeneration.

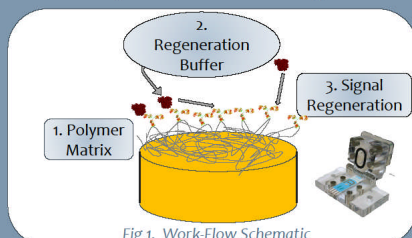


Fig 1. Work-Flow Schematic

1. Polymer Matrix

Previous research from our group proved the successful use of PANI:2-ABA copolymer², and a myoglobin sensor was made accordingly to investigate regeneration. After analyte binding & EIS interrogation, sensor regeneration was attempted using a range of conditions:

- pH was varied from 1-4
- Debind time was varied from 10-120 seconds

Using PANI:2-ABA three regeneration cycles were achieved using 100mM glycine at pH 2.75, though the reproducibility was low (Fig. 2) proving the polymer was chosen poorly.

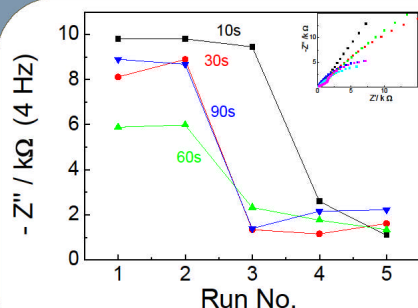


Fig 2. Regeneration of a PANI:2-ABA based biosensor, Nyquist data inset.

This was due to the electronic structure of the copolymer which has three states. Incubation at low pH therefore caused large change in impedance of the sensor itself, generating large amounts of noise. To correct this, polytyramine (Ptyr) was used as an alternative polymer matrix. With only one redox state it was found to be stable over a wide range of conditions (Fig.3).

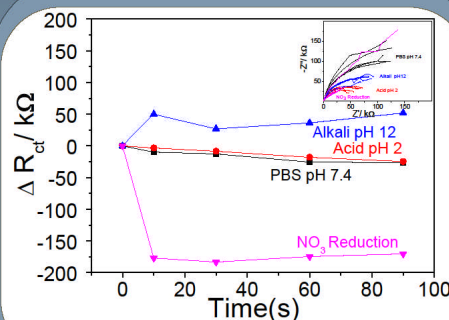


Fig 3. Stability of polytyramine sensor in different buffers, Nyquist data inset.

2. Regeneration Buffer

The stability of Ptyr was confirmed in high & low pH however the generation of alkali using electrochemical reduction of nitrate³ caused polymer stripping. Optimal regeneration was achieved using:

- 100 mM glycine in 50% propylene glycol + 1% DMSO at pH 2.75 for 10 seconds exposure (Fig.4).

3. Signal Regeneration

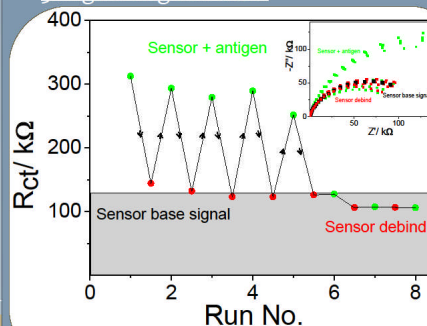


Fig 4. Regeneration of a polytyramine based biosensor, Nyquist data inset.

Conclusions

- The choice of polymer matrix is a key factor in sensor regeneration in order to avoid the regeneration buffer altering signal.
- The regeneration of an impedimetric immunosensor was achieved up to five cycles.
- This represents a reduction in the cost per test, in turn promoting the commercial uptake of biosensors.

1. Andersson, Hämäläinen & Malmqvist, 1999, Identification and Optimization of Regeneration Conditions for Affinity-Based Biosensor Assays. A Multivariate Cocktail Approach, *Anal.Chem.*, ACS, v.71:13, pg 2475-2481
 2. Gaybill, Hodges et al. 2012 Novel impedimetric biosensor for the detection and quantitation of Adenovirus using reduced antibody fragments immobilised onto a conducting copolymer surface. *Biosensors & Bioelectronics*, 33 pg 104-110
 3. Katsouranos & Kyriacou, 2005, Influence of nitrate concentration on its electrochemical reduction on tin cathode: identification of reaction intermediates. *Electrochimica Acta*, v.53:17, pg. 5477-5484

8.5 Poster Presented at MMT 2015

School of Biomedical Sciences
Faculty of Biological Sciences



The use of Nanobodies[®] in Reagentless Immunosensors

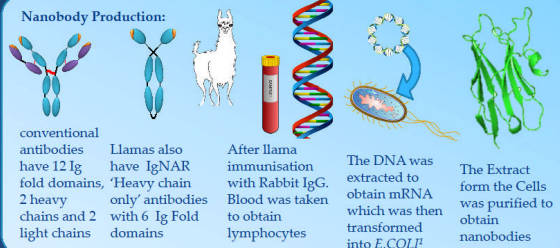
Jack A. Goode^{1,2}, Prof. Paul A. Miller¹ *Email: sm07jag@leeds.ac.uk,
¹University of Leeds, UK, ²Abcam Plc., Cambridge, UK

Introduction

Biosensors hold the potential to revolutionise diagnostic and commercial testing markets. Traditionally biosensors use antibodies as a widely available well understood receptor which can be readily generated. There is however a current shift away from the use of antibodies in favour of Non Antibody Binding Proteins (NABPs). This reduces the reliance on animal sacrifice and removes batch to batch variance; it may also prove much cheaper in time. When NABPs are used in immunosensors, they may have significantly different effects than antibodies. In this research, nanobodies have been investigated as a novel bioreceptor for impedimetric immunosensors.

The presented data shows the difference in sensor signal when using antibodies and nanobodies and highlights the issues that might be encountered when using NABPs in their native form applied to biosensors.

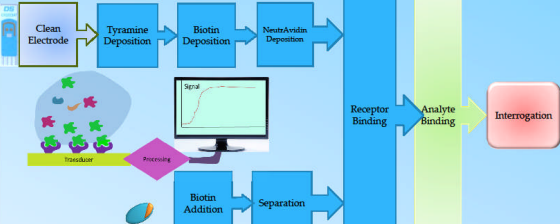
Nanobody Production:



Methods

A sensor to selectively detect rabbit IgG, our analyte, was constructed on screen printed gold electrodes (Dropsens[®] CX2223AT). A tethering layer was deposited by electropolymerising tyramine from solution (25mM in 0.6M NaOH in MeOH)². The receptor was conjugated by biotinylating both the receptor and the freshly deposited tyramine surface using Biotin-NHS. These were then cross-linked using 0.1 μM NeutrAvidin[®]. The concentration of receptor was optimised at ~7nM. The biosensor was interrogated using Electrochemical Impedance Spectroscopy (250kHz-250mHz). Consecutive concentrations of rabbit IgG analyte were tested. From these plots, data was modelled using a modified Randles' equivalent cell, where capacitance was substituted for by a constant phase element in order to account for non-ideality. This allowed the charge transfer resistance (R_{ct}) to be obtained.

Biosensor Fabrication



Results

We confirm the production of the biosensor itself both through the successful electropolymerisation of tyramine as shown in the Nyquist plot (Fig 1) and in the CV (Fig 1 inset). After polytyramine addition and fabrication of the full sensor the increase in arc size provides confirmation that the biosensor has been constructed and each layer is successfully deposited.

Upon analyte addition we observe a decreasing arc in the Nyquist plot (Fig 2 inset). This runs against the main body of evidence usually finding an increased arc upon analyte binding (discussed below). By analysing these Nyquist curves using the equivalent cell displayed (Fig 2, inset) charge transfer resistance (R_{ct}) values were determined. By comparing calibrations for a rabbit IgG sensor to which either rabbit IgG (specific analyte) or sheep IgG (control analyte) were added a clear difference was observed. A second negative control was done by adding Rabbit IgG to an Anti-Green Fluorescent Protein sensor (control receptor). These negative controls give a measure of non-specific binding. This data provides proof that the decrease in R_{ct} observed is analyte specific, caused by the binding of the analyte and that the sensor for rabbit IgG has good specificity and operational range.

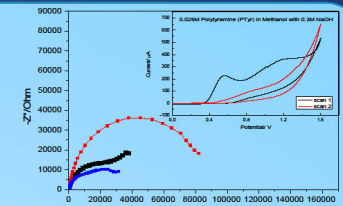


Fig 1: Confirmation of biosensor construction Nyquist Plot of a Biosensor construction shows bare gold (■) Polytyramine matrix (■) and fully constructed biosensor (■) Inset data: electropolymerisation of tyramine.

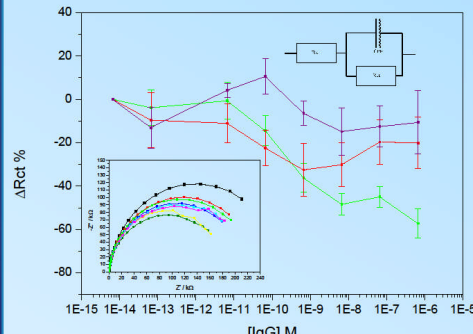


Fig 2: Calibration of a nanobody based biosensor for the detection of Rabbit IgG. Incubated with Rabbit IgG (■) Sheep IgG (■) and a sensor for the detection of GFP tested using Rabbit IgG (■). Inset Left Nyquist data showing incubation of sensor with rabbit IgG: 0M (■), 0.06 fM (■), 0.6 fM (■), 6 fM (■), 60 fM (■), 600 fM (■), 6000 fM (■). Inset right equivalent cell used to simulate data.

Comparison to Antibody based Immunosensors

When comparing data obtained from immunosensors constructed using nanobodies to conventional antibody based sensors (Fig 3) a clear difference can be observed. The decrease in impedance is significantly different and opposite to the positive increase in resistance is observed when using antibodies, which follows similar findings in the field.

It is commonly argued that the increase in resistance is due to the presence of analyte proteins preventing charge flow across the sensor surface, however, it is clear that when biotinylating nanobodies and using them directly on the sensor surface a decrease in the resistance is observed. It is important to note that the size of resistance change is much larger than when using antibodies albeit negative.

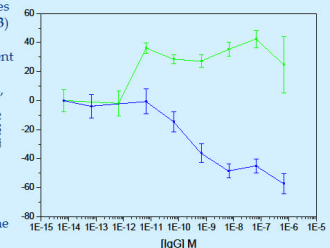
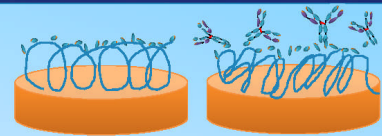


Fig 4: Comparison of biosensors developed to detect Rabbit IgG. Both the nanobody based sensor (■) and a conventional IgG based sensor (■).

Summary

In this work, a nanobody based sensor for Rabbit IgG has been successfully fabricated and whilst a calibration of decreasing resistance was obtained. We can be confident that this is an analyte specific response and a feature of using nanobodies as a receptor, which is distinctly different from data obtained in sensors constructed using antibody receptors.

Our current hypothesis for this phenomenon concerns the size of the nanobody relative to the IgG analyte: it is proposed that the small receptor size means that as the relatively large analyte binds, a distortion in the polymer tethering layer occurs. As the polymer layer is by no means static, this may open up conduction pathways and lead to a consistent reduction in the charge transfer resistance across the sensor interface. This could be a critical piece of knowledge in the field of biosensors where an increasing body of work is being amassed in exploiting the opportunities of other non antibody binding proteins as the primary biological recognition component.



1. Molecules 11(2) 2009. Retrospect. Immunosensibil. 128, 179-185
2. Thomson. 19-11-2008 Analytical Chemistry Acta. 654, 59-60

Publications(QR)

